

CHARACTERISING THE ROLE OF CIRCULATING IMMUNE CELLS IN BRAIN METASTASIS

Lukxmi Balathanan

Lincoln College

A thesis submitted to the Medical Sciences Division of the University of Oxford in partial
fulfilment of the requirements for the degree of
Doctor of Philosophy



Gray Institute for Radiation Oncology & Biology

Department of Oncology

University of Oxford

Trinity 2012

Word count: 43 666

(Excluding references, figure legends and appendices)

ABSTRACT

Characterising the role of circulating immune cells in brain metastasis

Submitted for the degree of Doctor of Philosophy

Lukxmi Balathasan -Lincoln College-Trinity 2012

Brain metastasis is a frequent occurrence in cancer patients and carries a high mortality rate. The incidence of brain metastasis is on the rise, highlighting the need for improved therapeutic intervention. Immune cells have been shown to promote disseminated tumour cells to colonise the lung and liver. Therefore, we aim to determine whether immune cells also facilitate brain metastasis by describing the host immune response to tumour cells attached to the brain vasculature.

We developed a model of brain metastasis by using ultrasound guidance to perform intracardiac injection of tumour cells. Using this method, we identified highly and weakly brain metastatic cell lines. To understand how cancer cells develop into brain metastases, we analysed brains harvested 4 h- 14 d after tumour injections.

At 4 h after intracardiac injection, only cell lines that developed into brain metastases were found adhered to the brain vasculature in high numbers. A small number of arrested tumour cells clustered with CD45⁺ immune cells. These tumour-CD45 clusters persisted over time whilst the frequency of solitary tumour cells declined. Tumour-associated CD45⁺ immune cells were identified to be Ly6G⁺Gr-1⁺CD11c⁻ myeloid cells. Considerably more tumour-CD45⁺ immune cell clusters were found within the brain vasculature when tumour cells were injected into mice bearing a primary tumour. Increased tumour-CD45⁺ immune cells clusters correlated with an increased number of brain metastases in the same group of mice. We also found a positive association between increased tumour-immune clusters and levels of tumour and host derived G-CSF. To establish a causal relationship between tumour cell-CD45 clusters and metastases, we developed an experimental setup for transcranial imaging. Our results suggest that tumour recruited immune cells may promote tumour cell colonisation of the brain and provides a framework for further investigation.

ACKNOWLEDGEMENTS

First, I would like to thank my supervisor, Professor Ruth J Muschel, for encouraging me to apply to the DPhil program and for giving me the opportunity to undertake this project. I also thank CRUK and John and Ann-Margaret Walton for generously funding this project. I would not have completed this work without the help and guidance of Dr John Beech and I am very grateful for his patience and perseverance in developing the *in vivo* imaging. I thank Dr Sally Hill for helping to develop the initial intracardiac animal studies, and Karla Watson and Magda Flieger for their skilled technical support. I would like to acknowledge Drs Nicola Sibson and Daniel Anthony for their comments and suggestions.

I have had the pleasure of working with a fantastic research team and would like to thank the Muschel Lab and Anne-Marie. I especially want to thank two very talented scientists, Thomas and Esther for their scientific guidance and especially for proof-reading and editing this thesis. I am also very grateful for Cat's comments and feedback on this work and for the much needed Belgian bun breaks. I thank the past members of the RRI who have all contributed to a great working environment: members of the McKenna lab, Anna G, Julie H, Garth H, Laura P and Ling J.

To my parents, Sauce, Ben, Jane, PD and Kams: Thank you for your encouragement and for sticking by me as I moved around collecting degrees - it has been a long haul but I am finally done! Finally, I thank Paul for being by my side throughout this entire process. I would not have embarked on this journey and come through in one piece if it was not for your continued belief in my abilities.

LIST OF ABBREVIATIONS

<i>ad lib</i>	ad libitum (at one's pleasure)
ADAM 9	disintegrin and metalloproteinase domain-containing protein 9
ANGPTL4	angiopoietin-related protein 4
ATCC	American Type Culture Collection
BFGF	basic fibroblast growth factor
CAM	cell adhesion molecule
CD	cluster of differentiation
COX-2	cyclooxygenase-2
CSF	cerebral spinal fluid
CSF-1	colony stimulating factor - 1
DMEM	Dulbecco's Modified Eagle's Medium
DMSO	dimethyl sulfoxide
EAE	Experimental autoimmune encephalomyelitis
EDTA	ethylenediaminetetraacetic acid
<i>et al</i>	et alia (and others)
FBS	fetal bovine serum
FP	fat pad

G-CSF	granulocyte colony stimulating factor
GFP	green fluorescent protein
GM-CSF	granulocyte macrophage colony stimulating factor
HBEGF	heparin-binding EGF-like growth factor F
HER2	Human epidermal growth factor receptor 2
HRP	horseradish peroxidase
I.C	intracerebral
I.P	intraperitoneal
I.V	intravenous
ICA	intracardiac
ICAM	intracellular adhesion molecule
IFN- γ	interferon-gamma
IL	interleukin
IVIS	<i>in vivo</i> imaging system
JAM	junctional adhesion molecules
KC	keratinocyte-derived cytokine
LLC	Lewis Lung carcinoma
LPS	lipopolysaccharide

MAM	metastasis associated macrophages
MCP-1	monocyte chemotactic protein
MDSC	myeloid derived suppressor cells
MHC	major histocompatibility
MIG	monokine induced by gamma interferon
MIP	macrophage inflammatory protein
miRNA	micro-ribonucleic acid
MMP	matrix metalloproteinase
MT1-MMP	membrane type 1 matrix metalloprotease
MTF	mellanotransferrin
NGF	nerve growth factor
NO	nitric oxide
NSCLC	non-small cell lung carcinoma
OB	olfactory bulb
PBS	phosphate buffered saline
PDGF	platelet derive growth factor
PEDF	pigment epithelium-derived factor
PFA	paraformaldehyde

RANTES	regulated and normal T cell expressed and secreted
RCA-1	Ricinus communis agglutinin – 1
RPM	rotations per minute
SC	subcutaneous
SCID	severe combined immuno-deficient
SCLC	small cell lung carcinoma
SNA	Sambucus nigra agglutinin
TAM	tumour associated macrophages
TAN	tumour associated neutrophils
TEM	trans-endothelial migration
TGF- β	transforming growth factor – beta
TIMP-1	tissue inhibitor of metalloproteinase 1
TNF	tumour necrosis factor
uPA	urokinase-type plasminogen activator
VCAM	vascular cell adhesion molecule
VEGF	vascular endothelial growth factor
ZO	zona occludens

TABLE OF CONTENTS

ABSTRACT	II
ACKNOWLEDGEMENTS	III
LIST OF ABBREVIATIONS	IV
TABLE OF CONTENTS	VIII
LIST OF FIGURES	XIII
LIST OF TABLES	XVI
SUPPLEMENTARY FIGURES AND VIDEOS	XVI
CHAPTER 1: INTRODUCTION	1
1.1 THE BRAIN	1
1.1.1 Neuroglia	1
1.1.1.1 Microglia	3
1.1.1.2 Astrocytes	5
1.1.2 The Blood Brain Barrier	6
1.1.2.1 Cellular transport across the BBB	8
1.2 BRAIN METASTASIS	12
1.2.1 Treatment of brain metastasis	14
1.2.2 Mechanism of brain metastasis	15
1.2.2.1 Homing and arrest	16
1.2.2.1.1 Molecular determinants of brain metastasis	17
1.2.2.1.1.a Molecular signature	17
1.2.2.1.1.B Paracrine signalling	20
1.2.2.1.1.c Cancer stem cells	21
1.2.2.1.1.d miRNAs	21
1.2.2.2 Survival	22
1.2.2.3 Extravasation	23
1.2.2.3.1 Proteases and tumour cell extravasation	24
1.2.2.3.2 BBB permeability and tumour cell extravasation	26
1.2.2.4 Colonisation	26
1.2.2.4.1 Decision point: dormancy vs. angiogenesis	27
1.2.2.4.2 Astrocyte response to brain metastases	29
1.2.2.4.3 Microglia/macrophage response to brain metastases	31
	viii

1.3 RESEARCH MOTIVATION AND OVERVIEW OF FINDINGS	33
CHAPTER 2: MATERIALS AND METHODS	35
2.1 CELL CULTURE	35
2.1.1 <i>Cell lines</i>	35
2.1.2 <i>Cell maintenance</i>	36
2.1.3 <i>Cell line storage</i>	36
2.1.4 <i>Cell preparation for animal injections</i>	37
2.2 IN VIVO EXPERIMENTS	37
2.2.1 <i>Animals</i>	37
2.2.2 <i>Ultrasound-mediated intracardiac injections</i>	37
2.2.3 <i>Intracarotid arterial injections</i>	39
2.2.6 <i>Fat pad/ subcutaneous primary tumour injections</i>	40
2.3 BRAIN PROCESSING	40
2.4 IMMUNOFLUORESCENCE	41
2.5 QUANTIFICATION OF BRAIN TISSUE	43
2.6 MICROSCOPY	44
2.7 STATISTICAL ANALYSIS	44
CHAPTER 3 – DEVELOPMENT OF AN <i>IN VIVO</i> MODEL OF BRAIN METASTASIS	45
3.1 INTRODUCTION	45
3.1.1 <i>In vivo models of brain metastasis</i>	45
3.1.1.1 Brain metastatic cell lines	45
3.1.1.2 Route of tumour delivery to form brain metastases	47
3.2 AIMS	48
3.3 MATERIALS AND METHOD	48
3.3.1 <i>In vivo experiments</i>	48
3.3.1.1 Intracardiac tumour injections (Blind)	48
3.3.1.2 Intracranial tumour injections	49
3.3.1.3 <i>In Vivo</i> bioluminescence assay	49

3.4 RESULTS	50
3.4.1 <i>Ultrasound guided intracardiac injection of metastatic cancer cells consistently produce brain metastases</i>	50
3.4.2 <i>Not all metastatic cell lines form parenchymal brain metastases</i>	52
3.4.3 <i>The inability to develop parenchymal brain metastases is an attribute of the cell line and not due to the mouse strain</i>	57
3.4.4 <i>Intracarotid injections of LLC does not result in consistent development of brain metastases</i>	60
3.4.5 <i>Weakly brain metastatic cells are able to grow in the brain if directly injected into the striatum</i>	62
3.5 DISCUSSION	64
CHAPTER 4: CHARACTERISING THE STEPS REQUIRED FOR DISSEMINATED TUMOUR CELLS TO DEVELOP INTO BRAIN METASTASES	68
4.1 INTRODUCTION	68
4.1.1 <i>Host-mediated metastases</i>	69
4.1.1.1 Macrophages	69
4.1.1.1.1 Tumour associated macrophages	70
4.1.1.1.2 Metastasis associated macrophages	71
4.1.1.2 Neutrophils	72
4.1.1.2.1 Tumour-associated neutrophils	72
4.1.1.2.2 Metastasis-associated neutrophils	73
4.1.1.3 Myeloid derived suppressor cells (MDSC)	74
4.1.1.3.1 Tumour associated MDSC	75
4.1.1.3.2 Metastasis associated MDSC	75
4.1.1.4 Primary tumour directed metastasis	76
4.2 HYPOTHESIS	78
4.3 AIMS	78
4.4 MATERIALS AND METHOD	79
4.4.1 <i>Fluorescence activated cell sorting (FACS)</i>	79
4.3 RESULTS	81
4.3.1 <i>Attachment and survival within the brain vasculature are the limiting steps in brain metastasis</i>	81
4.3.2 <i>ST6GALNAC5, the gene that mediates breast cancer metastasis to the brain, is not expressed by brain metastatic 4T1 cells</i>	83

4.3.3 Platelets associate with intravascular tumour cells	84
4.3.4 Circulating leukocytes associate with a few intravascular brain metastatic cells	87
4.3.5 Tumour-leukocyte clusters persist, whilst solitary tumour cells decline with time	88
4.3.6 An increase in tumour-CD45 ^{hi} intravascular clusters correlates with increased tumour burden	92
4.3.7 The CD45 ^{hi} cells clustered with intravascular tumour cells are Gr-1 ⁺ circulating immune cells	98
4.3.8 Different populations of Ly6G ⁺ granulocytes are present in blood after intracardiac injection of MDA 231 cells in naïve and tumour conditioned mice	106
4.3.9 Intravascular tumour associated immune cells express F4/80	111
4.4 DISCUSSION	112
CHAPTER 5: IDENTIFYING THE FUNCTION OF THE GR-1⁺ CELLS ASSOCIATED WITH INTRAVASCULAR BRAIN METASTATIC TUMOUR CELLS	123
5.1 INTRODUCTION	123
5.1.1 CD11b ⁺ Gr-1 ⁺ cells	123
5.2 HYPOTHESIS	126
5.3 AIMS	126
5.4 MATERIALS AND METHOD	127
5.4.1 In vivo neutrophil and Gr-1 cell depletion assay	127
5.4.2 Adoptive transfer of tumour educated immune cells	128
5.4.3 Mouse bio-plex cytokine assay	130
5.5 RESULTS	132
5.5.1 Ly6G positive neutrophils are not involved in aiding brain metastasis.	132
5.5.2 Gr-1 depletion is not sustained in mice injected with 4T1 tumour cells	134
5.5.3 Gr-1 antibody does not deplete all Gr-1 ⁺ cells	137
5.5.4 Adoptive transfer of tumour educated immune cells does not augment brain metastasis	138
5.5.5 G-CSF concentration is substantially increased in blood of pre-conditioned mice after intracardiac injection with MDA 231 or 4T1 cells	141
5.5.6 GR-1 ⁺ cells accumulate in brains of mice bearing 4T1 tumours and in brains of MDA 231 tumour bearing mice intracardiac injected with MDA 231 cells	143
5.6 DISCUSSION	148

CHAPTER 6: DEVELOPING AN <i>IN VIVO</i> IMAGING METHOD TO VISUALISE BRAIN METASTATIC TUMOUR CELLS INTERACTING WITH IMMUNE CELLS	156
6.1 INTRODUCTION	156
6.1.1 <i>In vivo brain imaging</i>	156
6.2 AIMS	156
6.3 MATERIALS AND METHOD	157
6.3.1 <i>Cranial window placement</i>	157
6.3.2 <i>In vivo microscopic imaging</i>	157
6.3.3 <i>Labelling CD45 antibodies with Alexa Fluor 546</i>	158
6.4 RESULTS	159
6.4.1 <i>Intracarotid injection of tumour cells delivers more cells to the brain allowing visualisation of tumour cells arrested in the brain vasculature</i>	159
6.4.2 <i>Oregon Green high molecular weight dextran is better than CD31-PE antibody to image the brain vasculature using multiphoton microscopy</i>	161
6.4.3 <i>Adoptive transfer of Dil labelled immune cells can be imaged through the cranial window</i>	163
6.4.4 <i>Circulating immune cells can be imaged along with brain vasculature using PE labelled CD45 antibody</i>	163
6.4.5 <i>Multiphoton microscopy enables imaging of tumour cells lying deeper within the brain</i>	167
6.5 DISCUSSION	172
CHAPTER 7: GENERAL DISCUSSION	177
7.1 ATTACHMENT TO THE BRAIN ENDOTHELIUM IS AN INTRINSIC ABILITY OF HIGHLY BRAIN METASTATIC CELLS	177
7.2 GR-1 ⁺ CIRCULATING IMMUNE CELLS MAY PROMOTE BRAIN METASTASIS.	181
7.3 GR-1 ⁺ CELLS FORM THE PRE-METASTATIC NICHE IN THE BRAIN	183
7.4 G-CSF INVOLVEMENT IN BRAIN METASTASES	186
7.5 CONCLUDING REMARKS	188
REFERENCES	190
APPENDIX	213
SUPPLEMENTARY FIGURES	213
SUPPLEMENTARY VIDEOS	224

LIST OF FIGURES

CHAPTER 1

FIGURE 1.1: CELLULAR MAKE-UP OF THE BRAIN	2
FIGURE 1.2: MICROGLIA DERIVE FROM HAEMATOPOIETIC STEM CELLS.....	4
FIGURE 1.3: ASTROCYTES COVER THE BRAIN ENDOTHELIUM TO FORM THE GLIAL LIMITANS	6
FIGURE 1.4: MOLECULAR AND CELLULAR TRANSPORT ACROSS THE BBB	8
FIGURE 1.5 IMMUNE CELLS CAN ENTER THE BRAIN VIA THREE DIFFERENT ROUTES	12
FIGURE 2.1: ULTRASOUND MEDIATED INTRACARDIAC INJECTIONS.....	39
FIGURE 2.2: ARRANGEMENT OF BRAIN SECTIONS ON SLIDES	43
FIGURE 3.1: ULTRASOUND GUIDED INTRACARDIAC INJECTION ALLOWS FOR CONSISTENT DEVELOPMENT OF BRAIN METASTASES IN MICE.....	51
FIGURE 3.2: INTRACARDIAC INJECTION OF 4T1, 4T07 OR MDA -MB-231 CELLS USING ULTRASOUND GUIDANCE CONSISTENTLY GIVE RISE TO PARENCHYMAL BRAIN METASTASES	54
FIGURE 3.3: B16 F10, LLC AND MC38 CANCER CELLS INFREQUENTLY DEVELOP INTRACRANIAL METASTASES AFTER INTRACARDIAC INJECTION.....	56
FIGURE 3.4: MET-1 CELLS DO NOT CONSISTENTLY PRODUCE BRAIN METASTASES	57
FIGURE 3.5: C57 BL/6 SYNGENEIC CELLS LINES DO NOT PRODUCE PARENCHYMAL BRAIN METASTASES IN BALB/C SCID MICE.....	59
FIGURE 3.6: COMPARING THE ABILITY OF METASTATIC CELL LINES TO COLONISE THE BRAIN AFTER ULTRASOUND-GUIDED INTRACARDIAC INJECTION.....	61
FIGURE 3.7: LLC CELLS INFREQUENTLY DEVELOP INTO BRAIN METASTASES AFTER INTRACAROTID INJECTION BUT WILL CONSISTENTLY FORM TUMOURS IN THE BRAIN IF DIRECTLY INJECTED INTO THE BRAIN PARENCHYMA	63
FIGURE 4.1: ATTACHMENT AND SURVIVAL OF METASTATIC CELLS WITHIN THE BRAIN OVER TIME.....	82
FIGURE 4.2: ST6GALNAC5 IS EXPRESSED BY LLC AND MDA 231 CELLS BUT NOT BY BRAIN METASTATIC 4T1 CELLS.....	84
FIGURE 4.3: PLATELETS ASSOCIATE WITH INTRAVASCULAR TUMOUR CELLS	86
FIGURE 4.4: A FEW INTRAVASCULAR TUMOUR CELLS ARE ASSOCIATED WITH CD45 ^{HI} IMMUNE CELLS 24 H POST INTRACARDIAC CHALLENGE	88
FIGURE 4.5: PERCENTAGE OF TUMOUR-CD45 ^{HI} CLUSTERS INCREASE WITH TIME	91
FIGURE 4.6: PRIMARY TUMOUR PRE-CONDITIONING EXPERIMENTAL PROTOCOL	93

FIGURE 4.7: THE MAJORITY OF 4T1 AND MDA-231 TUMOUR CELLS ARE INTRAVASCULAR 3 D POST INTRACARDIAC INJECTION	94
FIGURE 4.8: MICE PRE-CONDITIONED WITH A PRIMARY TUMOUR HAVE AN INCREASED PERCENTAGE OF INTRAVASCULAR TUMOUR- CD45 ^{HI} CLUSTERS AND DEVELOP MORE BRAIN METASTASES COMPARED TO PRIMARY TUMOUR-FREE MICE AFTER INTRACARDIAC INJECTION OF TUMOUR CELLS.....	96
FIGURE 4.10: INTRAVASCULAR TUMOUR ASSOCIATED IMMUNE CELLS ARE NOT CD3 ⁺ T-CELLS	99
FIGURE 4.11: IDENTIFYING TUMOUR ASSOCIATED IMMUNE CELLS USING MACROPHAGE/MYELOID CELL MARKERS	101
FIGURE 4.12: SOME TUMOUR ASSOCIATED CD45 ^{HI} CELLS DO NOT EXPRESS THE MACROPHAGE/MICROGLIA MARKER IBA1.	102
FIGURE 4.13: TUMOUR ASSOCIATED CD45 ^{HI} IMMUNE CELLS CO-EXPRESS THE GRANULOCYTE MARKER MBS.....	104
FIGURE 4.14: BOTH GR-1 ⁺ AND LY6G ⁺ IMMUNE CELLS ARE FOUND IN THE BRAINS OF TUMOUR INJECTED MICE.....	105
FIGURE 4.15: BLOOD FROM NAÏVE OR PRIMARY TUMOUR BEARING MICE ANALYSED 3 DAYS AFTER INTRACARDIAC INJECTION WITH MDA 231 MICE HARBOUR DIFFERENT POPULATIONS OF LY6G ⁺ CELLS	110
FIGURE 4.16: BRAIN METASTATIC CELL-ASSOCIATED MBS ⁺ CELLS CO-LOCALISE WITH F4/80 ⁺ CELLS	111
FIGURE 5.1: SCHEMATIC OF ANTIBODY MEDIATED DEPLETION OF NEUTROPHILS (LY6G ⁺) AND GR-1 ⁺ CELLS.....	128
FIGURE 5.2: SCHEMATIC OF ADOPTIVE TRANSFER EXPERIMENTS	130
FIGURE 5.3: SCHEMATIC OF BLOOD COLLECTION FOR CYTOKINE ASSAY	131
FIGURE 5.4: DEPLETION OF NEUTROPHILS IN MICE DOES NOT AUGMENT THE DEVELOPMENT OF BRAIN METASTASES.....	133
FIGURE 5.5: DEPLETION OF GR-1 ⁺ CELLS IS NOT SUSTAINED IN MICE INJECTED WITH 4T1 CELLS.....	137
FIGURE 5.6: INJECTION OF GR-1 ANTIBODY DOES NOT DEplete ALL GR-1 CELLS.....	138
FIGURE 5.7 ADOPTIVE TRANSFER OF TUMOUR EDUCATED IMMUNE CELLS DOES NOT AUGMENT DEVELOPMENT OF BRAIN METASTASES	140
FIGURE 5.8: CYTOKINES PRODUCED BY MDA-231 CELLS IN CULTURE ARE DETECTED USING A MOUSE CYTOKINE ARRAY	144
FIGURE 5.9: G-CSF LEVELS ARE SIGNIFICANTLY INCREASED IN BLOOD OF MDA 231 PRE CONDITIONED MICE 3 DAYS AFTER INTRACARDIAC INJECTION OF MDA 231-GFP CELLS.	145
FIGURE 5.10: G-CSF LEVELS ARE SIGNIFICANTLY INCREASED IN SERUM OF 4T1 TUMOUR BEARING MICE 3 DAYS AFTER INTRACARDIAC INJECTION OF 4T1-GFP CELLS.	146
FIGURE 5.11: GR-1 ⁺ CELLS ACCUMULATE IN BRAINS OF 4T1 AND MDA 231 TUMOUR BEARING MICE	147
FIGURE 6.1: AN INVERTED MOUSE HOLDER ENABLES IMAGING THOUGH A CRANIAL WINDOW	160

FIGURE 6.2: INTRACAROTID DELIVERY IMPROVES SUSTAINED DETECTION OF TUMOUR CELLS BENEATH CRANIAL WINDOW OVER TIME	161
FIGURE 6.3: OREGON GREEN LABELLED DEXTRAN ALLOWS VISUALISATION OF BRAIN VASCULATURE DEEPER WITHIN THE BRAIN.....	162
FIGURE 6.4: ANTI-MOUSE CD45-PE ALLOWS DETECTION OF CIRCULATING IMMUNE CELLS AND BLOOD VESSELS	164
FIGURE 6.5: ANTI-MOUSE CD45-PE SPECIFICALLY BINDS CIRCULATING IMMUNE CELLS	165
FIGURE 6.6: MICE INJECTED WITH 5×10^5 4T1-GFP CELLS ENABLE IMAGING TUMOUR CELLS OVER A LONGER TIME COURSE	165
FIGURE 6.7: INJECTING 1×10^6 4T1-GFP CELLS INTO MICE INDUCED SLOWING DOWN OF CIRCULATING IMMUNE CELLS.....	166
FIGURE 6.8: 4T1-GFP TUMOUR GROWS AS SHEETS BENEATH THE CRANIAL WINDOW	168
FIGURE 6.9: MULTIPHOTON IMAGING ALLOWS VISUALISATION OF TUMOUR CELLS LYING BELOW THE MENINGES.....	169
FIGURE 6.10: ALEXA FLOUR 546 LABELLED ANTI-MOUSE CD45 ALLOWS FOR IMAGING OF TUMOUR-IMMUNE CLUSTERS LYING DEEPER IN THE BRAIN	170

LIST OF TABLES

TABLE 2.1: CELL LINES TESTED FOR THEIR ABILITY TO FORM BRAIN METASTASES <i>IN VIVO</i>	35
TABLE 2.2: ANTIBODIES/LECTINS USED TO LABEL BRAIN TISSUES.....	42
TABLE 4.1: ANTIBODIES USED FOR FACS	80
TABLE 6.1: OPTIMISATION OF <i>IN VIVO</i> TRANSCRANIAL IMAGING OF TUMOUR CELLS, CIRCULATING IMMUNE CELLS AND BRAIN VASCULATURE	171

SUPPLEMENTARY TABLES FIGURES AND VIDEOS

SUPPLEMENTARY TABLE 1: <i>IN VIVO</i> ADVERSE EFFECTS.....	214
SUPPLEMENTARY FIGURE 1: LY6G ANTIBODY DEPLETES LY6G ⁺ CELLS BUT MAY MASK GR-1 ⁺ CELLS	216
SUPPLEMENTARY FIGURE 2: GR-1 ANTIBODY DOES NOT SUSTAIN DEPLETION OF GR-1 ⁺ CELLS IN 4T1 INJECTED MICE.....	220
SUPPLEMENTARY FIGURE 3: USE OF GR-1 ANTIBODY TO DEplete GR-1 ⁺ CELLS IN MDA 231 INJECTED SCID MICE.....	221
SUPPLEMENTARY FIGURE 4: SINGLE STAINING AND ISOTYPE CONTROL STAINING OF BLOOD CELLS FROM MDA 231 INJECTED SCID MICE.....	222
SUPPLEMENTARY FIGURE 5: ANTIBODY LABELLING OF SPLEEN SECTIONS AS POSITIVE CONTROLS	223
SUPPLEMENTARY VIDEO 1: ADOPTIVE TRANSFER OF DII LABELLED IMMUNE CELLS CAN BE VISUALISED THROUGH THE CRANIAL WINDOW	224
SUPPLEMENTARY VIDEO 2: CD45-PE ANTIBODIES LABEL CIRCULATING IMMUNE CELLS	224
SUPPLEMENTARY VIDEO 3: INJECTING MICE WITH 10 ⁶ 4T1-GFP TUMOUR CELLS CAUSES SLOWING DOWN OF CIRCULATING IMMUNE CELLS.	224
SUPPLEMENTARY VIDEO 4: INJECTING MICE WITH 5.0x10 ⁵ 4T1-GFP TUMOUR CELLS OR PBS DOES NOT CAUSE SLOWING DOWN OF CIRCULATING IMMUNE CELLS.	224

CHAPTER 1: INTRODUCTION

1.1 THE BRAIN

The brain is a specialised organ with a unique cellular structure composed of neurons and neuroglial support cells. The network of neurons communicates with each other using chemical messengers (neurotransmitters) and electrical signals to control all other organs and co-ordinate our actions and thought processes. With the exception of neurons formed in the subventricular zone to re-populate olfactory bulb (OB) neurons, and subgranular zones to replace neurons in the hippocampus, neurogenesis does not occur in adult brains (Altman and Das 1965; Altman 1969). To account for this, several layers of neuroprotection exist. The brain is encased by a tough connective tissue membrane called the leptomeninges which, together with the skull, provides physical protection. The cerebral spinal fluid (CSF) bathes the brain to provide cushioning (Del Bigio 2010). Homeostasis and protection from systemic threats are maintained by neuroglial cells and the blood-brain-barrier (BBB). The brain lacks a lymphatic system, and is maintained in an immunosuppressive state by local production of suppressive cytokines, low levels of major histocompatibility (MHC) I and II expression, and a limited presence of antigen-presenting cells (Bechmann, Galea et al. 2007; Galea, Bechmann et al. 2007). These features ensure immune privilege within the brain to limit inflammation and tissue damage.

1.1.1 NEUROGLIA

Neuroglia, the major cellular components of the brain critical for maintaining homeostasis, are composed of microglia and macroglia (Figure 1.1). Neuroglia have

pleiotropic functions including holding neurons in place, supplying nutrients and oxygen to neurons, insulating one neuron from another, destroying pathogens and removing dead neurons; They also modulate neurotransmission (Baumann and Pham-Dinh 2001; Christopherson, Ullian et al. 2005; Sofroniew 2005; Carson, Thrash et al. 2006; Brown and Ransom 2007; Ding, Fellin et al. 2007). There are three subsets of macroglia, of which astrocytes are the principle cell type. The two other types of macroglia include oligodendrocytes, cells that wrap myelin sheath around neuronal axons, and ependymal cells, cells that line the ventricle cavities and produce CSF (Del Bigio 2010).

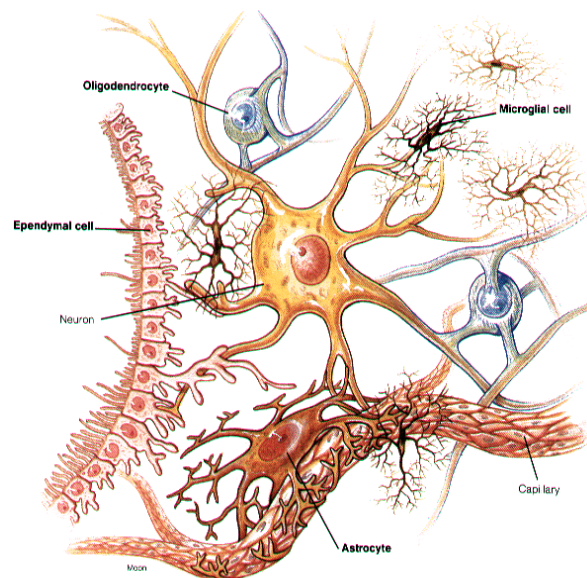


Figure 1.1: Cellular make-up of the brain

The brain is composed of neurons and neuronal support cells collectively called neuroglia. There are two types of neuroglia: microglia and macroglia. Microglia are brain specific macrophages and function to phagocytose dead neurons and debris and provide immune protection. There are three types of macroglia: astrocytes, oligodendrocytes and ependymal cells. Astrocytes and oligodendrocytes interact with neurons to provide structural and functional support. Ependymal cells line the ventricles of the brain and secrete CSF. The cilia found on ependymal cells constantly move in order to distribute the CSF. *Image adapted from www.celldiagram.net*

1.1.1.1 MICROGLIA

Microglia are the principal immune cells in the brain and account for 10-15% of total brain cells (Davis, Foster et al. 1994). Whilst neurons and macroglia develop from ectodermal progenitor cells, microglia develop from haematopoietic stem cells (Hickey and Kimura 1988). These haematopoietic stem cells enter the brain during development and differentiate into microglia, perivascular macrophages and pericytes (Ginhoux, Greter et al. 2010)(Figure 1.2a). Although microglia persist with little re-population, there is a high turn-over of pericytes and perivascular macrophages (Hickey and Kimura 1988; Guillemin and Brew 2004). Resting microglia morphologically display a small cell body with long protruding processes that are continuously at work surveying the brain microenvironment (Nimmerjahn, Kirchhoff et al. 2005) (Figure 1.2b). The activation of microglia can be detrimental to neurons and is therefore tightly controlled (von Zahn, Moller et al. 1997; DeWitt, Perry et al. 1998; Zujovic, Benavides et al. 2000; Nakajima and Kohsaka 2001; Streit, Davis et al. 2005) . Upon central nervous system (CNS) insult, nearby microglial cells retract their processes, up-regulate specific markers of activation and can become phagocytic in order to remove pathogens and debris (Nakajima and Kohsaka 2001; Colton and Wilcock 2010) (Figure 1.2b). Haematogenous macrophages can also enter the brain during pathology (Simard, Soulet et al. 2006; Getts, Terry et al. 2008; D'Mello, Le et al. 2009). Resting microglia can be distinguished from other macrophages based on surface expression of the leukocyte common antigen, CD45, as resting microglia exhibit low expression of CD45 compared to other myeloid cells (Sedgwick, Schwender et al. 1991; Carson, Thrash et al. 2006). However, activated

microglia up-regulate surface expression of CD45 and therefore distinction based on CD45 levels becomes ambiguous; there are currently no definitive markers to distinguish between these populations and to differentiate their specific roles in CNS pathology (Figure 1.2b).

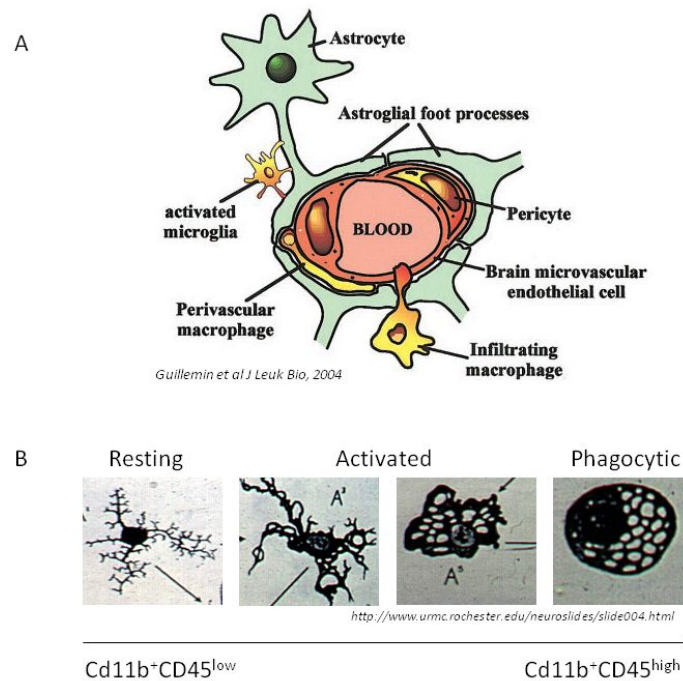


Figure 1.2: Microglia derive from haematopoietic stem cells

A: Microglia, perivascular macrophages, and pericytes in the brain all develop from haematopoietic stem cells. Pericytes cover the brain endothelium to provide structural support. Perivascular macrophages patrol the perivascular space –the area between the vascular basement membrane and the end feet of astrocytes which line the brain vasculature (glial limitans – see Figure 1.3). During pathology, circulating monocytes and perivascular macrophages can enter the brain parenchyma to support microglial cells. B: In the normal brain, microglia cells have small cell bodies with long processes which continuously survey the brain microenvironment. Resting microglia express the myeloid cell marker CD11b and have low expression of protein tyrosine phosphatase receptor type C (CD45). CD45 is a surface marker present on all leukocytes. In response to signalling cues (pathogens or damage), resting microglia retract their processes to become activated and additional stimuli converts activated microglia into phagocytes. Activated and phagocytic microglia up-regulate surface expression of CD45 and become indistinguishable from infiltrating macrophages. *Original source for figures are indicated.*

1.1.1.2 ASTROCYTES

Astrocytes are the most abundant cell type found in the brain and have essential roles in health and disease. Historically, astrocytes were described as 'glue' - structural support cells to hold neurons together and in place. However, several functional support roles have been identified (reviewed in (Sofroniew and Vinters 2010)). Astrocytes bridge capillaries and neurons to enable metabolic exchange (Obara, Szeliga et al. 2008) and contribute to neuronal regulation of blood flow (Gordon, Mulligan et al. 2007). They provide a fuel source for neurons (Brown and Ransom 2007) and maintain neuronal communication by neurotransmitter uptake and release (Sattler and Rothstein 2006), modulate synaptic transmission (Perea, Navarrete et al. 2009), promote myelination of neurons (Lutz, Zhao et al. 2009), and the development of synapses (Ullian, Sapperstein et al. 2001; Christopherson, Ullian et al. 2005). In response to extracellular cues, including damage, astrocytes become activated by a process termed *astrogliosis* and produce a variety of pro and anti-inflammatory molecules in a context-dependent manner (Eddleston and Mucke 1993; John, Lee et al. 2003; Sofroniew 2009). Severe astrogliosis can result in the formation of a glial scar. A glial scar can either promote recovery from damage or have detrimental effects such as preventing re-growth of damaged axons and causing neurodegeneration (Bush, Puvanachandra et al. 1999; Sofroniew 2009; Voskuhl, Peterson et al. 2009).

The end-feet of astrocytes are anchored by a transmembrane receptor, dystroglycan, to the parenchymal basement membrane (Wagner, Tagaya et al. 1997; Zaccaria, Di Tommaso et al. 2001) to form a second barrier encompassing the BBB and pericytes,

called the glial limitans (Abbott, Ronnback et al. 2006) (Figure 1.3). The glial limitans works in concert with the BBB to limit the passage of cells and molecules into the brain.

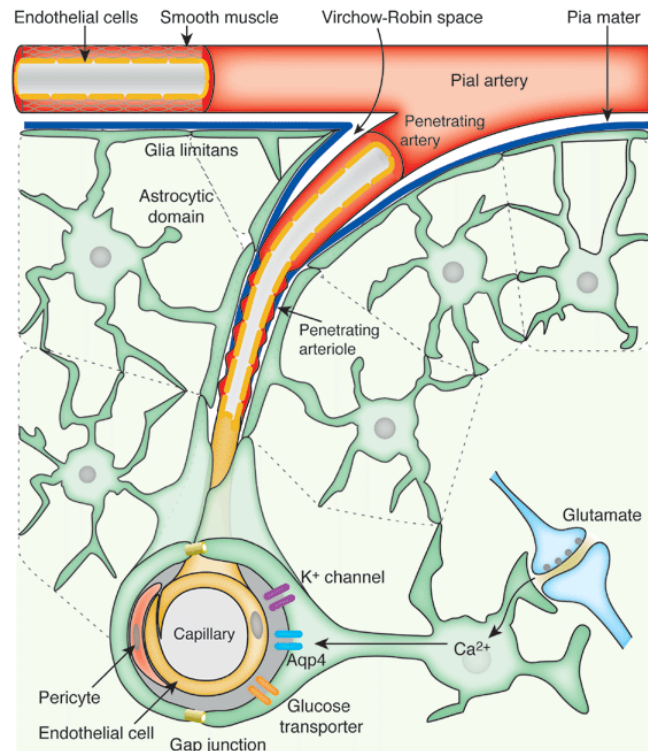


Figure 1.3: Astrocytes cover the brain endothelium to form the glial limitans

Blood vessels enter the brain through the meninges. The pia mater layer of the meninges surround arteries and arterioles but not veins (Zhang, Inman et al. 1990). The end feet of astrocytes surround endothelial cells and pericytes forming the glial limitans. The space between the glial limitans and the BBB is termed the perivascular space where patrolling perivascular macrophages are found. The arms of these astrocytes interact with neurons to mediate metabolic exchange. *Adapted from (Iadecola and Nedergaard 2007)*

1.1.2 THE BLOOD BRAIN BARRIER

The BBB is the endothelial interface that controls transport of most substances and cells from the blood into the brain. In the late 1800s, Paul Ehrlich discovered that injecting dye intravenously into rodents stained all organs excluding the brain (Ehrlich 1885).

Conversely, dye injected into the spinal cord was restricted to the brain. This restriction was due to the barrier formed by specialised tight junctions not present in the capillaries lining other organs (Wolburg and Lippoldt 2002). These tight junctions 'stitch' brain endothelial cells together, forming a highly selective filtration system which prevents paracellular entry of large macromolecules and cellular components (Lossinsky and Shivers 2004). The tight junctions are composed of small transmembrane protein subunits, including occludin, claudins, and junctional adhesion molecules (JAM). Each of these is anchored into endothelial cells by zonula occludens (ZO) protein complexes and associated proteins (Reese and Karnovsky 1967; Farrell and Shivers 1984; Wolburg and Lippoldt 2002; Gao and Shivers 2004). Particles of less than 20 nm in diameter, including oxygen, carbon dioxide and small lipophilic molecules, can diffuse across the barrier (Banks 2009). The presence of transport pumps enables the passage of substances and nutrients such as glucose and insulin to enter the brain via receptor-mediated transcytosis (Begley and Brightman 2003). There is little pinocytotic vesicle activity, which is usually used as a method of transport across endothelial and mesothelial cell layers (Abbott, Ronnback et al. 2006). On the parenchymal side, the BBB is supported by the basement membrane, pericytes, perivascular macrophages and the glial limitans (Wilson, Weninger et al. 2010). Refer to Figure 1.4 for an outline of the different transport mechanisms across the BBB

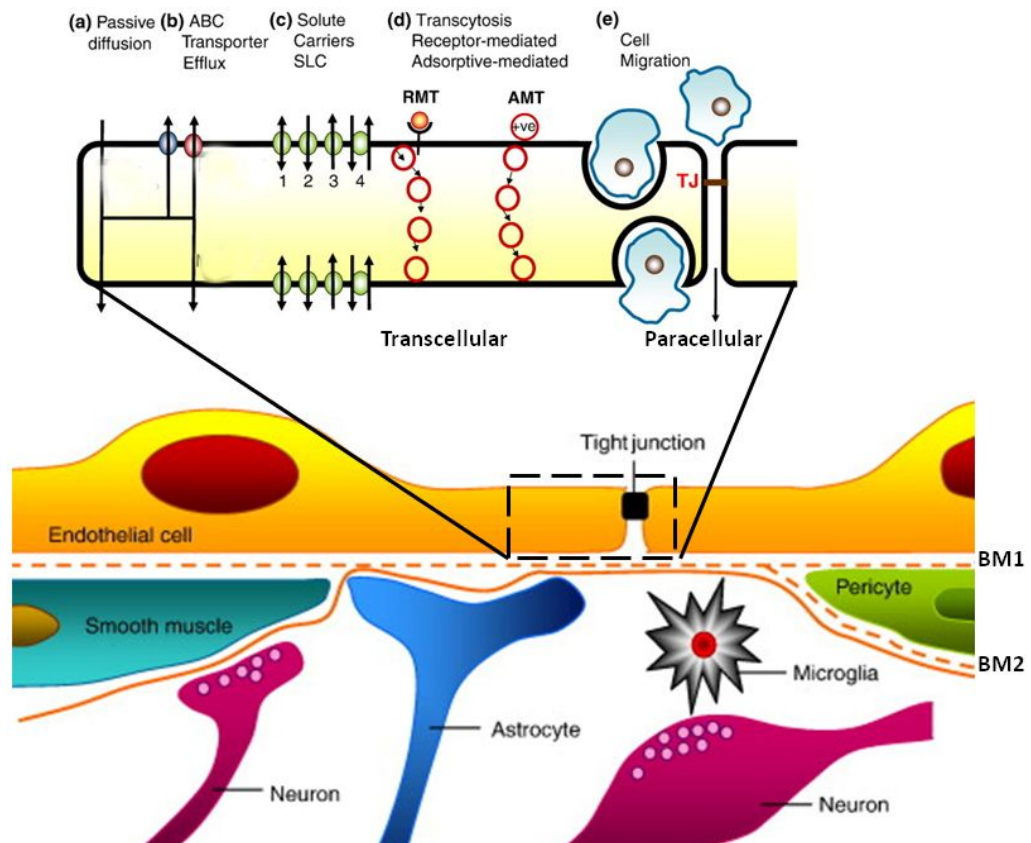


Figure 1.4: Molecular and cellular transport across the BBB

The endothelial cells of the BBB are non-fenestrated and are tightly held together by tight junctions to control the passage of molecules and cells into the brain. Molecular transport across the endothelium occurs across the endothelial cell (transcellular transport). Some molecules such as oxygen move into the brain by passive diffusion but larger molecules require special transport pumps. Immune cell trafficking into the brain is tightly controlled. Inflammatory conditions that weaken tight junctions may allow immune cell passage through endothelial cells (paracellular transport). There are two basement membranes in the brain: vascular basement membrane (BM1) and the parenchymal basement membrane (BM2). Astrocytes anchor to the parenchymal basement membrane to form a second barrier- the glial limitans. Image adapted from (Abbott, Patabendige et al. 2010)

1.1.2.1 CELLULAR TRANSPORT ACROSS THE BBB

The BBB maintains homeostasis and neuronal function by separating the brain from fluctuating events occurring externally (Cserr and Bundgaard 1984). However, the brain is not completely cut off and, as outlined above, interaction does occur with the external

surroundings. An early study showed that skin grafts placed in the brain will not be rejected but if graft antigens are presented first from outside the brain, then the skin graft would be rejected (Medawar 1948). There is also a low level of immune surveillance in the resting brain; activated T-cells are able to enter and patrol the brain but in the absence of antigen, T- cells do not persist (Engelhardt and Ransohoff 2005). In certain circumstances, immune cell infiltration into the brain can alleviate and resolve neuroinflammation (Israelski and Remington 1988; Byram, Carson et al. 2004; Du Pasquier, Kuroda et al. 2004; Simard, Soulet et al. 2006). However, inflammation also contributes to CNS dysfunction, as evident in Parkinson's, Alzheimer's, Multiple Sclerosis and viral infections (Compston and Coles 2002; Getts, Terry et al. 2008; Brochard, Combadiere et al. 2009; Sardi, Fassina et al. 2011).

Leukocyte extravasation into the brain follows similar steps that have been described for extravasation into other organs (Engelhardt and Ransohoff 2005; Bechmann, Galea et al. 2007). Chemokine signals originating from the brain can guide and capture immune cells at sites of extravasation. External cues can also influence immune infiltration into the brain; Systemic production of TNF during hepatic inflammation in mice was shown to cause up-regulation of adhesion molecules such as vascular CAM (V-CAM) on brain endothelium, thereby activating microglia to produce CCL2 and recruit CCR2-expressing, TNF-producing monocytes into the brain (D'Mello, Le et al. 2009). Once leukocytes slow down along the brain endothelium, they use selectin ligands to interact with endothelial selectins to tether and roll along the blood vessels. It has yet to be identified if there is a homing signature that attracts leukocytes to specific sites of the brain (Owens, Bechmann

et al. 2008). Arrest and firm adhesion is mediated by leukocyte integrin molecules interacting with complementary cell adhesion molecules (CAMs) on the endothelium. Leukocytes then crawl along the endothelium in search of an optimal location to extravasate. Monocytes and neutrophils predominantly use the Mac-1 integrin to crawl along inflamed vessels, whilst LFA-1 and VLA-4 have been implicated for lymphocytes (Schenkel, Mamdouh et al. 2004; Shulman, Shinder et al. 2009; Steiner, Coisne et al. 2010; Sumagin, Prizant et al. 2010) It has yet to be clarified whether immune cells use paracellular, transcellular, or other routes to extravasate (Butcher 1991).

Leukocytes extravasate from post-capillary venules and can enter the brain through three sites: across the choroid plexus into the CSF, into the subarachnoid space of the meninges, and into the parenchyma via the perivascular space (Ransohoff, KivisÃ¤kk et al. 2003) (Figure 1.5). Trans-endothelial migration (TEM) into the CSF and the meninges occurs across one layer (Wilson, Weninger et al. 2010). However, to enter the parenchyma from the perivascular space, leukocytes must breach the parenchymal basement membrane formed by the glial limitans (Wilson, Weninger et al. 2010). This second step is tightly regulated during homeostasis; Hematopoietic progenitor cells continuously enter the normal brain to give rise to pericytes and perivascular macrophages but these blood derived cells are restricted to the perivascular space (Hickey and Kimura 1988; Bechmann, Kwidzinski et al. 2001; Bechmann, Priller et al. 2001; Priller, Flugel et al. 2001). Studies have shown that CXCL12 expressed by brain endothelial cells of the microvasculature sequester CXCR4 expressing monocytes and T-cells within the perivascular space (McCandless, Wang et al. 2006; McCandless, Zhang et

al. 2008). However, in instances where homeostasis within the brain is threatened, appropriate cues permit the perivascular restricted immune cells to cross the glial limitans into the parenchyma and can have varying consequences: CXCR4 antagonism in experimental autoimmune encephalitis (EAE) enabled monocytes to enter the parenchyma and exacerbated disease (McCandless, Wang et al. 2006) whereas in West Nile virus infected mice, CXCR4 antagonism enhanced CD8⁺ T cells trafficking into the brain and alleviated symptoms (McCandless, Zhang et al. 2008) .

The mechanism(s) by which perivascular-restricted cells enter the brain parenchyma has yet to be fully elucidated but a few studies have indicated that proteases are involved. Whilst it was shown that MMPs were not required for leukocytes to traverse the endothelium into the perivascular space (Toft-Hansen, Buist et al. 2006), *Zhou et al* reported that neutrophil-produced MMP-9 was required for monocytes within the perivascular space to enter the brain parenchyma (Zhou, Stohlman et al. 2003). Depending on context, T-cell migration into the brain was also shown to require MMPs: Macrophage-secreted MMP-2 and 9 broke down dystroglycan, facilitating T-cell migration into the brain parenchyma (Agrawal, Anderson et al. 2006). However, MMP independent T-cell migration across the glial limitans has also been described (Savarin, Stohlman et al. 2010).

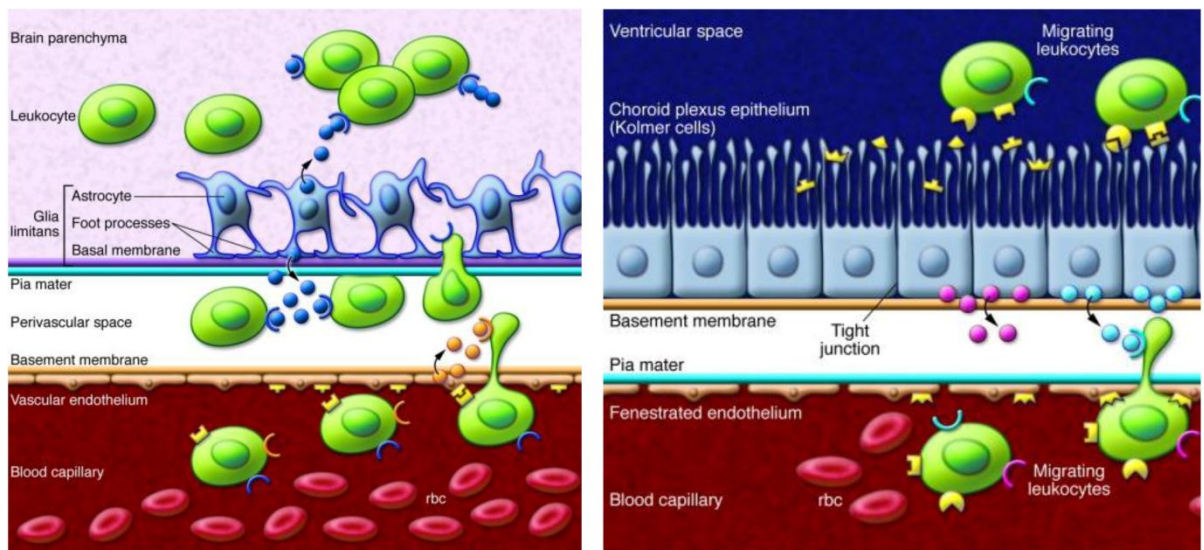


Figure 1.5 Immune cells can enter the brain via three different routes

Immune cells often cross the BBB at post-capillary venules to enter the perivascular space (left). Once past the endothelium, immune cells are sequestered within the perivascular space (space between the vascular basement membrane and the glial limitans) by signalling molecules such as CXCL12. Signals from within the brain may enable immune cells to traverse the glial limitans into the parenchyma. Immune cells can also cross the endothelium lining brain ventricles and through the choroid plexus directly into the ventricular space (right) or can cross from the blood into the subarachnoid space (not shown). Transport across the blood into the ventricular or subarachnoid space occurs across fenestrated endothelium (no tight junctions) and immune cells readily access the CSF. Adapted from (Wilson, Weninger et al. 2010)

1.2 BRAIN METASTASIS

Like immune cells, some disseminated tumour cells also have the ability to cross the BBB and 24-45% of all cancer patients will eventually develop brain metastases (Nussbaum, Djalilian et al. 1996). Lung cancer accounts for 50% of all brain metastases; followed by breast carcinomas, melanomas, renal carcinomas and gastro-intestinal tract carcinomas (Schouten, Rutten et al. 2002). Disseminated cancer cells that have accessed the CNS

commonly give rise to tumours within the brain parenchyma but metastases also form at other intracranial sites; 8% of intracranial metastases are found in the leptomeninges whilst 3-4% are found on the dura (Maroldi, Ambrosi et al. 2005). Non-parenchymal brain metastases arise through various routes including haematogenous spread, direct infiltration from vertebral metastases, and extension along nerve or perineural lymphatics (Kesari and Batchelor 2003; Maroldi, Ambrosi et al. 2005). Colonisation of the brain parenchyma most commonly occurs by the haematogenous spread of disseminated tumour cells (Maroldi, Ambrosi et al. 2005; Nayak, Abrey et al. 2009).

The incidence of brain metastasis is on the rise due to a plethora of factors: As improved therapies for primary cancer allow patients to live longer, the risk of developing recurrent disease increases, and the inability of current therapies to penetrate the BBB leaves the brain a sanctuary site for disseminated tumour cells. For example, breast cancer cells expressing the Her-2/neu receptor tyrosine kinase are associated with aggressive disease which metastasises to the lung, bone, liver, as well as the brain. The large monoclonal antibody trastuzumab is able to control systemic disease and prolong survival but, as it cannot penetrate the BBB, metastatic cells that escape into the brain have the chance to thrive; brain metastases are evident in 26-48% of trastuzumab-treated patients (Bendell, Domchek et al. 2003; Lai, Dang et al. 2004; Shmueli, Wigler et al. 2004; Stemmler, Kahlert et al. 2006; Lin and Winer 2007). On the other hand, the increasing incidence may simply be due to better imaging techniques that enable improved detection of brain metastases (Palmieri, Chambers et al. 2007). However, as brain imaging is not routine for

asymptomatic cancer patients, except those with certain lung cancers (Gavrilovic and Posner 2005), current incidence reports are most likely underestimated.

1.2.1 TREATMENT OF BRAIN METASTASIS

The prognosis upon detecting brain metastases is grim, with a median survival of 2-3 months (Nussbaum, Djalilian et al. 1996). Improved prospects depend on age of patient, tumour type and number of lesions presents (Gaspar, Scott et al. 1997). These factors also contribute to management and treatment. Unlike primary brain tumours, brain metastases are well encapsulated and demarcated from surrounding normal tissue making it possible for them to be removed with minimal damage to normal tissue (Krumina 2005). However, surgical resection is typically reserved for small solitary lesions in non-eloquent areas of the brain in patients with limited or controlled systemic disease (Patchell, Tibbs et al. 1990; Smalley, Laws et al. 1992; Auchter, Lamond et al. 1996; Fujimaki 2005; Claus 2011). Stereotactic radiosurgery is a non-surgical alternative that is also only available to patients with 1-3 brain metastases (O'Neill, Iturria et al. 2003; Warnick, Darakchiev et al. 2004; Koc, McGregor et al. 2005). Unfortunately, 70% of patients present with multiple metastases at the time of diagnosis, which limits treatment to whole brain radiation therapy (WBRT) to relieve neurological symptoms (Tosoni, Ermani et al. 2004).

The late presentation of brain metastases usually result in chemoresistant tumours and the BBB restricts penetrability of chemotherapeutics (Donelli, Zucchetti et al. 1992; Moscetti, Nelli et al. 2007). However, new agents with improved BBB permeability such as temozolomide has shown promise for treating a subset of brain metastatic patients

(Abrey and Christodoulou 2001), especially when combined with radiation therapy (Chalmers, Ruff et al. 2009; Devito, Yu et al. 2011; Gamboa-Vignolle, Ferrari-Carballo et al. 2012). Gefitinib, an oral tyrosine kinase inhibitor of epidermal growth factor receptor (EGFR), has been used to control brain metastases from non-small cell lung cancer (NSCLC) (Ceresoli, Cappuzzo et al. 2004). Recently, Dabrafenib treatment was shown to reduce the size of brain metastases in 90% of patients with BRAF mutated melanoma brain metastases (Falchook, Long et al. 2012). In mouse models of breast cancer metastasis to the brain, the microtubule-stabilizing agent taxane TPI-287 was reported to cross the BBB and reduce the growth of brain metastases by inhibiting tumour cell proliferation (Fitzgerald, Emerson et al. 2012).

1.2.2 MECHANISM OF BRAIN METASTASIS

Metastasis is a complex multi-step process. Cells from the primary tumour invade locally into normal tissue, intravasate into local lymph or blood vessels and travel within the circulation until they arrest, adhere, and extravasate into distant organs. At this point, tumour cells may remain dormant for years or if the conditions at the secondary site allow, proliferate to produce micrometastases. Metastases remain small until angiogenesis is stimulated. The entire process involves many unique molecular and cellular changes within the primary tumour and its local microenvironment as well as at sites of future colonisation.

The crucial changes required for successful metastases were thoroughly described more than 10 years ago (Hanahan and Weinberg 2000). The list of cancer hallmarks was recently updated to include a growing body of evidence showing that the host tumour

stroma and inflammation play a prominent role in cancer progression and metastasis (Colotta, Allavena et al. 2009; Hanahan and Weinberg 2011; Hanahan and Coussens 2012). Here, we specifically address the known mechanisms that enable disseminated tumour cells to develop into parenchymal brain metastases (hereafter referred to as brain metastases).

1.2.2.1 HOMING AND ARREST

Brain metastases develop from haematogenous spread of disseminated cancer cells within the arterial circulation (Gavrilovic and Posner 2005). However, the mechanism of homing and arrest at the brain microvasculature remains controversial and will most likely differ depending on the source and genetic make-up of the cancer cell. Ewing described secondary seeding at distant sites as a consequence of circulatory patterns of blood flow and mechanical arrest (Ewing 1928). This theory may account for the increased incidence of brain metastasis seen with lung cancer patients over other primary cancers as dislodged primary lung cancer cells first travel through the venous system to the heart where 15-20% of the blood pumped out is sent to the brain (Gavrilovic and Posner 2005). Clinical metastases are often found at the gray-white junction where narrowing of arterioles may capture large tumour emboli (Hwang, Close et al. 1996; Kruminina 2005) and in the watershed areas where decreased blood pressure may favour tumour attachment (Delattre, Krol et al. 1988). The distribution of brain metastases also follows blood flow - 80% are found in the cerebral hemispheres, 15% in the cerebellum, and 3% in the brain stem.

1.2.2.1.1 Molecular determinants of brain metastasis

Not all brain metastases fall within Ewing's mechanical model of arrest. The number of brain metastases in the cerebral hemisphere and cerebellum is greater in breast than lung cancer patients (Hengel, Sidhu et al. 2012) and not all lung tumours metastasise to the brain with comparable incidences and location. Small-cell lung cancers (SCLC) are more likely to metastasise to the brain than NSCLC, whilst lung adenocarcinomas are found more often in the brain than squamous lung carcinomas (Gavrilovic and Posner 2005). Colorectal cancers are frequently found in the posterior fossa, blood cancers frequent the meninges while breast cancers favour the pituitary gland (Hwang, Close et al. 1996). Melanoma cells have an increased propensity to form brain metastasis: 40% of all melanoma patients will develop brain metastasis as compared with 21% of all lung cancer patients (Nussbaum, Djalilian et al. 1996). Melanoma and SCLC cells may preferentially home to the brain as they share common heredity links with neural crest cells (Sharma, Korade et al. 1995). These findings give merit to Paget's 'seed and soil' hypothesis which states that metastatic spread is not a random process and disseminated cells, the 'seed' only grow in hospitable target sites, i.e. the 'soil' (Paget 1989).

1.2.2.1.1.a Molecular signature

A growing body of evidence suggests that one cannot adapt a cell line to grow in a specific organ; Within the primary tumour, there lie cells with the potential to metastasise to various organs and this specificity is determined by the different genetic mutations each cell carries (Chiang and Massague 2008). One study highlighted that different murine melanoma cells lines exhibit tropism for different sites of intracranial colonisation after

arterial injection. After intracarotid inoculation, the K-1735 melanoma produced brain metastases, whilst the B16 melanoma predominantly produced leptomeningeal metastases (Schackert and Fidler 1988). Injection of B16 melanoma cells into mice that were selected *in vitro* for increased ability to adhere brain tissue developed the same number of leptomeningeal metastases as the parental cell line (Netland and Zetter 1985). However, 26% of syngeneic mice injected with TGF- β 2-transfected B16 melanoma cells developed parenchymal brain micrometastases (Zhang, Zhang et al. 2009) suggesting that genetic changes need to occur to enable disseminated tumour cells to form brain metastases.

Genetic determinants of breast cancer-brain metastases have started to emerge. *Bos et al* compared brain-seeking clones with parental breast cancer cell lines, and analysed 368 human breast cancers, to identify a 17-gene signature, expression of which correlated with brain metastasis (Bos, Zhang et al. 2009). Within this 17-gene signature, many genes overlapped with the gene profile found on breast cancer cells which metastasise to the lung. However, the expression of sialyl transferase, *st6galnac5*, on breast cancer cells was specific for brain metastasis. ST6GALNAC5 protein expression by brain-metastasising breast cancer cells enabled adhesion and extravasation through an *in vitro* model of brain endothelium (Bos, Zhang et al. 2009). In another study, EGFR was implicated in breast cancer metastasis to the brain: knocking-down EGFR in the brain seeking variant of MDA-MB-231 breast cancer cells reduced adhesion, cell migration and invasion *in vitro* and produced fewer brain metastases *in vivo* (Nie, Yang et al. 2012). Recently, a functional bioinformatics approach to analysing site specific metastases revealed that breast cancer

cells that spread to the brain had a significant increase in proteins involved in signal transduction and in positive regulation of apoptosis, ER stress and Her-2 functions (Sanz-Pamplona, Aragues et al. 2011; Sanz-Pamplona, Garcia-Garcia et al. 2012).

Molecules that mediate brain metastasis from other primary cancers have also been identified. Some of the same genes expressed on breast cancer cells that metastasise to the brain identified by *Bos et al* were also found to be expressed by melanoma variants that metastasise to the brain including cyclooxygenase-2 (COX-2), matrix metalloproteinase-1 (MMP-1) and angiotensin-related protein 4 (ANGPTL4) (Izraely, Sagi-Assif et al. 2012). Others found that STAT3 was only expressed by metastatic, but not primary cutaneous melanoma and expression of STAT3 correlated with brain metastases (Xie, Huang et al. 2006). However, no connection was found with STAT3 expression and CNS metastases in stage IV melanoma patients (Lee, Fox et al. 2012). Increased $\alpha 3$ expression was noted on human lung cancer cells selected *in vivo* for enhanced brain metastases but not bone metastasis (Yoshimasu, Sakurai et al. 2004). Met protein activation and expression in patients with NSCLC was also found to be associated with increased frequency of brain metastasis (Benedettini, Sholl et al. 2010).

A reduction or lack of gene expression also plays a role in site-specific metastasis. Reduced expression of the metastasis suppressor genes *kiss1*, *kai1*, *brms1* and *mkk4* were associated with brain preference of breast cancer cells (Stark, Tongers et al. 2005) whilst decreased *nm23* expression was associated with melanoma brain metastases (Sarris, Scolyer et al. 2004). Down-regulated expression of the neuronal survival factor and tumour suppressor, pigment epithelium-derived factor (PEDF), in breast cancer cells

correlated with increased propensity of these cancer cells to proliferate *in vitro* and contributed to increased outgrowth in the brain (Cai, Parr et al. 2006; Fernandez-Garcia, Volpert et al. 2007; Hoshina, Abe et al. 2010; Fitzgerald, Subramanian et al. 2012). Increased incidence of brain metastases in NSCLC patients has been correlated with low expression of E-cadherin by the primary tumour (Yoo, Yang et al. 2012).

1.2.2.1.1.b Paracrine signalling

Paracrine signalling may play a role in organ-specific metastasis. Studies have shown that only tumour cells that express specific chemokine receptors are able to metastasise to organs that carry the cognate ligand (Muller, Homey et al. 2001; Andre, Xia et al. 2009). For example the ligand CXCL12 is expressed in the brain (Zlotnik 2004) and its receptor CXCR4 on breast cancer cells (Muller, Homey et al. 2001) and *in vitro* treatment of CXCR4-expressing MDA-MB-231 breast cancer cells with CXCL12 enabled trans-endothelial migration through human brain microvascular endothelial cells (Lee, Lee et al. 2004). However, migration studies using the bone and brain-seeking variants of MDA-MB-231 (MDA MB 231-Bo and Br) have shown that although the bone-seeking variant responded to CXCL12, the brain-seeking variant did not (Schmid, Reznicek et al. 2007). Instead, MDA-MB-231-Br cells expressed the Robo receptor and migrated in response to Slit2, a member of a family of secreted proteins which play important roles in neuronal development (Holmes, Negus et al. 1998; Wu, Wong et al. 1999; Schmid, Reznicek et al. 2007). Melanoma cells that express the p75^{NTR} cell-surface receptor have been reported to home towards the ligand, nerve growth factor (NGF) produced by astrocytes in the brain (Denkins, Reiland et al. 2004). Using matrigel invasion assays, NGF has also been

shown to enhance the invasiveness of lung cancer cells expressing a disintegrin and metalloprotease domain 9 (ADAM9) protein. ADAM9 expression also increased adhesion to brain slices, upregulated expression of integrin $\alpha 3$ and $\beta 1$, and produced brain metastases *in vivo* (Shintani, Higashiyama et al. 2004). A chemotactic role for neurotransmitters has been reported to guide breast cancer migration to the brain (Drell, Joseph et al. 2003).

1.2.2.1.1.c Cancer stem cells

The metastatic cells within the primary tumour not only contains a mixed population of cells with varying predilection for specific organs, they also harbour stem cells (Li, Tiede et al. 2007). Studies have shown that it is the stem cell population that has the capability to metastasise (Al-Hajj, Wicha et al. 2003; Dontu, Al-Hajj et al. 2003; Charafe-Jauffret, Ginestier et al. 2010). Notch signalling is involved in maintenance of stem cells (Bolos, Blanco et al. 2009) and Notch1 expression was found to correlate with increased brain metastases (Nam, Jeon et al. 2008; McGowan, Simeone et al. 2011). Spontaneous brain metastases have been shown to arise from H-RAS human mammalian epithelial cell tumours that over-express the stem cell maintenance factor B-lymphoma Moloney murine leukaemia virus insertion region-1 (BMI1) (Hoenerhoff, Chu et al. 2009).

1.2.2.1.1.d miRNAS

Micro RNAs (miRNA), small non-coding RNA molecules, are deregulated in many cancers (Osman 2012; Yang, Hao et al. 2012). Their involvement in brain metastasis from breast cancers (Tavazoie, Alarcon et al. 2008; Zhang, Sullivan et al. 2011), colon cancers (Li, Gu et al. 2012), and lung cancers (Arora, Ranade et al. 2011; Chen, Xu et al. 2012) have been

identified. miRNA-328 is over-expressed in both NSCLC lung tumours and paired brain metastases and therefore this miRNA may contribute to the brain-seeking property of a few lung cancer cells within the primary tumour (Arora, Ranade et al. 2011). miRNAs may also provide early prognostic marker of brain metastases (Teplyuk, Mollenhauer et al. 2012)

1.2.2.2 SURVIVAL

Arrival and arrest of circulating tumour cells to the secondary site does not guarantee access and most cells will not develop into metastases. *Fidler et al* showed that less than 0.01% of melanoma cells injected intravenously (i.v) into mice remained in the lung 24 h after injection and even fewer cells formed metastases (Fidler 1970). Disseminated tumour cells that arrest within the brain vasculature face the BBB, which forms an extra obstacle for tumour cells; Ultrastructural and histochemical studies of tumour cell extravasation at various sites have illustrated that it takes significantly longer for tumour cells to penetrate the BBB and extravasate than any other organ (Kawaguchi and Nakamura 1986; Paku, Dome et al. 2000; Loriger and Felding-Habermann 2010). In an experimental metastasis mouse model, 24 h after LLC tumour cells were injected, most tumour cells arrested in the vasculature of the liver, lung and adrenals had extravasated but 100% of LLC cells identified in the brain were still located within the microvasculature. Even at 72 h, majority of the tumour cells remained in the brain microvasculature. Although some were in an extracapillary position, none were in the process of extravasation (Paku, Dome et al. 2000). Similar results were reported in an experimental breast cancer brain metastasis model; the majority of the cancer cells remained

intravascular at day 3 after intracarotid injection and were only found within the brain at day 5 (Lorger and Felding-Habermann 2010). These and other studies suggest that survival within the brain vasculature is a key limiting step in the development of brain metastases (Kienast, von Baumgarten et al. 2010). Survival was limited due to the extended period of time brain metastatic cells remained in the vasculature, where they were continuously exposed to the pressures of blood flow and immune surveillance by circulating natural killer cells, leaving very few cells alive to extravasate.

1.2.2.3 EXTRAVASATION

The process by which tumour cells traverse the brain endothelium to enter the parenchyma has been studied using electron microscopy and ultrastructural analysis. Tumour cell arrest at the brain endothelium was shown to cause minor retraction of the endothelium, thereby facilitating extravasation (Kawaguchi and Nakamura 1986). Tumour cells themselves were also seen forming pores in the basement membrane to enable them to squeeze their way through (Kawaguchi and Nakamura 1986). Similar to leukocyte extravasation, tumour cells that transmigrate through the endothelium have been shown to be restricted to the perivascular space and require additional mechanisms to traverse the glial limitans, including the expression of MMPs (Saito, Hatori et al. 2007; Saito, Hatori et al. 2008). An alternative approach to active extravasation into the brain is the use of mechanical force, where tumour cells proliferate within the vessel lumen and burst their way through. Evidence for this mechanism is lacking as breakdown of the blood brain barrier (BBB) is infrequently seen with small micrometastases (Kawaguchi and Nakamura 1986; Fidler, Schackert et al. 1999).

1.2.2.3.1 Proteases and tumour cell extravasation

Several degradation proteases, including MMPs, plasmin, urokinase plasminogen activator (uPA), cathepsins and heparanase, secreted by primary tumour cells and stroma, help break through the extra cellular matrix (ECM) to invade local tissue and escape into the circulation (intravasation) (reviewed in (Mason and Joyce 2011). Some of these proteases are also involved in tumour cell extravasation into the secondary site.

Tumour expression of MMPs correlate with invasiveness and metastasis (reviewed in (Stamenkovic 2000). Increased MMP 2, 3, and 9 expression was detected in a rat breast cancer cell line that metastasises to the brain and inhibition of these MMPs decreased the invasive nature of this cell line and produced fewer brain metastases (Mendes, Kim et al. 2005). In a histological study, Jaalinoja *et al* showed that there was varying expression of MMP-2 in different primary human brain tumours but 100% of brain metastases expressed MMP-2 (Jaalinoja, Herva et al. 2000). Increased MMP-2 expression was also noted in brain metastatic melanoma cells compared to non-metastatic cutaneous melanoma cells (Izraely, Sagi-Assif et al. 2012). A pair-wise comparison of systemic primary tumours and their brain metastases showed that MMP-9 expression was up-regulated in all primary brain tumours and brain metastases with low or no expression of the MMP-9 inhibitor – tissue inhibitor of metalloprotease 1(TIMP-1) (Arnold, Young et al. 1999). Brain metastases from fibrosarcomas were reduced in mice over-expressing TIMP-1 compared to wild-type mice (Kruger, Sanchez-Sweatman et al. 1998). Lung cancer cells transfected with ADAM9 formed brain metastases in part by using the metalloprotease portion of ADAM9 to degrade the brain extra-cellular matrix (ECM) (Shintani,

Higashiyama et al. 2004). The passage of brain metastatic cells into the parenchyma from the perivascular space may also depend on local expression of MMP-2 and MMP-9 (Saito, Hatori et al. 2007).

Other proteases have also been shown to promote tumour cell extravasation into the brain. Heparanase, an enzyme that degrades ECM heparan sulphate molecules, has been shown to facilitate the invasion of melanoma cells into the brain (Nicolson, Nakajima et al. 1994; Reiland, Sanderson et al. 2004; Roy, Reiland et al. 2005). miRNA-1258, which inhibits heparanase production, is down-regulated in human brain metastatic breast cancers (Zhang, Sullivan et al. 2011). Inhibition of miRNA-1258 increased invasion of breast cancer cells *in vitro* and increased the number of brain metastases *in vivo* (Zhang, Sullivan et al. 2011). Urokinase-type plasminogen activator (uPA) converts plasminogen to plasmin, a trypsin-like enzyme which degrades the ECM and uPA has been reported to promote tumour dissemination (Carriero, Franco et al. 2011). Experimental melanoma brain metastases were reduced in plasminogen knock-out mice and in mice injected with inhibitors to plasminogen because of the reduced ability of melanoma cells to extravasate (Perides, Zhuge et al. 2006). Mellanotransferrin (Mtf), expressed on human melanoma cells, enabled extravasation into the brain in part by producing plasmin (Bertrand, Demeule et al. 2007; Rolland, Demeule et al. 2009). *In vitro* studies using the irreversible serine protease inhibitor, Pefobloc[®], reduced the rate of migration of human and mouse melanoma cells through brain microvascular endothelial cells (Fazakas, Wilhelm et al. 2011) and may prove to be a useful therapeutic tool in the clinic.

1.2.2.3.2 BBB permeability and tumour cell extravasation

In addition to proteases that breakdown the BBB, tumour cells also produce factors that increase BBB permeability. The 17-gene signature expressed by breast cancer cells that specifically form brain metastases identified by *Bos et al* includes COX-2, heparin binding epidermal growth factor (HBEGF), and ST6GALNAC5 (Bos, Zhang et al. 2009). Inhibition of any three proteins within the signature inhibited tumour cell migration through an *in vitro* model of the BBB (Bos, Zhang et al. 2009). COX has been shown to increase *in vitro* BBB permeability during inflammation (de Vries, Blom-Roosemalen et al. 1996) while HBEGF expression increased tumour cell motility and invasiveness (Miyamoto, Yagi et al. 2006).

Vascular endothelial growth factor (VEGF) stimulates vasculogenesis and angiogenesis and has been reported to increase permeability of cultured brain microvascular endothelial cells, exposing the underlying basement membrane to tumour cells and thereby facilitating extravasation (Lee, Avraham et al. 2003; Fan, Cai et al. 2011). Placental growth factor, secreted by SCLC cells, can bind to and activate VEGFR-1 on brain endothelial cells and VEGFR-1 activation can initiate Rho kinase (ROCK) and ERK signalling-mediated tight junction disassembly and increased endothelial permeability (Li, Wang et al. 2012). Inhibition of ROCK in *in vitro* assays was shown to prevent SCLC cells from transmigration (Li, Zhao et al. 2006).

1.2.2.4 COLONISATION

Organ-specific arrest followed by survival and extravasation is necessary, but not sufficient, for the development of brain metastases. Extravasated tumour cells face several fates within the brain microenvironment. Tumour cells may find the new

microenvironment unfavourable and undergo apoptosis, anoikis or lay dormant. Maintaining close contact to the abluminal side of blood vessels has been shown to be necessary for tumour survival and proliferation (Carbonell, Ansorge et al. 2009; Kienast, von Baumgarten et al. 2010). Extravasated cells that could not adhere to the vascular basement membrane either died or the few that proliferated eventually regressed (Kienast, von Baumgarten et al. 2010).

1.2.2.4.1 Decision point: dormancy vs. angiogenesis

Brain metastases typically present at the end stage of breast cancer indicating that either disseminated tumour cells do not survive well within the brain microenvironment or enter a state of prolonged dormancy. Iron oxide particles used to follow the fate of breast cancer cells in brain metastases showed that 4.5% of extravasated tumour cells lay dormant in the brain (Heyn, Ronald et al. 2006). *In vivo* transcranial imaging of human lung and melanoma cells also illustrated that a small percentage of extravasated brain metastatic tumour cells remained in a dormant state over the course of the study (Kienast, von Baumgarten et al. 2010).

Outgrowth of micrometastases to macrometastases requires angiogenesis. Melanoma cells expressing endostatin, an inhibitor of angiogenesis, formed small microscopic brain metastases compared to normal melanoma cells (Kirsch, Weigel et al. 2005). VEGF-A inhibition prevented VEGF-A producing lung cancer micrometastases from outgrowth and these cancer cells became dependent on co-option of existing vasculature and remained in a dormant state (Kienast, von Baumgarten et al. 2010). Knocking-out VEGF in human lung cancer cells partially decreased the growth of brain metastases compared to cells

expressing VEGF (Yano, Shinohara et al. 2000). MDA-MB-231 breast cancer cells engineered to constitutively express activated $\alpha\beta3$ had a significant growth advantage in the brain over $\alpha\beta3$ -null cell lines (Lorger, Krueger et al. 2009). Growth of brain metastases was dependent on VEGF; the difference in tumour growth in the brain was only evident after tumours reached a critical size when VEGF expression was required for angiogenesis. This growth enhancement was not seen when $\alpha\beta3$ -expressing tumour cells grew in the mammary fat pad implying that $\alpha\beta3$ regulates VEGF in a brain-specific manner (Lorger, Krueger et al. 2009). Systemic expression of VEGF causes BBB permeability but interestingly, one study reported that VEGF expression from within the brain reduced BBB leakage and was neuroprotective (Kaya, Gursoy-Ozdemir et al. 2005). Anti-VEGF therapeutics administered intracerebrally, rather than systemically, may prove to be more beneficial in shrinking brain metastases whilst also increasing BBB permeability around tumours to allow penetration of chemotherapeutic agents.

Breast cancers over-expressing Her-2 often metastasise to the brain but this is usually associated with the inability of the Her-2 antagonist, trastuzumab, to penetrate the BBB. However, some studies have shown that although Her-2 transfected breast cancer cells produced comparable number of brain metastases as un-transfected control cells, they were substantially larger (Palmieri, Bronder et al. 2007; Perera, Ribot et al. 2012). Anti-angiogenic therapies may be beneficial when treating Her-2⁺ breast cancer patients with brain metastases.

1.2.2.4.2 Astrocyte response to brain metastases

Upon entering the brain, tumours first come into contact with astrocytes and therefore it is not surprising that local activation of astrocytes has been found to be uniformly present around extravasated tumour cells (Lorger and Felding-Habermann 2010; Seike, Fujita et al. 2011). Astrocyte activation is most commonly defined by increased expression of the astrocyte-specific intermediate filament, glial fibrillary acidic protein (GFAP) and in a mouse xenograft model of human lung cancer brain metastasis, a strong correlation was found between tumour size and GFAP activity (Seike, Fujita et al. 2011).

Astrocytes may form part of the 'soil' that preferentially fosters growth of breast cancers in the brain. Sierra and colleagues report that brain-seeking breast cancer cells had enhanced proliferation and adhesion to stimulated astrocytes when compared to the parental or the lung-seeking metastatic variant (Sierra, Price et al. 1997). In a species cross-hybridization study, epigenetic changes in MDA-231 cells implanted in mouse brains correlated with the expression profile of the same cell lines co-cultured with murine astrocytes but not fibroblasts, indicating that brain astrocytes are crucial drivers of epigenetic changes in breast cancer brain metastases (Park, Kim et al. 2011).

It has been shown *in vitro* that activated astrocytes promote tumour cell survival and proliferation. Cultured astrocytes secreted soluble factors that increased proliferation of a variety of tumour cells lines in a time- and dose-dependent manner (Noda, Seike et al. 2009). mRNA and cytokine profiling of conditioned media from murine astrocytes either in co-culture or insert culture with human lung cancer cells, showed that IL-8 and MIF secreted by lung cancer cells induced cultured astrocytes to express TNF, IL-1 β , and IL-6

(Seike, Fujita et al. 2011). Expression of these cytokines by astrocytes cultured alone was minimal. The receptors for these cytokines produced by astrocytes were evident on the lung cancer cells when in co-culture but only the IL-6 receptor had sustained expression. Soluble IL-6 produced by astrocytes also induced proliferation of human breast cancer cells and protected them from apoptosis (Sierra, Price et al. 1997). The receptor for IL-6 was found to be significantly up-regulated in a subline of murine breast cancer cells that often metastasise to the brain, when compared to the non-brain metastatic counterpart (Nishizuka, Ishikawa et al. 2002). Astrocytes may also contribute to the failure of chemotherapeutic agents in the brain as physical contact between astrocytes and tumour cells was shown to protect tumour cells from chemotherapy-induced apoptosis (Lin, Balasubramanian et al. 2010) by up-regulating survival genes (Kim, Kim et al. 2011)

Astrocytes have also been shown to promote invasion of brain metastatic cells. Astrocyte-produced heparanase works synergistically with melanoma-produced heparanase to increase melanoma brain invasion (Marchetti, Li et al. 2000). MMP-2 production by astrocytes increased ENU1564 rat mammary carcinoma invasion *in vitro* and invasion was inhibited by the MMP-2 inhibitor TIMP-2 (Mendes, Kim et al. 2007). Astrocyte signalling also induced MMP expression in brain metastatic breast cancer cells (Mendes, Kim et al. 2007; Loriger and Felding-Habermann 2010) while transforming growth factor- β (TGF- β) produced by tumour cells (Menter, Herrmann et al. 1995; Zhang, Zhang et al. 2009) can induce MMP-9 expression in astrocytes (Hsieh, Wang et al. 2010), indicating a tumour-astrocyte feedback loop may exist to increase tumour invasiveness.

In contrast to the brain metastases-promoting properties of astrocytes, in the absence of tumour influence, they can be manipulated to kill cancer cells. *In vitro*, LPS and IFN- γ stimulated astrocytes produced nitric oxide (NO) to kill primary glioma cells and a variety of brain metastatic cancer cells. Intracerebral injection of LPS and IFN- γ increased survival of mice subsequently challenged with B16 melanoma (Samdani, Kuchner et al. 2004).

1.2.2.4.3 Microglia/macrophage response to brain metastases

A number of studies have reported varying degrees of microglial activation in response to brain metastases. Blood-borne monocytes have been shown to infiltrate brain metastases (Schackert, Simmons et al. 1988; Brantley, Guo et al. 2010), but as they are indistinguishable from activated microglia cells, the role of blood-borne cells versus resident brain microglia in brain metastasis is unknown. In mouse models of human and mouse breast cancer brain metastases, heterogeneous microglia/macrophage activation around extravasated mouse and human breast cancer cells have been reported (Lorger and Felding-Habermann 2010). This heterogeneity of microglia activation was also noted in tissue from human brain metastases (Berghoff, Lassmann et al. 2012). However, one other study reported consistent activation of microglia in histological samples of human brain metastases forming a defined microglial wall around the tumours (Shinonaga, Chang et al. 1988; Zhang and Olsson 1995; Fitzgerald, Palmieri et al. 2008). Fitzgerald *et al* showed that brain metastases produced in mice by the human breast cancer brain-seeking tumour cells, MDA MB 231-Br, were highly proliferative and induced a uniform inflammatory response in the brain with activated microglia/macrophage and astrocytes

forming a wall around the metastases (Fitzgerald, Palmieri et al. 2008). Microglia co-cultured with MDA MB 231-Br cells secreted factors that increased proliferation of tumour cells (Fitzgerald, Palmieri et al. 2008). Microglia have also been shown to promote invasion; Co-culture of murine microglia with weakly metastatic human breast cancer cells significantly enhanced migration of tumour cells through a Boyden chamber. Tumour cell invasion was inhibited by the Wnt signalling inhibitor DKK-1 (Pukrop, Dehghani et al. 2010). Normal brain slices co-cultured with tumour cells induced accumulation of microglia at the brain slice-tumour border. These microglia then migrated into the tumour cells to actively promote tumour invasion into the brain slice (Pukrop, Dehghani et al. 2010).

Histological studies using a xenograft model of Hara-B human lung cancer cells also report uniform up-regulation of microglia around and in the brain metastases and a positive correlation was found between tumour size and microgliosis (Noda, Seike et al. 2009). However, in contrast to breast cancer cells, when Hara-B cells were co-cultured with microglia or microglia conditioned media, proliferation of the tumour cells was significantly reduced in a dose-dependent manner. This reduction in proliferation was not due to increased apoptosis but the authors speculate that microglia secrete factors that may induce cell-cycle arrest in tumour cells (Noda, Seike et al. 2009). Other studies have shown that microglial cells need to be manipulated in order to be tumouricidal. Conditioned media from immortalized microglia cells activated with lipopolysaccharide (LPS) killed tumour cells in a dose- and time-dependent manner (He, Wang et al. 2006; Brantley, Guo et al. 2010). However, dilute conditioned media enhanced tumour survival

and growth (He, Wang et al. 2006). Fidler's group recently showed that LPS and IFN- γ treated mouse microglial cells in culture produced NO to induce apoptosis of melanoma cells (Brantley, Guo et al. 2010). Interestingly, no toxic effects were seen when normal cells were co-cultured with LPS and IFN- γ activated microglia. These findings suggest that microglia may be potent tumour killers if given the correct cues, and this could be a potential avenue for targeted therapy.

1.3 RESEARCH MOTIVATION AND OVERVIEW OF FINDINGS

The improvement of cancer therapies has led to an increase in patient survival. However, we now face a new problem – increased incidence of brain metastases. Therapeutic intervention focusing on eliminating established brain metastases has had limited success especially when multiple brain metastases are present (Gavrilovic and Posner 2005). Chemotherapies fail due to the impenetrability of the BBB and currently, radiotherapy is used as a palliative modality. To battle the increasing incidence of brain metastases we need to identify those tumour cells that will seed the brain and determine how they penetrate the BBB. This will enable development of screening modalities and therapies that may prevent cancer cells from seeding the brain.

Research into brain metastasis is limited in part due to the lack of animal models. In Chapter 3, we focus on developing a mouse model of brain metastasis that will enable quantitative characterisation of disseminated cancer cell arrest, survival and extravasation into the brain. Using this model, we show in Chapter 4 that not all metastatic cells will form brain metastases when introduced into the arterial circulation. Poorly brain metastatic cells lack the ability to adhere to the brain endothelium,

suggesting that disseminated cells need brain specific adhesion molecules in order to form brain metastases. Identifying these adhesion molecules will enable development of targeted therapies against brain metastatic cells.

In accordance with published data, we also show that tumour cells that adhere to the brain endothelium remain in the vasculature for days and are continually eliminated. Only a small number of metastatic cells survive to form brain metastases. We show in Chapter 4 that the few tumour cells that persist within the vasculature and ones that seem to be in the process of extravasation are often found associated with circulating immune cells. Furthermore, far more intravascular tumour-immune cell clusters are found when brain metastatic cells are injected into mice bearing primary tumours. Primary tumour bearing mice also develop more brain metastases than non-tumour bearing mice after tumour cell injection. Leukocytes that extravasate past the brain endothelium are limited to the perivascular space unless they navigate past the glial limitans (Owens, Bechmann et al. 2008). This process is sometimes mediated by accessory immune cells (Tran, Hoekstra et al. 1998; Zhou, Stohlman et al. 2003; Savarin, Stohlman et al. 2010). In Chapter 5, we look at the role of tumour associated immune cells to determine whether they support tumour cell survival within the vasculature and/or extravasation and in Chapter 6, we develop an imaging technique to study tumour-immune cell interactions in real-time. Our findings suggest that targeting brain metastasis-associated immune cells directly or indirectly by inhibiting the factors that recruit them to arrested tumour cells may be a valuable therapeutic tool to prevent brain metastasis.

CHAPTER 2: MATERIALS AND METHODS

2.1 CELL CULTURE

2.1.1 CELL LINES

Source of all cell lines used and whether GFP-transfected cell lines were pooled or single clones are listed in Table 2.1. 4T1, B16F1, B16F10 and LLC cells expressing GFP were transfected previously with pEGFP-C1 vector (Clontech, USA) by members of the Muschel Lab. Single clones were picked and expanded. 4T07 was also transfected with the pEGFP-C1 vector and stable clones expressing GFP were isolated using G418 selection. Using flow cytometry, the brightest fluorescent cells (top 5%) from each clone were expanded and frozen. 4T07-GFP clone-1 was used for all experiments.

Table 2.1: Cell lines tested for their ability to form brain metastases *in vivo*

Cell Line(type)	Source	Fluorophore selection
4T1 (mammary carcinoma)	American type culture collection– GFP transfected in house 4T1-luc (Caliper Life Sciences- single clone)	GFP – 400 µg/ml G418
4T07 (mammary carcinoma)	ATCC – GFP transfected in house (single clone)	GFP – 400 µg/ml G418
B16F1, B16F10 (melanoma)	ATCC - GFP transfected in house (single clone)	GFP – 2 mg/ml G418
LLC (lung carcinoma)	ATCC – GFP transfected in house (single clone)	GFP – 800 µg/ml G418
MC38 (colon carcinoma)	Generous gift from Carlos Arteaga (Vanderbilt Univ., USA – single clone)	GFP – 5 µg/ml puromycin
Met-1 (mammary carcinoma)	Generous gift from Jeffrey W. Pollard (Albert Einstein College of Medicine, New York, USA)	n/a
MDA-MB-231 (human pleural breast metastases)	Generous gift from Richard Treisman (CRUK London Research Institute - pooled) (Medjkane, Perez-Sanchez et al. 2009)	GFP - 200 µg/ml puromycin

2.1.2 CELL MAINTENANCE

All cell lines were maintained in Dulbecco's Modified Eagle Medium (DMEM) (GIBCO® Invitrogen, Paisley,UK) supplemented with 10% fetal bovine serum (FBS)(GIBCO®) and 1% L-glutamine (GIBCO®). Frozen cells stocks were thawed in a 37°C water bath, diluted with 10 ml of warm complete DMEM, and then centrifuged at 1200 rpm for 5 minutes. The cell pellet was re-suspended in 10 ml of complete media and transferred to a T25 culture flask (Sartedt, Leicester, UK). Appropriate antibiotics were added to maintain GFP expression (Table 2.1). Cells were incubated in a HERA 150i (Thermo Scientific, Asheville, USA) incubator at 37°C with 20% oxygen and 5% carbon dioxide. When cells reached between 80-90% confluence, they were rinsed with 1x phosphate buffered saline (PBS), and were lifted using 1-5 ml of 0.05% Trypsin-EDTA (GIBCO®) for 5 min at 37°C. Cells were checked to ensure they were all in suspension before inactivating the trypsin with 10 x the volume of complete DMEM. Cells to be maintained in subculture were re-plated at a dilution of 1:10 to 1:40 in either a T75 or T175 flask using complete DMEM. All cells were routinely checked for mycoplasma using a Cambrex MycoALert® Mycoplasma Detection Assay kit (Cambrex BioScience, Nottingham, UK).

2.1.3 CELL LINE STORAGE

Lifted, washed and pelleted cells were re-suspended in media consisting of 10% DMSO (Dimethyl sulfoxide – Sigma) and 20% FBS and 1.5 ml aliquots were transferred to cryovials (Greiner Bio-One, Frickenhausen, Germany). Cryovials were stored in an isopropanol filled Nalgene® Mr. Frosty (Thermo Scientific) holder at -80°C for 24 h before transferring to long term storage in a cryo-storage system (Taylor-Wharton, Husum, Germany) .

2.1.4 CELL PREPARATION FOR ANIMAL INJECTIONS

Cells were washed free of antibiotics 24 h prior to harvest for animal injections. Lifted, washed and pelleted cells were re-suspended in PBS and counted using a Nucleocounter (Chemometec, Lillerod, Denmark). Dead cell count was measured by directly sampling the prepared cell suspension using a nucleocassette (Chemometec). The total cell count was obtained by lysing 100 µl of the cell sample in equal volumes of lysing solution A and B (Chemometec) and taking readings with the nucleocassette. The live cell count was calculated by subtracting the dead cell count from the total cell count. Cells were then diluted in PBS to the required final concentration of live cells and stored on ice for injections.

2.2 IN VIVO EXPERIMENTS

2.2.1 ANIMALS

Female Balb/c, Balb/c Severe Combined Immuno-deficient (SCID), C57 Bl/6 mice (Charles River, Margate, UK) or FVB/N mice were used when they were 8-10 wks old. Mice were housed in ventilated cages and fed mouse diet food and water *ad lib*. All animal experiments were performed under UK Home Office licensing and ethics committee approval from the University of Oxford. The expected and actual major adverse effects for all *in vivo* procedures are summarised in Supplementary Table 1.

2.2.2 ULTRASOUND-MEDIATED INTRACARDIAC INJECTIONS

Mice were anaesthetised and placed supine slightly tilted towards the right side with all four limbs secured on a heated stand. The fur covering the thorax was removed by shaving and by use of hair removal cream as any residual fur would interfere with the ultrasound image quality. A thick layer of ultrasound gel was placed on the bare thorax above the heart and a

stand mounted 707B ultrasound probe (Visualsonics, Toronto, Canada) was used to find the left ventricle of the heart (Figure 2.1a). Tumour cells were re-suspended using a 23G needle and 100 μ l of the cell suspension was loaded into a 1 ml syringe. The syringe was fitted with a $\frac{3}{4}$ -inch long 27G needle, secured onto a needle holder and its position adjusted to be underneath the ultrasound probe until visualised in the ultrasound image. When the needle tract trajectory was deemed suitable, the needle was advanced through intercostal space into the left ventricle (Figure 2.1b). Cells were only injected after visual confirmation of the needle within the left ventricle of the heart and pulse of bright red blood was seen to flash back into the syringe. 10^5 tumour cells in 100 μ l were injected slowly in 20 μ l increments over 30 s.

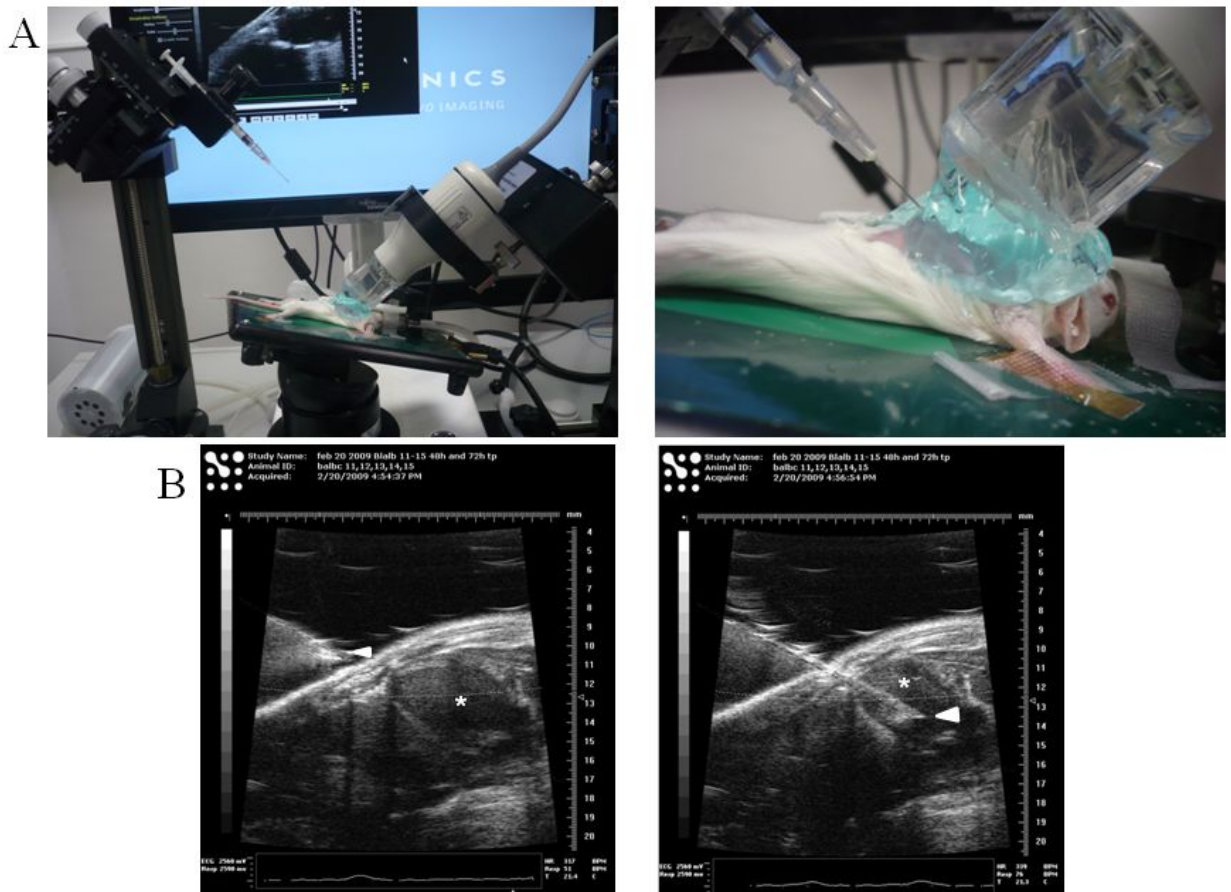


Figure 2.1: Ultrasound mediated intracardiac injections.

Balb/c mice were injected with 10^5 4T1-luc cells into the left ventricle of the heart using ultrasound guidance. A: The mouse was secured on an adjustable, heated platform and aligned beneath the 707b ultrasound probe until the left ventricle was visible on the monitor. The needle, aligned using fine adjustment knobs, was inserted into the intercostal space. B - The left ventricle is in view (*). Arrow shows the tip of the needle. Cells were injected into the heart upon visual confirmation of the needle placement into the left ventricle.

2.2.3 INTRACAROTID ARTERIAL INJECTIONS

Mice were maintained under inhalation anaesthesia, restrained on a cork board on their backs and all limbs secured. The fur over the throat was removed and under a dissection microscope, a midline incision was made over the trachea to expose the common carotid artery below the bifurcation into the internal and external arteries. The common carotid was tied off 3-4 mm below the bifurcation and a small incision was made above where the

artery was tied off. A long 30G catheter fitted with a 1 ml syringe filled with saline was inserted into the incision into the internal carotid artery and a small amount of saline was injected. The saline was then replaced with 100 μ l of a cell suspension which had been thoroughly re-suspended. Cells were injected slowly and then flushed with saline. The catheter was removed and the point above the incision was then tied off. The skin over the exposed arteries was sutured back together and mice were monitored until recovery from anaesthesia.

2.2.6 FAT PAD/ SUBCUTANEOUS PRIMARY TUMOUR INJECTIONS

For primary tumour assays, 5000 4T1 or 4T1 expressing luciferase (4T1-luc) cells were injected into the 4th mammary fat pad or 2×10^6 MDA MB 231 or LLC cells were injected subcutaneously on the right flank. Tumours were measured at least once a week using callipers.

2.3 BRAIN PROCESSING

At various times points after tumour cell injections, mice were placed under terminal anaesthesia using pentobarbitone and were transcardially perfused with 10-15 ml ice cold PBS followed by 15-20ml 4% paraformaldehyde (PFA) using a perfusion process pump (Watson-Marlow, Cornwall, UK) set to 20.31 ml/min. Organs were excised and placed in 30% sucrose for at least 48 h. Brains were sectioned using an OTF 5000 cryostat (Bright Instruments, Cambridgeshire, UK). Brains from mice subject to intracardiac injections were sectioned along the axial plane at 15 μ m. Brains from mice injected with tumour cells directly into the brain were sectioned along the coronal plane at 10-12 μ m.

2.4 IMMUNOFLUORESCENCE

Frozen slides were thawed at room temperature or at 37°C for 5-10 min, sections outlined with PAP pen and then rehydrated in three washes of 1x PBS for 5 min. Endogenous biotin was blocked using a Streptavidin/Biotin blocking kit (Vector labs) for 15 min with a 5 min PBS wash in between. Non-specific protein interaction was blocked using the TNB blocking solution provided with the TSA amplification kit (Perkin Elmer). The blocking solution was placed directly on the sections for 30 min after which the primary antibody (diluted in the blocking solution) was added. The primary antibodies and methods of detection used are listed in Table 2. After primary antibody incubation either for 2 h at room temperature or overnight at 4°C, the slides were rinsed 3 times in PBS for 5 min. Primary antibodies were amplified using a secondary antibody directly conjugated with a fluorophore or biotin. Biotinylated secondary was either detected using a streptavidin conjugated to a fluorophore or further amplification was carried out using the TSA kit. Antibody requiring TSA amplification had to be quenched of endogenous hydrogen peroxidase by immersing the slides in a 3% solution of hydrogen peroxide (Sigma) in PBS for 15-20 min. Horseradish peroxidase (HRP) conjugated streptavidin (1:200 or pre-diluted, Vector Labs) was added for 30 min followed either by TSA-Bio or TSA-fluorescent amplification reagent for 2-7 min depending on the antibody. If TSA-Bio was used, a further step was performed where a fluorophore conjugated to streptavidin was added to the sections for 30 min before rinsing in PBS. All reagents except the TSA reagent were diluted with the TNB blocking reagent (0.1 M TRIS-HCl, pH 7.5, 0.15 M NaCl, 0.5% blocking reagent). Hoechst was added to the final rinse step (1:100,000) to counterstain cell nuclei.

Table 2.2: Antibodies/lectins used to label brain tissues.

Antigen/Glycan	Host/Isotype/ Lectin	Clone	Company	Cat #	Dilution/ Detection
GFP (and CFP)	Chicken - IgY		Abcam	ab13970	1:500 overnight
CD34	rat - IgG2a	MEC 14.7	Abcam	ab8158	1:50 TSA
CD45	Rat – IgG2b, κ	30F11	BD	553081	1:100 TSA
F4/80	Rat – IgG2a	BM8	Abcam	Ab16911	1:100 TSA
CD11b	Rat – IgG2b	M1/70.15	Abd Serotec	mca74G	1:100 TSA
IBA1	Rabbit – poly		Wako	016- 20001	1:250 indirect with fluorophore
INTEGRIN α II β	Rat - IgG		Serotec	Sc-19963	1:50 TSA
Brain vasculature and microglia glycan	Ricinus communis agglutinin (RCA-1) biotin		Vector labs	AS-2084	1:100 - 1:250 indirect with streptavidin fluorophore
Brain vasculature glycan ST6GALNAC5	Sambucus nigra agglutinin (SNA) biotin		Vector labs	B-1305	1:200 indirect with streptavidin fluorophore
CD3	rabbit - IgG		abcam	ab5690	1:50- 1:100 indirect with biotin
Ly6G	Rat – IgG2a	IA8	BD	551459	1:100 indirect with biotin
Gr-1	Rat – IgG2b	RB6-8C5	eBioscience	14-5931- 85	1:100 indirect with biotin
Ly6C	rat - IgG2a	ER- MP20	abcam	ab54223	1:100 TSA
Neutrophil	Rat - IgG2b	NIMP R14	Abcam	ab2557	1: 50 TSA
CD11c	Hamster- IgG	N418	Abcam	Ab119342	1:100 TSA
MBS	Rabbit poly		D. Anthony		1:100 indirect fluorophore
COLLAGEN IV	rabbit - IgG		abcam	ab19808	1:250 TSA

2.5 QUANTIFICATION OF BRAIN TISSUE

Brains harvested from mice after intracardiac injections were cut along the axial plane. Each slide contained 10 different sections from the top half of the brain (up to 4th ventricle) or 8 different sections from the bottom half of the brain (4th ventricle to the pons) (Figure 2.2). There was approximately 75 μm difference between adjacent sections on each slide. One slide representing 10 brains sections from the top and one slide representing 8 brain sections from the bottom portion of the brain were counted per mouse (18 sections) and the total number of positively stained cells/metastases were summed to generate a single value per mouse (representing a single n value). Data is represented as mean score of the sum of 18 brain sections per mouse unless stated otherwise.

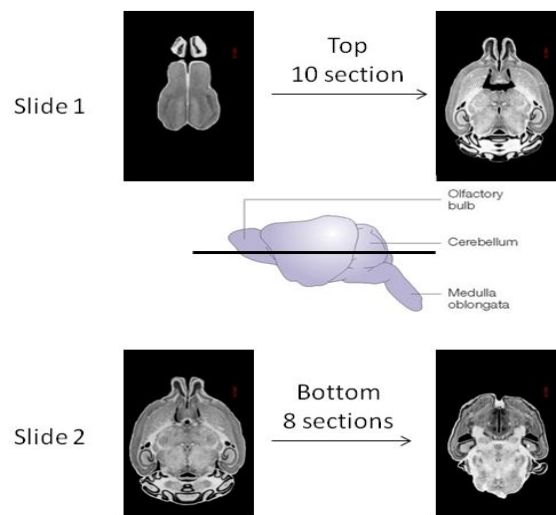


Figure 2.2: Arrangement of brain sections on slides

Brains from mice intracardiac injected with tumour cells were cut along the axial plane. A set of 15 slides was used to collect all the sections from the top of the brain until approximately the fourth ventricle and the remaining bottom half of the brain was collected over another 15 slides. One slide representing the top portion of the brain (10 sections per slide) and one slide representing the bottom half of the brain (8 sections per slide) were quantified to determine the numbers of tumours or tumour cells per mouse brain. Adapted from http://www.mbl.org/atlas232/atlas232_frame.html and (Cryan and Holmes 2005).

2.6 MICROSCOPY

Light micrographs were taken using a Nikon Eclipse E800 microscope fitted with a digital colour camera (DXM1200; Nikon). Fluorescent images were acquired using an inverted epi-fluorescence microscope (DM IRB; Leica Microsystems) fitted with a digital camera (Orca; Hamamatsu Photonics), and analyzed with Open Lab (Improvision; PerkinElmer Life and Analytical Sciences) and ImageJ Version 1.46 (<http://rsb.info.nih.gov/ij>) software. Confocal z-stack images were acquired with an inverted confocal microscope (LSM-710; Carl Zeiss Microimaging) and analysed using Zen (Carl Zeiss Microimaging) and Image J software.

2.7 STATISTICAL ANALYSIS

GraphPad Prism (GraphPad Software Inc, San Diego, USA) was used for all statistical analysis. The type of analysis used is detailed in the corresponding figures. Data are represented as mean \pm SD and was considered significant if $p < 0.05$. If a 1-way or 2-way ANOVA was deemed significant, then the Bonferroni post-hoc test was performed to compare treatment and groups and determine where the significance lies.

CHAPTER 3 – DEVELOPMENT OF AN *IN VIVO* MODEL OF BRAIN METASTASIS

3.1 INTRODUCTION

3.1.1 IN VIVO MODELS OF BRAIN METASTASIS

3.1.1.1 BRAIN METASTATIC CELL LINES

The murine cancer cells lines 4T1, LLC and B16 have been characterised previously in experimental models of brain metastasis (Schackert and Fidler 1988; Saito, Hatori et al. 2007; Tao, Fang et al. 2008; Zhang, Hatori et al. 2008; Carbonell, Ansorge et al. 2009; Serres, Soto et al. 2012). 4T1 is one of four sub-lines isolated from the 410.1 spontaneously arising mammary tumour in a BALB/cfC3H mouse (Dexter, Kowalski et al. 1978; Aslakson and Miller 1992). It is the most aggressive of the sub-lines and can spontaneously metastasise from the primary tumour to various secondary sites including the lung, liver, bone and brain (Pulaski and Ostrand-Rosenberg 1998). When injected into the carotid artery, 4T1 cells form aggressive parenchymal brain metastasis surrounded by extensive microgliosis (Fitzgerald, Palmieri et al. 2008; Longer and Felding-Habermann 2010) similar to that described in human clinical brain metastases (Zhang and Olsson 1995).

The B16 melanoma arose spontaneously on the ear of a C57Bl/6 mouse and the cell line developed from this melanoma has been shown to metastasise to the lung, liver and spleen (Wosko, Ferrara et al. 1984). The B16 melanoma cell line has undergone *in vivo* selection for specific organ tropism and several sub-clones are in use (Fidler and Nicolson 1976). The brain specific clones were selected by injecting the B16 F1 variant into mice

via intracardiac injection, harvesting brains and cultivating any rare intracranial tumours (Fidler and Nicolson 1976). The selection cycle was repeated seven times to obtain clones B16 B1-7. The parental B16 melanoma cell lines and the brain-selected sub-lines have been reported to form metastases on the dura, meninges or within blood vessels (Kawaguchi, Kawaguchi et al. 1983; Fidler, Schackert et al. 1999) while others have reported the development of parenchymal brain metastases after intracarotid injections of the lung metastatic variant, B16 F10 (Aboody, Najbauer et al. 2006; Perides, Zhuge et al. 2006).

Lewis lung carcinoma (LLC) was first identified in the lung of a C57 Bl/ 6 mouse in 1951 and was subsequently established as a cell line by culturing lung tumour nodules that arose from the subcutaneous implant of LLC in a C57 Bl/6 mouse (Sugiura and Stock 1955; Bertram and Janik 1980). It is used commonly as a lung metastasis model, but spontaneous and experimental brain metastases have been reported (Rashidi, Yang et al. 2000; Saito, Hatori et al. 2007; Zhang, Hatori et al. 2008; Saito, Hatori et al. 2009; Brantley, Guo et al. 2010).

Xenograft models of brain metastases have been established with several human cancer cells of which the human breast cancer MDA MB 231 (MDA 231 for brevity) and its brain seeking variant, MDA MB 231-BR are well characterised (Yoneda, Williams et al. 2001; Bos, Zhang et al. 2009; Lorgner and Felding-Habermann 2010). Intracardiac or intracarotid injection of MDA MB 231-BR cells have resulted in the development of parenchymal as well as leptomeningeal brain metastases (Fitzgerald, Palmieri et al. 2008).

3.1.1.2 ROUTE OF TUMOUR DELIVERY TO FORM BRAIN METASTASES

Brain colonisation is generated in experimental *in vivo* models by injecting cancer cells directly into the brain parenchyma, into the internal carotid artery, or into the left ventricle of the heart. Direct injection of tumour cells into the brain enables growth of tumour cells that would not normally be able to traverse the BBB or ones that have a low success rate of forming brain metastases (Carbonell, Ansorge et al. 2009). However, direct injection of tumour cells into the brain bypasses adhesion and extravasation at the secondary site and the injection itself may cause damage to the brain. Introduction of cancer cells into the arterial circulation via the carotid artery or the heart simulates the metastatic process once cells have left the primary site. Intracarotid injection allows precise delivery of tumour cells into the circulation with all cells first seeding the brain. However, this approach is technically demanding and carries an increased risk of developing systemic inflammation and ischemia. The development of tumours at the site of injection or head and neck has also been reported (Zhang, Hatori et al. 2008). The intracardiac route is the quickest and least technically involved method. Cardiac injection of tumour cells delivers fewer cells to the brain as only 15-20% of cardiac output reaches the brain and there is the potential for extra-cranial metastasis via the arterial circulation (Maroldi, Ambrosi et al. 2005). Even though cardiac injections are less invasive compared with intracarotid injections, without visualising the site of injection, one can never be sure if all or any tumour cells were injected correctly into the left ventricle of the heart (Conley 1982).

3.2 AIMS

Previously developed brain metastasis models are either time consuming or give variable results. In order to study and understand the steps required for disseminated tumour cells to give rise to brain metastases, **the first aim of this chapter is to optimise the intracardiac route of tumour injection to make it precise and reproducible. Once we develop a model that gives rise to consistent brain metastases, the second aim is to compare and characterise different cell lines for their ability to produce consistent brain metastases.**

3.3 MATERIALS AND METHOD

3.3.1 IN VIVO EXPERIMENTS

3.3.1.1 INTRACARDIAC TUMOUR CELL INJECTIONS (BLIND)

Mice were laid flat on their backs, with limbs secured and fur over the thorax was shaved. Determining the site of injection was followed as described (Basse, Hokland et al. 1988). Briefly, a ¾ inch 27 G needle fitted to a 1 ml syringe was placed parallel to the sternum, under the ribcage and injected angled 30° away from the sternum towards the heart. Repeated angling of the needle was necessary until a quick flashback of blood was observed in the syringe, indicating the needle was inserted into the heart. Cancer cells were then injected in 20 µl increments holding the syringe steady with the other hand. The same dose of cancer cells were always injected (10^5 cells/100 µl of PBS) unless otherwise stated.

3.3.1.2 INTRACRANIAL TUMOUR CELL INJECTIONS

Mice were anesthetized, heads shaved and secured onto a stereotaxic frame. A micro-drill was used to thin a 2-3 mm portion of the skull allowing it to be peeled back without causing damage to the underlying dura and 2000 cells in 1 μ l of PBS was injected using a glass micro-capillary (Alpha Laboratory Ltd., UK) over 5 min. The co-ordinates for the injection site were left 2 mm, forward 0.5 mm, and down 2.5 mm from bregma. After injection, the micro-capillary was removed and the skin was closed and sutured with coated 4-0 VICRYL (Ethicon, US) and mice were allowed to recover.

3.3.1.3 IN VIVO BIOLUMINESCENCE ASSAY

Mice injected with 4T1-luc (Caliper Life Sciences) were assessed for metastasis using non-invasive bioluminescent imaging at various times after tumour injection. Anaesthetised mice were placed in the *In Vivo* Imaging System (IVIS – Caliper Life Sciences, US) imaging chamber and injected intra-peritoneally (i.p) with 200 μ l of 15 mg/ml of D- luciferin (Caliper Life Sciences). Imaging commenced immediately after luciferin injection using various exposure times and binning settings adjusted according to the saturation levels of the observed signal. For imaging organs *ex vivo*, mice were injected i.p with the same dose of D-luciferin and culled 5 min after. Organs were excised and placed inside the IVIS chamber to be imaged.

3.4 RESULTS

3.4.1 ULTRASOUND GUIDED INTRACARDIAC INJECTION OF METASTATIC CANCER CELLS CONSISTENTLY PRODUCE BRAIN METASTASES

In order to develop a model of brain metastasis, we tested the reproducibility of intracardiac injections of 4T1-luc cells in forming brain metastases. Presence of brain metastases was determined by *in vivo* bioluminescent imaging of mice and histological assessment of brains. Majority of injected mice harboured intense luminescent signal in the thorax including the heart and lungs (Figure 3.1a) and post-mortem *ex-vivo* imaging of the brain and lung confirmed the *in vivo* results (Figure 3.1b). Using this technique, only 5 of 12 mice survived more than 7 days after tumour injection, of which 50% had lung metastases, 33% had tumour burden in the chest cavity and heart and only 33% developed brain metastases (summarised in Figure 3.1c).

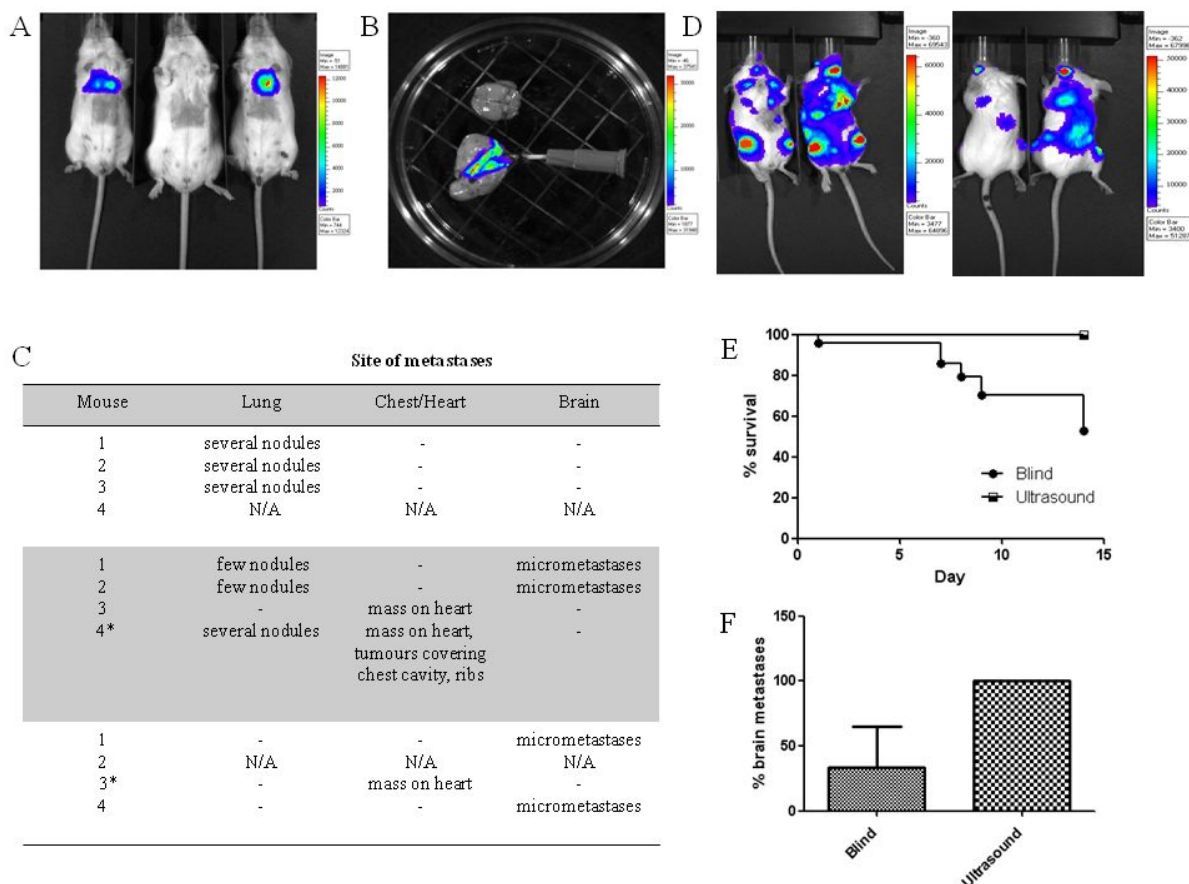


Figure 3.1: Ultrasound guided intracardiac injection allows for consistent development of brain metastases in mice.

4T1-luc cells (10^5) were injected into the left ventricle of the heart using a 27 G needle (blind). A: Surviving mice were assessed for brain metastases 10 days after injection using bioluminescent imaging as an indication of tumour growth and representative images highlight tumour growth either in the heart, chest cavity or lung. B: *Ex vivo* imaging of lungs and brain from one of the mice in (A) confirm tumour growth in the lungs but not the brain. C: Summary of autopsy findings from three different experiments using intracardiac injection (blind) of 4T1-luc cells ($n=12$). N/A indicates mice that had died immediately after intracardiac injection; * indicates mice that had undergone post-mortem examination. D: Representative images of mice injected with 10^5 4T1-luc cells into the left ventricle using ultrasound guidance. Injection of tumour cells using this technique resulted in widespread metastases as indicated by luminescent signal present in various organs, including the lungs, bones, heart, and brain. E: Kaplan-Meier curves comparing survival of mice injected with 10^5 4T1-luc cells either with ($n= 8$) or without ultrasound guidance ($n = 18$). F: Comparing brain metastases formation in 4T1-luc injected mice using the two different intracardiac methods indicates that the ultrasound method is 100% consistent. $n=13$ blind intracardiac injected; $n= 8$ ultrasound guided intracardiac injected. Refer to Supplementary Table 1 for expected and actual adverse effects of using both methods to develop brain metastases.

Due to the variations in the development of brain metastasis after intracardiac injections, we developed a method to increase accuracy by coupling intracardiac injections with ultrasound guidance. Bioluminescent imaging of mice 10 days post 4T1-luc intracardiac injection using ultrasound showed widespread metastases in the brain, lung, liver and bones (Figure 3.1d). Brain metastases were confirmed by histology. All mice injected using this method survived up to day 14-post tumour challenge whereas only 52% of mice injected blindly survived until this end-point (Figure 3.1e). This method was 100% reproducible in generating brain colonies compared to only 33% by blind injections (Figure 3.1f) and no tumours were observed within the thorax.

3.4.2 NOT ALL METASTATIC CELLS FORM PARENCHYMAL BRAIN METASTASES

We screened several cells lines known to form brain colonies as well as some not previously reported (4T07, MC38, Met-1) to evaluate their brain metastatic ability following ultrasound guided intracardiac injections. 4T1 and 4T07 cells were injected into Balb/c mice; B16 F10, LLC, and MC38 cells were injected into C57 BL/6 mice; Met-1 was injected into FVB/N mice and MDA 231 human cancer cells were injected into Balb/c SCID mice.

As previously reported, 4T1 breast cancer cells formed multiple brain metastases. An antibody against collagen IV, used to label vascular basement membrane, showed 4T1 cells proliferating outside and along the brain vessels (Figure 3.2- last panel). Microgliosis, as detected with a CD45 antibody, were also present around the metastases

consistent with previous reports (Figure 3.2, middle panel) (Fitzgerald, Palmieri et al. 2008).

4T07, another sub-clone derived from the 410.1 breast cancer, can spread to the lung and liver from the primary tumour but fail to develop into metastases (Aslakson and Miller 1992). However, mice fell ill by day 12-14 after intracardiac injection of 4T07 cells and brain histology revealed several large tumours within the brain parenchyma growing out from brain vessels and surrounded by activated microglia (Figure 3.2). Neither 4T1 nor 4T07 cells gave rise to dural and/or leptomeningeal metastases.

MDA-MB-231 cells consistently formed extra-vascular colonies in the brain parenchyma that were surrounded by activated microglia. These metastases were far fewer and smaller compared to those produced by 4T1 and 4T07 cells at the same time after tumour cell injection (Figure 3.2).

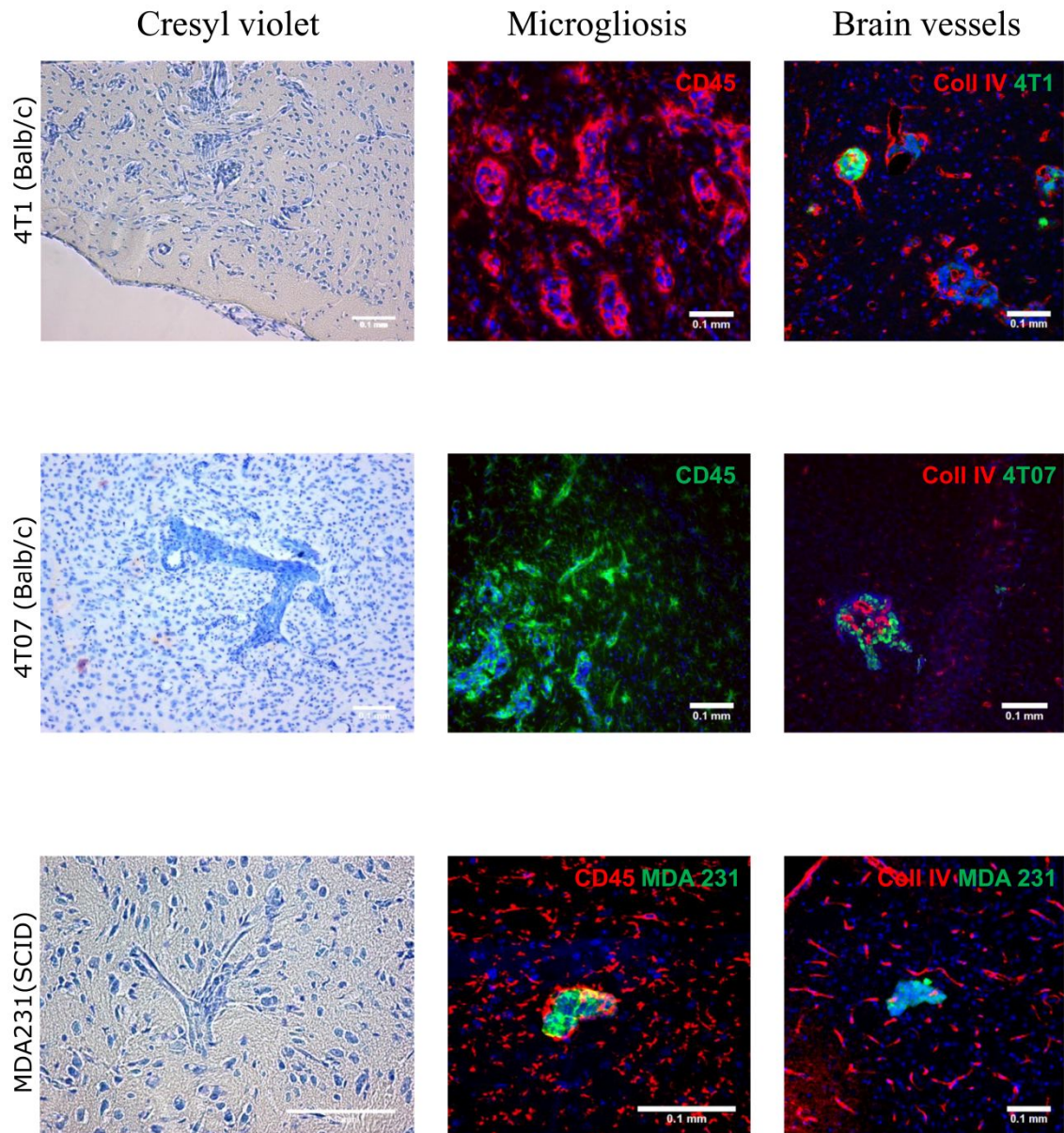


Figure 3.2: Intracardiac injection of 4T1, 4T07 or MDA -MB-231 cells using ultrasound guidance consistently give rise to parenchymal brain metastases

Balb/c (4T1, 4T07) or SCID mice (MDA-MB-231) were intracardiac injected using ultrasound guidance with 10^5 GFP-expressing cancer cells. Mice were culled when they showed signs of distress and cresyl violet stained brain sections were analysed for tumour development (left panel). Microgliosis was present around the metastases as indicated by increased expression of CD45 (red 4T1, MDA-231; green 4T07). Collagen IV (red) antibody was used to label the basement membrane and showed extra-vascular growth of all cells lines. Strong nuclear labelling of Hoechst (blue) identified large tumours that had lost their GFP expression. Scale bars represent 0.1mm

None of the C57 Bl/6 syngeneic cells lines consistently formed metastases in the brain. Two of the four mice injected with B16 F10 cells died 16 days after tumour injection and the remaining two healthy mice were also culled at this time. Visual inspection of systemic organs did not show any signs of macroscopic tumour growth. The brain of one sick mouse had an easily detachable dural tumour which was shown in histological analysis to not have invaded the brain (Figure 3.3). The brain of the other sick mouse had one small intravascular tumour growth.

All LLC-injected mice were culled 14 post after tumour injection and two of the ten mice injected had intracranial tumours. Macroscopic tumour growth was visible on top of the brain in one mouse. Inspection of the whole brain using epi-fluorescent microscopy revealed tumour growth on the surface. Histological analysis of brain sections confirmed that the tumour was growing within the meninges and had not invaded the parenchyma. Small clusters of intravascular LLC cells were also observed at other sites of the brain. This particular mouse also had extensive extra-cranial metastasis including the ovaries, intestines and lymph nodes. Another mouse had an invasive tumour growth limited to the olfactory bulb and did not have any visible extra-cranial metastasis (Figure 3.3). One mouse with no signs of brain metastases had a macroscopic lung tumour.

All mice injected with MC38 cells were culled 14 days after intracardiac injection as 2 out of the 5 mice injected fell ill at this time. Visual inspection of organs showed lung and ocular metastases in one of the mice while another mouse had lung metastases. No visible tumour were found in brains but histology revealed that 3 mice developed

intracranial metastases but these were small lesions restricted to the meninges, ventricle lining or were intravascular (Figure 3.3).

FVB/N mice injected with the Met-1 breast cancer cell line all developed brain metastases 14 days post tumour injection into the heart. Although the metastases were very small and infrequent, they were extravascular and elicited a microglial/macrophage response (Figure 3.4). However, further attempts at repeating the experiment using both ultrasound-guided intracardiac injections and intra-carotid injections were unsuccessful.

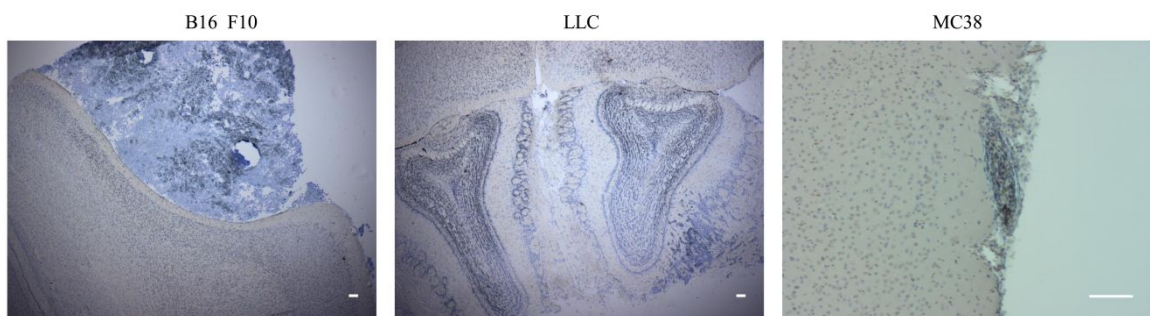


Figure 3.3: B16 F10, LLC and MC38 cancer cells infrequently develop intracranial metastases after intracardiac injection

GFP-expressing LLC, B16 F10 and MC38 cancer cell lines (10^5) were injected into C57 Bl/6 mice using ultrasound guidance and brains were harvested when mice became moribund. Brain sections were processed for histology and brain metastases were identified. B16 F10 and MC38 cells did not produce any parenchymal brain metastases. In one instance, LLC formed parenchymal brain metastases in an area of the brain that does not have an intact BBB (olfactory bulb- middle panel). Scale bar represents 0.1mm

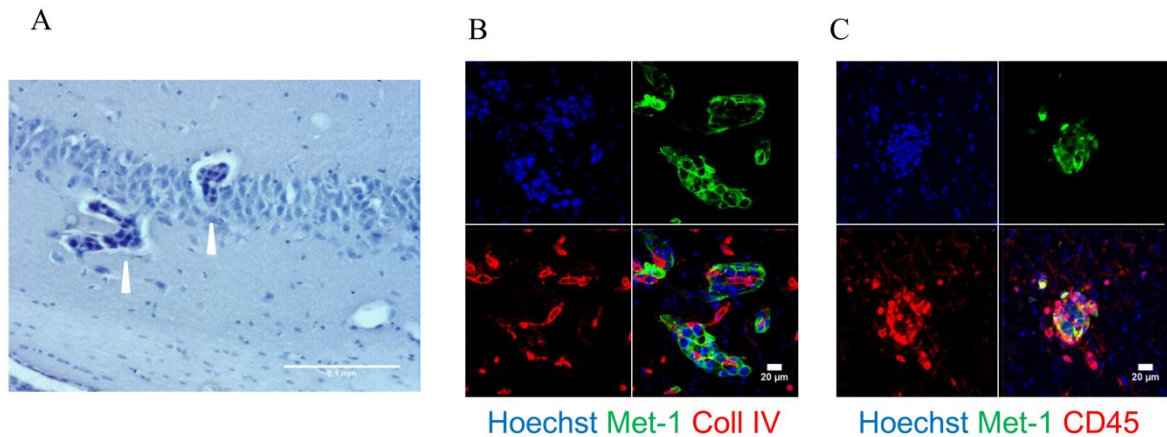


Figure 3.4: Met-1 cells do not consistently produce brain metastases

FVB/N mice were injected with 10^5 Met-1 breast cancer cells expressing cyan fluorescent protein (CFP -green). Mice were culled 14 days after tumour injection and brain sections were analysed. A: Cresyl violet staining of brain sections showed very small and infrequent metastases in all brains examined (arrows), which were confirmed to be extra-vascular by coll IV (red) antibody labelling of brain vasculature (B). C: Microgliosis was also evident around brain metastases as shown by anti CD45 immuno-reactivity (red). Hoechst was used to counter-stain cell nuclei (blue). Subsequent experiments where the same number of tumour cells were intracardiac injected (n = 9) or intracarotid injected (n=3) failed to give rise to any brain metastases.

3.4.3 THE INABILITY TO DEVELOP PARENCHYMAL BRAIN METASTASES IS AN ATTRIBUTE OF THE CELL LINE AND NOT DUE TO THE MOUSE STRAIN

Since cell lines derived from tumours formed in C57 Bl/6 mice could not form brain metastases, we asked whether the immune system of this particular mouse strain contributed to this failure. We therefore determined whether the LLC and B16F10 cell lines would give rise to brain metastases after intracardiac injection into Balb/c SCID mice. We also injected 4T1 cells into SCID mice as controls. As expected, 4T1 breast cancer cells displayed similar patterns of brain metastases in SCID mice as they did in syngeneic Balb/c mice, with extra-vascular invasive brain growth (Figure 3.5, top panels). In contrast, LLC and B16F10 cells were as poorly metastatic as they had been in syngeneic immuno-

competent mice. One of three mice injected with LLC cells displayed extra-vascular proliferations along the blood vessels of the cortex while the other two mice were metastases-free (Figure 3.5, middle panels). Only one of three mice challenged with B16 F10 cells had an intracranial lesion but this was restricted to a ventricle without evident invasion into the brain (Figure 3.5 bottom panels). The ability of different cells lines to form brain metastases in syngeneic and SCID mice are summarised in Figure 3.6.

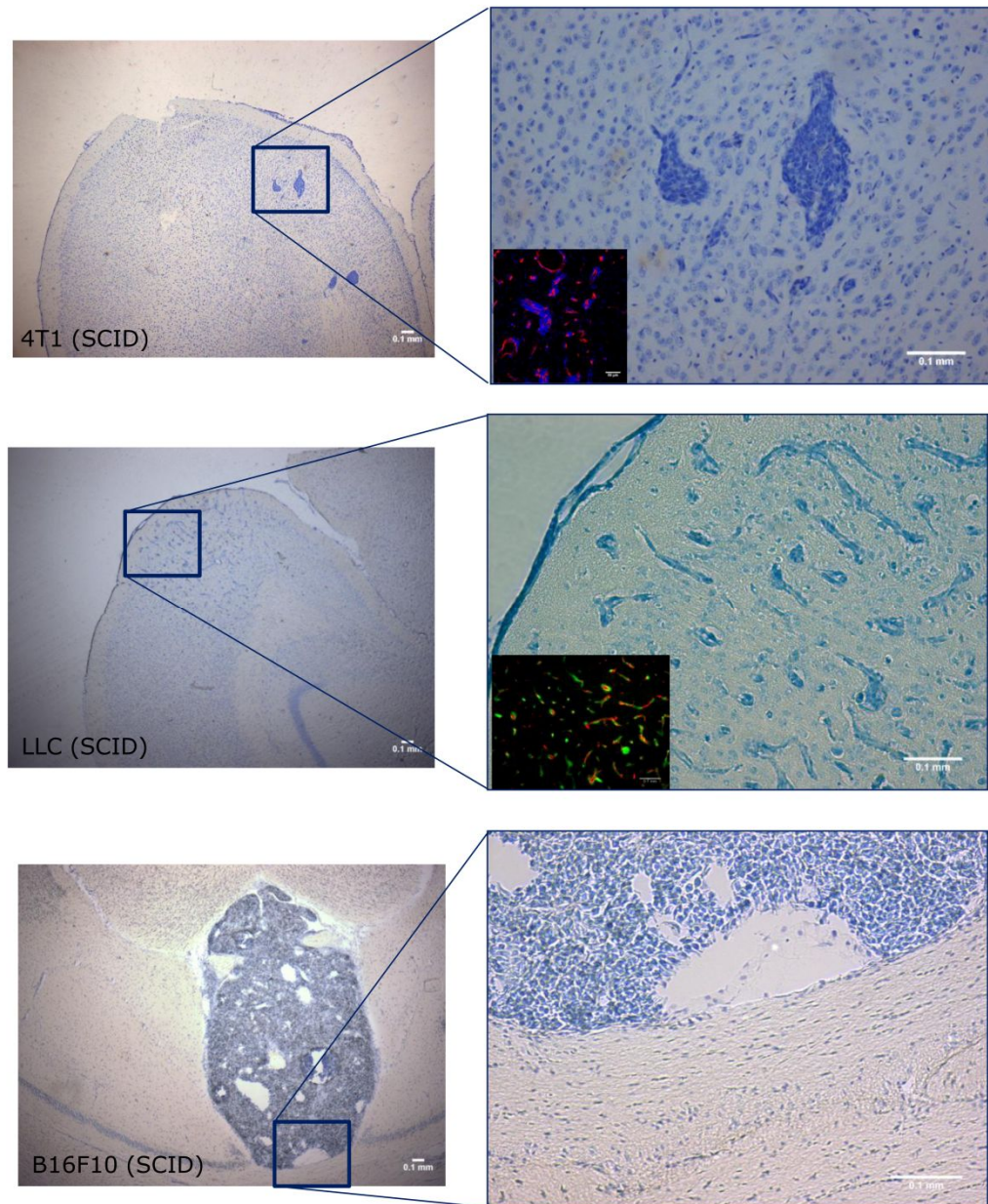


Figure 3.5: C57 Bl/6 syngeneic cells lines do not produce parenchymal brain metastases in Balb/c SCID mice

GFP-expressing LLC, B16 F10, and 4T1 cells (10^5) were intracardiac injected into Balb/c SCID mice using ultrasound guidance. Mice were culled when they showed signs of distress and brain tissue sections were analysed using cresyl violet staining and antibody labelling. 4T1 cells maintained their ability to form parenchymal brain metastases in SCID mice. Anti-collagen IV labelling of basement membrane (red – inset) showed 4T1 cells (deep blue) to be growing within the brain. LLC and B16 F10 cells were unable to produce parenchymal brain metastases in SCID mice. However, in one case, anti-collagen IV staining (red) showed LLC cells growing in peri-vascular regions of the cortex (inset, middle panel; LLC – green; coll IV - red).

3.4.4 INTRACAROTID INJECTIONS OF LLC CELLS INFREQUENTLY GIVE RISE TO BRAIN METASTASES

To limit extra-cranial tumour cell seeding and to deliver more cells, we injected LLC cells into the internal carotid artery. Mice were culled when they showed signs of distress, or 20 days post tumour injection. Although 81% of mice had intracranial tumours, the majority of tumours were located within the ventricles. Only 18% of mice had metastases in the parenchyma. However, these metastases were larger and more widespread throughout the brain than metastases seen after intracardiac injection (Figure 3.7- compare with Figure 3.3 middle panel).

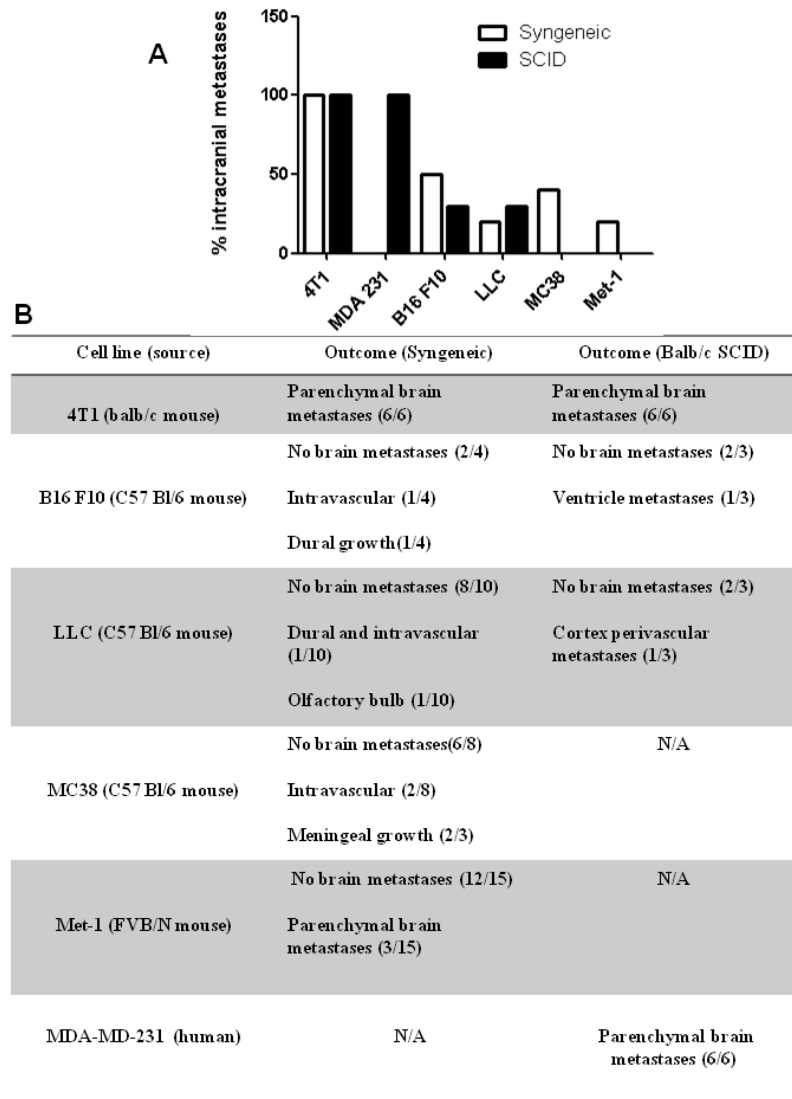


Figure 3.6: Comparing the ability of metastatic cell lines to colonise the brain after ultrasound-guided intracardiac injection

Syngeneic or SCID mice were intracardiac injected with 10^5 GFP expressing tumour cells using ultrasound guidance. Mice brains were analysed for brain metastases 2-4 wks after injection when the mice showed signs of distress. A: Percentage of mice that developed intracranial metastases after intracardiac injection with each cell line regardless of location within the cranium. B: Summary of the specific site of intracranial metastases found in A. Numbers in brackets indicates number of mice with indicated findings out of total mice tested.

3.4.5 WEAKLY BRAIN METASTATIC CELLS ARE ABLE TO GROW IN THE BRAIN IF DIRECTLY INJECTED INTO THE STRIATUM

There are several steps in the final stages of the metastatic cascade that may limit disseminated cancer cell from developing into brain metastases. These cells may be able to enter the brain i.e. extravasate, but are unable to survive or grow within the brain parenchyma. To test this, we directly injected LLC cells into the striatum of mice. Mice were culled 8 days after LLC injection and brains were assessed. Tumour growth was noted at the site of injection. An activated microglial wall surrounded the tumours formed by LLC cells and infiltration of IBA1⁺ microglia/macrophages were also present (Figure 3.7). Similar results were obtained after direct injection of B16F10 cells into the brain (personal correspondence and (Aboody, Najbauer et al. 2006).

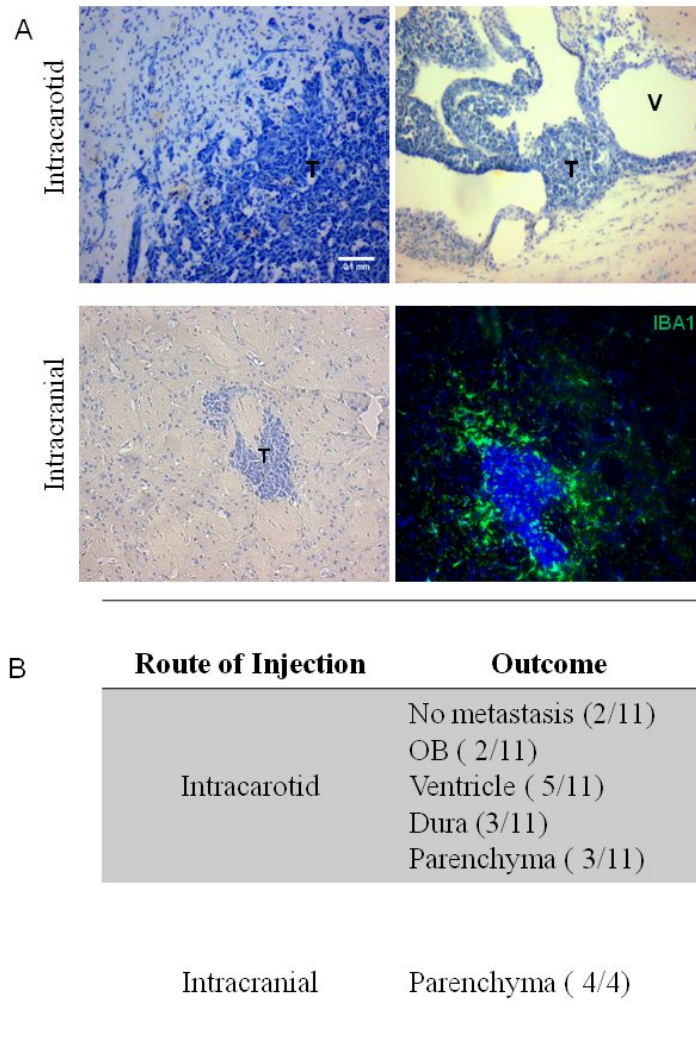


Figure 3.7: LLC cells infrequently develop into brain metastases after intracarotid injection but will consistently form tumours in the brain if directly injected into the brain parenchyma

A: C57 Bl/6 mice were injected with 10^5 LLC-GFP cells into the internal carotid artery and culled 8 days after ($n = 11$). Cresyl violet stained brain sections were analysed for the presence of brain metastases. Although majority of intracarotid injected mice developed intracranial tumours, almost all were located in ventricles or on the dura (top panel, T- tumour; V- ventricle). When LLC cells were directly injected into the striatum of mice ($n=4$), 100% of the mice developed tumours at the site of injection (bottom panel). The microglia marker IBA1 was used to label brain sections and microgliosis was seen around the tumours (IBA1 – green, bottom panel). Scale bar represents 0.1 mm. B: Summary of the outcome after injection of LLC cells using the two different routes; OB-olfactory bulb

3.5 DISCUSSION

Spontaneous models of brain metastasis enable the study of every aspect of the metastatic cascade. However, only few models exist and require extended experimental waiting times before brain metastases develop and these only occur in few mice (Cruz-Munoz, Man et al. 2008; Carbonell, Ansorge et al. 2009). To accelerate the process of forming brain metastases, experimental brain metastases have been established by introducing tumour cells into the arterial circulation through the left ventricle of the heart or the carotid artery. This approach has led to important information about the vascular localisation and establishment of brain metastases (Carbonell, Ansorge et al. 2009; Kienast, von Baumgarten et al. 2010). However, these methods have had the drawback of technical difficulty and limited reproducibility, which may contribute to the limited research into brain metastasis. Accordingly, we modified the intracardiac method by using ultrasound to guide the intracardiac injection. This resulted in reliable introduction of cells with widespread dissemination and reliable induction of cells into the brain.

The intracarotid route of injection produces consistent results with minimal injection error. However, this technique requires extensive microscopic surgery that limits the number of animals used in a single study. This route of injection also increases the risk of ischemia and induction of tumours at the site of injection. On the other hand, the intracardiac approach does not require open surgery, and is very quick but is limited by its inconsistency. Choi *et al* used intracardiac injection of MDA MB 231-BR cells to develop brain metastases in which, 3 of 12 animals died immediately following cardiac injection

and of the 9 remaining, only 6 developed brain metastases (Choi, Rizia et al. 2012). This 50% success rate in developing brain metastases is very limiting when performing large scale animal experiments especially when time-consuming post-mortem processing is required to determine successful brain metastases. Without visualising the heart, it is easy to miss the target and inject into the chest cavity, right ventricle or heart muscle. Therefore, a consistent dose of cells cannot be delivered repeatedly within an experiment and quantitative analysis cannot be performed.

To overcome the variability in results after intracardiac injection of tumour cells, we coupled this technique with ultrasound imaging. The method we developed was quick, easy to perform and most importantly, gave consistent results. Using ultrasound imaging to guide the intracardiac injection, we achieved a 100% success rate in developing brain metastases from brain metastatic cell lines and we also minimised animal loss. Our model allowed us to inject up to 6-8 mice in an hour using the same batch of cells whereas it took up to 40 minutes to inject a single mouse via the carotid artery.

Using ultrasound guidance to inject tumour cells, we were able to compare the brain metastatic ability of three C57 Bl/6 syngeneic cell lines, LLC, MC38 and B16F10 and one breast cancer cell line syngeneic to FVB/N mice. The Met-1 murine mammary carcinoma is metastatic to the lung from the primary tumour, and is used as a model for breast cancer lung metastasis (Borowsky, Namba et al. 2005; Qian, Li et al. 2011). To our knowledge, this cell line has not been tested for its ability to produce brain metastases. Two weeks after intracardiac injection, we infrequently found small brain metastases in

all tumour injected mice. Unfortunately, subsequent experiments failed to develop brain metastases. This cell line produced consistent lung metastases after tail vein injection and tested negative for mycoplasma. Given that intracarotid injections of Met-1 tumour cells also failed to produce any intracranial tumours, we concluded that it was not worth pursuing as a brain metastases model. LLC, B16F10 and MC38 cells were incapable of forming brain metastases and only sporadically formed metastases at other intracranial sites (leptomeningeal, dural and ventricular). Inability to form brain metastases was found in both syngeneic and SCID mice implying that the limited ability of these tumour cells to form brain metastases is an inherent property of the cell line and not due to the mouse strain. Furthermore, it was recently shown that the C57 Bl/6 breast cancer cell-line E0771 produced brain metastases in syngeneic mice after intracarotid injection (Lorger 2012). However, it is yet to be determined how consistent this result is.

Several studies have used LLC and B16F10 cell lines to produce brain metastases (Rashidi, Yang et al. 2000; Aboody, Najbauer et al. 2006; Perides, Zhuge et al. 2006; Saito, Hatori et al. 2007; Saito, Hatori et al. 2008; Zhang, Hatori et al. 2008; Saito, Hatori et al. 2009; Brantley, Guo et al. 2010) but our results contradict these findings. In one study using intracarotid injection of LLC, a 77% success rate of developing brain metastases was reported (Zhang, Hatori et al. 2008). However, these metastases were described to be located in the perivascular space, ventricles or the meninges with few mice developing parenchymal metastases. Therefore, the difference in findings may be because these groups used intracarotid injection to deliver tumour cells to the brain and also because these reports do not differentiate between parenchymal metastases and tumours formed

in other intracranial sites. When we performed intracarotid injections with LLC, we too found that 80% of injected mice developed intracranial tumours but only 37% of these mice had parenchymal metastases. Mice harbouring parenchymal brain metastases also had extensive metastases within the ventricles implying that cancer cells shed into the CSF may account for parenchymal metastases in this case. Although we did not inject B16 F10 cells into the carotid artery, other reports using this route indicate that this cell line does not form brain metastases and any intracranial tumours are restricted to the meninges (Fidler and Nicolson 1976; Schackert and Fidler 1988). Due to the inconsistent development of intracranial tumours, with rare instances of parenchymal growth, we conclude that both LLC and B16 F10 are poorly brain metastatic and are not suitable to use for studying brain metastasis.

Using direct intra-parenchymal injections of tumour cells, we have shown that LLC can grow in the brain. Similar experiments done with B16 F10 by others (Perides, Zhuge et al. 2006) and within our institute (personal correspondence) verify that this melanoma line is also capable of growing in the brain parenchyma when directly introduced. This implies that the failure of these cell lines to form brain metastasis is due to their inability to interact with and/or cross the BBB. Using the techniques developed in this chapter, we can quantitatively compare these weakly brain metastatic cells lines with ones capable of forming brain metastases (4T1 and MDA 231), to determine the critical step(s) required for disseminated tumour cells to enter the brain parenchyma.

CHAPTER 4: CHARACTERISING THE STEPS REQUIRED FOR DISSEMINATED TUMOUR CELLS TO DEVELOP INTO BRAIN METASTASES

4.1 INTRODUCTION

Several barriers must be overcome in order for cancer cells to successfully colonise a distant site and the majority of disseminated cancer cells do not survive to form brain metastases (Fidler 1970). Within the circulation, disseminated cells face destruction by natural killer cells (Hanna 1982; Hanna 1982) and the shear force of blood flow (Glinsky and Glinsky 1996). To survive, cancer cells up-regulate survival signals and mask themselves in platelets (Tsuruo, Kawabata et al. 1986; Stone and Wagner 1993). Platelet-coated tumours form an embolus which enables entrapment within capillaries where subsequent platelet signalling through integrin promotes tumour cell adhesion along the target vessel (Tsuruo, Kawabata et al. 1986; Felding-Habermann, Habermann et al. 1996). Tumour cell extravasation into most secondary sites occurs within 24 h, but crossing the brain endothelium occurs over several days (Paku, Dome et al. 2000). Using human and mouse breast cancer cell lines, it has been shown that extravasation does not occur until at least 3 days after vessel adherence and some intravascular cells were even noted at day 7 (Lorger and Felding-Habermann 2010). Extended time spent exposed to the circulation decreases a tumour cell's chance of survival and survival within the brain vasculature has been noted as the key limiting step which determines successful brain metastasis (Kienast, von Baumgarten et al. 2010; Lorger and Felding-Habermann 2010). The mechanisms by which tumour cells survive and extravasate into the brain are

unknown and may involve a similar two-step process used by leukocytes to migrate into the brain (Saito, Hatori et al. 2007; Owens, Bechmann et al. 2008).

4.1.1 HOST-MEDIATED METASTASES

Tumour infiltrating leukocytes are conditioned by the tumour microenvironment to take on a pro-tumour role (DeNardo, Johansson et al. 2008). These leukocytes promote tumour growth, invasion and dissemination by releasing survival, growth and angiogenic factors and proteases that enable ECM re-modelling (Balkwill and Coussens 2004; Wyckoff, Wang et al. 2007). A growing body of evidence now indicates that host immune cells are also directly involved in promoting colonisation of tumour cells at the secondary site (Hiratsuka, Watanabe et al. 2006; Qian, Li et al. 2011; Gil-Bernabe, Ferjancic et al. 2012).

4.1.1.1 MACROPHAGES

In response to inflammatory signals, blood monocytes migrate to inflamed tissue and differentiate into macrophages to perform a variety of functions. Tissue macrophages are phagocytic scavenger cells that engulf debris, dead cells and pathogens and present antigens to T-cells to mount an adaptive immune response (Unanue 1984). Macrophages also secrete cytokines and growth factors to maintain homeostasis and immunity (Gordon and Taylor 2005) and to promote tissue repair and fibrosis (Martinez, Helming et al. 2009; Lucas, Waisman et al. 2010). Macrophages are also critical for normal tissue development (Pollard 2009)

4.1.1.1.1 Tumour-associated macrophages

Initially, tumour-associated macrophages (TAM) were thought to mount an anti-tumour response but it was subsequently shown that they promote tumour growth, progression and immuno-suppression (Leek, Lewis et al. 1996; Dave, Wright et al. 2004; Paik, Shak et al. 2004; Budhu, Forgues et al. 2006). The relationship between tumourgenesis and macrophages were first shown in experiments using colony stimulating factor 1 (CSF-1) knock-out mice (Lin, Nguyen et al. 2001). As the CSF-1 receptor is only present on macrophages, CSF-1 null mice cannot recruit macrophages. Although no effects were evident in hyperplasia, adenoma or early carcinoma, deficient mice displayed delayed onset of invasive carcinoma and reduced lung metastases (Lin, Nguyen et al. 2001; Lin, Gouon-Evans et al. 2002). Subsequent experiments have shown that TAMs produced VEGF to enhance vascularisation of the tumour (Lin, Li et al. 2006; Lin, Li et al. 2007). Furthermore, Tie2 expressing monocytes (TEM) have been identified within primary tumours that specifically promote tumour angiogenesis (De Palma, Venneri et al. 2005).

The tumour-promoting role of macrophages stems from their ability to adapt to their surroundings and perform various functions in response to environmental cues. Two distinct activation states of macrophages have been identified and classified as M1 or M2. M1 macrophages are activated predominantly by interferon γ whereas alternative activation is triggered by IL-4 and IL-13 (reviewed in (Martinez, Helming et al. 2009; Varin and Gordon 2009)). M1 macrophages promote inflammation, extra-cellular matrix (ECM) re-modelling/destruction and apoptosis while M2 macrophages promote wound healing, cell proliferation, ECM construction, and angiogenesis (Varin and Gordon 2009). It is

these alternatively activated M2 macrophages that are present in primary tumours. These macrophages suppress the adaptive immune system from mounting an anti-tumour response and aid in tumour progression and metastasis (Mantovani, Sozzani et al. 2002; Allavena, Sica et al. 2008).

4.1.1.1.2 Metastasis-associated macrophages

Platelets play a central role in haematogenous spread of tumour cells. Not only do they provide physical protection to circulating tumour cells, emerging evidence indicate that platelets attract immune cells that aid the metastatic process (Borsig, Wong et al. 2002). Anti-coagulation has been shown to reduce lung metastasis by preventing interaction of monocytes/macrophages with lung metastatic mouse melanoma tumour cells (Gil-Bernabe, Ferjancic et al. 2012). In an experimental mouse model of lung metastasis, inhibition of macrophage recruitment in CSF-1 null mice and CD11b conditional knock-out mice (CD11b-DTR) or depletion of macrophages using liposome encapsulated clodronate resulted in significantly less lung metastases compared to WT mice (Qian, Deng et al. 2009). These metastasis associated macrophages (MAM) expressed CD11b, CCR2, CX3CR1, VEGFR1, but not Gr-1 and interacted with lung metastatic cells as early as 24 h after tumour injection (Qian, Deng et al. 2009). Extravasating portions of tumour cells are seen directly interacting with macrophages indicating that macrophages may physically aid lung metastases formation. Inflammatory CD11b⁺Gr1⁺CCR2⁺ monocytes were also recruited to the lung via tumour secreted CCL2 and aided extravasation of breast cancer cells (Qian, Li et al. 2011).

4.1.1.2 NEUTROPHILS

Neutrophils are innate immune cells that develop from the same myeloid progenitor as monocytes (Friedman 2002). They are the most abundant immune cells found in humans but are mostly restricted to the bone marrow with less than 2% found in circulation (Sadik, Kim et al. 2011). Neutrophils provide the first line of defence against bacteria and fungus by engulfing pathogens, secreting anti-microbial factors and form extracellular traps composed of neutrophil granules and chromatin to catch microbes (Brinkmann, Reichard et al. 2004; Segal 2005; Urban, Reichard et al. 2006) .

4.1.1.2.1 Tumour-associated neutrophils

Neutrophils have also been shown to be involved in tumourgenesis. Accumulation of tumour associated neutrophils (TAN) in cancer patients correlates with poor disease outcome (Jensen, Donskov et al. 2009; Zhou, Dai et al. 2012). Analogous to M1 and M2 macrophages, N1 neutrophils are tumour-killing, whilst N2 neutrophils are tumour-promoting (Mantovani 2009; Fridlender and Albelda 2012). In primary tumours, it has been shown that the conversion from N1 to N2 is mediated by tumour-derived transforming growth factor $-\beta$ (TGF- β) (Fridlender, Sun et al. 2009). Neutrophil depletion (N2) in naïve mice lead to tumour growth retardation. However, when TGF- β is chemically inhibited in mice, depletion of neutrophils (N1) resulted in tumour progression (Fridlender, Sun et al. 2009). Using the Pu.1 knock-out zebrafish model of experimental metastasis, the contribution of macrophages and neutrophils to metastasis was deciphered. Partial inhibition of Pu.1 (macrophage only) resulted in poor tumour vascularisation whereas complete knock-down of Pu.1 (macrophages and neutrophils)

resulted in poor vascularisation and decreased tumour invasion (He, Lamers et al. 2012). Invasion was independent of VEGF and was due to neutrophil deformation of nearby collagen (He, Lamers et al. 2012). TANs have also been shown to produce MMP-9 to support tumour progression and invasion by activating angiogenesis (Nozawa, Chiu et al. 2006).

4.1.1.2.2 Metastasis-associated neutrophils

As previously outlined, tumour secreted CCL2 has been shown to recruit monocytes to the lung to promote breast cancer cells to colonise the lungs (Qian, Li et al. 2011). Another study has shown that CCL2 produced by breast cancer cells also recruit neutrophils to the lung; these neutrophils destroy disseminated breast cancer cells arriving at the lungs to prevent lung metastases (Granot, Henke et al. 2011). However, other studies report pro-metastatic roles for neutrophils. *In vivo*, rats co-injected with adenocarcinoma cells and tumour conditioned neutrophils developed more lung metastases compared to rats co-injected with tumour cells and normal neutrophils (Welch and Schissel 1989). *In vitro*, it was shown that MDA-MB-231 human breast cancer cells transmigration through various endothelial barriers was significantly increased when tumour cells were mixed with human neutrophils exposed to tumour-conditioned media but not normal neutrophils (Wu, Wang et al. 2001). It was subsequently shown that enhanced transmigration was a result of GM-CSF produced by MDA-MB-231 cells. Tumour secreted GM-CSF caused increased expression of adhesion molecules (Mac-1: CD11b/CD18) on neutrophils enabling enhanced interaction with ICAM expressed on MDA-MB-231 cells (Wu, Wang et al. 2000). Recently, *in a xenograft model*, it was

reported that adhesion of human melanoma cells to mouse lung vasculature increased in the presence of human neutrophils (Huh, Liang et al. 2010). These melanoma cells secreted IL-8, a neutrophil chemoattractant, which increased $\beta 2$ integrin expression on neutrophils. $\beta 2$ engaged with ICAM-1 on the melanoma cell to mediate extravasation into the lung. Knock-down of the *Il-8* gene in the human melanoma cells decreased expression of $\beta 2$ on neutrophils, decreased retention of melanoma cells in the lung and decreased lung metastases (Huh, Liang et al. 2010). In a mouse model of lung cancer liver metastasis, neutrophil depletion using the Gr-1 antibody reduced liver metastases; the number of liver metastases increased when LPS stimulated neutrophils were exogenously delivered into Gr-1 depleted mice. Furthermore, the authors showed that direct interaction of tumour cells with neutrophils was essential for liver metastasis as blocking the Mac-1 receptor on neutrophils or ICAM on lung cancer cells *in vitro* decreased the number of liver metastases (Spicer, McDonald et al. 2012).

4.1.1.3 MYELOID DERIVED SUPPRESSOR CELLS (MDSC)

MDSC are a heterogeneous population of immature bone marrow derived myeloid cells capable of differentiating into granulocytes, macrophages or dendritic cells (Egan, Sukhumavasi et al. 2008). In normal tissue homeostasis, these immature cells curb inflammation and autoimmunity but in the context of cancer, MDSC promote tumourgenesis and metastasis (Gabrilovich and Nagaraj 2009; Nagaraj, Collazo et al. 2009).

4.1.1.3.1 Tumour-associated MDSC

Increased presence of MDSCs was noted in almost all human cancers (Almand, Clark et al. 2001; Nagaraj and Gabrilovich 2007; Diaz-Montero, Salem et al. 2009; Nagaraj and Gabrilovich 2010). The increased numbers of MDSC in tumours, blood and spleen of tumour bearing mice correlated with dampened anti-tumour immunity. MDSC suppress T-cell functions through a variety of mechanisms including secretion of peroxynitrate rendering T-cells incapable of recognizing antigens (Nagaraj, Gupta et al. 2007), and degrading arginine which prevents T-cell replication and decreases expression of the receptor ζ chain (Rodriguez, Zea et al. 2003; Rodriguez and Ochoa 2008).

MDSCs are tentatively characterized as CD11b⁺ cells which co-express Gr-1 (Ly6G⁺Ly6C⁺). Two populations of MDSC have been identified and classified as monocyte-like (Ly6G^{low},Ly6C^{hi}) or granulocyte like (Ly6G^{hi}Ly6C^{low}) and each population is described to have different immunosuppressive strengths (Dolcetti, Peranzoni et al. 2010). However, due to ambiguity in surface marker expression, they are mainly identified by their immunosuppressive activity. The role of these cells has been extensively studied in the primary tumours (Nagaraj and Gabrilovich 2008; Ostrand-Rosenberg and Sinha 2009; Nagaraj and Gabrilovich 2010) but have only recently been shown to play a direct role in promoting colonisation at the secondary site (Kowanetz, Wu et al. 2010; Yan, Pickup et al. 2010).

4.1.1.3.2 Metastasis-associated MDSC

Mice bearing orthotopic 4T1 breast tumours have been shown to accumulate Ly6G⁺Ly6C⁺ (Gr1⁺) granulocytic cells in their lungs prior to tumour cell arrival (Kowanetz, Wu et al.

2010; Yan, Pickup et al. 2010). These granulocyte-like cells were not present in organs where 4T1 cells do not commonly metastasise spontaneously (bone, brain). The presence of Gr1⁺ cells were shown to produce Bv8, a protein that aids tumour cell migration to the lung (Kowanetz, Wu et al. 2010). Depletion of CD11b⁺Gr1⁺ cells reduced the number of lung metastases (Kowanetz, Wu et al. 2010). Another similar study found that the CD11b⁺Gr-1⁺ cells present in the lung increased proliferation of metastatic cells and maintained immune-suppression in part by preventing lung macrophages from producing interferon- γ (IFN- γ). The same study also showed that MMP-9 produced by the CD11b⁺Gr-1⁺ cells increasing vessel leakiness and permeability thereby facilitating lung metastasis (Yan, Pickup et al. 2010).

4.1.1.4 PRIMARY TUMOUR DIRECTED METASTASIS

Factors secreted by the primary tumour have been reported to pre-condition the lung and other organs to direct metastasis. This concept, termed the pre-metastatic niche, was first described by Hiratsuka *et al* where they showed that LLC-bearing mice had increased expression of MMP-9 in the lungs and this contributed to increased lung metastases (Hiratsuka, Nakamura et al. 2002). Subsequently, the same study team showed that TGF- β , TNF, and VEGF secreted by the primary LLC tumour cells induced expression of S100A8 and S100A9 calcium binding inflammatory proteins in the lung. This inflammatory environment created by the S100 proteins attracted CD11b⁺ MMP9⁺ myeloid cells specifically to the lung to promote the formation of lung metastases (Hiratsuka, Watanabe et al. 2006). Interestingly, another study using 4T1 primary tumour-bearing mice, CD11b⁺Ly6G⁺Ly6C⁺ cells were shown to be specifically recruited to the lung by

tumour secreted G-CSF (Kowanetz, Wu et al. 2010). In the 4T1 model, the myeloid cells recruited to the lungs expressed MMP9 as well as S100A8 and S100A9 proteins that also promoted tumour cell recruitment and growth in the lungs (Kowanetz, Wu et al. 2010). Tumour-derived factors have also been shown to recruit VEGFR⁺ bone marrow derived cells to future sites of metastasis. The accumulation of VEGFR⁺ cells promoted colonisation of tumour cells at specific secondary sites (Kaplan, Riba et al. 2005). Recently, coagulation has been reported to contribute to the formation of the pre-metastatic niche (Gil-Bernabe, Ferjancic et al. 2012). Mice bearing subcutaneous melanoma primary tumour showed increased accumulation of CD11b⁺ monocyte/macrophage cells in the lung coated in platelets and in long-term metastases assays, these mice harboured significantly more lung metastases compared to non-tumour bearing mice. Anti-coagulation abolished the recruitment of CD11b⁺ cells and reduced the number of lung metastases (Gil-Bernabe, Ferjancic et al. 2012).

Metastatic efficiency is greatly increased when tumour cells form heterotypic clusters with factors in the circulation or homotypic clusters with themselves (Fidler 1973; Liotta, Saidel et al. 1976; Updyke and Nicolson 1986; Ruiters, van Krieken et al. 2001). Expanding on this idea, collective metastasis has been identified where tumour cells 'bring their own soil' to the secondary site to increase their ability to successfully metastasise (Duda, Duyverman et al. 2010). In normal brain and those bearing glioblastomas, fibroblasts are restricted to vessel-associated pericytes and smooth muscle cells. However, histological analysis of brain metastases from a variety of human cancers show the presence of metastases associated fibroblasts within the tumours (Duda, Duyverman et al. 2010).

An increasing body of evidence shows that immune cells are deregulated in cancer and function predominately to favour tumour progression and metastasis. The role of different host immune cells in facilitating disseminated tumour cells to colonise the lung and liver is now coming to light and it seems likely that immune cells also contribute to tumour cell colonisation of the brain.

4.2 HYPOTHESIS

Host immune cells contribute to successful brain metastasis by promoting intravascular tumour cell survival and/or extravasation into the brain.

4.3 AIMS

Research to date has focused mainly on inflammatory cells and associated factors that contribute to the survival, extravasation and establishment of secondary tumours at the lung and liver. Employing the brain metastasis model established in the previous chapter, we focus on identifying host immune cells which may contribute to the establishment of brain metastases. **The first aim of this chapter is to compare metastatic cells lines to determine at which steps after dissemination the poorly-brain metastatic cells fail. Expanding on these finding, we then aim to characterise the host response to metastatic cells after intracardiac injection and determine if immune cells are involved in the steps necessary for successful brain metastasis.**

4.4 MATERIALS AND METHOD

4.4.1 FLUORESCENCE ACTIVATED CELL SORTING (FACS)

In order to obtain quantitative measurements of leukocyte subsets in peripheral blood, anti-coagulated whole blood was collected from mice. Erythrocytes were lysed after a 20 min incubation in FACSlyse (BD Bioscience). Cells were washed twice in FACS buffer (PBS containing 0.5% FBS and 0.1% sodium azide) and diluted up to a volume of 1 ml. To decrease non-specific binding of immunoglobulins, cells were incubated for 10 min with anti-CD16/32 (Fc block) (BD Bioscience) and divided into 100 μ l aliquots. The appropriate quantities of monoclonal antibodies were added to each sample (listed in Table 4.1). Unstained, single antibody stained, and isotype controls were included. After a 20 min incubation on ice, cells were spun and washed thrice and resuspended in FACS buffer containing 2% PFA. Cells were examined with a four-color BD FACSCalibur cytometer (BD Biosciences) equipped with BD CellQuest Version 6 software (BD Biosciences) and data analyzed with FlowJo Version 7.6.5 software (Tree Star, Inc., Ashland, OR, USA)

Table 4.1: Antibodies used for FACS

Mouse Antigens	Dilution	Fluorochrome	Isotype	Clone	Company	Cat#
CD16/CD32 (Fc block)	1:50	-	rat IgG2b, κ	2.4G2	BD	553141
CD3e	1:80	APC	Armenian hamster IgG	145-2C11	eBioscience	17-0031
	1:20	PE-Cy7	Armenian hamster IgG	145-2C11	eBioscience	25-0031
CD11b	1:160	PE-Cy7	rat IgG2b, κ	M1/70	eBioscience	25-0112
	1:80	A488	rat (DA) IgG2b, κ	M1/70	BD	557672
	1:100	FITC	rat IgG2b, κ	M1/70	eBioscience	11-0112
	1:100	A488	rat IgG2b, κ	M1/70	eBioscience	53-0112
	1:80	APC-Cy7	rat (DA) IgG2b, κ	M1/70	BD	557657
CD11c	1:80	A647	Armenian hamster IgG	N418	eBioscience	51-0114
	1:80	FITC	Armenian hamster IgG	N418	eBioscience	11-0114
	1:40	PE-Cy7	Armenian hamster IgG	N418	eBioscience	25-0114
CD45	1:160	APC	rat IgG2b, κ	30-F11	eBioscience	17-0451
	1:100	PE	rat IgG2b, κ	30-F11	BD	553081
F4/80	1:50	PE	rat IgG2a	BM8	Invitrogen	MF48004
	1:50	A647	rat IgG2a	BM8	Invitrogen	MF48021

Gr-1	1:700	PE	rat IgG2b, κ	RB6-8C5	eBioscience	12-5931
	1:160	A647	rat IgG2b, κ	RB6-8C5	eBioscience	51-5931
Ly-6c	1:20	PerCP-Cy5.5	rat IgG2c	HK1.4	eBioscience	45-5932
	1:50	FITC	rat IgM, κ	AL-21	BD	553104
Ly6G	1:100	FITC	rat IgG2a, κ	IA8	BD	551460

4.3 RESULTS

4.3.1 ATTACHMENT AND SURVIVAL WITHIN THE BRAIN VASCULATURE ARE THE LIMITING STEPS IN BRAIN METASTASIS

To determine whether defects at the point of attachment, survival and/or extravasation limit brain metastasis, we compared the poorly brain metastatic LLC and B16F10 cell lines to the highly brain metastatic 4T1 and MDA 231 cell lines. We sacrificed mice at different times after intracardiac injection of GFP-expressing tumour cells and analysed the brains for the presence of tumour cells. Numbers of GFP positive tumour cells were counted in representative brain sections (18 sections per brain) and plotted against time (Figure 4.1). At the earliest time point (4 h), MDA-231 cancer cells (207.33 ± 151.47 cells/18 brain sections) were the most abundant, followed by 4T1 (143.75 ± 50.09 cells /18 brain sections). Only sporadic LLC (8 ± 9.2 cells/18 brain sections) or B16 F10 cells (1.75 ± 2.06 cells/18 brain sections) were observed. There were significantly more MDA 231 tumour cells arrested in blood vessels of the brain than 4T1, LLC and B16F10 4 h after tumour injection. The number of 4T1 cells continued to decline over 3 days (12.71 ± 19.08 cells/18 brain sections at day 3) and stabilised at this time whilst the number of MDA-231 continued to decline over 7 days. As almost no surviving LLC (0.33 ± 0.577 cells/18 brain

section) or B16 F10 cells were detected at day 3 (1.33 ± 1.53 cells/18 brain sections), the experiment was terminated at this time point for these cell lines.

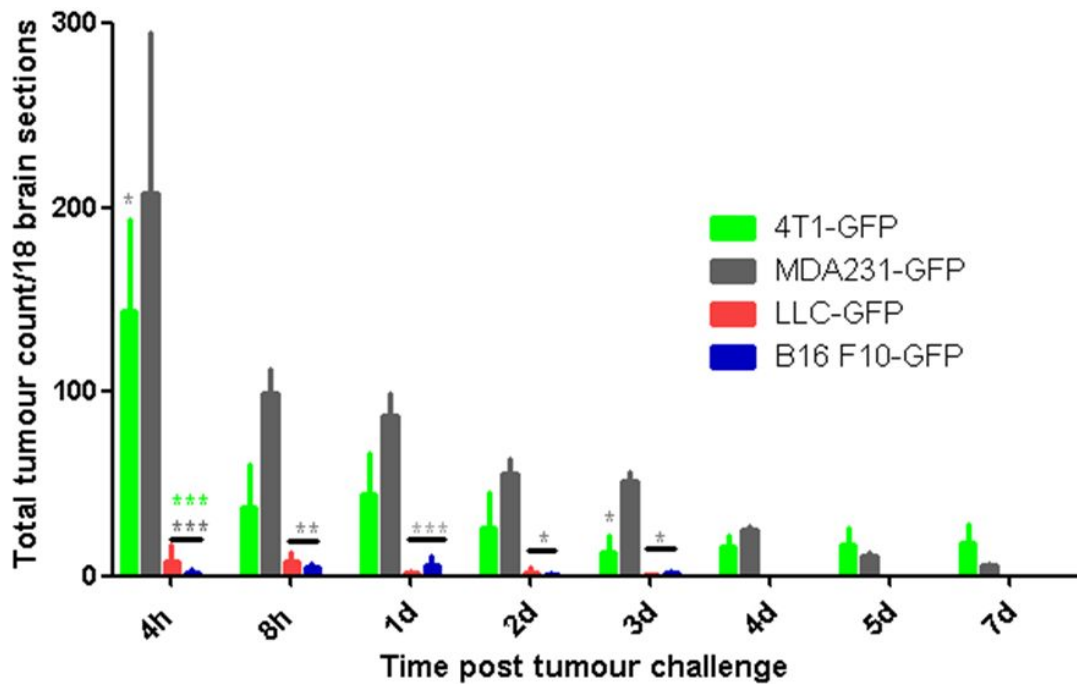


Figure 4.1: Attachment and survival of metastatic cells within the brain over time

Mice were intracardiac injected with 10^5 GFP-expressing highly brain metastatic 4T1 and MDA 231 cells or the poorly brain metastatic LLC and B16 F10 cells. Mice were culled at 4 h, 8 h and each subsequent day. Experiments were terminated at day 3 post tumour challenge for mice injected with LLC and B16 F10 cells and at day 7 for mice injected with 4T1 and MDA 231 cells. GFP positive cells (or metastases) were counted in 18 representative brains sections from each mouse brain and total numbers were plotted against time. At least 2 brains were counted for every cell line per time-point and the experiment was repeated at least twice. Data is presented as mean \pm SD and significance was determined using 2-way ANOVA and the Bonferroni post hoc test. Green asterisks indicates significance relative to 4T1; gray asterisks indicate significance relative to MDA-231; *** $p < 0.001$; ** $p < 0.01$; * $p < 0.05$.

4.3.2 ST6GALNAC5, THE GENE THAT MEDIATES BREAST CANCER METASTASIS TO THE BRAIN, IS NOT EXPRESSED BY BRAIN METASTATIC 4T1 CELLS

It has been shown that MDA 231 cells, and more so the brain-seeking variant MDA 231-Br, express a gene designated st6galnac5, which is required for this cell line to invade the brain (Bos, Zhang et al. 2009). We tested our cell lines for expression of the ST6GALNAC protein using the elderberry lectin, Sambucus nigra agglutinin (SNA) that specifically binds to ST6GALNAC5 (Kaku, Kaneko et al. 2007; Bos, Zhang et al. 2009). As reported, MDA 231 cells were SNA positive but surprisingly the very aggressive 4T1 breast cancer cell line was SNA negative (Figure 4.2). Furthermore, SNA bound strongly to LLC cells, a weakly brain metastatic cell line. No positive signal was seen when cells were labelled with an unrelated lectin.

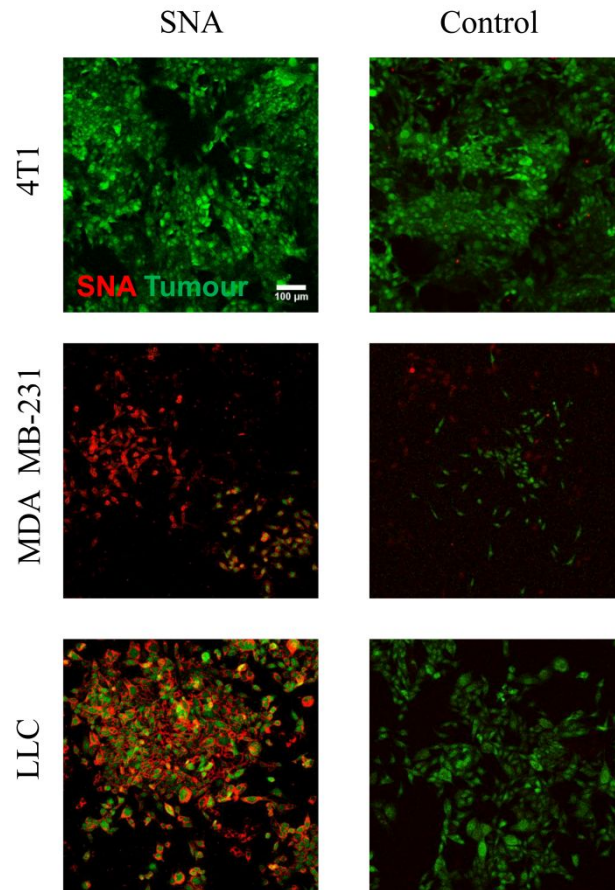


Figure 4.2: ST6GALNAC5 is expressed by LLC and MDA 231 cells but not by brain metastatic 4T1 cells

4T1, MDA 231 and LLC GFP-expressing cells were grown on 6-well tissue culture plates. When cells were 80% confluent, they were fixed with 4% PFA and incubated with the lectin *Sambucus nigra* agglutinin (SNA) to assess ST6GALNAC5 expression. Representative confocal images illustrate strong expression of ST6GALNAC5 (red) on MDA 231 and LLC cells (green). However, no expression was detected on 4T1 cells. Negative control images represent cells incubated with an unrelated lectin (RCA). Scale bar represents 100 μm

4.3.3 PLATELETS ASSOCIATE WITH INTRAVASCULAR TUMOUR CELLS

Platelets have been reported to play a role in enhancing metastasis and anti-coagulation and heparin has been suggested as a therapeutic intervention for melanoma brain metastasis (Camerer, Qazi et al. 2004; Maraveyas, Johnson et al. 2010). To determine

whether platelets contribute to adhesion and survival of tumour cells within the brain vasculature, we quantified platelet association with highly brain metastatic 4T1 and MDA 231 cells and the weakly brain metastatic LLC and B16F10 cells 4 h and 8 h after intracardiac injection. Platelets were detected using an antibody against the $\alpha\text{IIb}\beta$ integrin receptor that is uniquely expressed on platelets (Calvete 1995). Tumour cell – platelet association was quantified as percentage of tumour cells co-localised with platelets. 4T1 and MDA 231 cells adherent to the brain vasculature were predominantly associated with platelets (Figure 4.3 a, b). Although it was rare to find LLC and B16F10 cells attached to the brain vasculature 4-8 h after intracardiac injection, the few cells present were also coated with platelets. Platelet co-localization with 4T1 cells was assessed over a longer time course (Figure 4.3c). Between 1-3 days after intracardiac injection, majority of 4T1 cells were associated with platelets but the number of surviving cells continued to decrease. After day 3, surviving 4T1 cells were less likely to be associated with platelets either because platelets were replaced with a fibrin clot, or the tumour cells were in the process of or had completed extravasation into the brain.

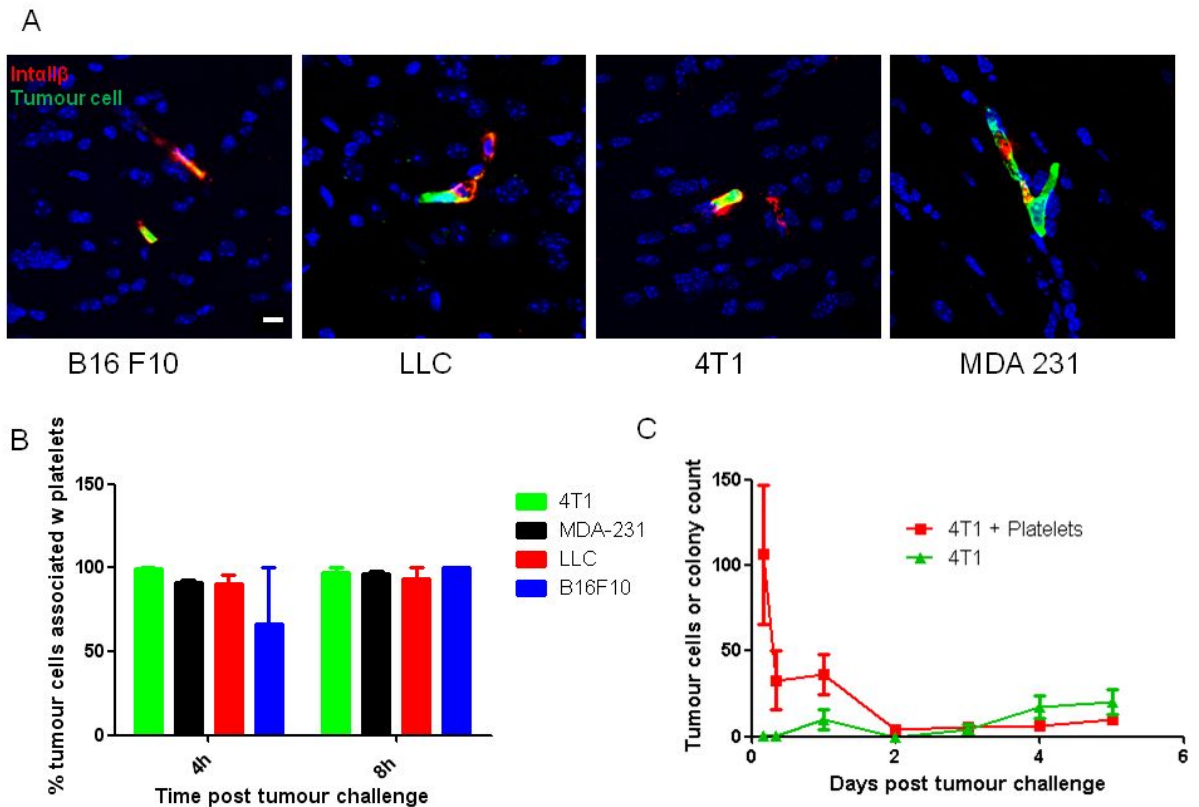


Figure 4.3: Platelets associate with intravascular tumour cells

A: Mice were intracardiac injected with 10^5 B16 F10, LLC, 4T1 or MDA 231 GFP-expressing cells and culled 4 h or 8 h after tumour challenge. Brain sections were co-labelled with anti-integrin $\alpha II\beta$ to detect platelets (red) and anti-GFP to detect tumour cells (green) and representative images are shown. Scale bar represents 10 μm . B: Total number of tumour cells co-localised with platelets were quantified in 10 representative brain sections per mouse brain. Percentage of tumour cells co-localised with platelets at 4 h and 8 h after intracardiac injection was plotted for each cell line (LLC, B16 F10 $n = 3$; 4T1, MDA 231 $n=4$). C: Balb/c mice were intracardiac injected with 10^5 4T1-GFP cells and culled at several time points after injection. Brain sections (10 per mouse brain) from each time point were quantified for total platelet-tumour co-localisation ($n \geq 3$ per time-point). Up to 2 days post tumour challenge, the majority of tumour cells found in brain sections were co-localised with platelets and the number of tumour cell-platelet aggregates (red line) declined over time.

4.3.4 CIRCULATING LEUKOCYTES ASSOCIATE WITH A FEW INTRAVASCULAR BRAIN METASTATIC CELLS

Platelets alone appear to be insufficient to support long term survival of intravascular tumour cells. However, it has been reported that platelets mediate tumour survival and lung metastasis through recruitment of metastasis promoting monocytes/macrophages to the tumour-platelet emboli (Gil-Bernabe, Ferjancic et al. 2012). To determine if a similar mechanism accounts for brain metastasis, we assessed brain tissues excised from mice 24 h after intracardiac injection with GFP expressing 4T1, MDA 231, LLC or B16 F10 cells. Brain tissues were stained with a pan-leukocyte marker, CD45, which detects circulating immune cells (CD45^{hi}) and brain resident microglia (CD45^{low}). Representative fluorescent images shown in Figure 4.4a illustrate intravascular tumour cells 24 h post intracardiac injection, some of which were associated with CD45^{hi} cells. Brain sections were quantified for the number of tumour-CD45^{hi} clusters formed at 24 h post tumour injection for each cell line. An average of 8.42 ± 3.17 4T1 cells/18 fields, 5.25 ± 1.26 MDA 231 cells/18 fields and 0.33 ± 0.58 LLC cells/18 fields were found adjacent to a CD45^{hi} immune cell(s). No association with CD45^{hi} immune cells was seen with B16F10 cells (Figure 4.4 b).

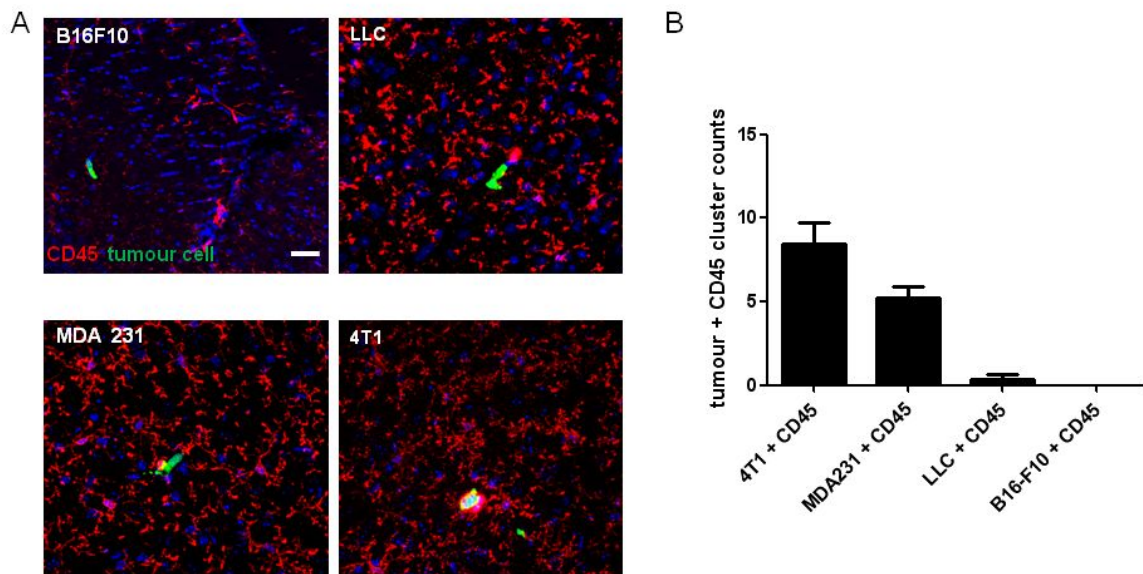


Figure 4.4: A few intravascular tumour cells are associated with CD45^{hi} immune cells 24 h post intracardiac challenge

Mice were intracardiac injected with 10^5 GFP-expressing B16F10, LLC, MDA 231 and 4T1 cells. Mice were culled 24 h after tumour injection and brain tissue sections were co-labelled with anti-CD45 antibody to detect circulating immune cells and microglia (red) and anti-GFP antibody to detect tumour cells (green). A: Representative images of intravascular GFP-expressing tumour cells 24 h post tumour challenge, some of which were associated with CD45^{hi} immune cells. Scale bar represents 20 μ m. B: Brain sections (18 per mouse) were analysed for tumour-CD45^{hi} clusters and quantified for each cell line (4T1 n= 6; MDA 231 n= 4; LLC n= 3; B16 F10 n=3).

4.3.5 TUMOUR-LEUKOCYTE CLUSTERS PERSIST, WHILST SOLITARY TUMOUR CELLS DECLINE WITH TIME

There are several possible consequences that arise from the association of CD45^{hi} immune cells with intravascular tumour cells. They may be present to recognise and clear tumour cells from within the vasculature or, in contrast, they may aid tumour cell survival and/or extravasation. To address this, we quantified tumour-immune interaction over 7 days after intracardiac challenge with 4T1 or MDA 231 breast cancer cells. Representative images of tumour-leukocyte clusters for 4T1 and MDA 231 cells at various time points are shown in Figure 4.5a and b. Quantification of the percentage of CD45-

tumour clusters or solitary tumour cells within the brain at each time point is shown in Figure 4.5c and 4.5d.

At 4 h post tumour challenge only a small percentage of brain metastatic tumour cells were associated with CD45^{hi} immune cells (5.61 ± 4.04 % of 4T1 cells/18 brain sections and 4.09 ± 2.79 % MDA 231 cells/18 brain sections). However, with time, the percentage of solitary tumour cells declined, and by 3 days post tumour challenge, an average of 42% of surviving 4T1 cells and 20% of surviving MDA 231 cells were clustered with one or more leukocytes. The phenotype of the CD45^{hi} tumour associated cells changed with time. Initially from 4 h – 3 d, CD45 cells were single, small, spherical and intensely CD45 positive compared to surrounding microglia (CD45^{low}). Between days 3- 7 post tumour challenge, as surviving tumour cells begin to extravasate, we noticed a mixed phenotype of the tumour associated CD45^{hi} cells. Tumour cells continued to be associated with bright CD45^{hi} round cells and by day 5, greater numbers of immune cells were present beside tumour cells. However, tumour cells in the process of extravasation were also surrounded by activated CD45⁺ microglia. Activated microglial cells were noted as CD45^{mid-hi} expressing cells with a stellate appearance in contrast to the ramified processes of quiescent microglia (See Figure 1.2). By day 7, an average of 18.12 ± 3.35 4T1 micrometastases/18 brain sections were counted, and 83.04 ± 10.01% of these were encased by a microglial wall and in some instances, we noted few bright CD45^{hi} round cells among the microglial wall (Figure 4.5a). At the same time, the few remaining 4T1 cells (3.24±0.87 cells/18 brain sections) not associated with CD45^{hi} immune cells were solitary and appeared intravascular. An average of 3.4 ± 0.98 MDA 231 cells/18 brain

sections was present at day 7 with $78.00 \pm 8.34\%$ encased within a microglial wall or a combination of microglial wall and bright, round CD45^{hi} immune cells. By day 7 post-tumour injection 4T1 cells were noted as small micrometastases composed of over 10 tumour cells, whilst MDA-231 cells formed small tumour clusters containing only 3-5 tumour cells. The MDA 231 cells not associated with CD45^{hi} immune cells by day 7 were all intravascular single cells (2.00 ± 00.56 cells/18 brain sections). The persistence of the tumour- CD45^{hi} immune clusters over time, and the decline of solitary tumour cells suggest that the CD45^{hi} immune cells associated with 4T1 and MDA 231 cells may in fact be aiding tumour cell survival and/or extravasation.

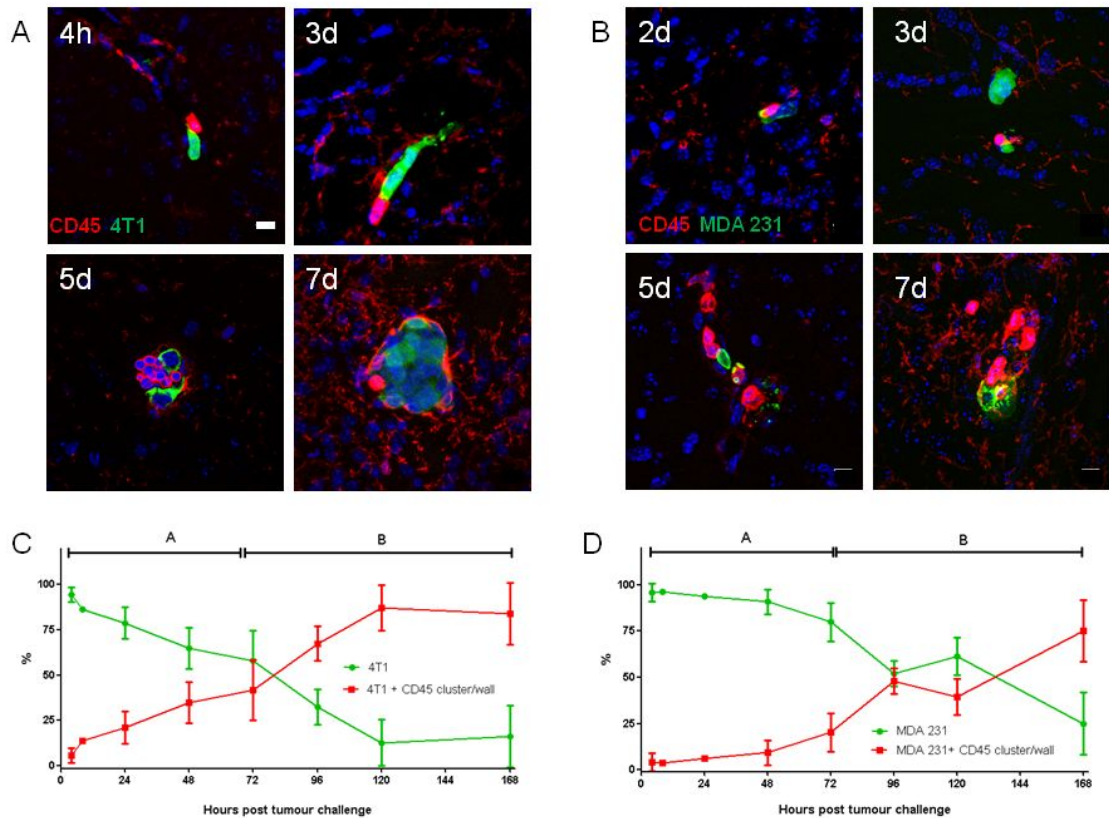


Figure 4.5: Percentage of tumour-CD45^{hi} clusters increase with time

Mice were intracardiac injected with 10^5 4T1-GFP or MDA 231-GFP cells. Mice were culled 4 h, 8 h, and then each subsequent day until day 7 post tumour injection. Brain tissue sections (18 per mouse) were co-labelled with anti-CD45 and anti-GFP antibodies and tumour-CD45^{hi} clusters were imaged (A,B) and quantified (C,D) for each time point. C-D: The red line represents percentage of CD45^{hi} circulating immune cells/activated microglia associated with tumour cells at each time point. The green line indicates tumour cells found alone. From 4 h – 3 days post tumour challenge, a few tumour cells were associated with single round CD45^{hi} cells (line A). After day 3, tumour cells were frequently associated with either CD45^{hi} round immune cells, activated microglia, or a combination of the two (line B). The experiment was repeated at least twice with 2 or more mice per time point. Data is presented as mean sum of total counts from 18 brain sections per mouse \pm SD. Scale bar represents 10 μ m.

4.3.6 AN INCREASE IN TUMOUR-CD45^{HI} INTRAVASCULAR CLUSTERS CORRELATES WITH INCREASED TUMOUR BURDEN

To investigate the relevance of tumour-CD45^{hi} clusters found within the brain vasculature, we asked whether we could augment this association and determine the effect on brain metastases development. The pre-metastatic niche, induced by the primary tumour at a distant site, enhances seeding of a second dose of tumour cells at the niche site (Kaplan, Riba et al. 2005; Hiratsuka, Watanabe et al. 2006). We pre-conditioned mice with either 4T1 or MDA 231 cells and when tumours reached 250 mm³, we intracardiac challenged these mice with the same tumour cells (GFP expressing) used to produce the primary tumour. Mice that received just the intracardiac dose of tumour cells served as controls. Mice were culled either 3 d post intracardiac challenge to quantify intravascular tumour-CD45^{hi} immune clusters, or 7 d (4T1) and 20 d (MDA 231) after the second tumour injection to quantify brain metastases. The experimental protocol is outlined in Figure 4.6.

To confirm previous findings that 4T1 and MDA 231 cells were predominantly intravascular 3 days post intracarotid injections (Larger and Felding-Habermann 2010), we co-labelled brain sections from mice culled 3 days post intracardiac injection with anti-GFP and anti-CD34 antibodies to visualise tumour location in relation to the brain vasculature. Using this method, we confirmed that 98-99% of 4T1 and MDA-231 cells were intravascular 3 days after intracardiac injection (Figure 4.7).

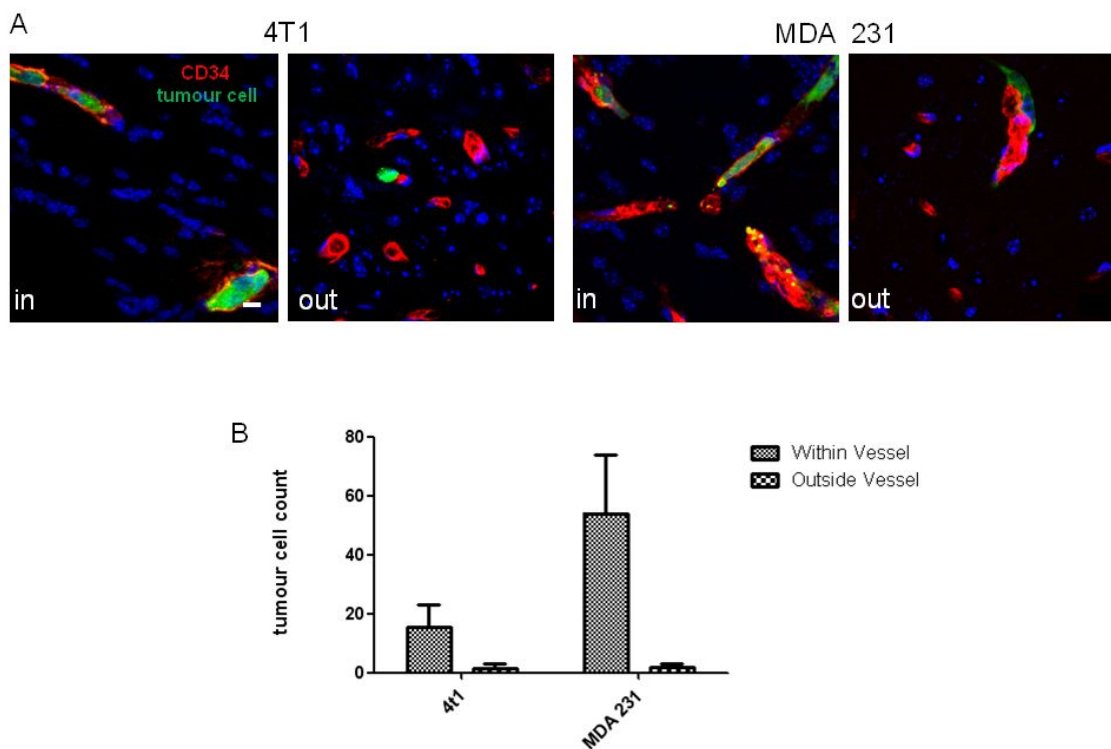


Figure 4.7: The majority of 4T1 and MDA-231 tumour cells are intravascular 3 d post intracardiac injection

Brain sections from mice culled 3 days after intracardiac injection with 10^5 4T1 or MDA 231 GFP-expressing cells were co-labelled with anti-GFP and anti-CD34 antibody to determine location of tumour cells in relation to the brain vasculature. A: Representative images from 4T1 and MDA 231 injected brains illustrate intravascular and extravascular tumour cells. Scale bar represents 10 μ m. B: Total tumour cells were counted in 18 brain sections per mouse and scored based on vessel location. Data is represented as the mean sum of total tumour cells counted in 18 brain sections \pm SD. Majority of 4T1 and MDA 231 cells were found within brain vessels at day 3 post intracardiac challenge (n=3).

Since tumour cells were predominately intravascular 3 d post intracardiac challenge, we quantified total intravascular tumour cells and percentage of these tumour cells associated with CD45^{hi} immune cells in pre-conditioned and control mice. Slightly fewer 4T1-GFP tumour cells were noted in brains of pre-conditioned mice (34.00 ± 21.95 4T1

cells/18 brain sections) compared to controls (47.08 ± 26.78 4T1 cells/18 brain sections). However, the percentage of 4T1-CD45^{hi} intravascular clusters was significantly increased in pre-conditioned mice compared to controls ($46.33 \pm 15.64\%$ conditioned vs. $32.48 \pm 8.89\%$ control) (Figure 4.8a). 7 days post intracardiac challenge, the number of brain metastases in pre-conditioned mice increased by 70% compared to controls (65.71 ± 48.80 4T1 metastases/18 fields conditioned vs. 38.57 ± 18.67 4T1 metastases/18 fields control). However, this increase was not significant (Figure 4.8b).

Similar results were obtained with mice pre-conditioned with MDA-231 cells. In brains of mice culled 3 days after intracardiac injection, there was slightly fewer MDA 231-GFP cells in pre-conditioned mice (58.25 ± 31.19 cells/18 brain sections) compared to control mice (86.50 ± 26.89 cells/18 brain sections control) (Figure 4.8c). There was, however, a significant increase in percentage of intravascular MDA 231-CD45^{hi} immune clusters at this time-point ($36.13 \pm 13.51\%$ clusters/18 brain sections) compared to controls ($15.23 \pm 6.22\%$ clusters/18 brain sections control) (Figure 4.8c). As shown in Figure 4.8d, 20 days after intracardiac injection, there were significantly more brain metastases in tumour bearing mice compared to control animals (37.40 ± 16.10 brain metastases/18 brain sections conditioned vs. 7.250 ± 2.99 brain metastases/18 brain sections control).

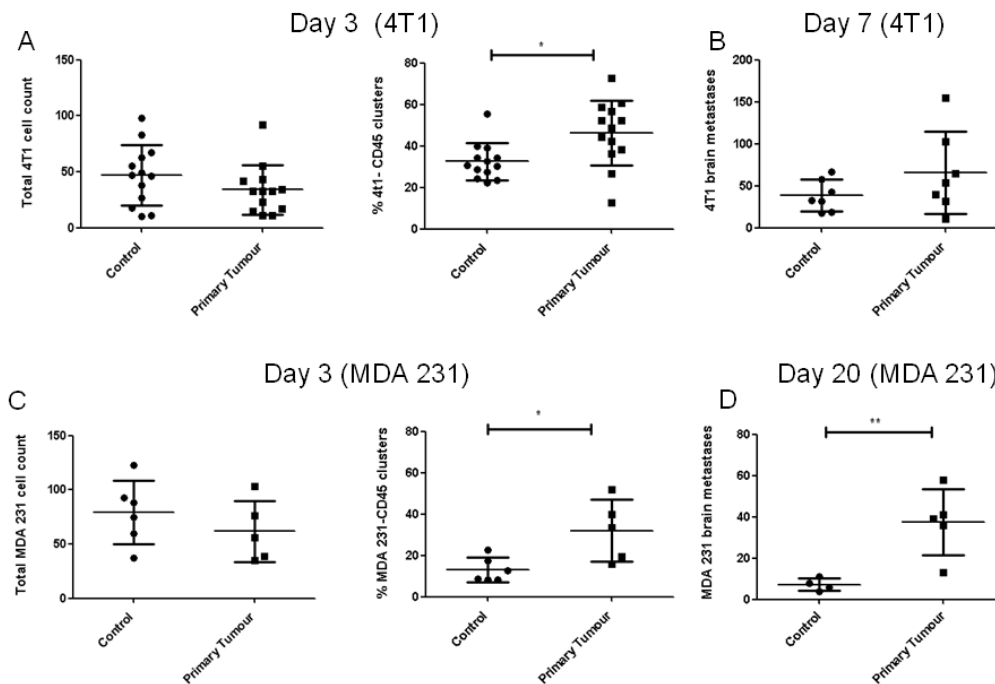


Figure 4.8: Mice pre-conditioned with a primary tumour have an increased percentage of intravascular tumour-CD45^{hi} clusters and develop more brain metastases compared to primary tumour-free mice after intracardiac injection of tumour cells.

Naïve Balb/c mice or ones bearing a 4T1 primary tumour were intracardiac injected with 10^5 4T1-GFP cells. A: Mice were culled 3 days after intracardiac challenge and brain sections were co-labelled with anti-CD45 and anti-GFP antibodies. The total number of tumour cells (left) and percentage of tumour cells associated with CD45^{hi} immune cells were quantified in 18 brain sections per mouse (right) (n=13). No differences were found in the numbers of tumour cells in the brain but a significant increase in the percentage of intravascular 4T1-CD45^{hi} clusters were found in pre-conditioned mice compared to control mice. B: The experiment was repeated but mice were culled 7 days after 4T1-GFP intracardiac injection and the total number of brain metastases in 18 brain sections per mouse were quantified (n=7). Slightly more metastases were found in pre-conditioned mice compared to control mice. C: Similar experiments were performed using the MDA 231 cell line. Naïve mice or ones bearing a subcutaneous MDA 231 primary tumour were intracardiac injected with 10^5 MDA 231-GFP cells and brains were harvested 3 days post intracardiac challenge. Brain sections were co-labelled with anti-CD45 and anti-GFP and total tumour cells (left) and percentage of tumour cells associated with CD45^{hi} immune cells (right) were quantified in 18 brain sections per mouse (n=5). No differences in the numbers of intravascular tumour cells were found but a significant increase in the percentage of MDA 231-CD45^{hi} clusters was noted in pre-conditioned mice compared to control mice. D: The experiment was repeated but mice were culled 20 days after tumour challenge and 18 brain sections per mouse were assessed for total brain metastases (n= 5). Significantly more metastases were present in pre-conditioned mice compared to control mice. Data is presented as mean sum of tumour cells/metastases per 18 brain sections \pm SD and unpaired t test was used to determine significance (normally distributed data) for all except percent CD45-4T1 clusters at day 3 (Mann-Witney); * p < 0.05. ** p < 0.01

To determine the specificity of pre-conditioning, we performed control experiments where 4T1-CD45^{hi} clusters were quantified in mice bearing the poorly brain metastatic LLC primary tumour (Figure 4.9). We also determined whether 4T1 pre-conditioning increased adherence of LLC to brain endothelium after intracardiac injection. These experiments were carried out in Balb/c SCID mice as LLC is syngeneic to C57 Bl/6 mice. As a positive control, we injected 4T1-GFP cells into 4T1 pre-conditioned SCID mice. Brain sections from mice culled 3 days after intracardiac injection showed that there were significantly more 4T1-CD45^{hi} clusters in 4T1 tumour bearing mice compared to non-tumour bearing mice ($53.32 \pm 6.231\%$ conditioned vs. $32.51 \pm 10.01\%$ in control). In contrast, no increase in 4T1-CD45^{hi} clusters were noted in mice pre-conditioned with LLC (Figure 4.9b). There were also no differences in total intravascular tumour cells in brains of mice pre-conditioned with 4T1 or LLC compared to controls (Figure 4.9a). Furthermore, pre-conditioning with 4T1 cells did not increase the ability of LLC to adhere and survive within the brain vasculature nor did it make a difference in the percentage of LLC-CD45^{hi} clusters compared to control brains.

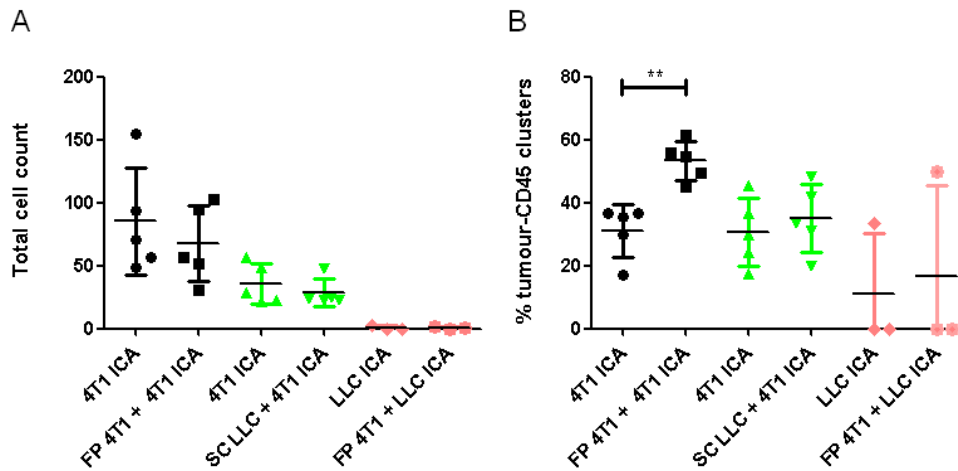


Figure 4.9: Pre-conditioning mice with a LLC primary tumour does not increase the percentage of 4T1-CD45^{hi} clusters in mice brains 3 days after intracardiac tumour injection

SCID mice were injected with 10^5 4T1 cells into the mammary fat pad or 2.5×10^5 LLC cells were injected subcutaneously into the right flank. Control mice were injected with PBS. When tumours reached 250 mm^3 , mice were intracardiac injected with 10^5 LLC-GFP or 4T1-GFP cells. Brains were harvested 3 days post tumour challenge and 18 brain sections per mouse were quantified for total number of tumour cells (A) and the percentage of total tumour cells associated with CD45^{hi} immune cells (B). Only mice pre-conditioned with a 4T1 tumour, then subsequently injected with 4T1-GFP cells resulted in a significant increase in percentage of tumour-CD45^{hi} clusters when compared to control mice (black n= 5). When LLC cells were used as the pre-conditioning cell line, there was no increase in the percentage of 4T1-CD45^{hi} clusters in the brain compared to control mice (green n=4). Pre-conditioning with a 4T1 primary tumour did not increase the adhesion and/or survival of LLC cells within the brain vasculature (pink n=3). Data is presented as mean sum of tumour cell or metastases count in 18 brain sections \pm SD and unpaired t test was used to determine significance (normally distributed data); ** p<0.01

4.3.7 THE CD45^{hi} CELLS CLUSTERED WITH INTRAVASCULAR TUMOUR CELLS ARE GR-1⁺ CIRCULATING IMMUNE CELLS

Because CD45 is a pan-leukocyte marker that detects cells of all immune lineages, we characterised other surface markers present on the tumour associated CD45^{hi} immune cells. As we found tumour-CD45^{hi} clusters in SCID mice, they were unlikely to be T-cells (Figure 4.5b and 4.10a). We verified this by staining brain tissue sections with anti- CD3 antibody, a marker of T-cells. A few T-cells were only noted within the metastases on or

after 5 days post tumour challenge (Figure 4.10b). Even within larger brain metastases that formed 10 days post tumour injection, CD3 reactivity was not consistently detected. Robust infiltration of CD3 cells into brain metastases were only seen at late stage of disease progression (day 12 and 22). Increased leakiness of the blood brain barrier was also present around these tumours, as detected by anti – IgG immuno-staining (Figure 4.10c).

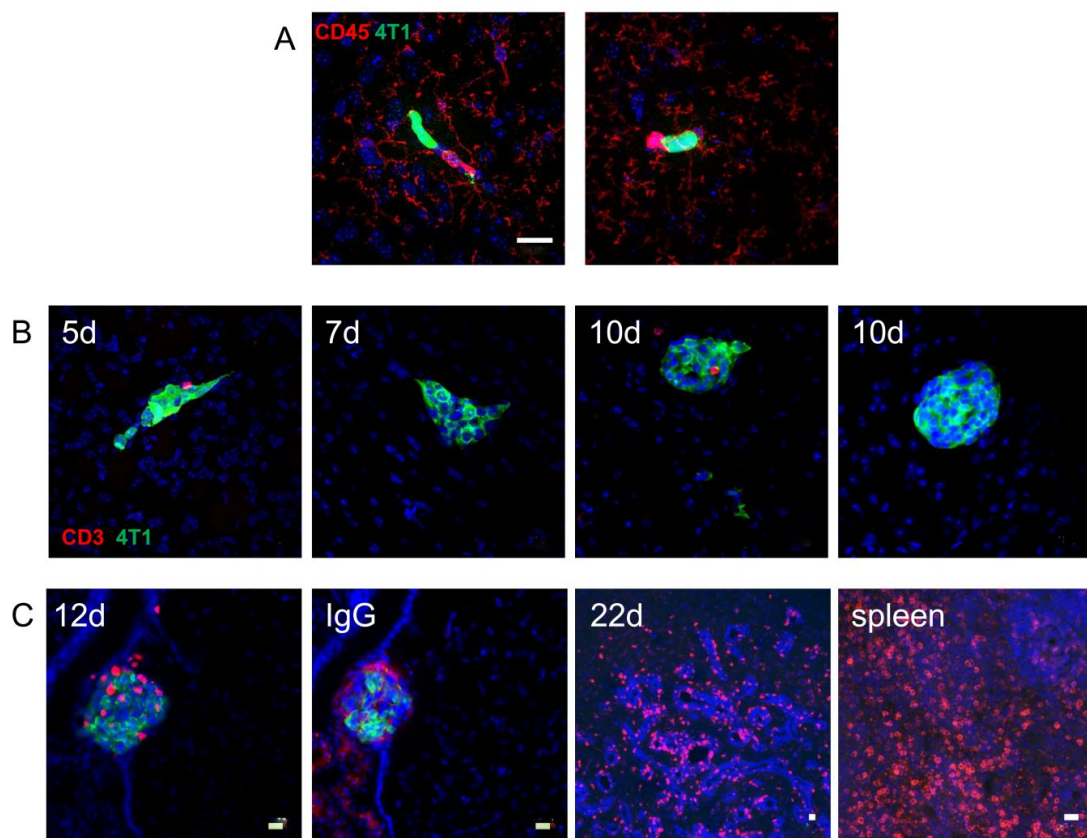


Figure 4.10: Intravascular tumour associated immune cells are not CD3⁺ T-cells

A: SCID mice injected with 10^5 4T1-GFP cells were culled 3 d after tumour challenge and brains assessed for tumour-CD45^{hi} clusters. Representative images show CD45^{hi} cells (red) associated with GFP-expressing 4T1 cells (green). B: Brain sections from balb/c mice bearing micrometastases (day 5, 7) or larger metastases (day 10) were labelled with anti-CD3 (T-cells-red) and not many T-cells were found in the brain or within brain metastases. C: Increased numbers of T-cells were seen around and within brain metastases in late stages when the BBB was breached (determined by IgG immunoreactivity - red). CD3 staining of spleen tissue is shown as positive control. Scale bar represents 20 μ m (Scale bar in A is same for B).

Monocytes/macrophages have been described to modulate metastasis, therefore we characterised expression of monocyte/macrophage markers in tumour challenged brain sections (Figure 4.11). CD11b is expressed on all myeloid cells including microglia. Upon, CNS insult, CD11b expression is up-regulated on activated microglia, making it difficult at this point to differentiate between bright circulating cells from activated microglia. The same problem was encountered with the mature macrophage marker F4/80, where it was hard to distinguish between circulating bright cells and activated microglia. Very few CD11c cells were detected in brains of tumour injected mice and none were associated with intravascular tumour cells. Although Ly6C staining identified immune cells in spleen sections (Supplementary Figure 5), Ly6C also reacts with antigens expressed on brain vasculature making it difficult to identify immune cells (Alliot, Rutin et al. 1998).

All the available antibodies against different myeloid cell surface antigens were raised in rat, the same species used to raise anti-CD45 antibody therefore we could not perform co-labelling experiments. However, antibodies against the microglia/macrophage specific ionised calcium binding adaptor molecule-1 (IBA1) were made in rabbit, which enabled co-labelling with anti-CD45. Most tumour associated CD45^{hi} round cells were not positive for IBA1 (Figure 4.12 – day 3). Furthermore, in extravascular metastases, where CD45 expression is up-regulated in activated microglia surrounding the brain metastases, CD45^{hi}/ IBA1 negative cells were clearly seen within the tumour (Figure 4.12 – day 7). Thus, the tumour-associated CD45^{hi} cells were not activated microglia, nor were they perivascular or circulating macrophages.

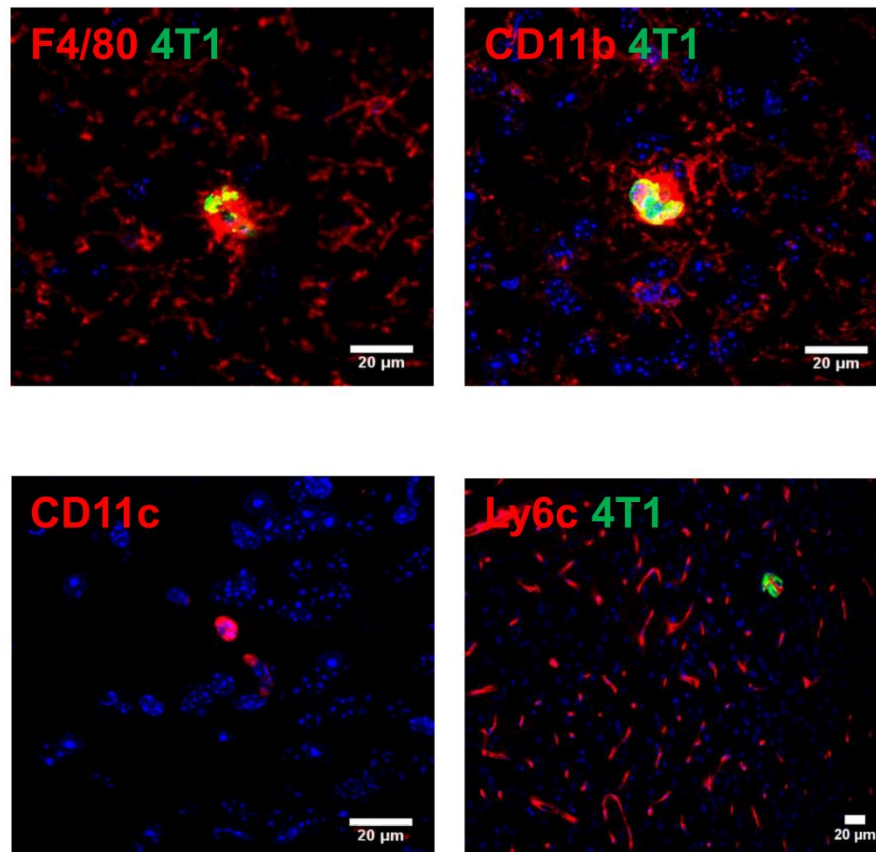


Figure 4.11: Identifying tumour associated immune cells using macrophage/myeloid cell markers

Brain tissue from mice collected 3 days post tumour injection with 4T1-GFP cells were labelled with several macrophage markers (red) to identify tumour associated immune cells. Increased expression of CD11b and F4/80 was noted around few tumour cells but as macrophages and activated microglia express similar levels of CD11b and F4/80, it was difficult to distinguish between the two cell types. Very few CD11c⁺ immune cells were seen in brain sections and none were associated with tumour cells. Ly6C, a monocyte/macrophage marker also reacts with blood vessels in the brain making it difficult to identify Ly6C⁺ immune cells in the brain. Positive controls for CD11c and Ly6C are shown in Supplementary Figure 5.

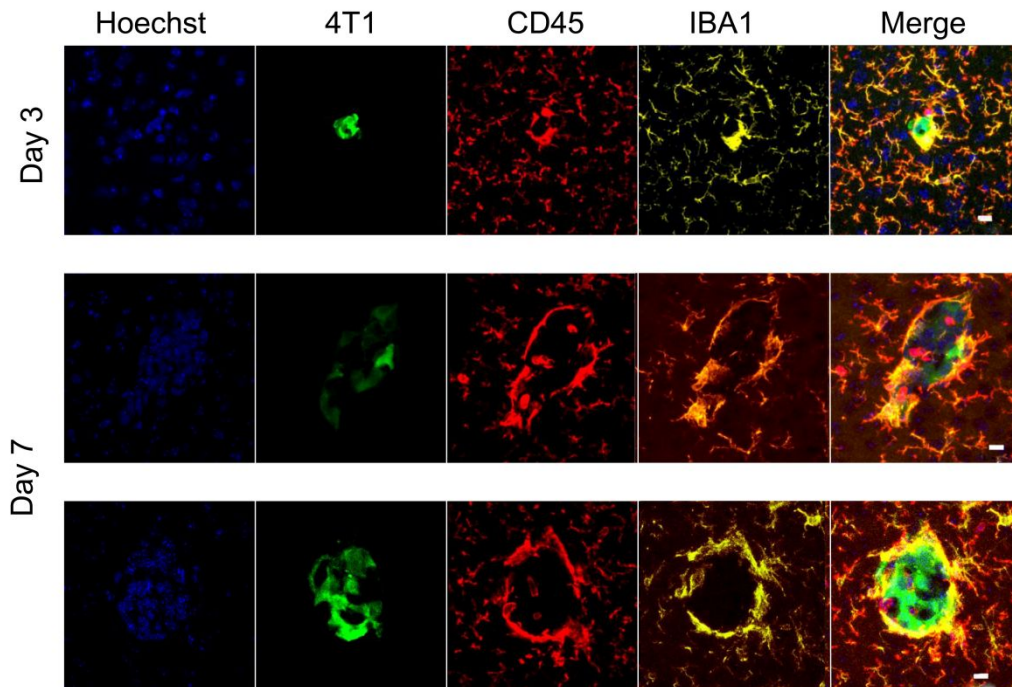


Figure 4.12: Some tumour associated CD45^{hi} cells do not express the macrophage/microglia marker IBA1.

Brain tissue from Balb/c mice injected with 4T1-GFP and culled 3 d and 7 d after tumour challenge were co-labelled with CD45 antibody and an antibody against the macrophage/microglia marker IBA1. Increased expression of CD45 around most tumours was also IBA1 positive. However, some CD45^{hi} cells were IBA1 negative and therefore neither microglia nor macrophages, but another immune cell of systemic origin. Scale bars represent 10 µm.

Myeloid derived suppressor cells (MDSC) and tumour associated neutrophils (TAN) have recently joined the repertoire of immune cells that promote primary tumour growth and metastasis. We looked for co-localisation of the tumour associated CD45^{hi} cells with markers for MDSC or TAN. Although Gr-1 and Ly6G are the standard markers, they are both raised in rat making it difficult to co-label with CD45. MBS, an antibody raised in rabbits against neutrophils were used to co-label mouse brain tissue collected 3 days after intracardiac injection of 4T1 or MDA 231. We saw consistent co-localization of MBS

positive cells with bright round tumour associated CD45^{hi} cells (Figure 4.13b). Further characterisation of the MBS positive cells by co-labelling indicated that these cells also expressed Gr-1 (Figure 4.14a). Gr-1 is expressed on neutrophils as well other myeloid cells, but Ly6G is specific marker for neutrophils therefore we quantified the number of tumour cells associated with either Gr-1⁺ or Ly6G⁺ cells in brains of mice culled 3 days after intracardiac injection of MDA-231 cells (Figure 4.14c). Both antibodies bound to immune cells in the brain and some of the Ly6G⁺ or Gr-1⁺ cells were associated with MDA-231 tumour cells (Figure 4.14b, c). However, fluorescent signal from tissue labelled with anti-Ly6G was weaker than tissue labelled with anti-Gr-1. Although visual scoring was possible with a weak signal, it was not possible to obtain an image with sufficient reduction of background fluorescence and no Ly6G images were captured.

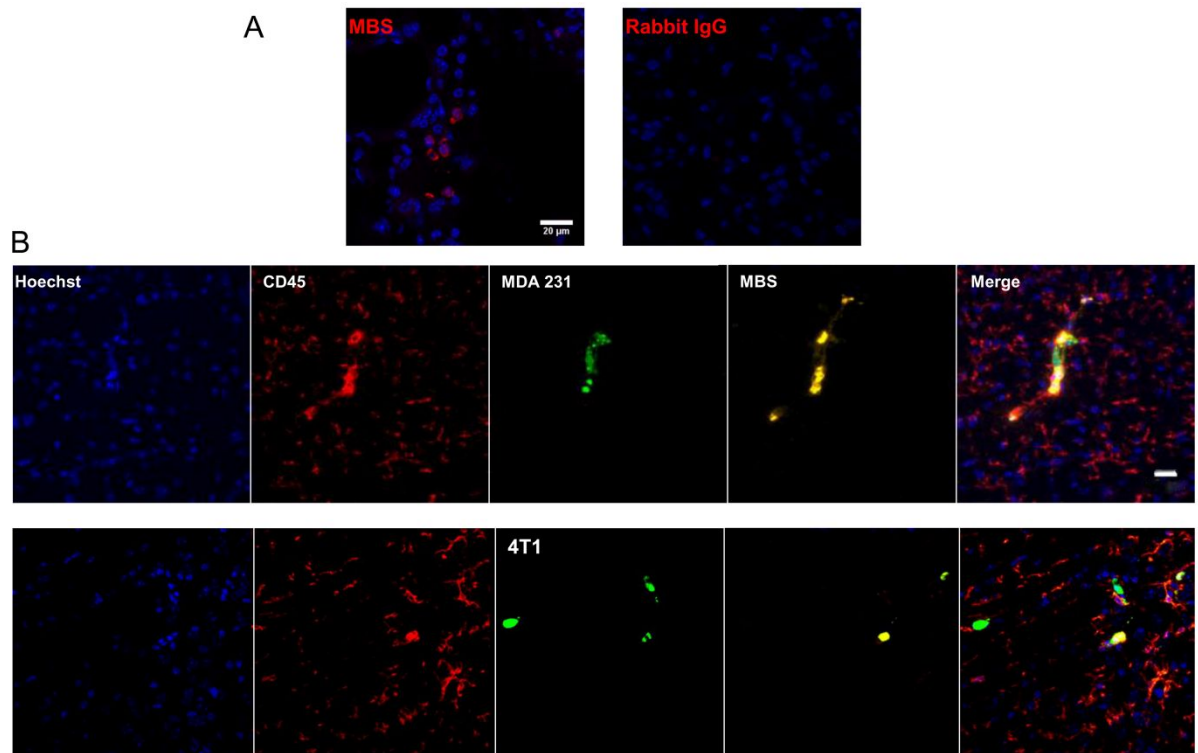


Figure 4.13: Tumour associated CD45^{hi} immune cells co-express the granulocyte marker MBS

A: Mouse lung tissue was labelled with the MBS antibody as a positive control. Adjacent lung tissue was labelled with rabbit IgG as an isotype control. B: Brain tissue from mice culled 3 days after intracardiac injections with either MDA 231 (top panel) or 4T1-GFP (bottom panel) were co-labelled with the MBS (yellow) and CD45 (red) antibodies and representative images are shown. Most CD45^{hi} bright round cells were MBS positive. Scale bars represent 20 μm.

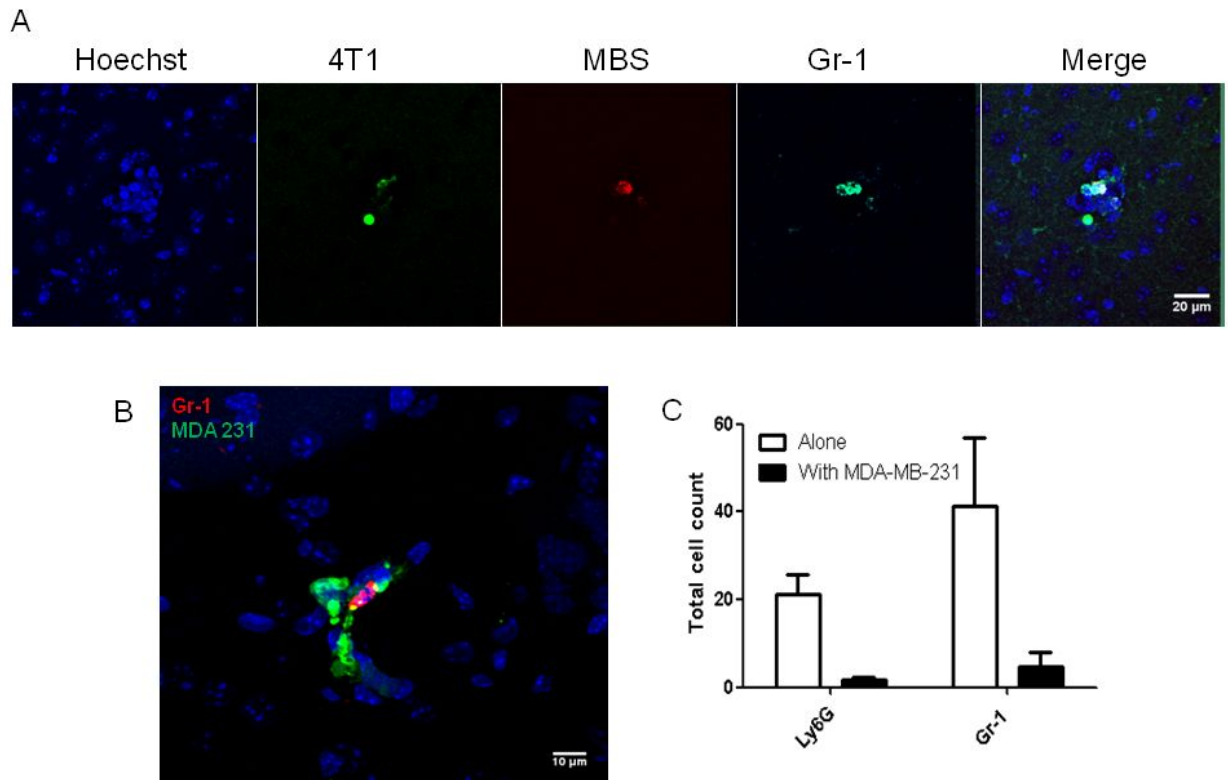


Figure 4.14: Both Gr-1⁺ and Ly6G⁺ immune cells are found in the brains of tumour injected mice.

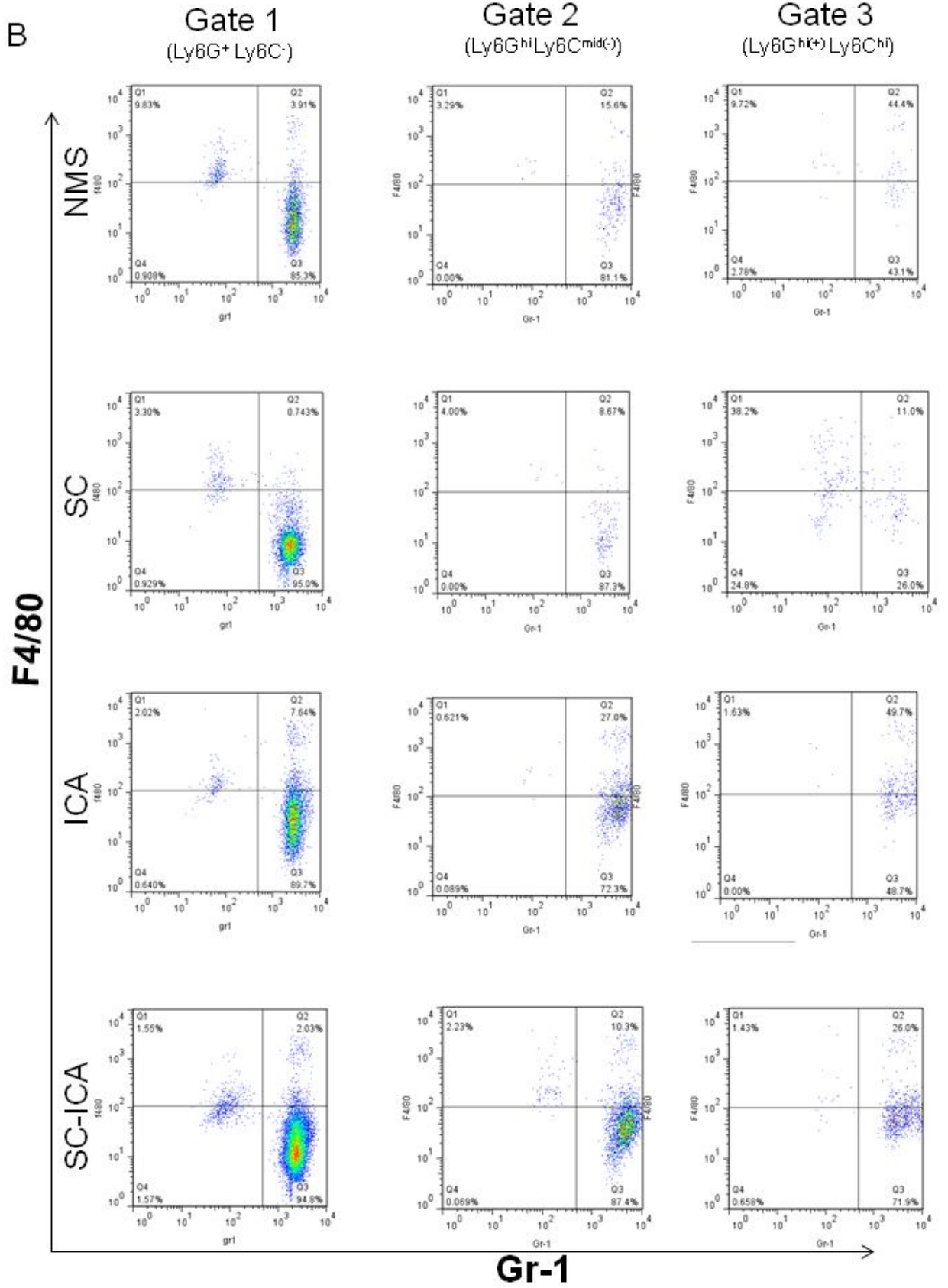
To identify whether tumour associated MBS⁺ immune cells in the brain are neutrophils or other granulocytes (eg. MDSCs), we analysed brain sections for the neutrophil specific marker Ly6G or the neutrophil/myeloid derived suppressor cell marker Gr-1. Ly6G⁺ cells in the brain were weakly positive and although the numbers of Ly6G⁺ cells could be quantified, it was not possible to obtain clear images and none are shown. A: Brain tissues from mice culled 3 days after intracardiac injection with 4T1-GFP were co-labelled with MBS as well as the neutrophils/myeloid derived suppressor cell marker Gr-1 and showed that MBS cells associated with brain metastatic cells also expressed Gr-1. B: A representative image showing Gr-1⁺ - MDA 231-GFP cluster in a brain section from mice culled 3 days post tumour challenge. C: The numbers of Gr-1⁺ and Ly6G⁺ cells in the brains of mice culled 3 days post cardiac challenge with MDA-231-GFP cells was quantified. Some tumour cells were found associated with Gr1⁺ and Ly6G⁺ immune cells (black bars). Data is presented as mean sum of total Ly6G⁺ or Gr-1⁺ cells counted in 18 brain sections (white bars) and as the mean sum of total number of Ly6G⁺ or Gr-1⁺ cells associated with tumour cells (black bars) in the same brain sections \pm SD (n= 2).

4.3.8 DIFFERENT POPULATIONS OF LY6G⁺ GRANULOCYTES ARE PRESENT IN BLOOD AFTER INTRACARDIAC INJECTION OF MDA 231 CELLS IN NAÏVE AND TUMOUR CONDITIONED MICE

We analysed cell populations in whole blood samples taken from SCID mice (normal mouse serum - NMS), SCID mice intracardiac injected with MDA 231-GFP (ICA), or mice pre-conditioned with a MDA 231 subcutaneous tumour prior to intracardiac injection with PBS (SC) or MDA 231-GFP (SC-ICA) (See Figure 4.15a for method outline). Blood was collected from mice 3 days after intracardiac injection and 50,000 white blood cells per sample were analysed using four-colour FACS. Total live cells (gated based on forward and side scatter data) were analysed based on surface marker expression. Gating strategy was based on single stained and isotype stained controls (Supplementary Figure 4).

As brain tissue co-labelling experiments indicated that the tumour associated immune cells were granulocytes, we focused on the Ly6G⁺ population. Within the Ly6G⁺ gate, we identified three different populations based on Ly6C expression: gate 1 - Ly6G⁺Ly6C⁻, gate 2 - Ly6G^{hi}Ly6C^{mid(-)} and gate 3 - Ly6G^{hi(+)}Ly6C^{hi} (Figure 4.15a). The three Ly6G⁺ populations (gates 1,2,3) were further separated based on surface expression of F4/80 and Gr-1 (Figure 4.15b) and each population was quantified as a percentage of total live cells (Figure 4.15c). In normal blood, most Ly6G⁺ cells were Ly6C⁻ (gate 1, neutrophils). The number of Ly6G⁺Ly6C⁻ cells increased 1.5-fold in SC and ICA mice and 4.5-fold in SC-ICA mice when compared to control blood. In all groups, the Ly6G⁺Ly6C⁻ populations were mostly Gr-1⁺F4/80^{low/-} while in SC mice, this population was Gr-1⁺F4/80⁻. A few cells seen in all groups were Gr-1⁻F4/80^{low} and Gr-1⁺F4/80^{hi}. In normal and SC blood, the numbers of

Ly6G^{hi}Ly6C^{mid(-)} cells (gate 2) were similar (0.258% of control blood and 0.264% of SC blood) and were predominately Gr-1⁺F480⁻. This cell population increased 5-fold in blood of naïve mice after intracardiac injection (ICA) and 13.5-fold in primary tumour conditioned mice after intracardiac injection (SC-ICA). These were also mainly Gr-1⁺F480⁻ but shifted up and to the right compared to blood from control and SC mice and to take on a Gr-1^{hi}F4/80^{low} phenotype. The Ly6G^{hi(+)}Ly6C^{hi} population (gate 3) increased approximately 2 fold in blood from SC and ICA mice and increased 6 fold in blood from SC-ICA mice compared to blood from control mice. These cells from gate 3 were mostly F480⁻ and Gr-1⁺ in control and SC mice. There were also a greater number of cells from gate 3 that were Gr-1⁻F4/80⁺ in blood from SC mice that was not present in blood of all other groups. As seen with gate 2, in blood of ICA and SC-ICA, the Ly6G^{hi(+)}Ly6C^{hi} cells in gate 3 had shifted up to be F4/80^{low} and two Gr-1 populations are seen, Gr-1⁺ and Gr-1^{hi}.



C

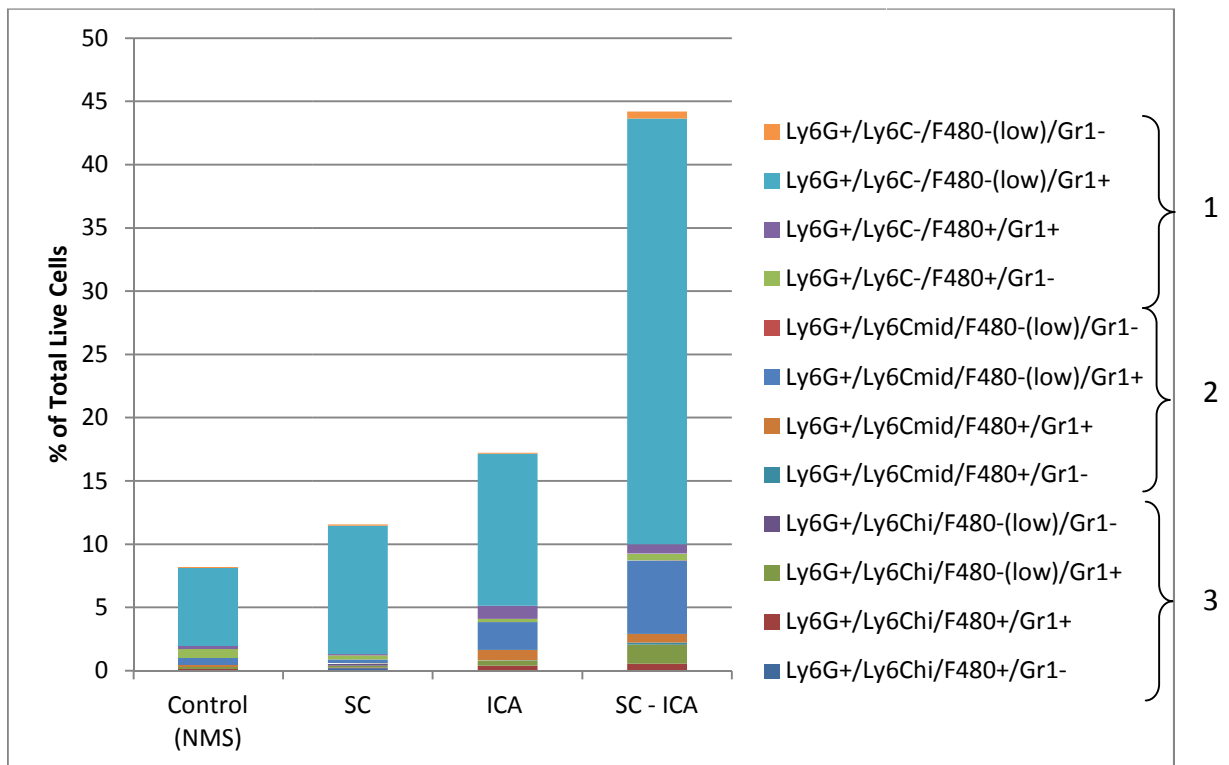


Figure 4.15: Blood from naïve or primary tumour bearing mice analysed 3 days after intracardiac injection with MDA 231 mice harbour different populations of Ly6G⁺ cells

A: Naïve or tumour bearing SCID mice were intracardiac injected with 10^5 MDA 231-GFP cells (ICA vs. SC-ICA). Some mice bearing a primary tumour were intracardiac injected with PBS (SC). Mice were culled 3 days after intracardiac injection and anti-coagulated blood were collected and processed for FACS analysis. Blood from naïve age-matched SCID mice (NMS) served as controls. Live cells were gated according to Ly6G (y-axis) and Ly6C (x-axis) expression and three Ly6G⁺ populations were identified: (Gate 1) Ly6G⁺Ly6C⁻, (Gate 2) Ly6G^{hi}Ly6C^{mid}, (Gate 3- all of quadrant 3) Ly6G^{+/hi}Ly6C^{hi}.

B: The three gated Ly6G⁺ populations from (A) were further classified based on F4/80 and Gr-1 expression. Gating strategy was based on single stains and isotype controls (Supplementary Figure 4)

C: The Ly6G⁺ populations in blood from control or experimental mice (as outlined in A) were separated into 12 populations based on expression of Ly6C, F4/80 and Gr-1 (from B). Each population was quantified as a percentage of total live cells. Data shown is representative of one mouse from each group (n=2).

4.3.9 INTRAVASCULAR TUMOUR ASSOCIATED IMMUNE CELLS EXPRESS F4/80

To determine if the populations detected in blood of tumour challenged mice correlate with immune cells found interacting with intravascular tumour cells in the brain, we assessed brain tissue for cells which express F4/80. Previous labelling of immune cells with Ly6C antibody proved to be unsuccessful as anti-Ly6C also binds to brain vasculature (Figure 4.11). We co-labelled brain tissues taken from mice 3 days after cardiac injection with 4T1-GFP with MBS and F4/80 antibodies and found tumour associated MBS⁺ cells to co-localise with F4/80⁺ cells (Figure 4.16)

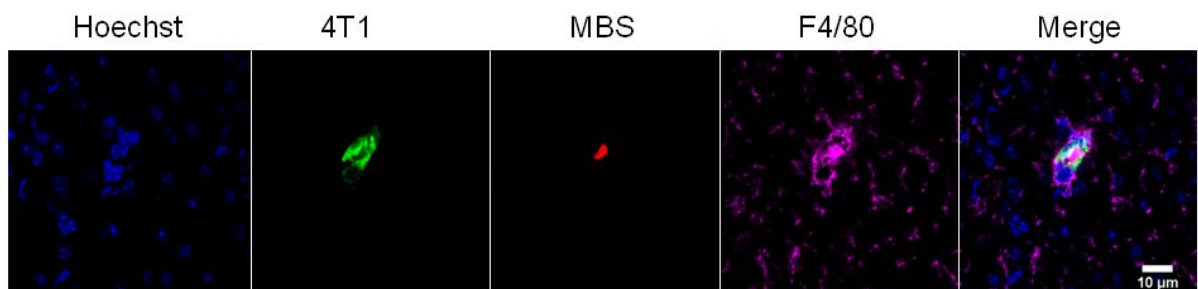


Figure 4.16: Brain metastatic cell-associated MBS⁺ cells co-localise with F4/80⁺ cells

Brain tissue harvested from mice 3 days after intracardiac injection with 4T1-GFP were labelled with antibodies against GFP, MBS, and F4/80 antigens. MBS⁺ cells associated with 4T1-GFP also co-localised with F4/80⁺ cells and may be the same cell (MBS⁺F4/80⁺).

4.4 DISCUSSION

Previous studies analysing tumour cell arrest and survival at the brain vasculature and subsequent extravasation of the metastatic cells into the brain have concluded that survival within the brain vasculature is the key limiting step that determines whether disseminated cancer cells develop into brain metastases (Kienast, von Baumgarten et al. 2010; Loriger and Felding-Habermann 2010). Here, we showed that not all metastatic cells intracardiac injected formed brain metastasis because some metastatic cells lacked the ability to adhere to the brain endothelium. Therefore, adhesion may precede survival as the limiting step in determining successful brain metastasis. However, after adhesion, survival within the blood vessel becomes an important step and we showed that the number of intravascular tumour cells arrested in the brain quickly diminished, and few cells remained to extravasate. Intravascular tumour cells were not alone, as some were found associated with circulating immune cells. These tumour-immune cell clusters persisted over time whilst solitary tumour cells declined. We focused on identifying the phenotype of the tumour-associated leukocytes in this chapter. The role of these cells will be addressed in the following chapter.

Using ultrasound guidance to inject tumour cells into the heart, we were able to quantify and compare the behaviour of different metastatic cells after release into the circulation. Although LLC and B16-F10 cells were capable of adhering to the lung vasculature hours after tail vein injection (unpublished data and Gil-Bernabe, Ferjancic et al. 2012), it was rare to find these tumour cells within the brain vasculature a few hours after intracardiac tumour injection. Previous studies have used the intracardiac route to deliver LLC

tumours cells into mice to study extravasation of these cells into brain, liver and adrenals. Although sufficient cells were found in the endothelium of the liver and adrenals to perform data analysis, not many cells were found in the brain vasculature and the authors switched to intracarotid injection to deliver more cells to the brain (Paku, Dome et al. 2000). This finding implies that the intracardiac route of injection is not a cause of failed attachment to the brain and is more likely due to the genetic make-up of these tumour cells. LLC cells have the ability to attach onto lung, liver and adrenal endothelium and form metastases at these sites but lack brain specific adhesion molecules and are therefore weakly brain metastatic. *In vitro* studies have compared adhesion of prostate cancer cells derived from brain metastases with primary prostate cancer cells (Brayton, Qing et al. 1998). Whilst primary cancer cells showed increased adhesion to inflamed brain endothelium, no difference in adhesion was found with the brain derived cell line. Here, we show that mice pre-conditioned with a brain metastatic primary tumour (4T1) did not increase the adhesion of highly or poorly brain metastatic cells (4T1 compared to LLC cells). Although in the *in vitro* studies, different inflammatory conditions may have been induced (tumour necrosis factor (TNF) and IL-1 α), it seems likely that the ability of metastatic cancer cells to adhere different endothelium is an inherent ability that determines organ-tropism. These findings also imply that mechanical entrapment of tumour cells within brain capillaries does not contribute to successful brain metastasis in our models.

Although identifying factors that mediate tumour adhesion to the brain vasculature was not within the scope of this work, we did look at tumour cell expression of ST6GALNAC5.

Expression of this particular protein was shown to be a key factor for human breast cancer metastasis to the brain (Bos, Zhang et al. 2009). LLC, a poorly brain-metastatic lung cell line expressed the protein implying that ST6GALNAC5 is not sufficient for promoting brain metastasis in non-breast cancer cells. LLC cells may require additional factors that are only expressed by breast cancer cells. However, the lack of ST6GALNAC5 expression on 4T1 murine breast cancer cells signify that other factors are involved that promote tumour cell adhesion to the brain vasculature and subsequent extravasation into the brain.

In experimental and spontaneous models of metastasis, inhibition of coagulation reduces metastatic burden (Camerer, Qazi et al. 2004; Palumbo, Talmage et al. 2005). Platelets aggregating with circulating tumour cells protect tumour cells from destruction by NK cells and blood flow (Palumbo, Talmage et al. 2005). Platelets may also mediate arrest of tumour cell at the secondary site by providing bulk and engaging signalling molecules on blood vessels (Laubli and Borsig 2010). We found that within 8 h after tumour injection of highly and weakly brain metastatic cells, the majority of tumour cells adherent to the brain cohered with platelets. However, the inability of LLC and B16F10 to adhere to the brain vasculature may be due to reduced ability of these cells to interact with platelets whilst in the circulation. Although we did not look at circulating tumour cells, other studies have shown that this is not the case. Within 8 h after tail vein injection, LLC and B16 F10 cells bound to the lung were coated in platelets and in long term metastasis assays, both these cell lines developed multiple lung metastases (Gil-Bernabe, Ferjancic et al. 2012) while anti-platelet therapy reduced retention of LLC and B16 F10 cells in the lung

(Zhang, Dang et al. 2012). Therefore, LLC and B16F10 were fully capable of interacting with platelets whilst in the circulation and platelets most likely do not influence adhesion of the brain metastatic cells to brain endothelium.

Metastatic inefficiency is a well known phenomenon described as the inability of most disseminated tumour cells to give rise to fully fledged macroscopic metastases. A manifestation of metastatic inefficiency is the decline in the number of circulating or vascular adherent tumour cells after introduction into the circulation. Our results are consistent with this concept. Although significantly more MDA 231 cells initially adhered to brain endothelium compared to 4T1 cells, 4T1 cells produced more brain metastases. Others have shown that *in vitro*, greater number of primary prostate cells adhered to normal and inflamed brain endothelial cells than brain metastatic prostate cancer cells (Brayton, Qing et al. 1998). Therefore adhesion of tumour cells to the brain endothelium may be an essential prerequisite for brain metastasis, but to develop into metastases, other factors subsequently become important.

Assuming that all adherent brain metastatic cells have equal opportunity to form brain metastases, we asked whether host derived cellular factors may play a part in survival and extravasation. We have shown that platelets most likely do not play a role in tumour cell adhesion to the brain and our data also imply that platelets alone also do not mediate survival of intravascular tumour cells. We found that although the majority of intravascular 4T1 cells were coated in platelets, the number of surviving tumour cells declined with time. However, platelets secrete cytokines to recruit immune cells and also express adhesion receptors that bridge immune cells to sites of damage and inflammation

(von Hundelshausen and Weber 2007; Mazzucco, Borzini et al. 2010). This homing of immune cells to platelet clots has been shown to enhance lung metastasis (Gil-Bernabe, Ferjancic et al. 2012; Zhang, Dang et al. 2012). In line with this, we used an antibody against CD45, a pan leukocyte marker, to determine whether intravascular brain metastatic cells interacted with circulating immune cells. Anti-CD45 was used as it allows for discrimination between quiescent microglia ($CD45^{low}$) and circulating immune cells ($CD45^{hi}$). However, at time-points beyond day 3 post tumour injection, tumour cells began to extravasate, causing activation of nearby microglial cells. Activated microglia up-regulate expression of CD45 and are therefore become indistinguishable from circulating immune cells by CD45 expression alone. In this case, we also took into account size and shape of the $CD45^{hi}$ cells. With this in mind, we did see early association (4-8 h) of few 4T1 and MDA 231 tumour cells with $CD45^{hi}$ immune cells. This association persisted whilst solitary tumour cells declined over time. When we compared all metastatic cell lines within the brain vasculature at 24 h post tumour injection, we found that although more MDA 231 cells adhered to brain vessels compared to 4T1, there were more 4T1- $CD45^{hi}$ clusters than MDA 231- $CD45^{hi}$ clusters. The number of tumour cells associated with $CD45^{hi}$ immune cells rather than total number of cells that initially arrested within blood vessels corresponded with number of brain metastases formed by 4T1 and MDA 231 cells. This implies that the presence of $CD45^{hi}$ cells around arrested brain metastatic cells may be important in aiding the formation of brain metastasis. There were only a few instances where $CD45^{hi}$ cells were adjacent to LLC. Most LLC- $CD45^{hi}$ clusters were

found in the olfactory bulb, a location where LLC sometimes forms extravascular brain metastases (Chapter 3, Figure 3.5).

To determine whether the tumour associated immune cells contribute to brain metastasis, we performed experiments where mice bearing primary tumours were intracardiac injected with tumour cells (pre-conditioned mice). Brains from pre-conditioned mice culled 3 days after intracardiac injection had significantly more intravascular tumour cells associated with CD45^{hi} immune cells and this correlated with increased brain metastases compared to unconditioned mice. Whilst insignificant, surprisingly, a slight decrease in total adherent 4T1 and MDA 231 cells were noted in pre-conditioned brains compared to brains from control mice. There may be several explanations for this observation. Factors secreted by the primary tumours have been shown to direct metastases (Kaplan, Riba et al. 2005) and 4T1 and MDA 231 may favour metastases to other organs such as the lung. Circulating tumour cells have also been shown to re-populate the primary tumour (Kim, Oskarsson et al. 2009). Therefore, after intracardiac injection in pre-conditioned mice, a fraction of the cells may home to the lung or primary tumour decreasing the number of tumour cells that arrest in the brain. Others have shown that 4T1 primary tumours recruit neutrophils to the lung to destroy disseminated tumour cells seeding the lung (Granot, Henke et al. 2011) and a similar mechanism may play a role in tumour pre-conditioned brains. Even with this slight decrease in total adherent tumour cells, pre-conditioned mice appeared to harbour more brain metastases compared to control mice. However, this increase in brain metastases was only significant in the MDA 231 pre-conditioning model. As noted in Chapter 3, 2

weeks after intracardiac injection of the same number of tumour cells, 4T1 cells formed multiple large metastases whilst very infrequent and small brain metastases were formed by MDA 231 cells. 4T1 cells are potent producers of several inflammatory cytokines and growth factors *in vitro* and *in vivo* (DuPre and Hunter 2007; DuPre, Redelman et al. 2007) and the intracardiac dose of these cells alone may contribute to sufficient quantities of these pro-tumourigenic factors required to recruit CD45^{hi} cells to intravascular tumours. A study comparing lung metastases formed in mice implanted with either 4T1 or MDA 231 primary tumours showed that mice with primary MDA 231 tumours had 10-fold less G-CSF levels in serum compared to mice bearing 4T1 primary tumours. Due to the reduced levels of G-CSF, mice bearing MDA 231 primary tumours recruited far less metastasis associated immune cells to the lung, and had less lung metastases when compared to mice bearing 4T1 primary tumours (Kowanetz, Wu et al. 2010). Therefore, the intracardiac dose of MDA 231 cells alone may not be sufficient to produce enough factors to quickly recruit CD45^{hi} cells to intravascular tumour cells and this cell line may be more reliant on pre-conditioning than 4T1.

The slower time of MDA 231 cells to extravasate into the brain compared to 4T1 may also explain why pre-conditioning had more affect on MDA 231 cells compared to 4T1. Whilst the majority of 4T1 cells had extravasated by day 5 post tumour injection, some MDA 231-Br cells remained intravascular even at day 7 (Lorger and Felding-Habermann 2010). As MDA 231 cells are reported to be less brain metastatic than MDA 231-Br, far more MDA 231 tumour cells may remain intravascular at day 7 post tumour cell injection. When we assessed the number of surviving tumour cells in brains of mice over time,

although there were significantly more MDA 231 cells at 4 h after tumour cell injection compared to 4T1, the numbers of surviving MDA 231 cells continued to decline past 3 days whereas the numbers of surviving 4T1 cells remained steady from 3 days onwards. Therefore, it seems that in our model, most surviving 4T1 cells also extravasate by day 3 whereas MDA 231 cells most likely do not start extravasation until day 5 or later. We also start to see several CD45^{hi} cells around intravascular 4T1 cells around day 3-5 post tumour injection but only start to see the same clustering at day 7 in the MDA 231 model. We hypothesise that the pre-conditioning in the MDA model enables CD45^{hi} cells to be present around intravascular tumour cells days before they would be in naïve intracardiac injected mice (3-5 days vs. 5-7days) allowing surviving cells to extravasate faster and avoid clearance by blood flow or NK cells. This will therefore result in more tumour cells developing into brain metastases. As 4T1 cells extravasate as early as 3 days post tumour injection, the early presence of CD45^{hi} immune cells in the pre-conditioning model may only makes a marginal increase to the number of brain metastases in 4T1 pre-conditioned mice.

The positive correlation between increased tumour-immune clusters and increased brain metastases implies that these tumour associated immune cells may be important for successful brain metastases. To elucidate the role of these immune cells, it was first important to identify their phenotype. We were able to rule out that these cells were macrophages/microglia due to the absence of IBA1 expression on tumour associated CD45^{hi} cells. Co-labelling brain tissue with CD45 and MBS antibodies indicated that tumour associated CD45^{hi} cells also expressed MBS. MBS is described to be a neutrophil

specific marker (D. Anthony, University of Oxford - personal correspondence) but we then showed that the tumour associated MBS⁺ cells co-expressed Gr-1. Gr-1 is expressed on neutrophils, immature granulocytes, MDSC, eosinophils, dendritic cells, and few T cells (Tepper 1994; Nakano, Yanagita et al. 2001; Ribechini, Greifenberg et al. 2010). To identify whether these cells were neutrophils or other Gr-1⁺ cells, we used Ly6G (neutrophil specific) or Gr-1 antibodies to stain brain sections from mice culled 3 days after intracardiac injection with MDA 231 cells. Although the total numbers of Ly6G⁺ cells in the brain were slightly less than the Gr-1⁺ cells, both were found associated with a few intravascular MDA 231 cells. The Gr-1 epitope is composed of both Ly6C and Ly6G and the anti-Ly6G antibody binds to the Ly6G epitope on Gr-1 cells (Ribechini, Leenen et al. 2009). This cross-reactivity has been described with the neutrophil marker NIMP-R14, which is reported to be neutrophil-specific (Lopez, Strath et al. 1984), but also binds to cells identified as Gr-1⁺ (Henderson, Hobbs et al. 2003). MBS may also bind to the Ly6G epitope on Gr-1⁺ cells as we found co-localisation of MBS⁺ cells with Gr-1⁺ cells. This leaves two possibilities: in the brains of tumour injected mice, there could be a mixed neutrophil and Gr-1⁺ myeloid population or the majority of these immune cells are Gr-1⁺ myeloid cells but the Ly6G portion of the Gr-1 epitope is also recognised by MBS and Ly6G antibodies (Ribechini, Leenen et al. 2009).

To be able to detect several surface markers on individual immune cells and identify immune populations within the blood that may be associated with brain metastasis, we used FACS to analyse blood from MDA 231-conditioned mice and controls. In blood from naïve SCID mice, the majority of Ly6G⁺ cells were Ly6C⁻, F4/80⁻ and Gr-1⁺ and further

analysis of their size and granularity indicate that these were neutrophils. The neutrophil population increased in all experimental groups with substantial increase in primary tumour bearing mice after intracardiac injection with tumour cells. There was a population of $F4/80^{\text{low}}$, $Gr-1^-$ cells in the neutrophil gate that did not differ in number between experimental groups and are most likely to be contaminating blood monocytes.

With the exception of control blood, $Ly6G^+$ populations with $Ly6C^{\text{mid}}$ or $Ly6C^{\text{hi}}$ expression were evident in all experimental groups. Intracardiac injection of tumour cells in preconditioned mice substantially increased all three $Ly6G$ gated populations ($Ly6G^+Ly6C^-$, $Ly6G^{\text{hi}}Ly6C^{(-)\text{mid}}$ and $Ly6G^{(+)/\text{hi}}Ly6C^{\text{hi}}$) in the blood compared to all other groups. In unconditioned mice that were intracardiac injected with tumour cells, there was a substantial increase in the $Ly6G^{\text{hi}}Ly6C^{(-)\text{mid}}$ population compared to primary tumour alone and control blood. In blood of primary tumour bearing mice intracardiac injected with PBS, there was no increase in the number of $Ly6G^{\text{hi}}Ly6C^{(-)\text{mid}}$ cells but the number of cells in the $Ly6G^{(+)/\text{hi}}Ly6C^{\text{hi}}$ increased compared to blood from control mice. Interestingly, within the $Ly6G^{(+)/\text{hi}}Ly6C^{\text{hi}}$ only mice bearing primary tumours and intracardiac injected with PBS (SC) had increased numbers of $Gr-1^-F4/80^+$ cells (macrophages). This finding suggest that when there is only a primary tumour, factors secreted by the primary tumour or tumour associated stroma may only recruit myeloid cells required for primary tumour growth (possibly $Ly6C^{\text{hi}}Gr-1^-F4/80^+$ TAM precursors). In primary tumour bearing mice, only when tumour cells are detected in the circulation (after intracardiac injection) are increased numbers of metastasis promoting immune cells recruited into the circulation ($Ly6G^{(+)/\text{hi}}Ly6C^+$). Circulating immune cells may engage with circulating

immune factors such as myeloid cells and/or platelets or even engage endothelium to stimulate the recruitment of metastasis promoting immune cells (Laubli, Spanaus et al. 2009)

The Ly6G⁺Ly6C⁻ blood populations (gate 1 - neutrophils) were mostly Gr-1⁺. A shift to Gr-1^{hi} was only seen in the Ly6G^{hi}Ly6C^{mid(-)} (gate 2) and Ly6G^{(+)/hi}Ly6C^{hi} (gate 3) population in blood from SC-ICA and ICA mice. Only the Gr-1^{hi} cells were shifted towards F4/80⁺ compared to Gr-1⁺ cells (F4/80^{low/-}). These data indicate that there may in fact be two populations detected in the brain, Ly6G⁺ Ly6C⁻F4/80⁻Gr-1⁺ neutrophils and Ly6G⁺Ly6C^{mid/hi}F4/80^{low}Gr-1^{hi} granulocytes and we may be able to differentiate which population interacts with intravascular tumour cells by staining for Ly6C or F4/80 in the brain. As the Ly6C antibody also binds to brain endothelium (Alliot, Rutin et al. 1998), we found it difficult to stain for Ly6C⁺ cells that may be attached to brain endothelium but we were able to assess F4/80⁺ cells in the brain. Even though F4/80 is expressed on microglia and macrophages, when we stained brains from mice culled 3 days after intracardiac injection of 4T1-GFP cells, we saw F4/80⁺ microglia around the tumour but also found co-localization of F4/80⁺ cells with MBS⁺ tumour associated immune cells. Although this finding suggests that the tumour associated immune cells are most likely not neutrophils, we were not able to quantify co-localisation of these markers over the time course of brain metastases development to determine if all MBS⁺ cells associated with intravascular tumour cells were also F4/80⁺.

The findings in this chapter indicate that host immune cells may play a role in aiding brain metastasis. We showed that tumour-bearing mice subsequently intracardiac injected

with tumour cells harboured more brain metastases than non tumour-bearing mice. This is not due to increased number of tumour cells adhering to the brain vasculature in tumour-bearing mice, but may be due to faster recruitment of brain metastasis promoting immune cells to intravascular tumour cells. 4T1 cells secrete a plethora of factors that recruit a mixed population of myeloid cells into the circulation (DuPre, Redelman et al. 2007) and some of these factors have been shown to promote lung metastasis (Kowanetz, Wu et al. 2010). The intracardiac dose of MDA-231 cells may not be as robust as 4T1 cells in quickly recruiting metastasis promoting immune cells and this may explain why although significantly more MDA-231 cells adhered and survived within brain vessels compared to 4T1 cells, they produced far fewer brain metastases. We have identified our brain metastasis associated host cells to be Gr-1⁺ circulating immune cells but whether they are neutrophils or other Gr-1⁺ immune cells is yet to be verified. Further functional studies are also needed to show convincingly that these cells are necessary for successful brain metastasis.

CHAPTER 5: IDENTIFYING THE FUNCTION OF GR-1⁺ CELLS ASSOCIATED WITH INTRAVASCULAR BRAIN METASTATIC TUMOUR CELLS

5.1 INTRODUCTION

5.1.1 CD11b⁺GR-1⁺ CELLS

CD11b⁺ Gr-1⁺ immature myeloid cells are present in high numbers in peripheral blood of cancer patients (Diaz-Montero, Salem et al. 2009; Nagaraj and Gabrilovich 2010; Raychaudhuri, Rayman et al. 2011) and spleen and blood of tumour bearing mice (Nagaraj

and Gabrilovich 2007). These immune cells contribute to cancer progression and metastasis (Diaz-Montero, Salem et al. 2009; Ostrand-Rosenberg and Sinha 2009; Nagaraj and Gabrilovich 2010) by dampening T-cell anti-tumour activity and are therefore referred to as myeloid derived suppressor cells (MDSC) (Nagaraj, Schrum et al. 2010; Dumitru, Moses et al. 2012; Youn, Collazo et al. 2012).

MDSCs are composed of a heterogeneous population of immature bone marrow derived cells. The Gr-1 surface marker used to identify MDSC is composed of both the Ly6G and Ly6C epitopes and expression levels of each epitope depend on the subtype of MDSC (Gabrilovich, Bronte et al. 2007; Ribechini, Greifenberg et al. 2010). The subsets of MDSC are loosely classified as monocytic ($Gr-1^{int/low} - Ly6G^{low}Ly6C^{int/hi}$) or granulocytic ($Gr-1^{int/hi} - Ly6G^{int/hi}Ly6C^{low}$) and each subset has similar nuclear morphology as neutrophils or monocytes (Dolcetti, Peranzoni et al. 2010; Peranzoni, Zilio et al. 2010). Normal neutrophils and monocytes are also identified based on surface marker expression of Gr-1 and either Ly6G ($Gr-1^+$ - neutrophils) or Ly6C ($Gr-1^{low}$ - monocytes) (Peranzoni, Zilio et al. 2010). Therefore, MDSC are indistinguishable from normal counterparts by phenotyping alone and are often identified based on T cell suppressor functions (Kusmartsev, Nagaraj et al. 2005; Nagaraj and Gabrilovich 2010; Dumitru, Moses et al. 2012). Antibodies against Ly6G have been used to deplete neutrophils (Daley, Thomay et al. 2008; Granot, Henke et al. 2011). While the Gr-1 antibody has also been reported to also deplete neutrophils (Granot, Henke et al. 2011), its effects on non-neutrophil Gr-1 expressing cells, which include a subset of blood monocytes (Geissmann, Jung et al. 2003), plasmacytoid dendritic cells (Nakano, Yanagita et al. 2001), and MDSCs (Ostrand-

Rosenberg and Sinha 2009) are not clear (Ribechini, Leenen et al. 2009; Wojtasiak, Pickett et al. 2010).

MDSCs are primarily recruited by tumour derived granulocyte colony stimulating factor (G-CSF) and granulocyte macrophage colony stimulating factor (GM-CSF) (Bronte, Chappell et al. 1999; Shojaei, Wu et al. 2009; Dolcetti, Peranzoni et al. 2010; Waight, Hu et al. 2011). Under normal conditions, these colony growth factors are produced by immune cells and endothelial cells and are essential for egress of granulocytes and monocytes from bone marrow into the circulation (Semerad, Liu et al. 2002; Hamilton and Anderson 2004).

Although, nothing is known about these cells in relation to brain metastasis, they have been shown to be present in primary brain tumours. Macrophages and microglia have been found to infiltrate human glioma but did not have the capability to stimulate anti-tumour T-cell responses (Hussain, Yang et al. 2006) and normal human monocytes take on MDSC-like properties when exposed to glioma cells (Rodrigues, Gonzalez et al. 2010). Recently, MDSCs have been shown to be present in peripheral human blood of glioma patients (Raychaudhuri, Rayman et al. 2011). The majority of the human MDSCs were of the granulocytic sub-type and suppressed T-cell functions *ex vivo*. In mouse models of glioblastoma, Ly6G⁺Ly6C^{low} MDSC cells were found in the brain where they supported tumour growth (Jia, Jackson-Cook et al. 2010; Fujita, Kohanbash et al. 2011).

In addition to being involved in T-cell immunity, CD11b⁺Gr-1⁺ (Ly6G⁺Ly6C⁺) granulocytes have been identified in pre-metastatic lungs where they produced MMP-9, S100A8,

S100A9, and Bv8 pro-inflammatory factors that promoted 4T1 breast cancer cells to metastasise to the lung (Kowanetz, Wu et al. 2010; Yan, Pickup et al. 2010). Whether these cells participate in promoting tumour cells to colonise the brain remains to be determined.

5.2 HYPOTHESIS

Gr-1⁺ granulocytes support brain metastatic cells arrested in the brain vasculature to survive and/or extravasate into the brain.

5.3 AIMS

In the previous chapter, we had identified Gr-1⁺ cells associated with a few intravascular brain metastatic cells. Here, we aim to identify the role of these cells by using three different experimental modalities. **First we will use antibodies to specifically deplete neutrophils and/or other Gr-1 expressing cells to determine the effects of these immune cells on brain metastasis. Secondly, we will induce brain metastases in mice which have been adoptively transferred with immune cells from tumour bearing mice to determine whether we can augment the development of brain metastases. Thirdly, we will identify factors secreted by tumour cells and/or host cells that may recruit brain metastasis associated Gr-1⁺ cells. We can then deplete these factors to determine whether they affect the development of brain metastases.**

5.4 MATERIALS AND METHOD

5.4.1 *IN VIVO* NEUTROPHIL AND GR-1 CELL DEPLETION ASSAY

Neutrophil depletion *in vivo* using antibodies against Ly6G and Gr-1 has been described in (Granot, Henke et al. 2011). In brief, to specifically deplete neutrophils, mice were injected i.p with 12.5 µg of anti-mouse Ly6G antibody (BD Bioscience), or isotype control 24 h before intracardiac injection of either 10^5 4T1 or MDA 231 GFP expressing tumour cells. To confirm depletion, blood was collected 24 h and at other time points after injection of antibodies from a tail prick using a 20 µl pipette tip filled with EDTA and analysed by FACS (Figure 5.1). The FACS protocol for blood analysis is described in the Materials and Method section of Chapter 3. Ly6G antibody was injected daily for 7 days (4T1 injected mice) or 15 days (MDA-231 injected mice). Mice were culled either 8 d (4T1) or 25 d (MDA-231) after tumour challenge, and brains and anti-coagulated blood were collected. Blood was analysed by FACS after *ex vivo* labelling with Ly6G, Ly6C, F4/80 and Gr-1 antibodies. Brain sections were labelled with anti-GFP and the numbers of brain metastases were quantified in 18 representative brain sections per mouse.

To deplete neutrophils and possibly other Gr-1 expressing cells, mice were injected i.p with 12.5 µg or 50 µg of anti-mouse Gr-1 antibody. Depletion was confirmed as described above and depleted mice were then intracardiac injected with 10^5 tumour cells expressing GFP. Due to the toxic effects of Gr-1 antibody, mice were culled either 6 days (MDA 231) or 5-8 days (4T1) post tumour challenge, to collect brains and anti-coagulated blood. Blood and brains were processed as described above. Brain sections from MDA-231 injected mice were also quantified for the number of extravasated tumour cells by

labelling brain tissue with anti-CD45 and determining the number of tumour cells associated with an activated microglial wall.

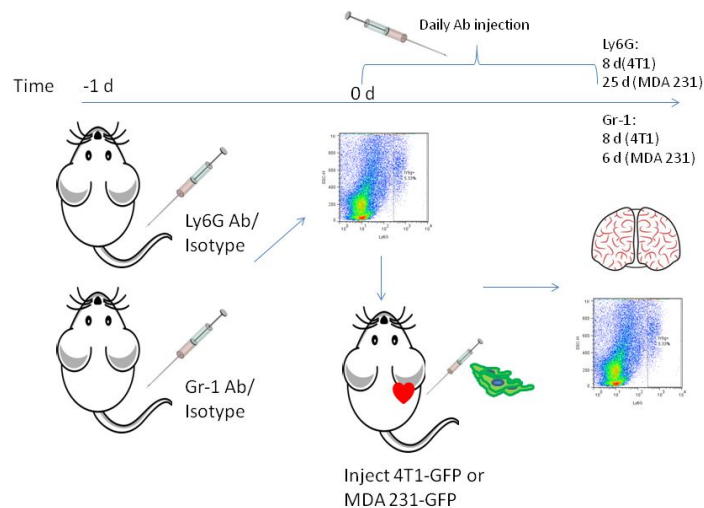


Figure 5.1: Schematic of antibody mediated depletion of neutrophils (Ly6G⁺) and Gr-1⁺ cells

Mice were injected i.p with either Ly6G, Gr-1 or isotype matched control antibodies. Blood was collected 24 h later for FACS analysis and after depletion was confirmed, mice were intracardiac injected with 10^5 GFP-expressing tumour cells. Daily i.p injections of antibody continued for 15 days (MDA 231) or the day before mice were culled. Mice were culled on the days indicated after tumour injection and blood and brains collected for analysis.

5.4.2 ADOPTIVE TRANSFER OF TUMOUR EDUCATED IMMUNE CELLS

Balb/c mice were injected into the mammary fat pad as described in Chapter 2 of Materials and Method. When primary tumours reached 250 mm^3 , mice were culled and blood (un-coagulated with EDTA), tibia, femurs and spleen were collected. Blood and spleen were also collected from naive age matched Balb/c mice. Spleens were minced with a scalpel and a single cell suspension was made by pushing minced spleens through a $70 \mu\text{m}$ sieve (BD Bioscience). Bone marrow cells were flushed out from femurs and tibias

using a 27 G needle fitted to a 20 ml PBS filled syringe. Erythrocytes were lysed in all samples using FACSLyse (BD Bioscience). Cells were counted using a haemocytometer, and diluted to 10^6 cells/ml in serum free warm DMEM. Immune cells were labelled by incubating with Dil dye (20 μ l) (Invitrogen) at 37°C for 20 min. Cells were washed 3 times in warm PBS and a sample was taken for microscopic verification of Dil labelling of immune cells. Labelled cells were spun and re-suspended in 120 μ l of PBS for injection. All procedures were performed under sterile conditions. To determine whether adoptively transferred cells were present in mice, mice were injected i.v with Dil labelled blood cells collected from a Balb/c mouse. Adoptively transferred mice were culled 24 h later and spleens were harvested, frozen and cryo-sectioned. Spleen sections were visualised using the TRITC filter on an epi-fluorescent microscope to confirm presence of adoptively transferred Dil labelled cells. For brain metastasis experiments, mice were injected i.v with either Dil labelled blood, spleen or bone marrow cells from tumour bearing or control mice. Immediately or 6 h after adoptive transfer, mice were intracardiac injected with 10^5 4T1-GFP cells. Mice were culled 3 days after tumour challenge and brains harvested for analysis (Figure 5.2 a). For co-injection experiments, 10^7 Dil labelled peripheral blood cells were mixed with 10^6 4T1-GFP cells in 1 ml of PBS and 100 μ l of this mixture was intracardiac injected into Balb/c mice (Figure 5.2b). Mice were culled 8 days after injection and brains were harvested to quantify numbers of brain metastases.

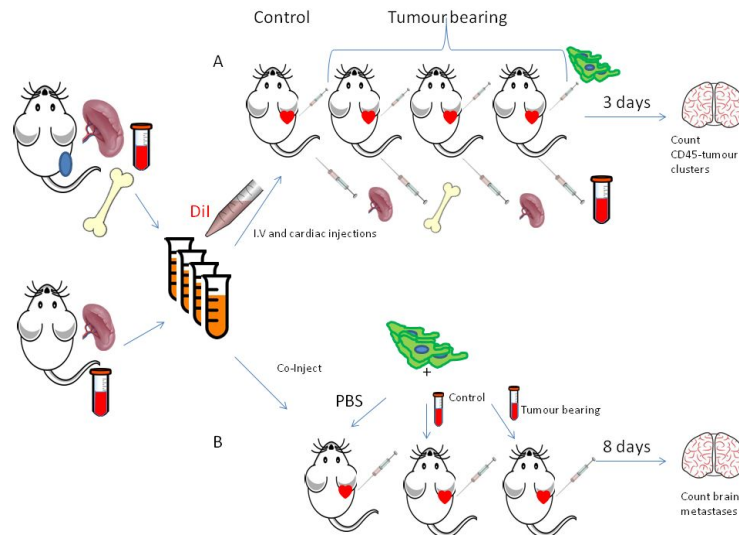


Figure 5.2: Schematic of adoptive transfer experiments

Balb/c mice implanted with a 4T1 primary tumour were culled to harvest blood, bone marrow and spleen (top). Spleen was also harvested from naïve mice to isolate normal splenocytes (bottom). Immune cells were purified from each organ and labelled *ex vivo* with Dil. A: Labelled immune cells were i.v injected into Balb/c mice and then 10^5 4T1-GFP cells were intracardiac injected either immediately or 6 h after adoptive transfer. Control mice were injected with spleen cells isolated from naïve mice. Mice were culled 3 days after tumour injection to collect brains. B: Immune cells purified from blood of tumour bearing or naïve Balb/c mice were labelled with Dil. Mice were injected into the heart with either 10^5 4T1-GFP tumour cells alone or mixed with control labelled peripheral immune cells or with tumour educated peripheral blood cells. Mice were culled 8 days after intracardiac injection to harvest brains.

5.4.3 MOUSE BIO-PLEX CYTOKINE ASSAY

Mice were injected with either 4T1 or MDA 231 primary tumours as described in Chapter 2 and when tumours reached 250 mm^3 , mice were intracardiac injected with either 10^5 MDA 231-GFP cells, 4T1-GFP cells or $100 \mu\text{l}$ of PBS. Naïve mice were also intracardiac injected with the same dose of GFP-expressing tumour cells. Mice were culled 3 days after intracardiac injection and serum was collected by coagulating whole blood at room temperature for 2 h, spinning and separating the supernatant to be stored at -80°C . Serum was also collected from age matched naïve SCID and Balb/c mice as controls (Figure 5.3). To analyse cytokines secreted from MDA 231 cells in culture, MDA 231 cells

were grown in T175 flasks and when 60% confluent, media was changed and collected 24 h later. Culture medium was passed through a 20 μm filter and stored at -80°C . On the day of cytokine assay, samples were thawed on ice and diluted 1:2 - 1:4 in sample buffer provided with the cytokine assay (Bio-Plex Pro [®] Mouse Cytokine 23-Plex and 9-Plex Assay, Biorad). The assay plate was prepared by adding antibody beads to all wells, after which the standards and serum/conditioned medium samples were added. After incubating for 30 min on a plate shaker, samples were washed thrice using a microplate washer. Detection antibodies were added to each well and incubated for another 30 min. Samples were washed thrice and streptavidin-PE was added to each well and incubated for 10 min. After 3 more washes, the samples were re-suspended and read using a plate reader.

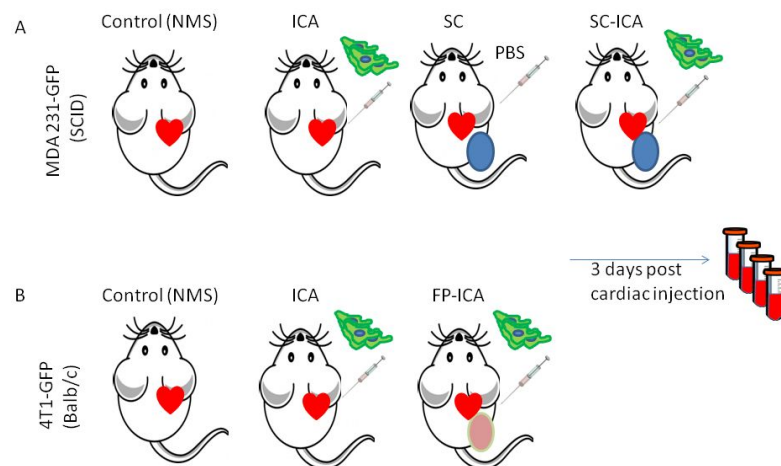


Figure 5.3: Schematic of blood collection for cytokine assay

A: SCID mice were injected with MDA 231 tumour cells into the right flank and when primary tumours reached 250 mm^3 , mice were intracardiac injected with PBS (SC) or 10^5 MDA-231-GFP

cells (SC-ICA). Non-tumour bearing mice were also intracardiac injected with 10^5 MDA 231- GFP cells (ICA). Mice were culled 3 days after tumour injection to collect serum. Serum was also collected from age-matched naïve SCID mice as control (NMS – normal mouse serum). B: Balb/c mice were injected with 4T1 tumour cells into the mammary fat pad and when primary tumours reached 250 mm^3 , mice were intracardiac injected with 10^5 4T1 -GFP cells (FP-ICA). Non-tumour bearing mice were also injected with 10^5 4T1-GFP cells (ICA). Mice were culled 3 days after tumour injection to collect serum. Serum was also collected from age-matched naïve Balb/c mice as controls.

5.5 RESULTS

5.5.1 LY6G POSITIVE NEUTROPHILS ARE NOT INVOLVED IN PROMOTING BRAIN METASTASIS.

The Ly6G (clone 1A8) antibody has been previously used to specifically deplete mouse neutrophils (Daley, Thomay et al. 2008; Kowanetz, Wu et al. 2010; Granot, Henke et al. 2011) therefore we used this antibody to determine whether neutrophils were involved in brain metastasis. FACS analysis of blood collected from mice injected with 4T1 cells at the end point of the experiment (day 8) confirmed that the Ly6G antibody depleted Ly6G positive cells whilst isotype injected mice retained Ly6G⁺ neutrophils (Figure 5.4a). The forward and side scatter profiles also showed depletion of a low forward scatter, high side scatter population characteristic of neutrophils (Figure 5.4a). As neutrophils also express Gr-1, further analysis of cell populations based on surface expression of Gr-1 confirmed absence of Gr-1⁺ cells in blood of Ly6G depleted mice (Supplementary Figure 1). Interestingly, we noted an increase in total cell number of Ly6G⁻ and Gr-1⁻ populations in blood from Ly6G antibody injected mice compared to blood from isotype injected mice (Supplementary Figure 1). When brain sections were analysed, no differences in the numbers of brain metastases formed by 4T1 or MDA 231 tumour cells were found between Ly6G depleted and isotype injected mice (Figure 5.4b).

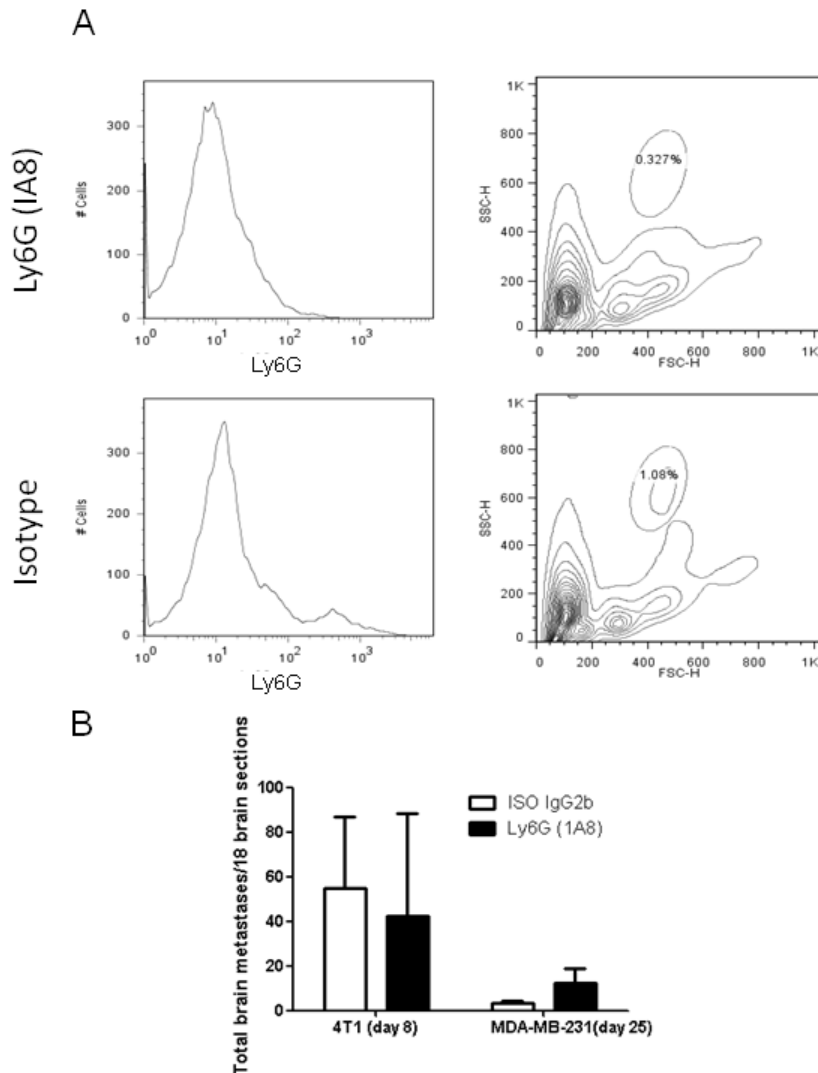


Figure 5.4: Depletion of neutrophils in mice does not augment the development of brain metastases

Mice were injected i.p with 12.5 μg (50 μl) of anti-mouse Ly6G antibody. 24 h after the first dose, 10-15 μl of blood was collected to confirm depletion of Ly6G⁺ cells. When depletion was confirmed, mice were then intracardiac injected with 10^5 4T1-GFP or MDA 231-GFP tumour cells. Mice received daily injections of Ly6G antibody until day 7 (4T1) or day 15 (MDA-231) after tumour challenge. 4T1-GFP injected mice were culled 8 d after tumour injection whilst MDA 231-GFP injected mice were culled 25 d after tumour injection. A: Representative FACS plot of blood collected from mice 8 days after 4T1-GFP injection. The histogram indicates that the Ly6G⁺ population was depleted in blood from Ly6G antibody injected mice but was present in blood from isotype-injected mice. The scatter plots show that the high side scatter and low forward scatter population typical of neutrophils (gated) was not present in Ly6G antibody injected mice. Refer to Supplementary Figure 1 for scatter plots based on Ly6G, Gr-1 and Ly6C staining. B: Eighteen representative brain sections per mouse were quantified for the number of brain metastases formed by each cell line and Student's t-test was used for statistical analysis. No differences in the number of brain metastases formed by 4T1 or MDA 231 cancer cells were found between neutrophil depleted and control mice (n = 4).

5.5.2 DEPLETION OF GR-1⁺ CELLS IS NOT SUSTAINED IN MICE INJECTED WITH 4T1 TUMOUR CELLS

As depleting Ly6G⁺ neutrophils did not augment the development of brain metastases, we then looked at the effects of depleting Gr-1⁺ cells using Gr-1 antibody (Figure 5.5). We followed the same protocol used to specifically deplete neutrophils. Blood was collected from mice 3 days after 4T1-GFP tumour challenge and analysed by FACS (Figure 5.5a). FACS histograms confirm absence of Gr-1⁺ cells in blood of Gr-1 antibody injected mice while the scatter plots indicate depletion of a neutrophil population (high side scatter, low forward scatter – gated population). By day 5, one of two Gr-1 antibody injected mice showed signs of distress and was culled, while the remaining mouse continued to receive daily i.p injections of Gr-1 antibody until day 7 post tumour challenge and culled the day after (day 8). Although Gr-1⁺ cells were absent in blood at day 3, these cells were subsequently detected at day 8, suggesting that the Gr-1 antibody ceased to maintain depletion of Gr-1⁺ cells (Figure 5.5a). In an attempt to sustain depletion of Gr-1⁺ cells, we repeated the experiment using an increased dose of the antibody (50 µg per mouse). At this dose, no toxic effects were evident in any of the Gr-1 antibody injected mice throughout the course of the experiment but Gr-1⁺ cells were present in blood of mice collected 8 days after tumour injection (Figure 5.5b and Supplementary Figure 2). FACS histograms of blood from Gr-1 antibody injected mice indicated an increase in Gr-1^{int} cells and scatter-plots showed almost twice the number of cells with high side scatter and low forward scatter compared to blood from isotype injected mice (Figure 5.5b – gated population and Supplementary Figure 2). Even though Gr-1 antibody did not sustain depletion of Gr-1⁺ cells, brains from these mice were still analyzed for metastases. Brain

sections labelled with anti-GFP were quantified and no differences in the number of 4T1 brain metastases were found between Gr-1 antibody injected mice and isotype control injected mice (Figure 5.5d).

We performed the Gr-1 antibody depletion experiments in SCID mice intracardiac injected with MDA 231-GFP cells. Depletion of Gr-1⁺ cells was confirmed 24 h after the first dose of antibody (50 µg/mouse/day - data not shown). One of three Gr-1 antibody injected mice had to be culled 24 h after tumour challenge and the remaining mice showed signs of distress 6 days after tumour injection therefore the experiment was terminated at this time. Blood from mice culled at day 6 was analysed by FACS and showed depletion of Gr-1⁺ cells (Figure 5.5c and Supplementary Figure 3). Since not all of the MDA 231-GFP tumour cells would have extravasated to form brain metastases by day 6 after tumour challenge, we therefore quantified the number of surviving MDA-231 cells in 18 representative brain sections. No differences in numbers of surviving tumour cells were found between Gr-1 and isotype injected mice (Figure 5.5d).

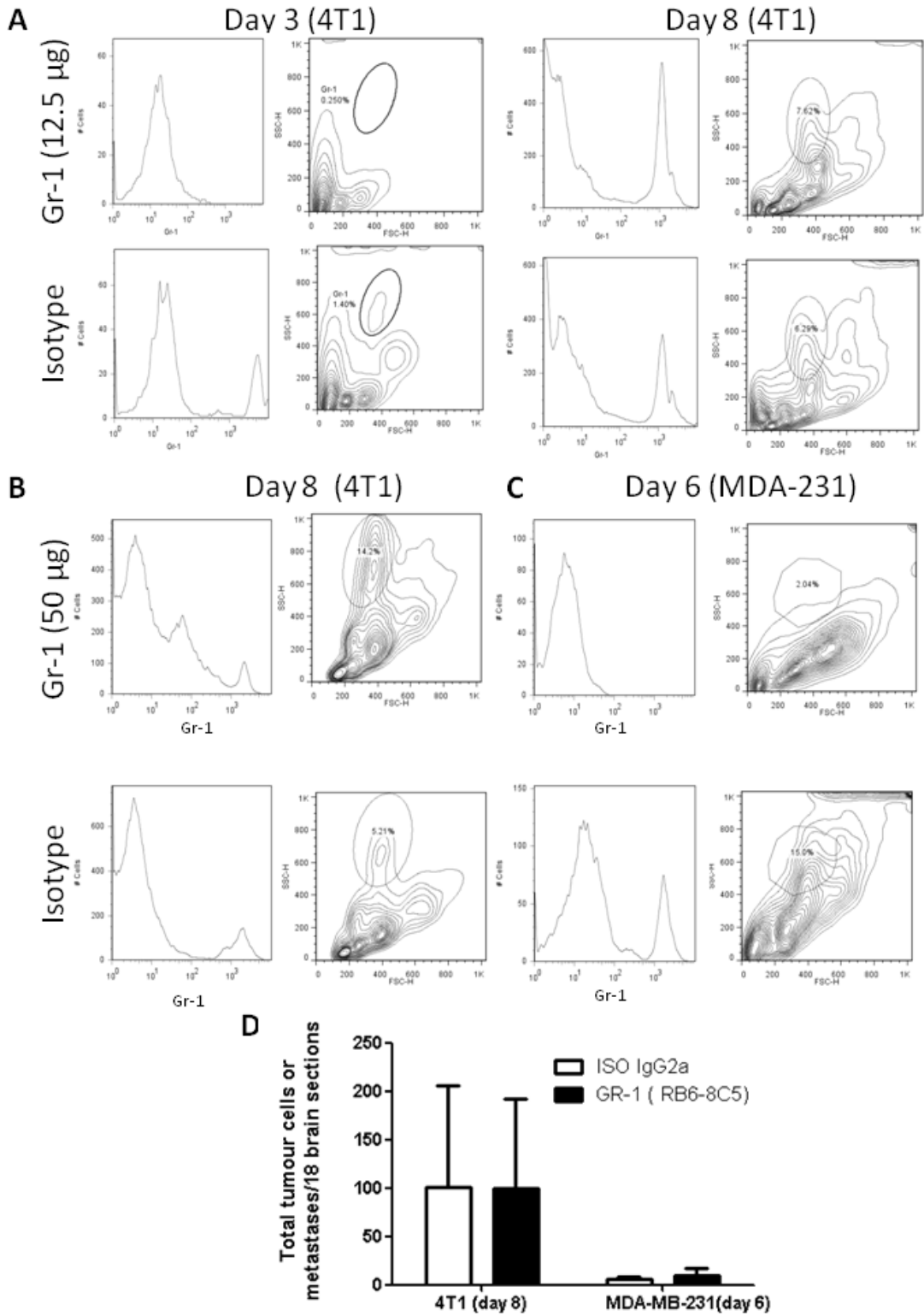


Figure 5.5: Depletion of Gr-1⁺ cells is not sustained in mice injected with 4T1 cells

12.5 µg of Gr-1 antibody was injected i.p into Balb/c mice and 24 h later, depletion of Gr-1⁺ cells was confirmed by FACS analysis of blood before mice were intracardiac injected with 10⁵ 4T1-GFP cells. Gr-1 antibody was administered daily until the day before the end-point of the experiment. A: Blood from mice were analysed by FACS 3 days and 8 days after tumour cell injection. Although Gr-1⁺ cells were not present in blood on mice 3 days after tumour injection compared to isotype injected mice (left plot – gated population), this population returned 8 days after tumour challenge (right plot; n=2). B: The dose of Gr-1 antibody was increased to 50 µg and the experiment was repeated. The increased dose of antibody was not enough to maintain depletion of Gr-1⁺ cells 8 days after tumour challenge (n= 3). Refer to Supplementary Figure 2-3 for scatter plots based on Ly6G and Gr-1 labelling of blood. C: 50 µg of Gr-1 antibody was used to deplete Gr-1⁺ cells in SCID mice 24 h prior to injection with 10⁵ MDA-231-GFP cells. Gr-1 antibody was administered daily until the experiment was terminated 6 days post tumour challenge when mice became ill. Blood collected from mice at this time was analysed by FACS. In blood from Gr-1 antibody injected mice, Gr-1⁺ cells were not present (gated population) when compared to blood from isotype injected mice (n=3 isotype; n=2 anti-Gr-1). D: 18 brain sections per mouse injected with 50 µg of Gr-1 or isotype antibodies were quantified for the number of brain metastases (4T1) or surviving tumour cells (MDA 231). No differences were found between Gr-1 depleted mice and isotype control injected mice.

5.5.3 GR-1 ANTIBODY INJECTION DOES NOT DEplete ALL GR-1⁺ CELLS

At the end point of the Gr-1 antibody experiment (6 days post tumour injection), a few MDA 231 cells remained intravascular or were just starting to extravasate. Since we showed that Gr-1 depletion worked at this time but had no effect on MDA 231 cell survival, we assessed whether Gr-1 depletion affected tumour cell extravasation. Extravasated tumour cells activate microglia, therefore we used anti-CD45 antibody to label brain sections from Gr-1 and isotype antibody injected mice. Although, we did not find any differences in microglia activation between depleted and control mice, we did note CD45^{hi} bright round cells associated with a few tumour clusters in brains of mice injected with Gr-1 or isotype control antibodies (Figure 5.6a). We then used a Gr-1 antibody to label adjacent brain sections to find the same tumour cells and determine if they were associated with Gr-1⁺ cells. Unfortunately, we did not find the same tumour

cells in adjacent brain sections but were able to identify Gr-1⁺ cells within the same area of the brain and sporadically throughout several brain sections (Figure 5.6b). As the Gr-1 antibody did not seem to deplete all Gr-1⁺ cells, we turned to other methods to determine the function of these cells.

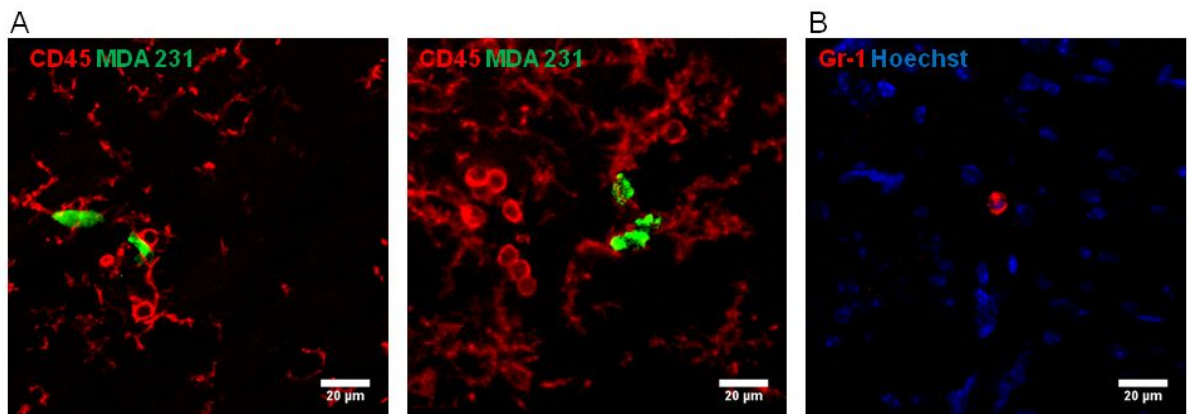


Figure 5.6: Injection of Gr-1 antibody does not deplete all Gr-1 cells.

SCID mice were injected with Gr-1 or isotype control antibodies and 24 h later, mice were intracardiac injected with 10^5 MDA 231-GFP tumour cells. Mice were injected daily with antibodies and culled 6 days after tumour challenge. Brain sections were analysed after labelling with anti-CD45 and anti-GFP (A) or anti-Gr-1 and anti-GFP (B) A: CD45^{hi} bright round cells were found associated with few MDA 231 cells in brains of Gr-1 depleted mice. B: Gr-1⁺ cells were seen in brains of mice injected with Gr-1 depleting antibody.

5.5.4 ADOPTIVE TRANSFER OF TUMOUR EDUCATED IMMUNE CELLS DOES NOT AUGMENT THE DEVELOPMENT OF BRAIN METASTASES

To address the question whether tumour cell colonisation of the brain is facilitated by circulating immune cells, we performed adoptive transfer experiments. Using epifluorescent microscopy, we confirmed that the Dil dye uniformly labelled immune cells *in vitro* (Figure 5.7a). Labelled cells were injected i.v and the mouse was culled 24 h later to harvest the spleen. We inspected spleen sections to confirm the presence of Dil labelled cells in adoptively transferred mice (Figure 5.7b). In brain metastasis experiments where

mice were adoptively transferred with tumour educated immune cells derived from the bone marrow, blood or spleen, we detected Dil labelled cells in the brains of tumour challenged mice (Figure 5.7c). However, numbers of these Dil cells were not sufficient for quantitative analysis. To determine whether adoptive transfer of tumour educated cells increased the number of immune cells interacting with intravascular 4T1-GFP cells, we used CD45 antibody to label brain sections and quantified the percentage of tumour-CD45^{hi} clusters. No differences in the percentage of tumour-CD45^{hi} clusters was found between mice adoptively transferred with tumour educated immune cells and mice adoptively transferred with normal immune cells (Figure 5.7 d,e). To rule out the possibility that the majority of adoptively transferred cells were homing to the lung due to the route of injection (i.v), we performed intracardiac co-injection experiments and culled mice 8 days after injection to quantify brain metastases. No differences in brain metastases were found between mice co-injected with 4T1 tumour cells and tumour educated peripheral blood cells, naïve blood cells, or PBS (Figure 5.7f).

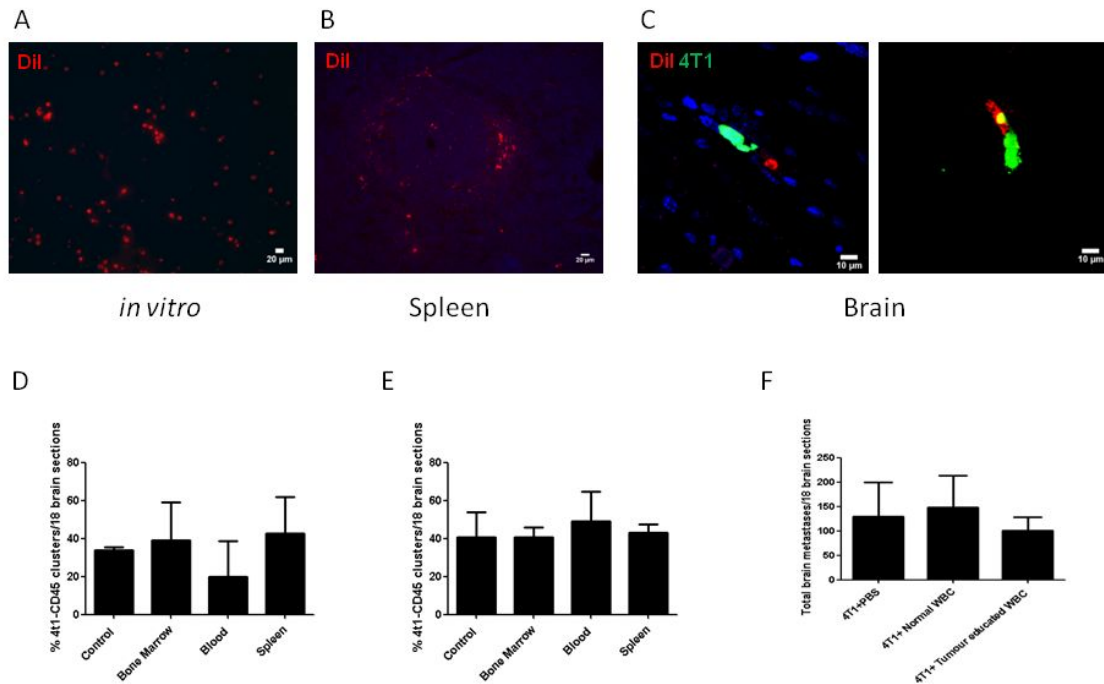


Figure 5.7 Adoptive transfer of tumour educated immune cells does not augment development of brain metastases

Anti-coagulated peripheral blood cells were isolated from a naïve Balb/c mouse. After red blood cell lysis, the immune cells were labelled *in vitro* with Dil dye. A: Dil labelled cells were inspected using epi-fluorescent microscopy to confirm labelling. B: 10^6 labelled cells were injected i.v into a naïve Balb/c mouse. The mouse was culled 24 h after adoptive transfer and the spleen was harvested. Spleen sections were visualised to confirm the presence of Dil labelled cells. C-D: Spleen, blood and bone marrow collected from mice bearing a 4T1 primary tumour were made into a single cell suspension and labelled with Dil and 10^6 labelled immune cells from the three different sources were injected i.v into three different mice. Splenocytes isolated from an age matched naïve Balb/c mouse were also labelled with Dil and injected i.v into naïve mice. Mice were culled 3 days after tumour injection and brains were harvested. Brain sections were assessed for the presence of Dil labelled cells (B). Brain sections from mice intracardiac injected 6 h after adoptive transfer (D - n=3) or immediately after (E - n=2) were labelled with CD45 and GFP antibodies and total tumour-CD45^{hi} clusters were quantified in 18 brain sections. Data was analysed using one-way ANOVA and no significant differences in the percentage of tumour cell-CD45^{hi} clusters were found between mice injected with tumour educated immune cells or control cells. F: Mice were co-injected in the heart with a mixture of 10^6 Dil labelled blood cells from naïve (n= 4) or tumour educated mice (n=5) and 10^5 4T1-GFP cells. Some mice were just injected with 10^5 4T1-GFP cells (n= 7). Data was analysed using one-way ANOVA and no significant differences in brain metastases were found between all groups.

5.5.5 G-CSF CONCENTRATION IS SUBSTANTIALLY INCREASED IN BLOOD OF PRE-CONDITIONED MICE AFTER INTRACARDIAC INJECTION WITH MDA 231 OR 4T1 CELLS

Ly6G antibody injected mice depleted of neutrophils or mice adoptively transferred with tumour educated immune cells showed no difference in the number of brain metastases compared to control mice. Since Gr-1 antibodies did not maintain depletion of Gr-1⁺ immune cells, we asked whether we could manipulate factors that recruit these immune cells to intravascular tumour cells. First, we screened serum collected from tumour injected mice and controls to find candidate molecules (See Figure 5.3 for a schematic). We initially used a mouse cytokine assay to analyse serum samples, and also assayed MDA 231 culture supernatant to detect any human cytokines that may cross react with mouse antibodies. Several cytokines were detected in MDA 231 conditioned media (Figure 5.8). Cytokines detected above 10 pg/ml included GM-CSF, IL-10, IL-12(p70), IL-15, IL-18, IL-2, IL-9, IL-1 β , TNF, and VEGF. VEGF levels were the highest (2178 \pm 6.52 pg/ml).

Next we analysed serum from mice injected with MDA 231 and controls. Levels of 17 of the 32 cytokines tested were increased in preconditioned mice that were also intracardiac injected with tumour cells (SC-ICA) when compared to all other groups (Figure 5.9). G-CSF was the only cytokine that was significantly increased in blood of SC-ICA mice, with 50 fold-increase compared to blood from ICA mice, 132 fold-increase compared to blood from SC mice and 20 fold-increase compared to blood from naïve mice. Cytokines that were at least 2-fold increased in blood of SC-ICA mice compared to blood of naïve mice included: IL-9(2-fold), IL-6 (2.6 fold), monocyte chemotactic protein-1(MCP-1 - 2.5 fold),

IL-1 α (2-fold), and macrophage inflammatory protein-1 α (MIP-1 α - 2-fold), platelet derived growth factor (PDGF - 2-fold), and monokine induced by gamma interferon (MIG - 4-fold). Cytokines that increased in blood of SQ-ICA mice compared to SQ only mice included IL-6(6-fold), MIP-1 α (2.5-fold), and MIG (3-fold). Only MIP-1 α and MIG were more than 2-fold increased in SC-ICA blood compared to ICA only blood. MIP-2 and VEGF were decreased by approximately 2-fold in SC-ICA mice compared to both SQ and ICA controls. Minimal differences in cytokine expression were found between pre-conditioned (SC) and intracardiac injection only mice (ICA) and when each of these groups were compared to control blood. Only basic fibroblast growth factor (BFGF) was increased (approximately 2-3 fold) in blood from SC mice compared to all other groups.

Levels of fewer cytokines were altered in serum from 4T1 pre-conditioned then intracardiac injected mice (FP-ICA) when compared to blood from mice injected with MDA 231 cells (Figure 5.10). G-CSF levels in naïve and ICA mice were similar (22.85 ± 0.02 pg/ml vs. 20.25 ± 1.0 pg/ml) although a substantial and significant increase in G-CSF level was detected in serum of FP-ICA mice. There was a 60-fold increase in levels of G-CSF after intracardiac injection of tumour-bearing mice compared to blood from naïve mice and 68-fold increase compared to blood from cardiac challenged naïve mice. IL-18 increased 2-fold in blood from ICA mice compared to both NMS and FP-ICA mice. Most other cytokines stayed the same or decreased in blood from FP-ICA mice compared to blood from naïve or ICA only mice. Cytokines that decreased more than 2 fold in FP-ICA mice compared to blood from naïve mice included IL-13 (2-fold), IL-1 β (3-fold), keratinocyte-derived cytokine (KC - 5-fold), MIP-1 β (3 fold), regulated and normal T cell

expressed and secreted (RANTES - 2.5 fold), and TNF (2-fold). Cytokines that decreased more than 2-fold in blood from FP-ICA mice compared to ICA mice included IL-18 (2-fold), IL-1 β (3-fold), KC (6-fold), and RANTES (2.5-fold). IL-17 was 3.5-fold decreased in blood from ICA mice compared to the other two groups.

5.5.6 GR-1⁺ CELLS ACCUMULATE IN BRAINS OF TUMOUR-BEARING MICE

To determine the link between G-CSF secretion and accumulation of Gr-1⁺ cells, brains taken from the cytokine assay experiment were stained with Gr-1 antibodies. Compared to brains from naïve Balb/c mice, 4T1 primary tumour bearing mice with or without intracardiac injection of 4T1-GFP cells had substantial accumulation of Gr-1⁺ cells in the brain (Figure 5.11a). There was a less prominent increase in the numbers of Gr-1⁺ cells in brains of naïve Balb/c mice 3 days after intracardiac injection with 4T1-GFP cells. We then determined the number of Gr-1⁺ cells in brains of naïve or MDA 231 primary tumour bearing SCID mice after intracardiac injection with MDA 231-GFP cells. Brains from MDA 231 tumour bearing mice intracardiac injected with PBS were not available for analysis. A considerable increase in the number of Gr-1⁺ cells was seen in MDA 231 tumour bearing mice after intracardiac injection (Figure 5.11b).

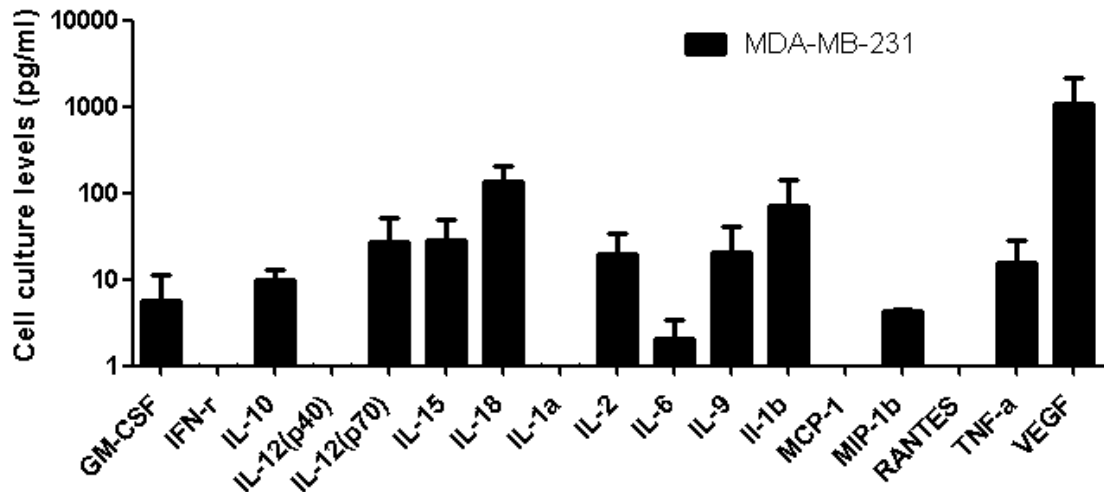


Figure 5.8: Cytokines produced by MDA-231 cells in culture are detected using a mouse cytokine array

Culture medium of MDA-231 cells was collected when cells were 80% confluent. Cytokines in the culture medium and control DMEM were analysed using a 24-plex mouse cytokine array. Increased levels of some human cytokines were detected by the mouse cytokine assay likely due to close sequence homology of the human and mouse epitopes. Cytokines were assayed in duplicates and the experiment was done once. Background values from DMEM was subtracted from experimental data and presented as the mean \pm SD.

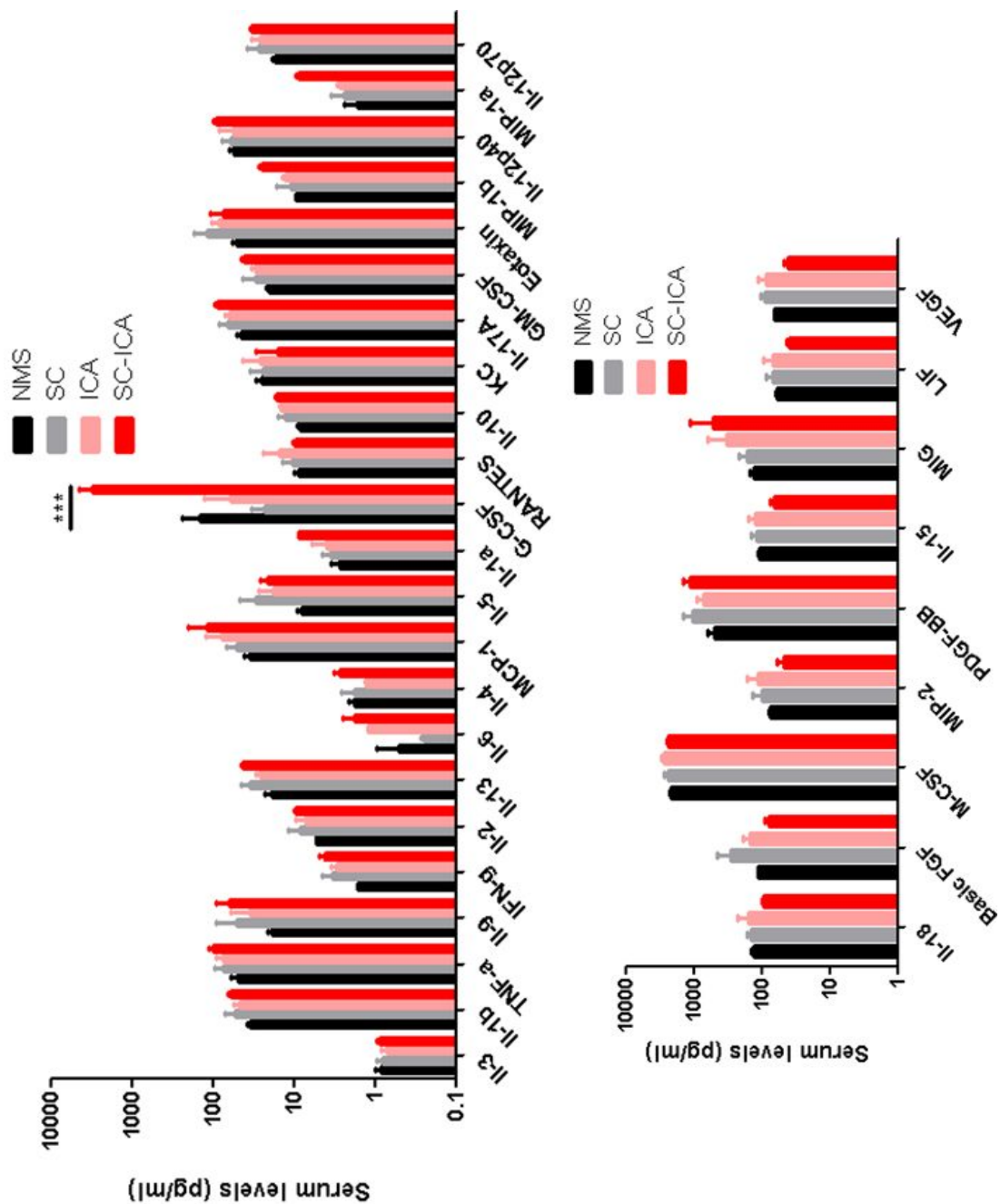


Figure 5.9: G-CSF levels are significantly increased in blood of MDA 231 pre conditioned mice 3 days after intracardiac injection of MDA 231-GFP cells.

Blood was collected from naïve or primary tumour bearing mice 3 days after intracardiac injection of 10^5 MDA 231-GFP cells (ICA vs. SC-ICA). Blood was also collected from tumour bearing mice 3 days after intracardiac injection with PBS (SC). Blood from age-matched SCID mice was collected as controls (NMS). A 23-plex and 9-plex mouse cytokine assay was performed on serum samples pooled from two different experiments and data analysed to remove outliers. Data is presented as means \pm SD from two different pooled experiments and 2-way ANOVA was used to determine statistical significance; *** $p < 0.001$

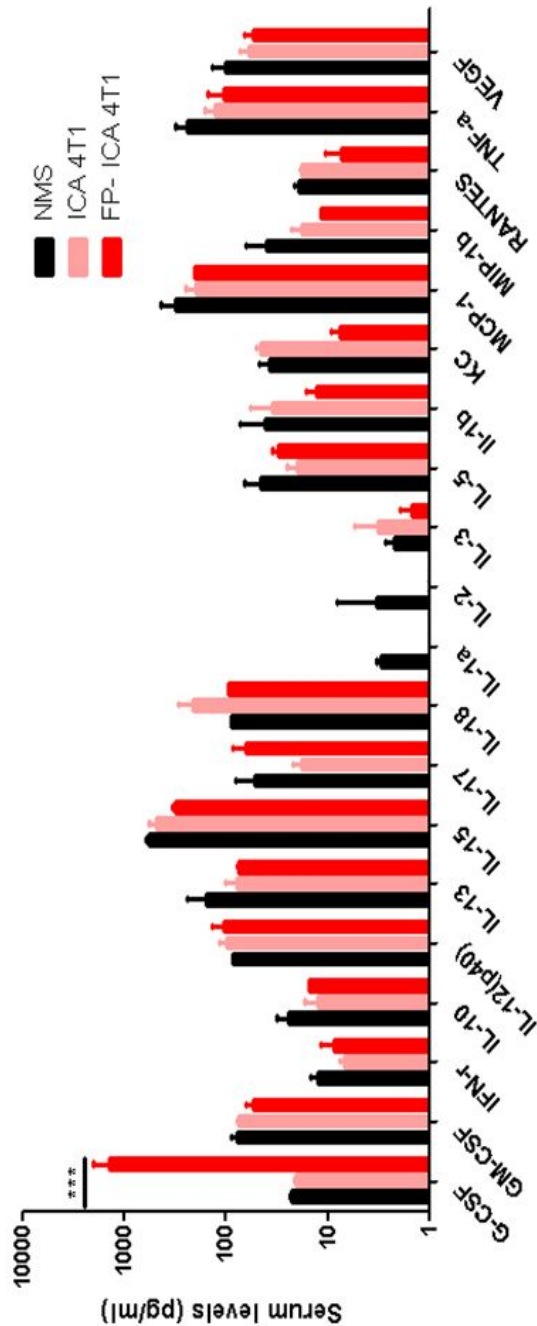


Figure 5.10: G-CSF levels are significantly increased in serum of 4T1 tumour bearing mice 3 days after intracardiac injection of 4T1-GFP cells.

Blood was collected from naïve or 4T1 tumour bearing Balb/c mice 3 days after intracardiac injection with 10^5 4t1-GFP cells. Blood was also collected from age-matched Balb/c mice as controls. Serum samples from primary tumour bearing mice that were intracardiac injected with PBS (FP) were unavailable. Cytokine analysis was performed using a 26-plex cytokine array and presented as mean \pm SD. Data from Eotaxin, IL-12 (p70), IL-4, IL-6, IL-9, MIP-1 α was omitted as they were below detection level. 2-way ANOVA was used to determine the significant differences in cytokine levels produced by the different experimental groups; *** $p < 0.001$

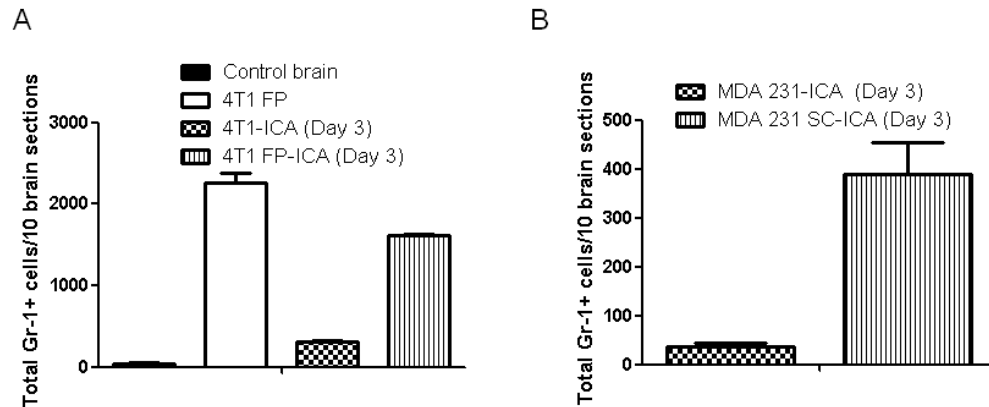


Figure 5.11: Gr-1⁺ cells accumulate in brains of 4T1 and MDA 231 tumour bearing mice

A: Brain sections from naïve Balb/c mice, naïve mice intracardiac injected with 10^5 4T1-GFP cells (ICA) or mice bearing a 4T1 primary tumour intracardiac injected with 4T1-GFP cells (FP-ICA) or PBS (FP) were labelled with Gr-1 antibody and total number of Gr-1⁺ cells were quantified in 10 brain sections per mouse. Substantial increase in Gr-1⁺ cells was found in brains from FP and FP-ICA mice compared to brains from naïve and ICA mice. B: The numbers of Gr-1⁺ cells were counted in representative brain sections from naïve or MDA 231 tumour bearing mice intracardiac injected with 10^5 MDA 231 - GFP cells (ICA vs. SC-ICA). Brains from naïve SCID mice (NMS) or ones bearing a MDA 231 tumour (SQ) were not available for analysis. A substantial increase in Gr-1⁺ cells was noted in brains of SC-ICA mice. Gr-1⁺ cells were quantified from 10 representative brain sections per mouse ($n=2$) and presented as mean \pm SD. Statistical analysis could not be done as there were not enough data points.

5.6 DISCUSSION

We have previously shown that Gr-1⁺ cells associated with intravascular tumour cells (Chapter 4) and in this chapter we attempted to characterize the effects of Gr-1⁺ cells on brain metastasis. Although, we were not able to determine the function of tumour associated Gr-1⁺ cells, we have now developed the methods that would allow further consideration of our hypothesis.

Gr-1 is expressed on neutrophils therefore we used the neutrophil specific Ly6G antibody to deplete these cells (Daley, Thomay et al. 2008). However, this did not change the number of brain metastases produced by both the 4T1 and MDA 231 tumour cells. This is consistent with our supposition that the Gr-1⁺ and MBS⁺ cells associated with intravascular brain metastatic tumour cells are most likely not neutrophils. Injection of mice with Gr-1 antibody (clone RB6-8C5) to deplete neutrophils and other Gr-1 expressing cells was inconclusive. The amount of antibody delivered in 4T1 injected Balb/c mice was not enough to sustain depletion and toxicity was also noted. Eliminating Gr-1⁺ cells via Gr-1 antibody administration not only depletes neutrophils and other Gr-1⁺ cells but also impairs the function of other innate immune cells such as NK cells (Jaeger, Donadieu et al. 2012) and increased susceptibility to infection has been described in immuno-competent mice (reviewed in (Egan, Sukhumavasi et al. 2008)). As immuno-deficient SCID mice are more reliant on innate immune cells, they are even more sensitive to Gr-1 antibody injection and we had to terminate depletion experiments before brain metastases could develop.

We are only aware of one study which has characterised the effects of Gr-1 depletion in mice (Ribechini, Leenen et al. 2009). *In vitro*, the Gr-1 antibody did not deplete non-neutrophil cells in mouse bone marrow but instead masked the Ly6G epitope on Gr-1⁺ non-neutrophil cells, and cells appeared to be depleted when analysed by FACS (Gr-1/Ly6G^{hi} → Gr-1/Ly6G^{low}) (Ribechini, Leenen et al. 2009). In our study, FACS analysis of blood from Ly6G antibody injected mice showed depletion of Ly6G⁺ cells and most of the Gr-1⁺ cells (Supplementary Figure 1a-b). The Ly6G antibody has been shown to bind Gr-1⁺ cells (Ribechini, Leenen et al. 2009) and therefore in FACS analysis, Gr-1⁺ cells appeared as Gr-1^{low/-} and Ly6G^{low/-}, which could be incorrectly interpreted as depletion. This shift explains why we detect more Gr-1/Ly6G^{low/-} cells in Ly6G depleted mice compared to isotype controls (Supplementary Figure 1b). The Ly6G and Gr-1 antibodies therefore only deplete neutrophils but mask the presence of other Gr-1⁺ cells. This phenomenon explains why we find CD45^{hi} bright round cells, characteristic of previously identified tumour associated immune cells, and Gr-1⁺ cells in brains of Gr-1 depleted SCID mice. It also accounts for lack of reduction in brain metastases or tumour cell survival in Gr-1 depleted mice. This finding further validates our hypothesis that the CD45^{hi}/MBS⁺/Gr-1⁺/Ly6G⁺ cells associated with brain metastatic tumour cells are not neutrophils.

Although the Gr-1 antibody does not deplete non-neutrophil cells in the spleen and bone marrow, it does however reduce the suppressive activity of Gr-1⁺ MDSC cells in the bone marrow (Ribechini, Leenen et al. 2009). This occurrence explains why some groups report reduction in tumour growth and metastases after using Gr-1 antibody in mice and assume tumour regression is due to depletion of MDSC cells (Pekarek, Starr et al. 1995; Fujita,

Kohanbash et al. 2011). Ribechini *et al* also report that the Gr-1 antibody even stimulates myeloid cell expansion within the bone marrow. Although we did not analyse bone marrow, we noted increased presence of Gr-1^{int} and Gr-1^{hi} cells in peripheral blood of mice injected with 50 µg of Gr-1 antibody which was not seen when mice were injected with 12.5 µg of anti-Gr-1 (Figure 5.5). This suggest that the Gr-1 antibody induced myelopoiesis in a dose dependent manner and this function of the Gr-1 antibody accounts for why we found increased numbers of Gr-1⁺ cells instead of depletion.

As the depletion experiments were not conclusive, we attempted to investigate the functions of Gr-1⁺ cells by adoptively transferring tumour conditioned immune cells. Adoptive transfer of tumour conditioned immune cells did not augment brain metastases. There are two key pitfalls of this experiment. First, we only attempted to deliver tumour-educated immune cells 6 h or at the same time as tumour injection. For pre-conditioning to favour brain metastasis, tumour educated immune cells may need to be present for a longer period of time before tumour challenge. Second, the numbers of adoptively transferred immune cells (10^6) may not compare to the numbers induced by 4T1 tumours. 4T1 primary tumour bearing mice have extensive numbers of immature granulocytes in peripheral blood and spleen resulting in splenomegaly (DuPre, Redelman et al. 2007). We too noticed very large spleens in mice bearing 4T1 primary tumours but not in mice bearing MDA 231 primary tumours. We also found considerably more white blood cells in blood from 4T1 primary tumour bearing mice compared to naïve mice. It was never possible to adoptively transfer the large quantities of immune cells purified from tumour bearing mice and is most likely the reason why we were not able to

augment the number of brain metastases developed in mice adoptively transferred with 4T1 conditioned immune cells.

Excess production of immature immune cells in 4T1 tumour bearing mice is linked to increased tumour secretion of G-CSF (DuPre and Hunter 2007; Waight, Hu et al. 2011). We also found a significant increase in G-CSF levels in serum collected from 4T1 and MDA 231 tumour bearing mice 3 days after intracardiac injection. Although we were not able to analyse serum of 4T1 tumour bearing mice that were not intracardiac injected with tumour cells, we found a substantial accumulation of Gr-1⁺ cells in brains from FP and FP-ICA mice. Therefore the increased levels of G-CSF in blood of FP-ICA mice were most likely due to the primary tumour and not the intracardiac injection of tumour cells. In contrast, we found the host to be the major source of G-CSF in MDA 231 tumour bearing mice that were also intracardiac injected (SC-ICA). Mouse G-CSF levels were undetectable in serum from mice bearing a MDA 231 primary tumour (SC) or in serum from mice 3 days after intracardiac injection (ICA). We also did not detect any mouse G-CSF from MDA 231 culture supernatant even though human and mouse G-CSF share 70% sequence homology (Demetri and Griffin 1991). Although we did not analyse serum or culture supernatant using human cytokine assays, others have shown that MDA 231 tumours produce human G-CSF in mice (Kowanetz, Wu et al. 2010). When we analysed brains from mice pre-conditioned with a primary tumour, we saw 5-fold less accumulation of Gr-1⁺ cells in brains of MDA 231 SQ-ICA mice compared to 4T1 FP-ICA mice even though mouse G-CSF levels in blood were 3-fold more in MDA 231 injected mice. Other studies have shown that mice bearing MDA 231 primary tumours expressed 10-fold less human G-CSF

in blood compared to murine G-CSF levels in blood of mice bearing 4T1 tumours (Kowanetz, Wu et al. 2010). The MDA 231 tumour bearing mice also developed fewer spontaneous lung metastases compared to 4T1 tumour bearing mice (Kowanetz, Wu et al. 2010). Even though human G-CSF is bioactive in mice (Demetri and Griffin 1991), the levels secreted by MDA 231 primary tumours may not be as robust as that secreted by 4T1 and we hypothesise that host secreted G-CSF may be more important in the MDA 231 model of brain metastases. Macrophages and monocytes predominately produce G-CSF, but under inflammatory conditions, endothelial cells, fibroblasts and mesothelial cells can also secrete G-CSF (Demetri and Griffin 1991). MDA 231 cells released into the circulation of pre-conditioned mice may interact with other tumour secreted factors, circulating immune cells and/or mouse endothelium to cause a robust release of G-CSF. We need to analyse blood samples using a human array to determine the importance of mouse G-CSF vs. human G-CSF. If mouse G-CSF is more important for the development of brain metastases from MDA-231 tumour cells, we could then examine the effects of exogenously injected mouse G-CSF on MDA 231 brain metastasis instead of pre-conditioning with a primary tumour.

The G-CSF receptor is highly expressed on mature and immature neutrophils and intermediate expression is found on other haematopoietic progenitor cells including monocytes and NK cells (Singh, Hu et al. 2012). Therefore it is not surprising that several studies have shown the link between G-CSF production by tumour cells and induction of neutrophils and immature myeloid cells to aid cancer progression and specifically, lung metastasis (DuPre and Hunter 2007; Kowanetz, Wu et al. 2010; Raychaudhuri, Rayman et

al. 2011; Waight, Hu et al. 2011; Scott and Jeremy 2012). We now show a link between increased G-CSF levels in mice with increased brain metastases. Although we propose that tumour secreted G-CSF functions to recruit brain metastasis promoting immune cells, cytokines themselves may play a role in tumour cell extravasation into the brain, with or without immune cell assistance. G-CSF receptor is found on endothelial cells and G-CSF has been shown to induce endothelial cell proliferation and migration (Bussolino, Wang et al. 1989; Bocchietto, Guglielmetti et al. 1993). In cultured endothelial cells, G-CSF treatment induced production of plasminogen activator (Kojima, Tadenuma et al. 1989). Plasminogen, a proteolytic enzyme that breaks-down basement membrane, is implicated in tumour cell invasion (Carriero, Franco et al. 2011; Mason and Joyce 2011) and has been shown to play a role in brain metastasis (Perides, Zhuge et al. 2006). However, others have shown that G-CSF has no effects on human vein endothelial cells (Yong, Cohen et al. 1991) and the role of G-CSF on brain endothelial cells remains to be identified.

IL-1 β , TNF and VEGF have been used to increase BBB permeability (Blamire, Anthony et al. 2000; Tsao, Hsu et al. 2001; Lee, Avraham et al. 2003). However, we only found detectable levels of these cytokines in MDA 231 conditioned media and not in serum from tumour bearing mice. In MDA 231 tumour bearing mice, these factors may be restricted to the primary tumour and may not accumulate in blood or tumour associated stromal cells halt production of these factors from the tumour. However, we cannot discount human levels of these factors. In blood from 4T1 tumour pre-conditioned mice after intracardiac injection, IL-1 β and TNF levels were decreased when compared to levels in blood from naïve mice. Even though VEGF was not tested in blood from 4T1 injected

mice, we do not think that increased brain metastases in preconditioned mice are due to increased permeability of the BBB.

In tumourgenesis, Ly6G⁺Ly6C⁺ cells have been identified to be MDSCs based on their T-cell suppressor function. Although we have not shown that these cells are MDSCs, we did note robust infiltration of T cells in brains of mice intracardiac injected with 4T1 cells at very late time points (Figure 4.13) when the mice were very sick. As MDSCs have been described in the 4T1 model, it was not surprising that these brain metastases associated T cells were not restricting tumour growth. The suppressive function of MDSCs is linked to tumour expression of GM-CSF (Dolcetti, Peranzoni et al. 2010) and even though GM-CSF was readily found in MDA 231 culture supernatant, we were surprised to not detect GM-CSF in serum of MDA-231 tumour bearing mice. However, we may find high levels of GM-CSF when we analyse serum samples using an assay which detects human cytokines. GM-CSF has been reported to be secreted by 4T1 primary tumours (Dolcetti, Peranzoni et al. 2010), but others report that while mRNA for GM-CSF and G-CSF are found in 4T1 cells, only G-CSF protein was detected in serum of tumour bearing mice (DuPre and Hunter 2007). We also did not find detectable levels of GM-CSF in 4T1 bearing mice. This discrepancy may be due to variations in tumour size and/or developmental stage of the tumour as biphasic growth of 4T1 primary tumours has been described (Tao, Fang et al. 2008). Tumour secreted GM-CSF may also only act within the primary tumour to recruit MDSCs to promote tumour growth and when circulating tumour cells are detected, host factors may secrete G-CSF to recruit metastasis promoting Gr-1⁺ cells. The Gr-1⁺ cells associated with intravascular brain metastatic cells may possibly be MDSCs but instead of

functioning solely to suppress T-cells, they may have other metastasis promoting functions. Tumour secreted G-CSF has been shown to recruit Gr-1⁺ cells to the lung; These immune cells produced an inflammatory environment to promote disseminated tumour cells to colonise the lung (Kowanetz, Wu et al. 2010). Our findings suggest that a similar mechanism operates in brain metastasis.

In this chapter, we attempted to determine the role of immune cells associated with intravascular brain metastatic cells. Although we did not determine the function of these immune cells, we were able to determine that these cells were not neutrophils and discovered that tumour and host derived G-CSF may be the driving force behind brain metastasis. G-CSF is significantly increased in blood of mice pre-conditioned with 4T1 and MDA 231 after intracardiac injection and we show a link between G-CSF expression and accumulation of Gr-1⁺ cells in brains of these mice. Therefore, the next step was to neutralise G-CSF in tumour bearing mice to determine if we could abolish recruitment of Gr-1⁺ cells and thus prevent or decrease the number of brain metastases. Unfortunately, due to time constraints, we were unable to commence these experiments. Future experiments targeting G-CSF may enable us to determine the role of Gr-1⁺ cells in brain metastasis. G-CSF can be targeted by injecting mice with G-CSF antibodies or by knocking out the gene from tumour cell lines. As MDA 231 may be more reliant on host derived G-CSF, we can exogenously deliver mouse G-CSF into naïve mice before intracardiac injection of MDA 231 cells and determine the effect on brain metastases development.

CHAPTER 6: DEVELOPING AN *IN VIVO* IMAGING METHOD TO VISUALISE BRAIN METASTATIC TUMOUR CELLS INTERACTING WITH IMMUNE CELLS

6.1 INTRODUCTION

6.1.1 IN VIVO BRAIN IMAGING

Trans-cranial window imaging is a well established technique in neuroscience used to visualise and elucidate the function of neurons (Denk 1994; Chen, Lendvai et al. 2000; Dombeck, Khabbaz et al. 2007), microglia (Davalos, Grutzendler et al. 2005; Nimmerjahn, Kirchhoff et al. 2005; Nimmerjahn 2012) and astrocytes (Ding, Fellin et al. 2007; Ding, Wang et al. 2009). This technique has also been expanded to observe immune trafficking to organs, including the brain, (Villringer, Dirnagl et al. 1991; Voisin, Woodfin et al. 2009; Woodfin, Voisin et al. 2009; Woodfin, Voisin et al. 2011) and to visualise and study the primary tumour microenvironment (Sahai, Wyckoff et al. 2005; Sidani, Wyckoff et al. 2006). Multi-photon imaging enables deeper visual penetration of live tissue whilst minimising damage. This technique has been employed to study vascularisation of primary brain tumours (Winkler, Kienast et al. 2009) and the very early steps of brain metastases development (Kienast, von Baumgarten et al. 2010) but has not yet been utilized to determine the role of circulating immune cells interacting with brain metastatic cells.

6.2 AIMS

To develop an *in vivo* method to image intravascular tumour cells interacting with systemic leukocytes over time.

6.3 MATERIALS AND METHOD

6.3.1 CRANIAL WINDOW PLACEMENT

For window placement, the same protocol was followed as intracranial injections to thin the skull (Chapter 2 Materials and Method). A 3-4 mm² piece of skull was removed and replaced with a 5 mm in diameter circular plastic coverslip (VWR International, Lutterworth, UK). The skin over the window was sutured back in place and mice were allowed to recover for a minimum of 4 weeks before further experimentation took place.

6.3.2 IN VIVO MICROSCOPIC IMAGING

Intracardiac/intracarotid injections of tumour cells are described in Chapter 2 (Materials and Method). Prior to imaging, mice were anaesthetised, and placed on an in-house constructed mouse holder and secured using cheek bars and tape. The cranial window was exposed and cleaned using a cotton swab and sterile saline. The holder was attached to the microscope stage and the mouse was re-positioned so that the window lay flat. The holder and stage was inverted and fixed onto a heated microscope stand. Mouse physiology was monitored using a thigh sensor (Mouse Ox[®] Starr Life Sciences Corp. Oakmont, PA, USA). For mice holder optimisation studies, mice fitted with a cranial window were imaged after i.v injection of 100 µl of CD31-PE antibody (eBioscience). For brain metastasis studies, mice were imaged at various time points after intracardiac or intracarotid injection of tumour cells. If mice were imaged immediately after tumour cell injection, 50-100 µl of fluorescently labelled antibody was also injected into the carotid artery after tumour cell injection. For imaging studies starting a day or more after tumour

cell injection, mice were injected i.v. with 50-100 μ l of anti-CD31 PE and/or Oregon Green dextran (Invitrogen) to detect vasculature or 50-100 μ l of anti-mouse CD45 (PE, Brilliant Violet or Alexa Fluor 546) antibody to detect circulating immune cells and vasculature. All confocal images and videos were obtained using the LSM-710 Zeiss confocal microscope. Multiphoton imaging was performed using the MaiTai sapphire laser (Spectra Physics, Stahnsdorf, Germany) with a tuning range of 700-1040 nm.

6.3.3 LABELLING CD45 ANTIBODIES WITH ALEXA FLUOR 546

100 μ g (in 100 μ l) of purified anti-mouse CD45 antibody (Abcam) was mixed with one vial of amine reactive Alexa Fluor 546 dye (Invitrogen) and incubated for 1 h in the dark. A size exclusion column was prepared by adding rehydrated sephadex beads (Fisher Life Sciences) into a glass Pasteur pipette plugged at the narrow end with cotton wool. PBS was added to the beads and allowed to flow through before adding the labelled antibody. PBS was added in increments so that the antibody flowed through the column. When the labelled antibody approached the narrow opening of the Pasteur pipette, and the flow through was collected in 100 μ l aliquots. Each aliquot was analysed using a fluorospectrometer (Nanodrop, Thermo Scientific) to determine which tubes contained A546 labelled antibodies and to determine the concentration. Tubes containing protein were combined and spun using an Amicon-Ultra 0.5 ml centrifugal filter (Millipore) to concentrate the labelled antibody. The concentrated antibody was diluted in PBS to a final volume of 100 μ l and stored at 4°C until use.

6.4 RESULTS

6.4.1 INTRACAROTID INJECTION OF TUMOUR CELLS DELIVERS MORE CELLS TO THE BRAIN ALLOWING VISUALISATION OF TUMOUR CELLS ARRESTED IN THE BRAIN VASCULATURE OVER TIME

Our final approach to determine the role of Gr-1⁺ immune cells associated with intravascular brain metastatic cells was through trans-cranial imaging. In order to use this technique, we first optimised the conditions necessary to image tumour cells and immune cells over time through a cranial window. As we only had access to an inverted confocal microscope, we first developed a stage that enabled the mouse to be imaged whilst on its back (Figure 6.1). The effectiveness of the stage holder was tested by trans-cranial imaging of the brain vasculature after injecting mice with a CD31 antibody labelled with PE (Figure 6.1d).

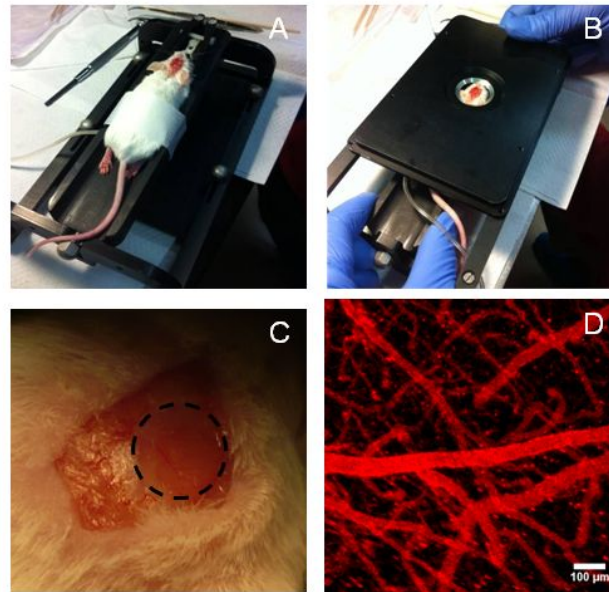


Figure 6.1: An inverted mouse holder enables imaging through a cranial window

A: The mouse was secured to a holder fitted with cheek bars to hold the head steady. Anaesthesia was provided through tubing attached to the holder beneath the mouse. B: The imaging stage was attached to the mouse holder and the mouse was adjusted until the cranial window lay flat beneath the field of view. C: An example of a cranial window in place. The circular window was placed over a 3-4 mm² removed piece of skull as indicated by the dashed lines and windows were visually inspected to ensure no damage before imaging. D: Mice were injected i.v with 100 µl of anti-mouse CD31-PE antibody prior to imaging. Brain vessels were visualised using the 561 laser in confocal imaging.

With the stage apparatus in place, we optimised conditions to image tumour cells within the brain vasculature. We used intracardiac injection to deliver 10^5 4T1-GFP cells into Balb/c mice and set-up trans-cranial imaging 24 h post tumour challenge. Although we were able to see 4T1-GFP cells growing in culture using confocal settings (Figure 6.2a), we found that 24 h after tumour cell injection, not many cells remained to be imaged. In order to increase our chance of detecting tumour cells, we changed the route of injection

and injected 10^5 4T1-GFP cells into the carotid artery. We were only able to detect GFP expressing tumour cells when mice were imaged immediately after intracarotid injection but not when mice were imaged the subsequent day. To sustain detection of tumour cells over time, we injected 2.5×10^5 4T1-GFP cells into the carotid artery, resulting in consistent detection of tumour cells under the window 24 h after injection (Figure 6.2b).

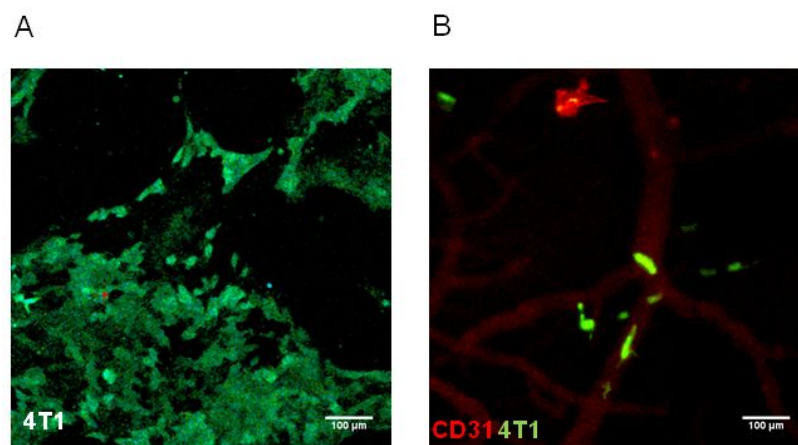


Figure 6.2: Intracarotid delivery improves sustained detection of tumour cells beneath cranial window over time

Mice fitted with a cranial window were injected with 10^5 4T1-GFP cells into the carotid artery. Although 4T1-GFP cells in culture could be imaged (A), we could not detect any tumour cells in brains of mice 24 h after tumour cell injection. B: The number of tumour cells injected into the carotid artery was increased to 2.5×10^5 . Mice were imaged 24 h later after injecting $100 \mu\text{l}$ of CD31-PE i.v to label blood vessels. GFP tumour cells were seen within the brain vasculature (red).

6.4.2 OREGON GREEN HIGH MOLECULAR WEIGHT DEXTRAN IS BETTER THAN CD31-PE ANTIBODY TO IMAGE THE BRAIN VASCULATURE USING MULTIPHOTON MICROSCOPY

PE labelled CD31 antibody and high molecular weight (70,000 MW) Oregon Green (OG) 514 dextran have been utilised by our lab to visualise blood vessels of mice *in vivo*. We compared both methods to determine which would work best for trans-cranial imaging.

Both CD31-PE and OG dextran were detected using confocal imaging when excited using their respective lasers (561 for PE, 488 for OG), but only OG dextran was visible using multi-photon microscopy (Figure 6.3a). However, due to the close wavelength overlap between GFP and OG, it was impossible to detect tumour cells in the brain and we used lambda un-mixing parameters on the ZEN software to differentiate between OG vessels and GFP tumour cells (Figure 6.3b).

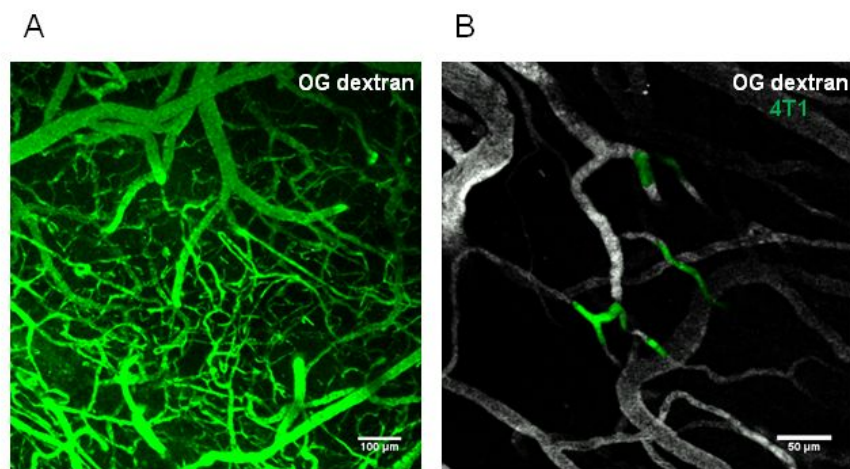


Figure 6.3: Oregon green labelled dextran allows visualisation of brain vasculature deeper within the brain.

A: Mice were injected with 2.5×10^5 4T1-GFP cells and 100 µl of CD31-PE antibody into the carotid artery and imaged within 4 h of tumour cell injection. 100 µl of OG dextran (70,000 MW) was injected i.v prior to imaging. Only OG labelled blood vessels were visible when mice were imaged using multiphoton excitation (850 nm) B: Due to the close emission spectra of OG dextran (524 nm) and GFP (519 nm), the ZEN software was used to un-mix the two signals in order to see 4T1-GFP cells within the blood vessels (white).

6.4.3 ADOPTIVE TRANSFER OF DII LABELLED IMMUNE CELLS CAN BE IMAGED THROUGH THE CRANIAL WINDOW

Using OG 514 high molecular weight dextran as our vessel marker, we optimised methods to visualise circulating immune cells using trans-cranial imaging. We re-explored adoptive transfer of Dil labelled immune cells (Chapter 5). Anti-coagulated whole blood was isolated from a naïve Balb/c mouse and purified white blood cells were dyed *in vitro* with Dil dye. Tumour cells and Dil labelled immune cells were both injected into the internal carotid artery and before imaging commenced, 100 µl of OG dextran were injected i.v. In 2 out of 3 experiments, we were able to see Dil labelled cells immediately after carotid injections and these were captured as videos (Supplementary Video 1). However, very few Dil cells were noted when mice were imaged 24 h and 72 h after injection and none were found in association with 4T1 tumour cells.

6.4.4 CIRCULATING IMMUNE CELLS CAN BE IMAGED ALONG WITH BRAIN VASCULATURE USING PE LABELLED CD45 ANTIBODY

To improve detection of host immune cells interacting with intravascular tumour cells, we utilised fluorescently labelled antibodies against circulating immune cells. Injecting FITC tagged CD11b antibodies i.v. was not successful. However, we were able to see bright round cells in the circulation as well as vascular channels using CD45-PE antibodies (Figure 6.4 and Supplementary Video 2). We verified the specificity of the anti-CD45 antibody by FACS analysis of blood samples from anti CD45-PE or isotype PE injected mice *ex vivo* labelled with anti CD45-APC or isotype APC (Figure 6.5). Only blood from mice injected with CD45-PE and *ex vivo* labelled with CD45-APC were double positive.

Using CD45-PE, we attempted time course imaging experiments after injecting mice with tumour cells. The majority of GFP tumour cells seen between 4-24 h after tumour injection cleared from within the vasculature and it was difficult to find tumour cells beyond 3 days after tumour injection. To overcome this difficulty, we injected more tumour cells via the carotid artery. By injecting 5.0×10^5 or 10^6 4T1-GFP cells, we were able to continually detect tumour cells over time (Figures 6.6, 6.7). Interestingly, we noticed substantial slowing down and rolling of CD45-PE labelled circulating immune cells 3 days after mice were injected with 10^6 4T1-GFP cells (Figure 6.7 and Supplementary Video 3). This was not seen with PBS injected mice or mice injected with 4T1-GFP cells (Supplementary Video 4). Since injecting mice with 5×10^5 4T1-GFP cells sustained detection of tumour cells over a longer time course with no apparent immune effects, we decided to use this cell dose for subsequent time course experiments.

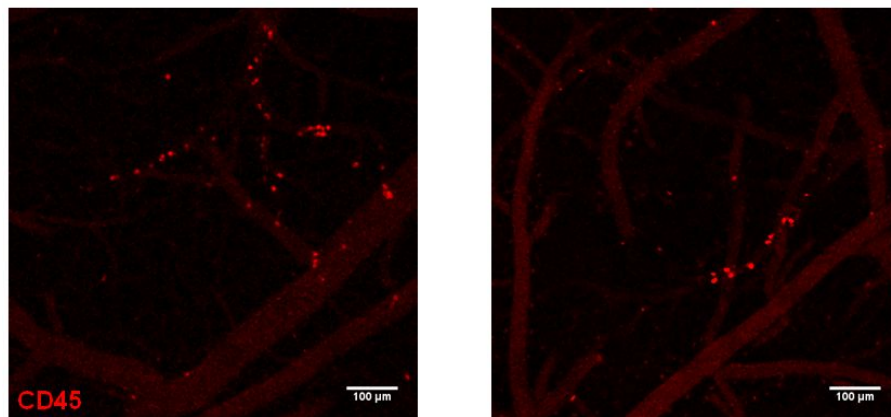


Figure 6.4: Anti-mouse CD45-PE allows detection of circulating immune cells and blood vessels

Mice were injected i.v with 100 µl of PE labelled anti-CD45 antibody and cells brightly labelled with PE were seen moving within the brain vasculature using epi-fluorescent and confocal microscopy. Free unbound antibody circulating in the blood highlighted blood vessels enabling simultaneous imaging of circulating immune cells and brain vasculature. See Supplementary Video 2 for confocal time-course images.

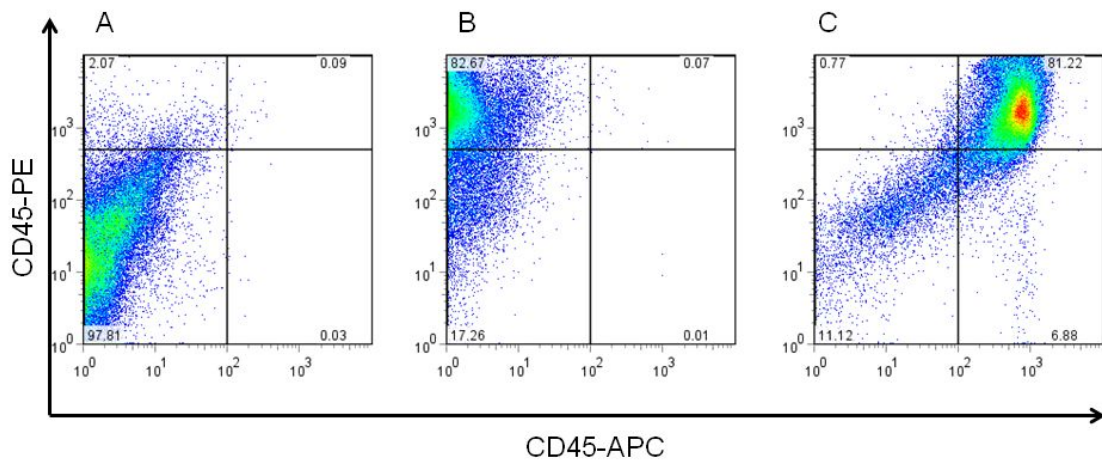


Figure 6.5: Anti-mouse CD45-PE specifically binds circulating immune cells

Mice were injected with 100 μ l of anti-mouse CD45-PE or isotype matched PE antibodies. 4 h after injection, mice were culled and anti-coagulated blood was collected for FACS analysis. A: Blood cells from Isotype-PE injected mice were not positive for PE. B: Blood from anti-mouse CD45-PE antibody injected mice were *ex vivo* labelled with mouse anti-IgG APC isotype control (B) or anti-CD45-APC (C). Only blood from mice injected with CD45-PE antibody was co-labelled with antibody against CD45-APC (double positive) indicating that CD45-PE was specifically labelling immune cells *in vivo*.

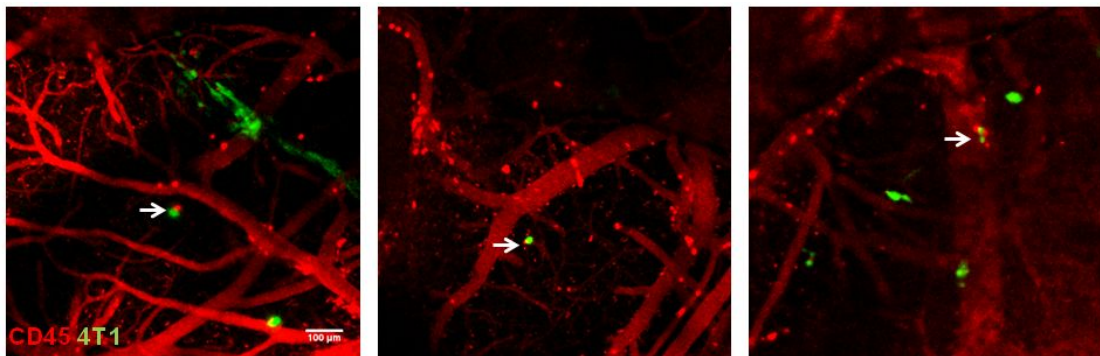


Figure 6.6: Mice injected with 5×10^5 4T1-GFP cells enable imaging tumour cells over a longer time course

Mice were injected with 5×10^5 4T1-GFP cells into the carotid artery and imaged 4 days later. Mice were injected i.v with 100 μ l of anti-mouse CD45-PE prior to imaging. 4T1 tumour clusters and individual cells were seen beneath the cranial window. 4T1 tumour-CD45 clusters were also noted (arrows). Unfortunately, this mouse could not be recovered after the imaging session and we could not follow the fate of these tumour cells.

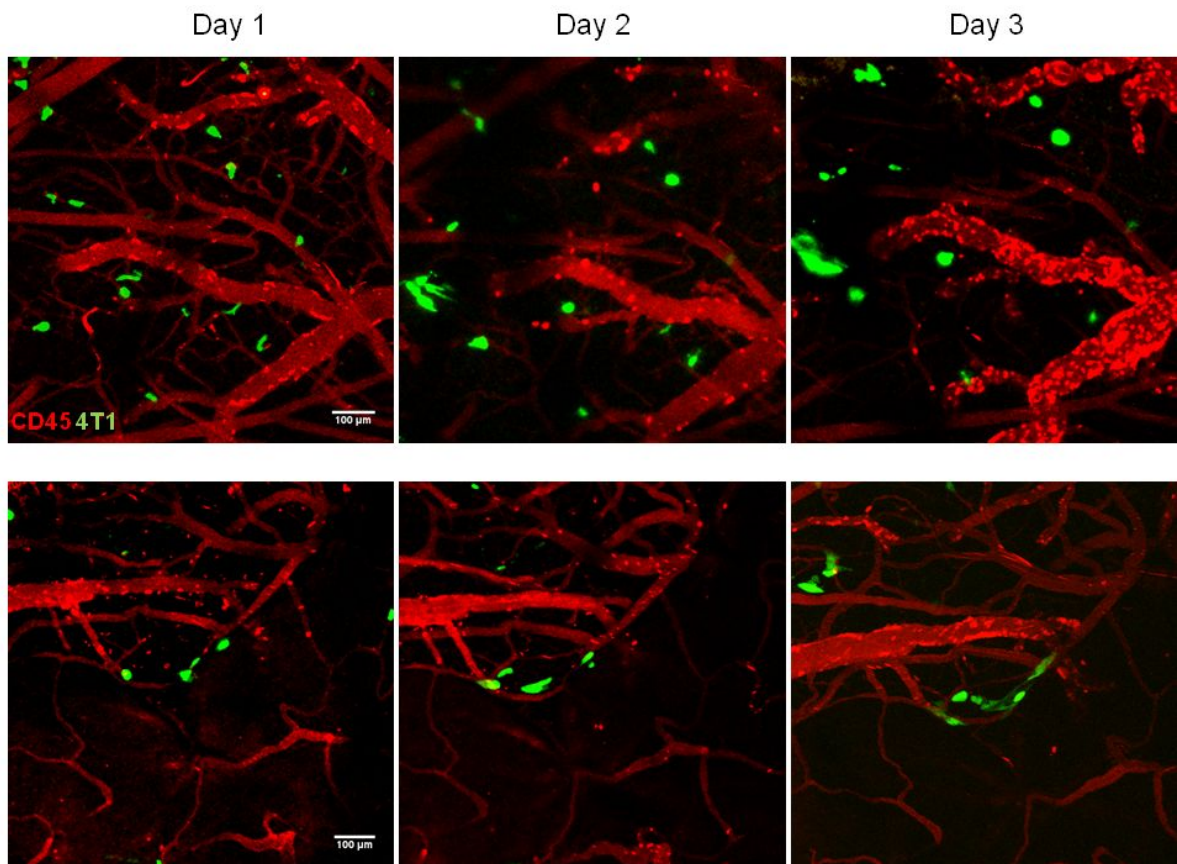


Figure 6.7: Injecting 1×10^6 4T1-GFP cells into mice induced slowing down of circulating immune cells.

Mice were injected into the carotid artery with 1×10^6 4T1-GFP cells and confocal imaging commenced 24 h after tumour injection and repeated every day for 7 days. Prior to each imaging session, mice were injected i.v with 100 μ l of anti-mouse CD45-PE. Each row represents brain images from two different mice. Each mouse was imaged over the same area on days 1, 2 and 3. Substantial slowing down of CD45-PE labelled cells was seen 3 days after tumour cell injection (see Supplementary Video 3). This increased slowing down of CD45 bright cells was not seen in mice injected with a lower dose of cells (5×10^5 4T1-GFP cells) or with PBS (Supplementary Video 4). Note proliferation of 4T1-GFP cells along blood vessels on day 3 (lower panel)

6.4.5 MULTIPHOTON MICROSCOPY ENABLES IMAGING OF TUMOUR CELLS LYING DEEPER WITHIN THE BRAIN

Using Balb/c mice injected with 5×10^5 4T1-GFP cells and CD45-PE antibody, we commenced time course experiments. Mice were imaged on days 1, 3, 5, 7-10 post tumour injection to follow any interactions between tumour cells and immune cells. We used vessel architecture as maps to image the same areas over time (Figure 6.7-6.8). During these imaging sessions we did notice a few interesting cells that lay beyond our focal depth. Unfortunately, most tumours that were visible using confocal imaging grew as sheets beneath the window and we were unable to follow single cells that lay deeper within the brain (Figure 6.8).

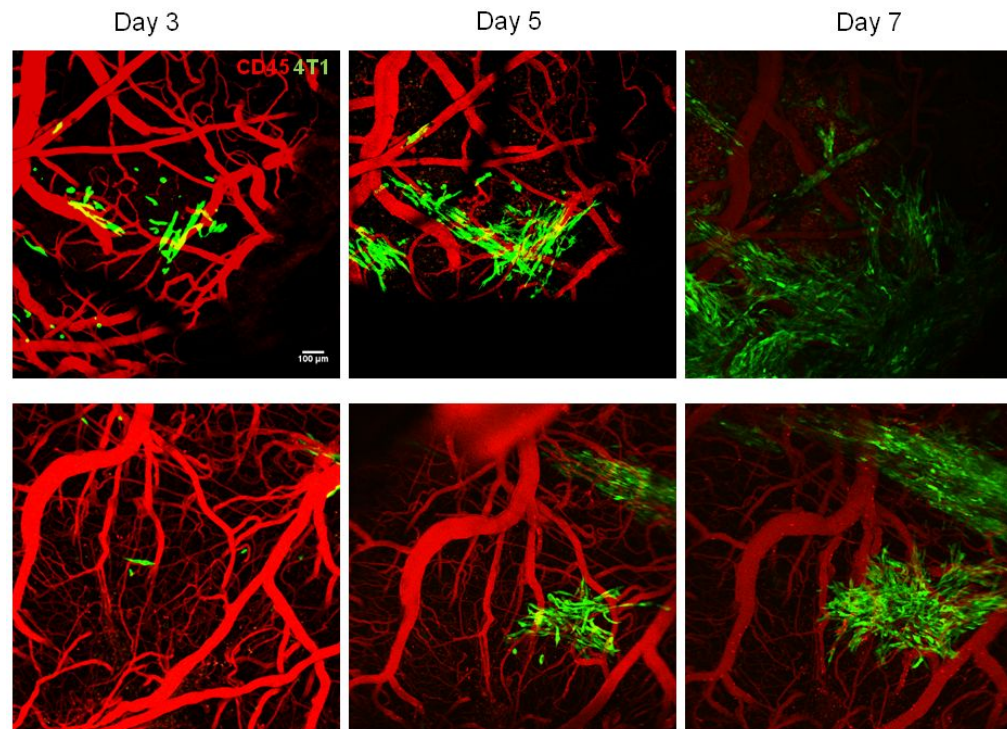


Figure 6.8: 4T1-GFP tumour grows as sheets beneath the cranial window

Mice fitted with a cranial window were injected with 5.0×10^5 4T1-GFP tumour cells into the carotid artery. Mice were injected i.v with CD45-PE prior to each imaging session. Vessel architecture, as visualised by free anti-mouse CD45-PE antibody, was used to follow the growth of tumour cells over time. However, using confocal imaging we were limited to imaging tumour cells which predominantly grew as sheets on the meninges beneath the cranial window and could not focus on brain metastases growing deeper in the brain.

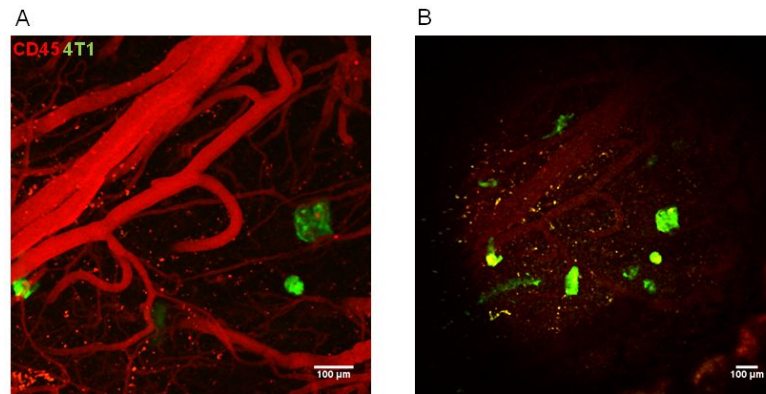


Figure 6.9: Multiphoton imaging allows visualisation of tumour cells lying below the meninges

Mice fitted with a cranial window were injected with 5.0×10^5 4T1-GFP tumour cells into the carotid artery. Mice were imaged daily after i.v injection with $100 \mu\text{l}$ of anti-mouse CD45-PE. A: Confocal image of the brain beneath the cranial window 9 days after tumour challenge shows tumour cells growing in the brain. B: When the same area was imaged using multiphoton microscopy, more tumours were detected that lay beneath the depth of view attained by confocal microscopy. However, with multiphoton imaging, signal from the PE labelled CD45 antibody was lost.

To visualise the development of brain metastases beneath the meninges, we turned to multiphoton microscopy. Although we could detect deep residing tumour cells, PE excitation is outside the range of our multiphoton laser and we lost the ability to simultaneously image tumour cells, immune cells and the vasculature (Figure 6.9). Mouse anti-CD45 is also commercially available labelled with brilliant violet but in our hands, this antibody was undetectable by epi-fluorescent, confocal and multiphoton microscopy (data not shown). To circumvent this issue, we labelled purified anti-mouse CD45 with Alexa flour 546 (A546), a dye whose excitation lies within the maximum laser wavelength of multiphoton microscopy. Mice were injected with 4T1-GFP tumour cells and 24 h later, mice were injected with CD45-A546 antibody i.v and imaged using multiphoton microscopy. We imaged over a spectrum of wavelengths and found 820 nm optimal for

concomitantly detecting GFP expressing tumour cells and A546 labelled immune cells (Figure 6.10a). We were also able to detect tumour cells lying deeper within the brain and a few tumour cells were seen associated with immune cells (Figure 6.10b). A summary of all parameters optimised in this chapter are listed in Table 6.1

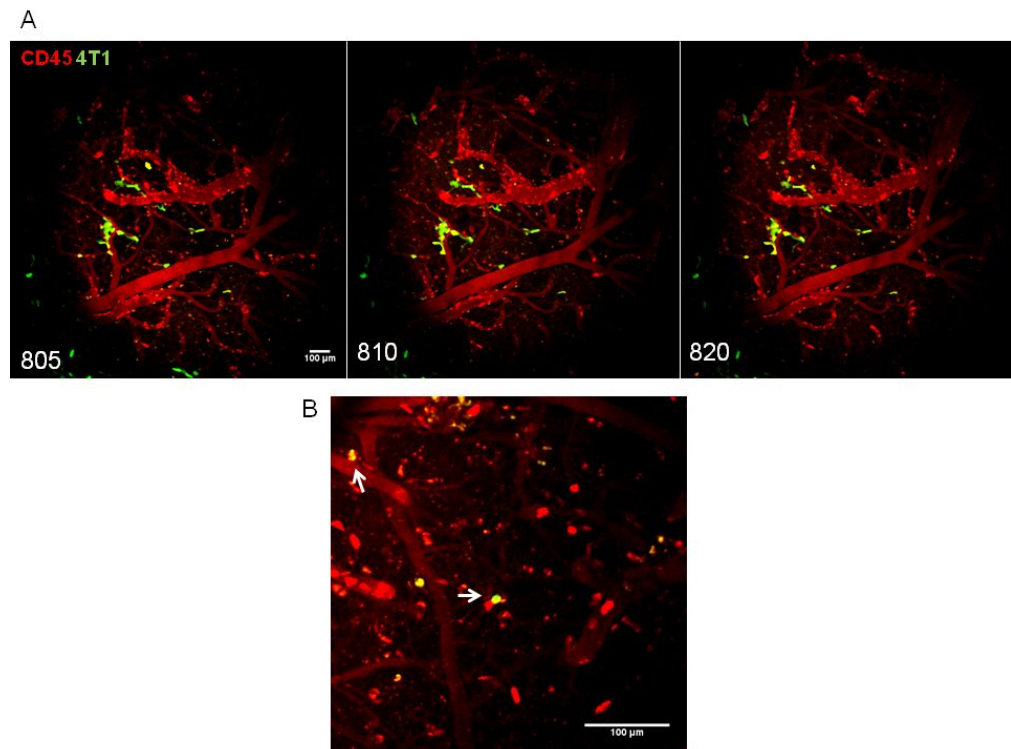


Figure 6.10: Alexa Flour 546 labelled anti-mouse CD45 allows for imaging of tumour-immune clusters lying deeper in the brain

Mice fitted with a cranial window were injected with 5×10^5 4T1-GFP cells into the intracarotid artery and 48 h later, mice were injected i.v with anti-CD45 A456 to image brains using multiphoton microscopy A: Images were taken using different laser wavelengths (810-830 nm) to determine settings which allow optimal detection of CD45-A546 immune cells and GFP tumour cells simultaneously. B: Different sections of the brain were imaged with the laser set to 820 nm. Tumour cells were seen lying below the meninges and a few tumour cells were seen associated with CD45 cells (arrows)

Table 6.1: Optimisation of *in vivo* transcranial imaging of tumour cells, circulating immune cells and brain vasculature

Optimisation parameters	Imaging tools used	Outcome
Trans-cranial imaging of mouse brains using inverted microscope	Inverted mouse holder; CD31-PE antibody to label brain vasculature	Secured mouse head with minimal movement Increased field of view
Imaging tumour cells	$10^5 - 10^6$ GFP expressing 4T1 tumour cells injected into the heart or carotid artery	5.0×10^5 4T1-GFP cells injected into the carotid artery was optimal for sustained detection of tumour cells over time.
Imaging brain vasculature	1)CD31-PE 2)Oregon Green 514 high molecular weight dextran 3)CD45-PE; CD45-A546	1) Detection of brain meningeal and superficial cortical vasculature using confocal microscope. Simultaneous imaging of vessels and tumour cells 2) Superior detection of vasculature including deep lying microvasculature using multiphoton microscopy; overlap with GFP reduces detection of tumour cells 3) Anti-CD45 did not bind vessels but vessel architecture was imaged due to free flowing unbound antibody. Simultaneous imaging of vessels and 4T1-GFP; PE is limited to confocal but A546 can be detected by both confocal and multiphoton microscopy.
Imaging circulating immune cells	1)Adoptive transfer of <i>ex vivo</i> Dil labelled immune cells 2)CD11b-FITC 3)CD45-PE 4)CD45- Brilliant violet 5)CD45-A546	1)Very few labelled immune cells were seen immediately after injection with even less were seen 24-72 h later 2)Did not work 3)Simultaneous detection of blood vessels and circulating immune cells by confocal microscopy 4)Did not work 5)Simultaneous detection of blood vessels and circulating immune cells using confocal and multiphoton microscopy

6.5 DISCUSSION

In this chapter we optimised the parameters necessary for simultaneous imaging of tumour cells, blood vessels of the brain and immune cells. Even though we did not have the time to continue the imaging studies, we have paved the way to use real time imaging to study immune cells interacting with tumour cells adhered to the brain vasculature over time. This method may prove that immune cells are necessary for successful brain metastases.

Upright microscopes are preferable when performing brain imaging studies as it is easier to position and align the cranial window underneath the lens using stereotactic frames (Kienast, von Baumgarten et al. 2010) and to easily find the cranial window when looking through the microscope lens. As we only had access to an inverted microscope, we encountered several issues. It was difficult to hold the mouse head upside down and flat without movement. It was also very difficult to find the cranial window when looking through the microscope lens. In order to resolve these issues, we made a mouse holder fitted with cheek bars to hold the head steady. Once the holder was attached to the stage, it could be adjusted so that the cranial window lay flat. Although it was still difficult to find the cranial window, we noticed a marked improvement in imaging brain vasculature when mice were set-up using the inverted holder.

With the imaging apparatus optimised, we next developed methods to simultaneously image tumour cells, blood vessels and circulating immune cells. Unfortunately, intracardiac injection of 10^5 4T1-GFP cells was not enough to image tumour cells over time. Although time consuming and technically challenging, injecting into the carotid

artery allowed more tumour cells to be delivered to the brain in order for them to be imaged under the cranial window over time. Delivering 5.0×10^5 4T1-GFP cells into the carotid artery sometimes caused ischemia in mice and the experiment had to be terminated. Fortunately, this did not occur often and we were able to use most mice for imaging experiments.

Fluorescent microparticles have been used to detect leukocytes *in vivo* (Villringer, Dirnagl et al. 1991). However, only immune cells that phagocytose these fluorescent beads can be imaged (Getts, Terry et al. 2008) and may not label our cell of interest. The use of transgenic animals engineered so that host cells constitutively express fluorescent markers have greatly advanced imaging studies (Qian, Li et al. 2011; Gil-Bernabe, Ferjancic et al. 2012). Unfortunately, these mice are of a genetic background where there are no isogenic cell lines that form brain metastases (C57 Bl/6 or FVB/N). However, it was recently reported that the E0771 breast cancer cell line isolated from a C57 Bl/6 mice formed brain metastases (Lorger 2012) and could be a potential model to use in future *in vivo* imaging of brain metastasis. To be able to image immune cells in our established models of brain metastasis, we used fluorescently labelled antibodies. Antibodies have effects on the cells they bind to and can affect results. We could not use fluorescently labelled Ly6G or Gr-1 antibodies as we and others have shown that both these antibodies deplete neutrophils and the Gr-1 antibody has additional effects on other myeloid cells (Daley, Thomay et al. 2008; Ribechini, Leenen et al. 2009). Surface markers such as CD11b are important for immune cell interaction with vessels and tumour cells (Spicer, McDonald et al. 2012) and antibodies against CD11b may interfere with this interaction.

We tried labelling circulating cells by injecting mice with CD11b-FITC or CD45-PE. CD11b-FITC did not label immune cells *in vivo* but CD45-PE antibody did. To determine whether mice injected with CD45-PE antibodies had effects on brain metastasis, we quantified the number of 4T1 brain metastases formed in mice injected daily with CD45-PE antibody or isotype-PE injected mice and found similar number of metastases in both groups (data not shown). Unexpectedly, unbound CD45-PE outlined the blood vessels and therefore we did not have to use OG dextran. There were two benefits of not relying on OG dextran. First, as OG overlapped with the emission spectra of GFP, we could not detect GFP-expressing tumour cells by eye and were dependent on software un-mixing parameters. Second, macrophages phagocytose OG dextran and when mice were imaged 24 h after i.v injection of OG, fluorescent green macrophages were evident beneath the cranial windows and interfered with detecting and imaging GFP expressing tumour cells.

Unfortunately, in most imaging studies, tumour growth on the dura or meninges occurred often and limited confocal imaging of tumour cells that were beneath the meninges. This could be a natural tendency of this cell line but we did not see 4T1 tumour growth at these locations in previous histological examinations of mice not fitted with cranial windows (see Chapter 3). Tumour growth directly under the cranial window may be a result of local inflammation. Mice fitted with a cranial window were often not experimented on until 6 weeks after window placement and the tissue beneath the window was microscopically inspected for signs of damage and inflammation before mice were used for imaging experiments. In one case, histological examination of a mouse fitted with a cranial window culled 10 days after tumour cell injection had extensive

tumour growth covering the entire surface area beneath the cranial window and penetrated deep into the cortex (data not shown). This was an exception as most brains inspected at the end of imaging experiments had evenly distributed brain metastases throughout the brain and were not limited to the site of the cranial window. To circumvent the issue of only imaging tumour cells on the brain surface, we explored the use of multiphoton microscopy. Multiphoton imaging enables detection of tumour cells residing deeper in the brain parenchyma (Kienast, von Baumgarten et al. 2010). Unfortunately, to employ multiphoton imaging, we had to utilise CD45 antibodies labelled with a fluorophore within the range of the multiphoton laser. CD45 antibodies that were commercially available included ones labelled with FITC or Brilliant Violet. We could not use FITC as this would overlap with GFP expressing 4T1 cells and although brilliant violet emission is within the range of multiphoton imaging, we could not detect any signal after injecting the antibody into mice. We were able to use CD45 antibody that we labelled with A546 to image deep lying tumour cells, blood vessels of the brain, and circulating immune cells. We imaged mice 3 days after tumour injection and found some deep lying tumour cells associated with immune cells. Unfortunately, this particular mouse had to be euthanized immediately after imaging and we did not have the time to follow up with other mice.

In this final chapter, we have optimised the conditions that allow for real time video imaging of circulating immune cells, brain vessels and tumour cells in the brain. This technique alone will not conclusively determine the role of Gr-1⁺ cells in brain metastasis but can be a powerful tool when used in conjunction with other experiments. We found

increased CD45^{hi}-tumour intravascular clusters when tumour cells were intracardiac injected into primary tumour bearing mice (Chapter 4) and can therefore employ *in vivo* imaging in tumour bearing mice. If G-CSF proves to be important for the development of brain metastases, then transcranial imaging could be used in experiments where mice are exogenously injected with G-CSF. This may show that G-CSF causes recruitment of immune cells to intravascular tumours. Transcranial imaging in these models to follow tumour-immune interaction over-time may prove that it is only those tumour cells that interact with CD45^{hi}/Gr1⁺ cells that endure to develop into brain metastases. Research can then progress into looking at methods to prevent this interaction.

CHAPTER 7: GENERAL DISCUSSION

The overall goal of this thesis was to investigate the hypothesis that host immune cells promote brain metastasis. In order to consider this theory, we first developed methods to identify the steps after dissemination which restrict tumour cells from forming brain metastases. Using ultrasound guidance to deliver tumour cells to the brain, we found that some metastatic cells that colonise the lungs and liver did not form brain metastases because they lacked the ability to adhere to brain endothelium. The metastatic cells which gave rise to brain metastases readily attached to the brain vasculature but were limited by their ability to survive within the vessel lumen. We found a few intravascular tumour cells in close association with circulating CD45^{hi} leukocytes and this interaction persisted over time. Furthermore, in mice implanted with a primary tumour, we found a correlation between increased tumour-CD45^{hi} leukocyte interaction within the brain vasculature and increased brain metastases. The tumour-associated leukocytes were identified to be Ly6G⁺Gr-1⁺ myeloid cells. Antibody-mediated depletion of neutrophils did not prevent interaction of intravascular tumour cells with circulating leukocytes nor did it decrease brain metastases, suggesting that the Gr-1⁺ cells are not neutrophils. Our findings indicate that our hypothesis is plausible and warrants further work.

7.1 ATTACHMENT TO THE BRAIN ENDOTHELIUM IS AN INTRINSIC ABILITY OF HIGHLY BRAIN METASTATIC CELLS

The brain vasculature forms a unique barrier whose selective nature stems from specialised tight junctions which stitch brain endothelial cells together (Begley and Brightman 2003). The BBB restricts passage of molecules and cells, including cancer cells,

from gaining access to the brain. Releasing B16-F10 metastatic cells into the arterial circulation did not give rise to brain metastases and LLC only sometimes formed brain metastases. However, we and others have shown that direct injection of B16F10 or LLC cells into the brain parenchyma, bypassing the BBB, results consistently in tumour formation (Perides, Zhuge et al. 2006). Therefore, these cells have the ability to grow in the brain parenchyma but are not able to traverse the BBB.

To determine what limits disseminated tumour cells within the circulation from developing into brain metastases, we developed a better method to model brain metastasis in mice. Using ultrasound guidance to perform intracardiac injection of tumour cells, we were able to quantify numbers of tumour cells that initially attach to the brain vasculature. We showed that the failure of B16F10 and LLC tumour cells to develop into brain metastases is due to their inability to adhere to brain endothelium. Our findings outline another function of the brain endothelium in restricting brain metastasis – limiting tumour cell adhesion (Chapter 4). We therefore propose that attachment to the brain is the first limiting step that determines whether disseminated tumour cells will colonise the brain.

The vascular basement membrane has been shown to be the 'soil' once tumour cells have extravasated into the brain (Carbonell, Ansorge et al. 2009). Brain metastatic cells use integrin $\beta 1$ to adhere to the vascular basement membrane and tumour cells must maintain close contact with the basement membrane in order to survive in the brain and proliferate (Carbonell, Ansorge et al. 2009; Kienast, von Baumgarten et al. 2010). Both LLC and B16F10 express $\beta 1$ integrin and expression of this integrin may be why these cancer

cells grow in the brain if directly injected (Carbonell, Ansorge et al. 2009). Since we have shown that both these cell lines cannot adhere to brain endothelium, $\beta 1$ is not likely to be important for adhesion to the brain endothelium. Based on these findings, we hypothesise that in the brain there are two components of the 'soil', endothelial and parenchymal, and both must be permissive for successful brain metastases.

The molecule that enables human breast cancer cells to attach to the brain endothelium have been identified as ST6GALNAC5, a sialyl transferase found on human and murine brain endothelium and by triple-negative breast cancer cells that metastasise specifically to the brain (Bos, Zhang et al. 2009). This protein was shown to mediate attachment and extravasation of breast cancer cells to cultured brain endothelial cells (Bos, Zhang et al. 2009). However, we show that 4T1 breast cancer cells, which are also triple-negative, do not express ST6GALNAC5 but are able to adhere to and extravasate into the brain, whilst LLC lung cancer cells express ST6GALNAC5 but cannot adhere to the brain endothelium. Therefore, we conclude that other factors must be involved that facilitate 4T1 cells to attach onto the brain endothelium. It was recently reported that Her-2 over-expressing MDA 231 breast cancer cells (MDA-231-Her2) express more αv integrin than parental cell lines (Wu, Muldoon et al. 2012). When MDA-231-Her2 breast cancer cells were treated with intetumumab, an antibody specific for αv integrin, a reduction in cancer cell adhesion was seen *in vitro*. Daily infusion of intetumumab into rats injected with MDA-231-Her2 did not affect the ability of tumour cells to adhere to the brain but did delay the onset of brain metastases and reduced the total number of brain metastases (Wu, Muldoon et al. 2012). However, since this inhibitor has also been used to reduce lung

metastases (Ning, Tian et al. 2010), αv over-expression does not seem to be specific for breast cancer cells which metastasise to the brain. VCAM-1 is an important adhesion molecule enabling leukocyte attachment to brain microvasculature (Laschinger and Engelhardt 2000; Vajkoczy, Laschinger et al. 2001; Man, Tucky et al. 2009; Steiner, Coisne et al. 2010) and has been recently shown to be expressed around established brain metastases (Serres, Soto et al. 2012). However, it is yet to be shown whether VCAM-1 or other CAMs are involved in tumour cell attachment to the brain. Screening highly and poorly brain metastatic cells for differential expression of activated integrins which bind CAMs expressed on the brain would be an attractive area for further investigation. If factors that mediate tumour cell adhesion to the brain are consistent among most brain metastatic cells or within a specific subtype, identification of these factors may provide a screening tool to determine which cancers will likely colonise the brain. This will allow for the development of tools for early detection of brain metastases and for the development of drugs which target brain specific adhesion molecules in order to prevent brain metastases.

Anticoagulation studies in mice have shown the importance of platelets in lung metastases (Im, Fu et al. 2004; Gil-Bernabe, Ferjancic et al. 2012; Zhang, Dang et al. 2012). Platelets promote tumour cell attachment and retention within the vessel lumen (Varon and Brill 2001; Im, Fu et al. 2004). The mechanism of tumour cell arrest within the brain endothelium may in part be due to physical entrapment of tumour-platelet emboli within small capillaries or due to specific molecular interactions of platelet receptors and selectin (P-selectin) molecules on inflamed vessels (Gupta and Massague 2004). Platelets

are involved in LLC and B16 lung metastases and anticoagulation reduces retention of these cells in lungs (Zhang, Dang et al. 2012). However, we found that these same tumour cells did not attach to the brain endothelium and thus infer that tumour interaction with platelets within the circulation is not sufficient for attachment to the brain vasculature. However, we did find that tumour cells attached to the brain endothelium were coated in platelets (Figure 4.3). Platelets may only adhere to tumour cells that have already attached to the endothelium, but others have reported that platelets interact with tumour cells whilst in the circulation (Varon and Brill 2001; Camerer, Qazi et al. 2004). We propose that platelets bound to circulating tumour cells may mediate loose interactions with brain endothelium (tethering, rolling), but for firm adhesion to occur, additional molecules only expressed by certain cancer cells are most likely involved. Our attempts to study the effects of anticoagulation prior to intracardiac tumour injection failed due to the detrimental effects on mice and we found anticoagulation 4 h after intracardiac injection to be ineffective. To study the effects of anticoagulation in brain metastasis may require the use of brain-seeking cell lines that form brain metastases after i.v injection.

7.2 GR-1⁺ CIRCULATING IMMUNE CELLS MAY PROMOTE BRAIN METASTASIS.

Macrophages, neutrophils and Gr-1⁺ myeloid cells have all been shown to facilitate lung metastases (Qian, Deng et al. 2009; Kowanetz, Wu et al. 2010; Gil-Bernabe, Ferjancic et al. 2012). Recently, a role for neutrophils in promoting liver metastases has been

described (Spicer, McDonald et al. 2012). Our work now implicates host Gr-1⁺ myeloid immune cells in promoting brain metastases.

Among the tumour cells which were able to seed the brain vasculature, the majority did not survive to colonise the brain. Over time, the small number of tumour cells that persisted were associated with cells that express high levels of the pan leukocyte marker, CD45, implying that these immune cells may be important for tumour cell survival. By day 4-5 after tumour injection, the surviving tumour cells began the process of extravasation and many more CD45^{hi} cells were found surrounding tumour cells. These CD45 expressing cells were morphologically distinct from resting microglia. Furthermore, when we analysed surface marker expression on these tumour associated leukocytes in brain tissues, we found these cells to be MBS⁺Gr-1⁺Ly6G⁺CD11c⁻CD3⁻ cells.

We and others have found that after injection into the arterial circulation, LLC tumour cells grew predominantly in the meninges and ventricles of the brain. The failure of the few LLC cells that attached to the brain vasculature to develop into brain metastases could be because these tumour cells are often limited to the perivascular space (Saito, Hatori et al. 2007). Monocytes and T cells which enter the brain are also often restricted to the perivascular space and do not cross the glial limitans (Tran, Hoekstra et al. 1998; Zhou, Stohlman et al. 2003; Savarin, Stohlman et al. 2010). These immune cells were only permitted to enter the brain parenchyma under certain inflammatory conditions such as West Nile virus infection or EAE and a few studies have shown that accessory immune cells were required for access past the glial limitans (McCandless, Wang et al. 2006; McCandless, Zhang et al. 2008). Even though very few LLC cells adhered to the brain

vasculature, we did note some of these associated with CD45^{hi} immune cells. Interestingly, these clusters were predominantly located in the olfactory bulb, an area of the brain where LLC sometimes formed brain metastases (Figure 3.3). Therefore, analogous to the two step model of leukocyte entry into the brain, the immune cells associated with intravascular tumour cells may be necessary for tumour cell invasion through the perivascular space. To our knowledge, ultrastructural studies of tumour cell extravasation into the brain have only been carried out with the poorly brain metastatic LLC cells (Paku, Dome et al. 2000), but our findings warrants careful analysis of tumour extravasation using highly brain-metastatic tumour cell lines such as 4T1.

7.3 GR-1+ CELLS FORM THE PRE-METASTATIC NICHE IN THE BRAIN

Factors secreted by the primary tumour set up an inflammatory setting at future sites of metastasis, termed the pre-metastatic niche (Hiratsuka, Nakamura et al. 2002; Kaplan, Riba et al. 2005). This niche has only been characterised in the lung (Hiratsuka, Watanabe et al. 2006; Kowanetz, Wu et al. 2010). We show, for the first time, that primary tumours can set up a pre-metastatic niche in the brain to increase brain metastases. Surprisingly, the increase in brain metastases is not due to increased adhesion of tumour cells to the brain as pre-conditioned mice have slightly less tumour cells adherent to the brain compared to unconditioned mice. Pre-conditioning also does not enhance the ability of the weakly brain metastatic LLC cells to adhere to the brain. We found that the increased percentage of immune-tumour clusters within the brain vasculature was linked to the increased number of brain metastases. As we found elevated levels of G-CSF in pre-conditioned mice, we propose that tumours themselves secrete G-CSF or stimulate the

host to produce G-CSF to recruit Gr-1⁺ cells to the brain. We hypothesise that these immune cells form the pre-metastatic niche in the brain to encourage the survival of tumour cells within the brain vasculature and to facilitate extravasation.

Mice bearing either MDA 231 or 4T1 primary tumours secrete G-CSF to mobilise Ly6G⁺Ly6C⁺ cells to accumulate in organs where these tumour cells spontaneously metastasise – lungs and liver (Kowanetz, Wu et al. 2010). This study reports that Ly6G⁺Ly6C⁺ cells do not accumulate in the brain or muscle (Kowanetz, Wu et al. 2010). In contrast, we find surplus numbers of Gr-1⁺ cells in brain tissue sections from 4T1 tumour bearing mice. This discrepancy could be due to the stage of tumour growth. We found that only large primary tumours pre-conditioned the brain to increase brain metastases and as lung and liver metastases occur earlier than brain metastases (Tao, Fang et al. 2008) therefore the stage of tumour growth that fosters lung and liver metastases may not yet favour brain metastases.

The immune cells implicated in forming the pre-metastatic niche to facilitate lung metastases may be different from ones involved in brain metastases. In the 4T1 spontaneous lung metastases model, neutrophils were found to be anti-metastatic (Granot, Henke et al. 2011). The anti-metastatic neutrophils were conditioned and recruited to the lung by tumour secreted CCL2 whilst G-CSF recruited neutrophils had no effect on lung metastases (Granot, Henke et al. 2011). However, another group reported that in the same mouse model, tumour secreted G-CSF recruited Ly6G⁺Ly6C⁺ cells to the lung and these immune cells promoted lung metastases (Kowanetz, Wu et al. 2010). Injecting mice that bore 66cl2 (410.1 metastatic subline related to 4T1) mammary

tumours with antibodies against Ly6G or Gr-1 reduced the number of spontaneous lung metastases (Kowanetz, Wu et al. 2010). Even though they refer to these immune cells as Ly6G⁺Ly6C⁺, they imply that lung promoting immune cells were neutrophils. We also used the same 4T1 model and saw an increase in G-CSF production but we were unable to show a reduction in brain metastases after using antibodies that deplete neutrophils. Furthermore, in an inflammatory setting, only local expression of KC and MIP-1 α resulted in recruitment of neutrophils to sites of inflammation (Wengner, Pitchford et al. 2008). We found that levels of KC were down-regulated in both MDA 231 and 4T1 tumour-bearing mice after intracardiac injection implying that neutrophils were not likely being recruited.

The different models used to assess metastases may account for why we do not see any effects on brain metastases after depleting neutrophils. Kowanetz and colleagues used a spontaneous model of lung metastasis. They did not report whether depleting antibodies had an effect on the primary tumour and they did not show whether injecting Ly6G or Gr-1 antibodies affected accumulation of Ly6G⁺Ly6C⁺ in the lung. As Gr-1 antibodies have been shown to suppress MDSC function (Ribechini, Leenen et al. 2009), this phenomenon could be the reason why they report decreased lung metastasis from the primary tumour. The reduction in spontaneous lung metastases seen after injection of Ly6G and Gr-1 antibodies in their model may likely be due to reduced tumour cell dissemination from the primary tumour and not due to decreased accumulation of Ly6G⁺Ly6C⁺ cells in the lung.

We do not believe that the metastasis associated immune cells in the brain are neutrophils. Although we found a considerable accumulation of neutrophils (Ly6G⁺Ly6C⁻Gr1⁺F4/80⁻) in the blood of pre-conditioned SCID mice after intracardiac injection with MDA 231, there were also increased numbers of Ly6G⁺Ly6C^{mid} and Ly6G⁺Ly6C^{hi} immune cells. These Ly6C expressing populations also had increased expression of Gr-1 compared to the neutrophil populations and low expression of F4/80. In tissue sections we also found tumour associated MBS⁺ immune cells to express F4/80. Although we did not quantify the numbers of F4/80 cells associated with tumour cells over time, this finding implies that the brain metastasis associated Gr-1⁺ cells are not neutrophils but most likely an immature granulocyte precursor not dissimilar to MDSC (Gabilovich, Bronte et al. 2007; Peranzoni, Zilio et al. 2010).

7.4 G-CSF INVOLVEMENT IN BRAIN METASTASES

Both brain metastatic breast cancer cell lines used in this work, 4T1 and MDA 231, secrete G-CSF (DuPre and Hunter 2007; Kowanetz, Wu et al. 2010; Waight, Hu et al. 2011). Studies have shown that G-CSF produced by 4T1 cells stimulated accumulation of granulocytic MDSC to promote primary tumour growth (Waight, Hu et al. 2011; Scott and Jeremy 2012). G-CSF produced by 4T1 and MDA 231 primary tumours has also been shown to promote recruitment of pro-metastatic Ly6G⁺Ly6G⁺ cells to the lung and neutralising G-CSF reduced lung metastases (Kowanetz, Wu et al. 2010). We found significant increase in blood levels of mouse G-CSF in tumour-bearing mice after intracardiac injection of tumour cells. These high levels of G-CSF correlated with increased accumulation of Gr-1⁺ cells in the brain. We also found a positive association

between G-CSF levels and increased tumour-immune cell clusters within the brain vasculature. Our findings implicate tumour or host derived G-CSF in recruiting Gr-1⁺ cells to the brain to promote brain metastases.

G-CSF may also play a more direct role in brain metastasis. The cytokine, SDF-1 (CXCL12), retains neutrophils within the bone marrow (Eash, Greenbaum et al. 2010). Increased expression of G-CSF locally within the bone marrow or acting from a distance dampens the effects of SDF-1, allowing neutrophils to enter the circulation (Suratt, Petty et al. 2004; Wengner, Pitchford et al. 2008). Interestingly, SDF-1 is also constitutively expressed by endothelial cells in the brain (McCandless, Wang et al. 2006; Li and Ransohoff 2008) and has been shown to sequester monocytes and T –cells within the brain perivascular space (McCandless, Wang et al. 2006; McCandless, Zhang et al. 2008). However, monocytes and T cells transmigrate through an *in vitro* model of the BBB only after stimulation with SDF-1 (Man, Tucky et al. 2012). An analogous role of SDF-1 has been shown in metastasis. *In vitro*, parental MDA 231 breast cancer cells responded to SDF-1 stimuli and migrated in response (Schmid, Rezniczek et al. 2007). However when SDF-1 was used to stimulate the bone-seeking and brain-seeking variants of MDA 231, only the bone-seeking variant responded; the brain-seeking variant had down-regulated expression of the SDF-1 receptor, CXCR4. Therefore, SDF-1 expressed within the bone marrow may cause bone metastasis (Wang, Loberg et al. 2006) and SDF-1 expressed by brain endothelium may enable tumour cells to migrate through the BBB but SDF-1 retains the tumour cells within the perivascular space. The brain-seeking variant of MDA 231 may readily form brain metastases because it lacks expression of CXCR4 and easily passes

through the perivascular space. We propose that in our brain metastasis model, G-CSF may facilitate tumour escape into the brain parenchyma by over-riding the effects of SDF-1. Receptors for G-CSF are found on brain endothelium and G-CSF readily crosses the BBB (Schneider, Kuhn et al. 2005). Therefore, G-CSF may have a dual role in brain metastasis: G-CSF may recruit metastasis promoting Gr-1⁺ cells to the brain in order to enable tumour cells arrested within the brain vasculature to extravasate through the BBB and G-CSF may also counteract the effects of SDF-1 in the perivascular space to promote passage of tumour cells through the glial limitans. Since 4T1 and MDA 231 cells endogenously express CXCR4 (Smith, Luker et al. 2004; Schmid, Reznicek et al. 2007) but do not have receptors for G-CSF (Waight, Hu et al. 2011), it is plausible that Gr-1⁺ cells, which express both receptors (Hiratsuka, Duda et al. 2010), are needed to support extravasation through the glial limitans. Analysing the effects of neutralising G-CSF and CXCR4 on cancer cell survival and extravasation into the brain will allow for this hypothesis to be tested.

7.5 CONCLUDING REMARKS

The findings presented in this work describe two steps that are crucial for disseminated tumour cells to form brain metastases. First we showed that the attachment to the brain endothelium is restrictive and requires expression of a specific receptor(s) by disseminated metastatic cells. Analysing the differential expression of adhesion molecules expressed by highly brain metastatic 4T1 and MDA 231 and the weakly brain metastatic B16F10 and LLC may reveal new targets for study and development of therapeutics. Secondly, we showed that those tumour cells which specifically adhere to the brain

endothelium face the impenetrability of the BBB and spend an extended period of time exposed to the circulation, minimising their chance of survival and subsequent extravasation into the brain. We have shown that circulating immune cells interact with a small percentage of tumour cells within the brain vasculature. It is yet to be determined what the exact purpose of this interaction is but we propose that tumour- or host-secreted G-CSF recruits non-neutrophil Gr-1⁺ cells to intravascular brain metastatic cells to support their survival and/or extravasation. We have developed an *in vivo* imaging method to observe what these immune cells might do and our data provide a framework for further investigation into the functional role of G-CSF and tumour associated Gr-1⁺ cells. Future studies where G-CSF is neutralised in tumour bearing mice or knocked-out of brain metastatic cell-lines may provide conclusive data to back-up our hypothesis. If true, this provides a great starting point to develop therapies targeting G-CSF in order to prevent brain metastases.

REFERENCES

- Abbott, N., L. Ronnback, et al. (2006). "Astrocyte-endothelial interactions at the blood-brain barrier." Nature reviews. Neuroscience **7**(1): 41-94.
- Abbott, N. J., A. A. Patabendige, et al. (2010). "Structure and function of the blood-brain barrier." Neurobiol Dis **37**(1): 13-25.
- Aboody, K. S., J. Najbauer, et al. (2006). "Targeting of melanoma brain metastases using engineered neural stem/progenitor cells." Neuro Oncol **8**(2): 119-26.
- Abrey, L. E. and C. Christodoulou (2001). "Temozolomide for treating brain metastases." Semin Oncol **28**(4 Suppl 13): 34-42.
- Agrawal, S., P. Anderson, et al. (2006). "Dystroglycan is selectively cleaved at the parenchymal basement membrane at sites of leukocyte extravasation in experimental autoimmune encephalomyelitis." J Exp Med **203**(4): 1007-19.
- Al-Hajj, M., M. S. Wicha, et al. (2003). "Prospective identification of tumorigenic breast cancer cells." Proc Natl Acad Sci U S A **100**(7): 3983-8.
- Allavena, P., A. Sica, et al. (2008). "The Yin-Yang of tumor-associated macrophages in neoplastic progression and immune surveillance." Immunol Rev **222**: 155-61.
- Alliot, F., J. Rutin, et al. (1998). "Ly-6C is expressed in brain vessels endothelial cells but not in microglia of the mouse." Neurosci Lett **251**(1): 37-40.
- Almand, B., J. Clark, et al. (2001). "Increased production of immature myeloid cells in cancer patients: a mechanism of immunosuppression in cancer." Journal of immunology **166**(1): 678-767.
- Altman, J. (1969). "Autoradiographic and histological studies of postnatal neurogenesis. IV. Cell proliferation and migration in the anterior forebrain, with special reference to persisting neurogenesis in the olfactory bulb." J Comp Neurol **137**(4): 433-57.
- Altman, J. and G. D. Das (1965). "Autoradiographic and histological evidence of postnatal hippocampal neurogenesis in rats." J Comp Neurol **124**(3): 319-35.
- Andre, F., W. Xia, et al. (2009). "CXCR4 expression in early breast cancer and risk of distant recurrence." Oncologist **14**(12): 1182-8.
- Arnold, S. M., A. B. Young, et al. (1999). "Expression of p53, bcl-2, E-cadherin, matrix metalloproteinase-9, and tissue inhibitor of metalloproteinases-1 in paired primary tumors and brain metastasis." Clin Cancer Res **5**(12): 4028-33.
- Arora, S., A. Ranade, et al. (2011). "MicroRNA-328 is associated with (non-small) cell lung cancer (NSCLC) brain metastasis and mediates NSCLC migration." International journal of cancer. Journal international du cancer **129**(11): 2621-2652.
- Aslakson, C. J. and F. R. Miller (1992). "Selective events in the metastatic process defined by analysis of the sequential dissemination of subpopulations of a mouse mammary tumor." Cancer Res **52**(6): 1399-405.
- Auchter, R. M., J. P. Lamond, et al. (1996). "A multiinstitutional outcome and prognostic factor analysis of radiosurgery for resectable single brain metastasis." Int J Radiat Oncol Biol Phys **35**(1): 27-35.
- Balkwill, F. and L. Coussens (2004). "Cancer: an inflammatory link." Nature **431**(7007): 405-411.

- Banks, W. A. (2009). "Characteristics of compounds that cross the blood-brain barrier." BMC Neurol **9 Suppl 1**: S3.
- Basse, P., P. Hokland, et al. (1988). "Fate of tumor cells injected into left ventricle of heart in BALB/c mice: role of natural killer cells." J Natl Cancer Inst **80**(9): 657-65.
- Baumann, N. and D. Pham-Dinh (2001). "Biology of oligodendrocyte and myelin in the mammalian central nervous system." Physiol Rev **81**(2): 871-927.
- Bechmann, I., I. Galea, et al. (2007). "What is the blood-brain barrier (not)?" Trends in immunology **28**(1): 5-16.
- Bechmann, I., E. Kwidzinski, et al. (2001). "Turnover of rat brain perivascular cells." Exp Neurol **168**(2): 242-9.
- Bechmann, I., J. Priller, et al. (2001). "Immune surveillance of mouse brain perivascular spaces by blood-borne macrophages." Eur J Neurosci **14**(10): 1651-8.
- Begley, D. J. and M. W. Brightman (2003). "Structural and functional aspects of the blood-brain barrier." Prog Drug Res **61**: 39-78.
- Bendell, J. C., S. M. Domchek, et al. (2003). "Central nervous system metastases in women who receive trastuzumab-based therapy for metastatic breast carcinoma." Cancer **97**(12): 2972-7.
- Benedettini, E., L. Sholl, et al. (2010). "Met activation in non-small cell lung cancer is associated with de novo resistance to EGFR inhibitors and the development of brain metastasis." The American journal of pathology **177**(1): 415-438.
- Berghoff, A., H. Lassmann, et al. (2012). "Characterization of the inflammatory response to solid cancer metastases in the human brain." Clinical & experimental metastasis.
- Bertram, J. S. and P. Janik (1980). "Establishment of a cloned line of Lewis Lung Carcinoma cells adapted to cell culture." Cancer Lett **11**(1): 63-73.
- Bertrand, Y., M. Demeule, et al. (2007). "Melanotransferrin induces human melanoma SK-Mel-28 cell invasion in vivo." Biochem Biophys Res Commun **353**(2): 418-23.
- Blamire, A. M., D. C. Anthony, et al. (2000). "Interleukin-1beta -induced changes in blood-brain barrier permeability, apparent diffusion coefficient, and cerebral blood volume in the rat brain: a magnetic resonance study." J Neurosci **20**(21): 8153-9.
- Bocchietto, E., A. Guglielmetti, et al. (1993). "Proliferative and migratory responses of murine microvascular endothelial cells to granulocyte-colony-stimulating factor." J Cell Physiol **155**(1): 89-95.
- Bolos, V., M. Blanco, et al. (2009). "Notch signalling in cancer stem cells." Clin Transl Oncol **11**(1): 11-9.
- Borowsky, A. D., R. Namba, et al. (2005). "Syngeneic mouse mammary carcinoma cell lines: two closely related cell lines with divergent metastatic behavior." Clin Exp Metastasis **22**(1): 47-59.
- Borsig, L., R. Wong, et al. (2002). "Synergistic effects of L- and P-selectin in facilitating tumor metastasis can involve non-mucin ligands and implicate leukocytes as enhancers of metastasis." Proceedings of the National Academy of Sciences of the United States of America **99**(4): 2193-2201.
- Bos, P. D., X. H. Zhang, et al. (2009). "Genes that mediate breast cancer metastasis to the brain." Nature **459**(7249): 1005-9.

- Brantley, E. C., L. Guo, et al. (2010). "Nitric oxide-mediated tumoricidal activity of murine microglial cells." Transl Oncol **3**(6): 380-8.
- Brayton, J., Z. Qing, et al. (1998). "Influence of adhesion molecule expression by human brain microvessel endothelium on cancer cell adhesion." Journal of neuroimmunology **89**(1-2): 104-116.
- Brinkmann, V., U. Reichard, et al. (2004). "Neutrophil extracellular traps kill bacteria." Science **303**(5663): 1532-5.
- Brochard, V., B. Combadiere, et al. (2009). "Infiltration of CD4+ lymphocytes into the brain contributes to neurodegeneration in a mouse model of Parkinson disease." J Clin Invest **119**(1): 182-92.
- Bronte, V., D. B. Chappell, et al. (1999). "Unopposed production of granulocyte-macrophage colony-stimulating factor by tumors inhibits CD8+ T cell responses by dysregulating antigen-presenting cell maturation." J Immunol **162**(10): 5728-37.
- Brown, A. M. and B. R. Ransom (2007). "Astrocyte glycogen and brain energy metabolism." Glia **55**(12): 1263-71.
- Budhu, A., M. Forgues, et al. (2006). "Prediction of venous metastases, recurrence, and prognosis in hepatocellular carcinoma based on a unique immune response signature of the liver microenvironment." Cancer Cell **10**(2): 99-111.
- Bush, T. G., N. Puvanachandra, et al. (1999). "Leukocyte infiltration, neuronal degeneration, and neurite outgrowth after ablation of scar-forming, reactive astrocytes in adult transgenic mice." Neuron **23**(2): 297-308.
- Bussolino, F., J. M. Wang, et al. (1989). "Granulocyte- and granulocyte-macrophage-colony stimulating factors induce human endothelial cells to migrate and proliferate." Nature **337**(6206): 471-3.
- Butcher, E. C. (1991). "Leukocyte-endothelial cell recognition: three (or more) steps to specificity and diversity." Cell **67**(6): 1033-6.
- Byram, S. C., M. J. Carson, et al. (2004). "CD4-positive T cell-mediated neuroprotection requires dual compartment antigen presentation." J Neurosci **24**(18): 4333-9.
- Cai, J., C. Parr, et al. (2006). "Decreased pigment epithelium-derived factor expression in human breast cancer progression." Clin Cancer Res **12**(11 Pt 1): 3510-7.
- Calvete, J. J. (1995). "On the structure and function of platelet integrin alpha IIb beta 3, the fibrinogen receptor." Proc Soc Exp Biol Med **208**(4): 346-60.
- Camerer, E., A. A. Qazi, et al. (2004). "Platelets, protease-activated receptors, and fibrinogen in hematogenous metastasis." Blood **104**(2): 397-401.
- Carbonell, W. S., O. Ansorge, et al. (2009). "The vascular basement membrane as "soil" in brain metastasis." PLoS One **4**(6): 5857.
- Carriero, M. V., P. Franco, et al. (2011). "Regulation of cell migration and invasion by specific modules of uPA: mechanistic insights and specific inhibitors." Curr Drug Targets **12**(12): 1761-71.
- Carson, M., J. Thrash, et al. (2006). "The cellular response in neuroinflammation: The role of leukocytes, microglia and astrocytes in neuronal death and survival." Clinical neuroscience research **6**(5): 237-482.
- Ceresoli, G. L., F. Cappuzzo, et al. (2004). "Gefitinib in patients with brain metastases from non-small-cell lung cancer: a prospective trial." Ann Oncol **15**(7): 1042-7.

- Chalmers, A. J., E. M. Ruff, et al. (2009). "Cytotoxic effects of temozolomide and radiation are additive- and schedule-dependent." Int J Radiat Oncol Biol Phys **75**(5): 1511-9.
- Charafe-Jauffret, E., C. Ginestier, et al. (2010). "Aldehyde dehydrogenase 1-positive cancer stem cells mediate metastasis and poor clinical outcome in inflammatory breast cancer." Clin Cancer Res **16**(1): 45-55.
- Chen, B. E., B. Lendvai, et al. (2000). "Imaging high-resolution structure of GFP-expressing neurons in neocortex in vivo." Learn Mem **7**(6): 433-41.
- Chen, L.-T., S.-D. Xu, et al. (2012). "MicroRNA-378 is associated with non-small cell lung cancer brain metastasis by promoting cell migration, invasion and tumor angiogenesis." Medical Oncology **29**(3): 1673-80.
- Chiang, A. C. and J. Massague (2008). "Molecular basis of metastasis." N Engl J Med **359**(26): 2814-23.
- Choi, M.-R., B. Rizia, et al. (2012). "Delivery of nanoparticles to brain metastases of breast cancer using a cellular Trojan horse." Cancer Nanotechnology **3**(1-6): 47-54.
- Christopherson, K. S., E. M. Ullian, et al. (2005). "Thrombospondins are astrocyte-secreted proteins that promote CNS synaptogenesis." Cell **120**(3): 421-33.
- Claus, E. (2011). "Neurosurgical management of metastases in the central nervous system." Nature reviews. Clinical oncology **9**(2): 79-165.
- Colotta, F., P. Allavena, et al. (2009). "Cancer-related inflammation, the seventh hallmark of cancer: links to genetic instability." Carcinogenesis **30**(7): 1073-1154.
- Colton, C. A. and D. M. Wilcock (2010). "Assessing activation states in microglia." CNS Neurol Disord Drug Targets **9**(2): 174-91.
- Compston, A. and A. Coles (2002). "Multiple sclerosis." Lancet **359**(9313): 1221-31.
- Conley, F. K. (1982). "Murine models of metastatic neoplasia to the central nervous system." Cancer Metastasis Rev **1**(3): 203-13.
- Cruz-Munoz, W., S. Man, et al. (2008). "Development of a preclinical model of spontaneous human melanoma central nervous system metastasis." Cancer Res **68**(12): 4500-5.
- Cryan, J. F. and A. Holmes (2005). "The ascent of mouse: advances in modelling human depression and anxiety." Nat Rev Drug Discov **4**(9): 775-90.
- Cserr, H. F. and M. Bundgaard (1984). "Blood-brain interfaces in vertebrates: a comparative approach." Am J Physiol **246**(3 Pt 2): 277-88.
- D'Mello, C., T. Le, et al. (2009). "Cerebral microglia recruit monocytes into the brain in response to tumor necrosis factor- α signaling during peripheral organ inflammation." J Neurosci **29**(7): 2089-102.
- Daley, J., A. Thomay, et al. (2008). "Use of Ly6G-specific monoclonal antibody to deplete neutrophils in mice." Journal of leukocyte biology **83**(1): 64-134.
- Davalos, D., J. Grutzendler, et al. (2005). "ATP mediates rapid microglial response to local brain injury in vivo." Nat Neurosci **8**(6): 752-8.
- Dave, S. S., G. Wright, et al. (2004). "Prediction of survival in follicular lymphoma based on molecular features of tumor-infiltrating immune cells." N Engl J Med **351**(21): 2159-69.
- Davis, E., T. Foster, et al. (1994). "Cellular forms and functions of brain microglia." Brain research bulletin **34**(1): 73-81.

- De Palma, M., M. A. Venneri, et al. (2005). "Tie2 identifies a hematopoietic lineage of proangiogenic monocytes required for tumor vessel formation and a mesenchymal population of pericyte progenitors." Cancer Cell **8**(3): 211-26.
- de Vries, H. E., M. C. Blom-Roosemalen, et al. (1996). "The influence of cytokines on the integrity of the blood-brain barrier in vitro." J Neuroimmunol **64**(1): 37-43.
- Del Bigio, M. R. (2010). "Ependymal cells: biology and pathology." Acta Neuropathol **119**(1): 55-73.
- Delattre, J. Y., G. Krol, et al. (1988). "Distribution of brain metastases." Arch Neurol **45**(7): 741-4.
- Demetri, G. D. and J. D. Griffin (1991). "Granulocyte colony-stimulating factor and its receptor." Blood **78**(11): 2791-808.
- DeNardo, D., M. Johansson, et al. (2008). "Immune cells as mediators of solid tumor metastasis." Cancer metastasis reviews **27**(1): 11-19.
- Denk, W. (1994). "Two-photon scanning photochemical microscopy: mapping ligand-gated ion channel distributions." Proc Natl Acad Sci U S A **91**(14): 6629-33.
- Denkins, Y., J. Reiland, et al. (2004). "Brain metastases in melanoma: roles of neurotrophins." Neuro Oncol **6**(2): 154-65.
- Devito, N., M. Yu, et al. (2011). "Retrospective study of patients with brain metastases from melanoma receiving concurrent whole-brain radiation and temozolomide." Anticancer Res **31**(12): 4537-43.
- DeWitt, D. A., G. Perry, et al. (1998). "Astrocytes regulate microglial phagocytosis of senile plaque cores of Alzheimer's disease." Exp Neurol **149**(2): 329-40.
- Dexter, D. L., H. M. Kowalski, et al. (1978). "Heterogeneity of tumor cells from a single mouse mammary tumor." Cancer Res **38**(10): 3174-81.
- Diaz-Montero, C. M., M. L. Salem, et al. (2009). "Increased circulating myeloid-derived suppressor cells correlate with clinical cancer stage, metastatic tumor burden, and doxorubicin-cyclophosphamide chemotherapy." Cancer Immunol Immunother **58**(1): 49-59.
- Ding, S., T. Fellin, et al. (2007). "Enhanced astrocytic Ca²⁺ signals contribute to neuronal excitotoxicity after status epilepticus." J Neurosci **27**(40): 10674-84.
- Ding, S., T. Wang, et al. (2009). "Photothrombosis ischemia stimulates a sustained astrocytic Ca²⁺ signaling in vivo." Glia **57**(7): 767-76.
- Dolcetti, L., E. Peranzoni, et al. (2010). "Hierarchy of immunosuppressive strength among myeloid-derived suppressor cell subsets is determined by GM-CSF." European journal of immunology **40**(1): 22-57.
- Dombeck, D. A., A. N. Khabbaz, et al. (2007). "Imaging large-scale neural activity with cellular resolution in awake, mobile mice." Neuron **56**(1): 43-57.
- Donelli, M. G., M. Zucchetti, et al. (1992). "Do anticancer agents reach the tumor target in the human brain?" Cancer Chemother Pharmacol **30**(4): 251-60.
- Dontu, G., M. Al-Hajj, et al. (2003). "Stem cells in normal breast development and breast cancer." Cell Prolif **36 Suppl 1**: 59-72.
- Drell, T. L. t., J. Joseph, et al. (2003). "Effects of neurotransmitters on the chemokinesis and chemotaxis of MDA-MB-468 human breast carcinoma cells." Breast Cancer Res Treat **80**(1): 63-70.

- Du Pasquier, R. A., M. J. Kuroda, et al. (2004). "A prospective study demonstrates an association between JC virus-specific cytotoxic T lymphocytes and the early control of progressive multifocal leukoencephalopathy." Brain **127**(Pt 9): 1970-8.
- Duda, D., A. M. Duyverman, et al. (2010). "Malignant cells facilitate lung metastasis by bringing their own soil." Proceedings of the National Academy of Sciences of the United States of America **107**(50): 21677-21759.
- Dumitru, C., K. Moses, et al. (2012). "Neutrophils and granulocytic myeloid-derived suppressor cells: immunophenotyping, cell biology and clinical relevance in human oncology." Cancer immunology, immunotherapy **61**(8): 1155-67.
- DuPre, S. and K. Hunter (2007). "Murine mammary carcinoma 4T1 induces a leukemoid reaction with splenomegaly: association with tumor-derived growth factors." Experimental and molecular pathology **82**(1): 12-36.
- DuPre, S. A., D. Redelman, et al. (2007). "The mouse mammary carcinoma 4T1: characterization of the cellular landscape of primary tumours and metastatic tumour foci." Int J Exp Pathol **88**(5): 351-60.
- Eash, K. J., A. M. Greenbaum, et al. (2010). "CXCR2 and CXCR4 antagonistically regulate neutrophil trafficking from murine bone marrow." J Clin Invest **120**(7): 2423-31.
- Eddleston, M. and L. Mucke (1993). "Molecular profile of reactive astrocytes--implications for their role in neurologic disease." Neuroscience **54**(1): 15-36.
- Egan, C. E., W. Sukhumavasi, et al. (2008). "Understanding the multiple functions of Gr-1(+) cell subpopulations during microbial infection." Immunol Res **40**(1): 35-48.
- Ehrlich, M. (1885). Königthum und staatswesen der alten Hebräer : nach biblischen und talmudischen quellen bearbeitet. Steinamanger, Gedruckt bei J. v. Bertalanffy.
- Engelhardt, B. and R. Ransohoff (2005). "The ins and outs of T-lymphocyte trafficking to the CNS: anatomical sites and molecular mechanisms." Trends in immunology **26**(9): 485-580.
- Ewing, J. (1928). Neoplastic diseases; a treatise on tumors. Philadelphia, London,, W.B. Saunders.
- Falchook, G. S., G. V. Long, et al. (2012). "Dabrafenib in patients with melanoma, untreated brain metastases, and other solid tumours: a phase 1 dose-escalation trial." Lancet **379**(9829): 1893-901.
- Fan, J., B. Cai, et al. (2011). "Integrin beta4 signaling promotes mammary tumor cell adhesion to brain microvascular endothelium by inducing ErbB2-mediated secretion of VEGF." Ann Biomed Eng **39**(8): 2223-41.
- Farrell, C. L. and R. R. Shivers (1984). "Capillary junctions of the rat are not affected by osmotic opening of the blood-brain barrier." Acta Neuropathol **63**(3): 179-89.
- Fazakas, C., I. Wilhelm, et al. (2011). "Transmigration of melanoma cells through the blood-brain barrier: role of endothelial tight junctions and melanoma-released serine proteases." PLoS One **6**(6): 20758.
- Felding-Habermann, B., R. Habermann, et al. (1996). "Role of beta3 integrins in melanoma cell adhesion to activated platelets under flow." J Biol Chem **271**(10): 5892-900.
- Fernandez-Garcia, N. I., O. V. Volpert, et al. (2007). "Pigment epithelium-derived factor as a multifunctional antitumor factor." J Mol Med (Berl) **85**(1): 15-22.

- Fidler, I. J. (1970). "Metastasis: quantitative analysis of distribution and fate of tumor embolilabeled with 125 I-5-iodo-2'-deoxyuridine." J Natl Cancer Inst **45**(4): 773-82.
- Fidler, I. J. (1973). "The relationship of embolic homogeneity, number, size and viability to the incidence of experimental metastasis." Eur J Cancer **9**(3): 223-7.
- Fidler, I. J. and G. L. Nicolson (1976). "Organ selectivity for implantation survival and growth of B16 melanoma variant tumor lines." J Natl Cancer Inst **57**(5): 1199-202.
- Fidler, I. J., G. Schackert, et al. (1999). "The biology of melanoma brain metastasis." Cancer Metastasis Rev **18**(3): 387-400.
- Fitzgerald, D., D. Emerson, et al. (2012). "TPI-287, a new taxane family member, reduces the brain metastatic colonization of breast cancer cells." Molecular cancer therapeutics **11**(9): 1959-67.
- Fitzgerald, D. P., D. Palmieri, et al. (2008). "Reactive glia are recruited by highly proliferative brain metastases of breast cancer and promote tumor cell colonization." Clin Exp Metastasis **25**(7): 799-810.
- Fitzgerald, D. P., P. Subramanian, et al. (2012). "Opposing effects of pigment epithelium-derived factor on breast cancer cell versus neuronal survival: implication for brain metastasis and metastasis-induced brain damage." Cancer Res **72**(1): 144-53.
- Fridlender, Z. G. and S. M. Albelda (2012). "Tumor-associated neutrophils: friend or foe?" Carcinogenesis **33**(5): 949-55.
- Fridlender, Z. G., J. Sun, et al. (2009). "Polarization of tumor-associated neutrophil phenotype by TGF-beta: "N1" versus "N2" TAN." Cancer Cell **16**(3): 183-94.
- Friedman, A. D. (2002). "Transcriptional regulation of granulocyte and monocyte development." Oncogene **21**(21): 3377-90.
- Fujimaki, T. (2005). "Surgical treatment of brain metastasis." Int J Clin Oncol **10**(2): 74-80.
- Fujita, M., G. Kohanbash, et al. (2011). "COX-2 blockade suppresses gliomagenesis by inhibiting myeloid-derived suppressor cells." Cancer research **71**(7): 2664-2738.
- Gabrilovich, D. I., V. Bronte, et al. (2007). Cancer Res **67**(1): 425-426.
- Gabrilovich, D. I. and S. Nagaraj (2009). "Myeloid-derived suppressor cells as regulators of the immune system." Nat Rev Immunol **9**(3): 162-74.
- Galea, I., I. Bechmann, et al. (2007). "What is immune privilege (not)?" Trends in immunology **28**(1): 12-20.
- Gamboa-Vignolle, C., T. Ferrari-Carballo, et al. (2012). "Whole-brain irradiation with concomitant daily fixed-dose temozolomide for brain metastases treatment: a randomised phase II trial." Radiother Oncol **102**(2): 187-91.
- Gao, P. and R. R. Shivers (2004). "Correlation of the presence of blood-brain barrier tight junctions and expression of zonula occludens protein ZO-1 in vitro: a freeze-fracture and immunofluorescence study." J Submicrosc Cytol Pathol **36**(1): 7-15.
- Gaspar, L., C. Scott, et al. (1997). "Recursive partitioning analysis (RPA) of prognostic factors in three Radiation Therapy Oncology Group (RTOG) brain metastases trials." Int J Radiat Oncol Biol Phys **37**(4): 745-51.
- Gavrilovic, I. T. and J. B. Posner (2005). "Brain metastases: epidemiology and pathophysiology." J Neurooncol **75**(1): 5-14.
- Geissmann, F., S. Jung, et al. (2003). "Blood monocytes consist of two principal subsets with distinct migratory properties." Immunity **19**(1): 71-153.

- Getts, D. R., R. L. Terry, et al. (2008). "Ly6c+ "inflammatory monocytes" are microglial precursors recruited in a pathogenic manner in West Nile virus encephalitis." J Exp Med **205**(10): 2319-37.
- Gil-Bernabe, A. M., S. Ferjancic, et al. (2012). "Recruitment of monocytes/macrophages by tissue factor-mediated coagulation is essential for metastatic cell survival and premetastatic niche establishment in mice." Blood **119**(13): 3164-75.
- Ginhoux, F., M. Greter, et al. (2010). "Fate mapping analysis reveals that adult microglia derive from primitive macrophages." Science **330**(6005): 841-5.
- Glinsky, G. V. and V. V. Glinsky (1996). "Apoptosis and metastasis: a superior resistance of metastatic cancer cells to programmed cell death." Cancer Lett **101**(1): 43-51.
- Gordon, G. R., S. J. Mulligan, et al. (2007). "Astrocyte control of the cerebrovasculature." Glia **55**(12): 1214-21.
- Gordon, S. and P. R. Taylor (2005). "Monocyte and macrophage heterogeneity." Nat Rev Immunol **5**(12): 953-64.
- Granot, Z., E. Henke, et al. (2011). "Tumor entrained neutrophils inhibit seeding in the premetastatic lung." Cancer Cell **20**(3): 300-314.
- Guillemin, G. J. and B. J. Brew (2004). "Microglia, macrophages, perivascular macrophages, and pericytes: a review of function and identification." J Leukoc Biol **75**(3): 388-97.
- Gupta, G. P. and J. Massague (2004). "Platelets and metastasis revisited: a novel fatty link." J Clin Invest **114**(12): 1691-3.
- Hamilton, J. A. and G. P. Anderson (2004). "GM-CSF Biology." Growth Factors **22**(4): 225-31.
- Hanahan, D. and L. Coussens (2012). "Accessories to the crime: functions of cells recruited to the tumor microenvironment." Cancer Cell **21**(3): 309-331.
- Hanahan, D. and R. Weinberg (2000). "The hallmarks of cancer." Cell **100**(1): 57-127.
- Hanahan, D. and R. Weinberg (2011). "Hallmarks of cancer: the next generation." Cell **144**(5): 646-720.
- Hanna, N. (1982). "Inhibition of experimental tumor metastasis by selective activation of natural killer cells." Cancer Res **42**(4): 1337-42.
- Hanna, N. (1982). "Role of natural killer cells in control of cancer metastasis." Cancer Metastasis Rev **1**(1): 45-64.
- He, B. P., J. J. Wang, et al. (2006). "Differential reactions of microglia to brain metastasis of lung cancer." Mol Med **12**(7-8): 161-70.
- He, S., G. Lamers, et al. (2012). "Neutrophil-mediated experimental metastasis is enhanced by VEGFR inhibition in a zebrafish xenograft model." The Journal of pathology **227**(4): 431-476.
- Henderson, R., J. Hobbs, et al. (2003). "Rapid recruitment of inflammatory monocytes is independent of neutrophil migration." Blood **102**(1): 328-363.
- Hengel, K., G. Sidhu, et al. (2012). "Attributes of brain metastases from breast and lung cancer." Int J Clin Oncol **epub ahead of print**
- Heyn, C., J. A. Ronald, et al. (2006). "In vivo MRI of cancer cell fate at the single-cell level in a mouse model of breast cancer metastasis to the brain." Magn Reson Med **56**(5): 1001-10.

- Hickey, W. and H. Kimura (1988). "Perivascular microglial cells of the CNS are bone marrow-derived and present antigen in vivo." Science (New York, N.Y.) **239**(4837): 290-292.
- Hiratsuka, S., D. G. Duda, et al. (2010). "C-X-C receptor type 4 promotes metastasis by activating p38 mitogen-activated protein kinase in myeloid differentiation antigen (Gr-1)-positive cells." Proc Natl Acad Sci U S A **108**(1): 302-7.
- Hiratsuka, S., K. Nakamura, et al. (2002). "MMP9 induction by vascular endothelial growth factor receptor-1 is involved in lung-specific metastasis." Cancer Cell **2**(4): 289-300.
- Hiratsuka, S., A. Watanabe, et al. (2006). "Tumour-mediated upregulation of chemoattractants and recruitment of myeloid cells predetermines lung metastasis." Nature cell biology **8**(12): 1369-1444.
- Hoenerhoff, M., I. Chu, et al. (2009). "BMI1 cooperates with H-RAS to induce an aggressive breast cancer phenotype with brain metastases." Oncogene **28**(34): 3022-3054.
- Holmes, G. P., K. Negus, et al. (1998). "Distinct but overlapping expression patterns of two vertebrate slit homologs implies functional roles in CNS development and organogenesis." Mech Dev **79**(1-2): 57-72.
- Hoshina, D., R. Abe, et al. (2010). "The role of PEDF in tumor growth and metastasis." Curr Mol Med **10**(3): 292-5.
- Hsieh, H.-L., H.-H. Wang, et al. (2010). "Transforming growth factor- β 1 induces matrix metalloproteinase-9 and cell migration in astrocytes: roles of ROS-dependent ERK- and JNK-NF- κ B pathways." Journal of neuroinflammation **7**: 88.
- Huh, S., S. Liang, et al. (2010). "Transiently entrapped circulating tumor cells interact with neutrophils to facilitate lung metastasis development." Cancer research **70**(14): 6071-6153.
- Hussain, S. F., D. Yang, et al. (2006). "The role of human glioma-infiltrating microglia/macrophages in mediating antitumor immune responses." Neuro Oncol **8**(3): 261-79.
- Hwang, T. L., T. P. Close, et al. (1996). "Predilection of brain metastasis in gray and white matter junction and vascular border zones." Cancer **77**(8): 1551-5.
- Iadecola, C. and M. Nedergaard (2007). "Glial regulation of the cerebral microvasculature." Nat Neurosci **10**(11): 1369-76.
- Im, J. H., W. Fu, et al. (2004). "Coagulation facilitates tumor cell spreading in the pulmonary vasculature during early metastatic colony formation." Cancer Res **64**(23): 8613-9.
- Israelski, D. M. and J. S. Remington (1988). "Toxoplasmic encephalitis in patients with AIDS." Infect Dis Clin North Am **2**(2): 429-45.
- Izraely, S., O. Sagi-Assif, et al. (2012). "The metastatic microenvironment: Brain-residing melanoma metastasis and dormant micrometastasis." International journal of cancer. Journal international du cancer **131**(5): 1071-1153.
- Jaalinoja, J., R. Herva, et al. (2000). "Matrix metalloproteinase 2 (MMP-2) immunoreactive protein is associated with poor grade and survival in brain neoplasms." J Neurooncol **46**(1): 81-90.

- Jaeger, B. N., J. Donadieu, et al. (2012). "Neutrophil depletion impairs natural killer cell maturation, function, and homeostasis." J Exp Med **209**(3): 565-80.
- Jensen, H. K., F. Donskov, et al. (2009). "Presence of intratumoral neutrophils is an independent prognostic factor in localized renal cell carcinoma." J Clin Oncol **27**(28): 4709-17.
- Jia, W., C. Jackson-Cook, et al. (2010). "Tumor-infiltrating, myeloid-derived suppressor cells inhibit T cell activity by nitric oxide production in an intracranial rat glioma + vaccination model." Journal of neuroimmunology **223**(1-2): 20-50.
- John, G. R., S. C. Lee, et al. (2003). "Cytokines: powerful regulators of glial cell activation." Neuroscientist **9**(1): 10-22.
- Kaku, H., H. Kaneko, et al. (2007). "Elderberry bark lectins evolved to recognize Neu5Ac alpha2,6Gal/GalNAc sequence from a Gal/GalNAc binding lectin through the substitution of amino-acid residues critical for the binding to sialic acid." J Biochem **142**(3): 393-401.
- Kaplan, R. N., R. D. Riba, et al. (2005). "VEGFR1-positive haematopoietic bone marrow progenitors initiate the pre-metastatic niche." Nature **438**(7069): 820-7.
- Kawaguchi, T., M. Kawaguchi, et al. (1983). "Brain meninges tumor formation by in vivo-selected metastatic B16 melanoma variants in mice." Clin Exp Metastasis **1**(3): 247-59.
- Kawaguchi, T. and K. Nakamura (1986). "Analysis of the lodgement and extravasation of tumor cells in experimental models of hematogenous metastasis." Cancer Metastasis Rev **5**(2): 77-94.
- Kaya, D., Y. Gursoy-Ozdemir, et al. (2005). "VEGF protects brain against focal ischemia without increasing blood-brain permeability when administered intracerebroventricularly." J Cereb Blood Flow Metab **25**(9): 1111-8.
- Kesari, S. and T. T. Batchelor (2003). "Leptomeningeal metastases." Neurol Clin **21**(1): 25-66.
- Kienast, Y., L. von Baumgarten, et al. (2010). "Real-time imaging reveals the single steps of brain metastasis formation." Nat Med **16**(1): 116-22.
- Kim, M. Y., T. Oskarsson, et al. (2009). "Tumor self-seeding by circulating cancer cells." Cell **139**(7): 1315-26.
- Kim, S.-J., J.-S. Kim, et al. (2011). "Astrocytes upregulate survival genes in tumor cells and induce protection from chemotherapy." Neoplasia (New York, N.Y.) **13**(3): 286-384.
- Kirsch, M., P. Weigel, et al. (2005). "Therapy of hematogenous melanoma brain metastases with endostatin." Clin Cancer Res **11**(3): 1259-67.
- Koc, M., J. McGregor, et al. (2005). "Gamma Knife radiosurgery for intracranial metastatic melanoma: an analysis of survival and prognostic factors." J Neurooncol **71**(3): 307-13.
- Kojima, S., H. Tadenuma, et al. (1989). "Enhancement of plasminogen activator activity in cultured endothelial cells by granulocyte colony-stimulating factor." J Cell Physiol **138**(1): 192-6.
- Kowanetz, M., X. Wu, et al. (2010). "Granulocyte-colony stimulating factor promotes lung metastasis through mobilization of Ly6G+Ly6C+ granulocytes." Proceedings of the

- National Academy of Sciences of the United States of America **107**(50): 21248-21303.
- Kruger, A., O. H. Sanchez-Sweatman, et al. (1998). "Host TIMP-1 overexpression confers resistance to experimental brain metastasis of a fibrosarcoma cell line." Oncogene **16**(18): 2419-23.
- Krumina, G. (2005). "Metastatic disease of the brain: parenchyma." Eur Radiol **15**(3): 608-16.
- Kusmartsev, S., S. Nagaraj, et al. (2005). "Tumor-associated CD8+ T cell tolerance induced by bone marrow-derived immature myeloid cells." J Immunol **175**(7): 4583-92.
- Lai, R., C. T. Dang, et al. (2004). "The risk of central nervous system metastases after trastuzumab therapy in patients with breast carcinoma." Cancer **101**(4): 810-6.
- Laschinger, M. and B. Engelhardt (2000). "Interaction of alpha4-integrin with VCAM-1 is involved in adhesion of encephalitogenic T cell blasts to brain endothelium but not in their transendothelial migration in vitro." J Neuroimmunol **102**(1): 32-43.
- Laubli, H. and L. Borsig (2010). "Selectins promote tumor metastasis." Semin Cancer Biol **20**(3): 169-77.
- Laubli, H., K. S. Spanaus, et al. (2009). "Selectin-mediated activation of endothelial cells induces expression of CCL5 and promotes metastasis through recruitment of monocytes." Blood **114**(20): 4583-91.
- Lee, B. C., T. H. Lee, et al. (2004). "Involvement of the chemokine receptor CXCR4 and its ligand stromal cell-derived factor 1alpha in breast cancer cell migration through human brain microvascular endothelial cells." Mol Cancer Res **2**(6): 327-38.
- Lee, I., P. Fox, et al. (2012). "The expression of p-STAT3 in stage IV melanoma: risk of CNS metastasis and survival." Oncotarget **3**(3): 336-380.
- Lee, T. H., H. K. Avraham, et al. (2003). "Vascular endothelial growth factor modulates the transendothelial migration of MDA-MB-231 breast cancer cells through regulation of brain microvascular endothelial cell permeability." J Biol Chem **278**(7): 5277-84.
- Leek, R. D., C. E. Lewis, et al. (1996). "Association of macrophage infiltration with angiogenesis and prognosis in invasive breast carcinoma." Cancer Res **56**(20): 4625-9.
- Li, B., C. Wang, et al. (2012). "Elevated PLGF contributes to small-cell lung cancer brain metastasis." Oncogene **epub ahead of publication**
- Li, B., W. D. Zhao, et al. (2006). "Involvement of Rho/ROCK signalling in small cell lung cancer migration through human brain microvascular endothelial cells." FEBS Lett **580**(17): 4252-60.
- Li, F., B. Tiede, et al. (2007). "Beyond tumorigenesis: cancer stem cells in metastasis." Cell Res **17**(1): 3-14.
- Li, M. and R. M. Ransohoff (2008). "Multiple roles of chemokine CXCL12 in the central nervous system: a migration from immunology to neurobiology." Prog Neurobiol **84**(2): 116-31.
- Li, Z., X. Gu, et al. (2012). "microRNA expression profiles in human colorectal cancers with brain metastases." Oncology letters **3**(2): 346-696.

- Lin, E. Y., V. Gouon-Evans, et al. (2002). "The macrophage growth factor CSF-1 in mammary gland development and tumor progression." J Mammary Gland Biol Neoplasia **7**(2): 147-62.
- Lin, E. Y., J. F. Li, et al. (2007). "Vascular endothelial growth factor restores delayed tumor progression in tumors depleted of macrophages." Mol Oncol **1**(3): 288-302.
- Lin, E. Y., J. F. Li, et al. (2006). "Macrophages regulate the angiogenic switch in a mouse model of breast cancer." Cancer Res **66**(23): 11238-46.
- Lin, E. Y., A. V. Nguyen, et al. (2001). "Colony-stimulating factor 1 promotes progression of mammary tumors to malignancy." J Exp Med **193**(6): 727-40.
- Lin, N. U. and E. P. Winer (2007). "Brain metastases: the HER2 paradigm." Clin Cancer Res **13**(6): 1648-55.
- Lin, Q., K. Balasubramanian, et al. (2010). "Reactive astrocytes protect melanoma cells from chemotherapy by sequestering intracellular calcium through gap junction communication channels." Neoplasia (New York, N.Y.) **12**(9): 748-802.
- Liotta, L., M. Saidel, et al. (1976). "The significance of hematogenous tumor cell clumps in the metastatic process." Cancer research **36**(3): 889-983.
- Lopez, A., M. Strath, et al. (1984). "Differentiation antigens on mouse eosinophils and neutrophils identified by monoclonal antibodies." British journal of haematology **57**(3): 489-583.
- Lorger, M. (2012). "Tumour microenvironment in the brain." Cancers **4**(1): 218-243.
- Lorger, M. and B. Felding-Habermann (2010). "Capturing changes in the brain microenvironment during initial steps of breast cancer brain metastasis." Am J Pathol **176**(6): 2958-71.
- Lorger, M., J. S. Krueger, et al. (2009). "Activation of tumor cell integrin alphavbeta3 controls angiogenesis and metastatic growth in the brain." Proc Natl Acad Sci U S A **106**(26): 10666-71.
- Lossinsky, A. S. and R. R. Shivers (2004). "Structural pathways for macromolecular and cellular transport across the blood-brain barrier during inflammatory conditions. Review." Histol Histopathol **19**(2): 535-64.
- Lucas, T., A. Waisman, et al. (2010). "Differential roles of macrophages in diverse phases of skin repair." J Immunol **184**(7): 3964-77.
- Lutz, S. E., Y. Zhao, et al. (2009). "Deletion of astrocyte connexins 43 and 30 leads to a dysmyelinating phenotype and hippocampal CA1 vacuolation." J Neurosci **29**(24): 7743-52.
- Man, S., B. Tucky, et al. (2009). "alpha4 Integrin/FN-CS1 mediated leukocyte adhesion to brain microvascular endothelial cells under flow conditions." Journal of neuroimmunology **210**(1-2): 92-101.
- Man, S., B. Tucky, et al. (2012). "CXCL12-induced monocyte-endothelial interactions promote lymphocyte transmigration across an in vitro blood-brain barrier." Sci Transl Med **4**(119): 119-14.
- Mantovani, A. (2009). "The yin-yang of tumor-associated neutrophils." Cancer Cell **16**(3): 173-177.

- Mantovani, A., S. Sozzani, et al. (2002). "Macrophage polarization: tumor-associated macrophages as a paradigm for polarized M2 mononuclear phagocytes." Trends Immunol **23**(11): 549-55.
- Maraveyas, A., M. Johnson, et al. (2010). "Malignant melanoma as a target malignancy for the study of the anti-metastatic properties of the heparins." Cancer metastasis reviews **29**(4): 777-861.
- Marchetti, D., J. Li, et al. (2000). "Astrocytes contribute to the brain-metastatic specificity of melanoma cells by producing heparanase." Cancer Res **60**(17): 4767-70.
- Maroldi, R., C. Ambrosi, et al. (2005). "Metastatic disease of the brain: extra-axial metastases (skull, dura, leptomeningeal) and tumour spread." Eur Radiol **15**(3): 617-26.
- Martinez, F. O., L. Helming, et al. (2009). "Alternative activation of macrophages: an immunologic functional perspective." Annu Rev Immunol **27**: 451-83.
- Mason, S. D. and J. A. Joyce (2011). "Proteolytic networks in cancer." Trends Cell Biol **21**(4): 228-37.
- Mazzucco, L., P. Borzini, et al. (2010). "Platelet-derived factors involved in tissue repair-from signal to function." Transfus Med Rev **24**(3): 218-34.
- McCandless, E., Q. Wang, et al. (2006). "CXCL12 limits inflammation by localizing mononuclear infiltrates to the perivascular space during experimental autoimmune encephalomyelitis." Journal of Immunology **177**(11): 8053-8117.
- McCandless, E., B. Zhang, et al. (2008). "CXCR4 antagonism increases T cell trafficking in the central nervous system and improves survival from West Nile virus encephalitis." Proceedings of the National Academy of Sciences of the United States of America **105**(32): 11270-11275.
- McGowan, P., C. Simeone, et al. (2011). "Notch1 inhibition alters the CD44^{hi}/CD24^{lo} population and reduces the formation of brain metastases from breast cancer." Molecular cancer research : MCR **9**(7): 834-878.
- Medawar, P. B. (1948). "Immunity to homologous grafted skin; the fate of skin homografts transplanted to the brain, to subcutaneous tissue, and to the anterior chamber of the eye." Br J Exp Pathol **29**(1): 58-69.
- Medjkane, S., C. Perez-Sanchez, et al. (2009). "Myocardin-related transcription factors and SRF are required for cytoskeletal dynamics and experimental metastasis." Nat Cell Biol **11**(3): 257-68.
- Mendes, O., H. T. Kim, et al. (2007). "MMP2 role in breast cancer brain metastasis development and its regulation by TIMP2 and ERK1/2." Clin Exp Metastasis **24**(5): 341-51.
- Mendes, O., H. T. Kim, et al. (2005). "Expression of MMP2, MMP9 and MMP3 in breast cancer brain metastasis in a rat model." Clin Exp Metastasis **22**(3): 237-46.
- Menter, D., J. Herrmann, et al. (1995). "The role of trophic factors and autocrine/paracrine growth factors in brain metastasis." Clinical & experimental metastasis **13**(2): 67-155.
- Miyamoto, S., H. Yagi, et al. (2006). "Heparin-binding epidermal growth factor-like growth factor as a novel targeting molecule for cancer therapy." Cancer Sci **97**(5): 341-7.

- Moscetti, L., F. Nelli, et al. (2007). "Up-front chemotherapy and radiation treatment in newly diagnosed nonsmall cell lung cancer with brain metastases: survey by Outcome Research Network for Evaluation of Treatment Results in Oncology." Cancer **109**(2): 274-81.
- Muller, A., B. Homey, et al. (2001). "Involvement of chemokine receptors in breast cancer metastasis." Nature **410**(6824): 50-56.
- Nagaraj, S., M. Collazo, et al. (2009). "Regulatory myeloid suppressor cells in health and disease." Cancer Res **69**(19): 7503-6.
- Nagaraj, S. and D. I. Gabrilovich (2007). "Myeloid-derived suppressor cells." Adv Exp Med Biol **601**: 213-23.
- Nagaraj, S. and D. I. Gabrilovich (2008). "Tumor escape mechanism governed by myeloid-derived suppressor cells." Cancer Res **68**(8): 2561-3.
- Nagaraj, S. and D. I. Gabrilovich (2010). "Myeloid-derived suppressor cells in human cancer." Cancer J **16**(4): 348-53.
- Nagaraj, S. and D. I. Gabrilovich (2010). "Regulation of suppressive function of myeloid-derived suppressor cells by CD4(+) T cells." Semin Cancer Biol **22**(4): 282-8.
- Nagaraj, S., K. Gupta, et al. (2007). "Altered recognition of antigen is a mechanism of CD8+ T cell tolerance in cancer." Nat Med **13**(7): 828-35.
- Nagaraj, S., A. G. Schrum, et al. (2010). "Mechanism of T cell tolerance induced by myeloid-derived suppressor cells." J Immunol **184**(6): 3106-16.
- Nakajima, K. and S. Kohsaka (2001). "Microglia: activation and their significance in the central nervous system." J Biochem **130**(2): 169-75.
- Nakano, H., M. Yanagita, et al. (2001). "CD11c(+)B220(+)Gr-1(+) cells in mouse lymph nodes and spleen display characteristics of plasmacytoid dendritic cells." The Journal of experimental medicine **194**(8): 1171-1179.
- Nam, D. H., H. M. Jeon, et al. (2008). "Activation of notch signaling in a xenograft model of brain metastasis." Clin Cancer Res **14**(13): 4059-66.
- Nayak, L., L. E. Abrey, et al. (2009). "Intracranial dural metastases." Cancer **115**(9): 1947-53.
- Netland, P. A. and B. R. Zetter (1985). "Metastatic potential of B16 melanoma cells after in vitro selection for organ-specific adherence." J Cell Biol **101**(3): 720-4.
- Nicolson, G. L., M. Nakajima, et al. (1994). "Malignant melanoma metastasis to brain: role of degradative enzymes and responses to paracrine growth factors." J Neurooncol **18**(2): 139-49.
- Nie, F., J. Yang, et al. (2012). "Involvement of epidermal growth factor receptor overexpression in the promotion of breast cancer brain metastasis." Cancer **118**(21): 5198-209.
- Nimmerjahn, A. (2012). "Two-photon imaging of microglia in the mouse cortex in vivo." Cold Spring Harb Protoc **epub ahead of publication**.
- Nimmerjahn, A., F. Kirchhoff, et al. (2005). "Resting microglial cells are highly dynamic surveillants of brain parenchyma in vivo." Science **308**(5726): 1314-8.
- Ning, S., J. Tian, et al. (2010). "Anti-alpha v integrin monoclonal antibody intetumumab enhances the efficacy of radiation therapy and reduces metastasis of human cancer xenografts in nude rats." Cancer Res **70**(19): 7591-9.

- Nishizuka, I., T. Ishikawa, et al. (2002). "Analysis of gene expression involved in brain metastasis from breast cancer using cDNA microarray." Breast Cancer **9**(1): 26-32.
- Noda, M., T. Seike, et al. (2009). "The role of immune cells in brain metastasis of lung cancer cells and neuron-tumor cell interaction." Russ Fiziol Zh Im I M Sechenova **95**(12): 1386-96.
- Nozawa, H., C. Chiu, et al. (2006). "Infiltrating neutrophils mediate the initial angiogenic switch in a mouse model of multistage carcinogenesis." Proc Natl Acad Sci U S A **103**(33): 12493-8.
- Nussbaum, E. S., H. R. Djalilian, et al. (1996). "Brain metastases. Histology, multiplicity, surgery, and survival." Cancer **78**(8): 1781-8.
- O'Neill, B. P., N. J. Iturria, et al. (2003). "A comparison of surgical resection and stereotactic radiosurgery in the treatment of solitary brain metastases." Int J Radiat Oncol Biol Phys **55**(5): 1169-76.
- Obara, M., M. Szeliga, et al. (2008). "Regulation of pH in the mammalian central nervous system under normal and pathological conditions: facts and hypotheses." Neurochem Int **52**(6): 905-19.
- Osman, A. (2012). "MicroRNAs in health and disease--basic science and clinical applications." Clin Lab **58**(5-6): 393-402.
- Ostrand-Rosenberg, S. and P. Sinha (2009). "Myeloid-derived suppressor cells: linking inflammation and cancer." J Immunol **182**(8): 4499-506.
- Owens, T., I. Bechmann, et al. (2008). "Perivascular spaces and the two steps to neuroinflammation." J Neuropathol Exp Neurol **67**(12): 1113-21.
- Paget, S. (1989). "The distribution of secondary growths in cancer of the breast. 1889." Cancer Metastasis Rev **8**(2): 98-101.
- Paik, S., S. Shak, et al. (2004). "A multigene assay to predict recurrence of tamoxifen-treated, node-negative breast cancer." N Engl J Med **351**(27): 2817-26.
- Paku, S., B. Dome, et al. (2000). "Organ-specificity of the extravasation process: an ultrastructural study." Clin Exp Metastasis **18**(6): 481-92.
- Palmieri, D., J. L. Bronder, et al. (2007). "Her-2 overexpression increases the metastatic outgrowth of breast cancer cells in the brain." Cancer Res **67**(9): 4190-8.
- Palmieri, D., A. F. Chambers, et al. (2007). "The biology of metastasis to a sanctuary site." Clin Cancer Res **13**(6): 1656-62.
- Palumbo, J. S., K. E. Talmage, et al. (2005). "Platelets and fibrin(ogen) increase metastatic potential by impeding natural killer cell-mediated elimination of tumor cells." Blood **105**(1): 178-85.
- Park, E., S. Kim, et al. (2011). "Cross-species hybridization of microarrays for studying tumor transcriptome of brain metastasis." Proceedings of the National Academy of Sciences of the United States of America **108**(42): 17456-17517.
- Patchell, R. A., P. A. Tibbs, et al. (1990). "A randomized trial of surgery in the treatment of single metastases to the brain." N Engl J Med **322**(8): 494-500.
- Pekarek, L. A., B. A. Starr, et al. (1995). "Inhibition of tumor growth by elimination of granulocytes." J Exp Med **181**(1): 435-40.
- Peranzoni, E., S. Zilio, et al. (2010). "Myeloid-derived suppressor cell heterogeneity and subset definition." Current opinion in immunology **22**(2): 238-282.

- Perea, G., M. Navarrete, et al. (2009). "Tripartite synapses: astrocytes process and control synaptic information." Trends Neurosci **32**(8): 421-31.
- Perera, M., E. Ribot, et al. (2012). "In Vivo Magnetic Resonance Imaging for Investigating the Development and Distribution of Experimental Brain Metastases due to Breast Cancer." Translational oncology **5**(3): 217-242.
- Perides, G., Y. Zhuge, et al. (2006). "The fibrinolytic system facilitates tumor cell migration across the blood-brain barrier in experimental melanoma brain metastasis." BMC Cancer **6**: 56.
- Pollard, J. W. (2009). "Trophic macrophages in development and disease." Nat Rev Immunol **9**(4): 259-70.
- Priller, J., A. Flugel, et al. (2001). "Targeting gene-modified hematopoietic cells to the central nervous system: use of green fluorescent protein uncovers microglial engraftment." Nat Med **7**(12): 1356-61.
- Pukrop, T., F. Dehghani, et al. (2010). "Microglia promote colonization of brain tissue by breast cancer cells in a Wnt-dependent way." Glia **58**(12): 1477-89.
- Pulaski, B. A. and S. Ostrand-Rosenberg (1998). "Reduction of established spontaneous mammary carcinoma metastases following immunotherapy with major histocompatibility complex class II and B7.1 cell-based tumor vaccines." Cancer Res **58**(7): 1486-93.
- Qian, B., Y. Deng, et al. (2009). "A distinct macrophage population mediates metastatic breast cancer cell extravasation, establishment and growth." PLoS One **4**(8): 6562.
- Qian, B. Z., J. Li, et al. (2011). "CCL2 recruits inflammatory monocytes to facilitate breast-tumour metastasis." Nature **475**(7355): 222-5.
- Ransohoff, R., P. KivisÃkk, et al. (2003). "Three or more routes for leukocyte migration into the central nervous system." Nature reviews. Immunology **3**(7): 569-650.
- Rashidi, B., M. Yang, et al. (2000). "A highly metastatic Lewis lung carcinoma orthotopic green fluorescent protein model." Clin Exp Metastasis **18**(1): 57-60.
- Raychaudhuri, B., P. Rayman, et al. (2011). "Myeloid-derived suppressor cell accumulation and function in patients with newly diagnosed glioblastoma." Neuro-oncology **13**(6): 591-600.
- Reese, T. S. and M. J. Karnovsky (1967). "Fine structural localization of a blood-brain barrier to exogenous peroxidase." J Cell Biol **34**(1): 207-17.
- Reiland, J., R. D. Sanderson, et al. (2004). "Heparanase degrades syndecan-1 and perlecan heparan sulfate: functional implications for tumor cell invasion." J Biol Chem **279**(9): 8047-55.
- Ribechini, E., V. Greifenberg, et al. (2010). "Subsets, expansion and activation of myeloid-derived suppressor cells." Medical microbiology and immunology **199**(3): 273-354.
- Ribechini, E., P. Leenen, et al. (2009). "Gr-1 antibody induces STAT signaling, macrophage marker expression and abrogation of myeloid-derived suppressor cell activity in BM cells." European journal of immunology **39**(12): 3538-3589.
- Rodrigues, J., G. Gonzalez, et al. (2010). "Normal human monocytes exposed to glioma cells acquire myeloid-derived suppressor cell-like properties." Neuro-oncology **12**(4): 351-416.

- Rodriguez, P. C. and A. C. Ochoa (2008). "Arginine regulation by myeloid derived suppressor cells and tolerance in cancer: mechanisms and therapeutic perspectives." Immunol Rev **222**: 180-91.
- Rodriguez, P. C., A. H. Zea, et al. (2003). "L-arginine consumption by macrophages modulates the expression of CD3 zeta chain in T lymphocytes." J Immunol **171**(3): 1232-9.
- Rolland, Y., M. Demeule, et al. (2009). "Inhibition of melanoma brain metastasis by targeting melanotransferrin at the cell surface." Pigment Cell Melanoma Res **22**(1): 86-98.
- Roy, M., J. Reiland, et al. (2005). "Antisense-mediated suppression of Heparanase gene inhibits melanoma cell invasion." Neoplasia **7**(3): 253-62.
- Ruiter, D., J. van Krieken, et al. (2001). "Tumour metastasis: is tissue an issue?" The lancet oncology **2**(2): 109-121.
- Sadik, C., N. Kim, et al. (2011). "Neutrophils cascading their way to inflammation." Trends in immunology **32**(10): 452-512.
- Sahai, E., J. Wyckoff, et al. (2005). "Simultaneous imaging of GFP, CFP and collagen in tumors in vivo using multiphoton microscopy." BMC Biotechnol **5**: 14.
- Saito, N., T. Hatori, et al. (2009). "Dynamics of global gene expression changes during brain metastasis formation." Neuropathology **29**(4): 389-97.
- Saito, N., T. Hatori, et al. (2007). "A double three-step theory of brain metastasis in mice: the role of the pia mater and matrix metalloproteinases." Neuropathol Appl Neurobiol **33**(3): 288-98.
- Saito, N., T. Hatori, et al. (2008). "Comparison of metastatic brain tumour models using three different methods: the morphological role of the pia mater." Int J Exp Pathol **89**(1): 38-44.
- Samdani, A. F., E. B. Kuchner, et al. (2004). "Astroglia induce cytotoxic effects on brain tumors via a nitric oxide-dependent pathway both in vitro and in vivo." Neurosurgery **54**(5): 1231-7; discussion 1237-8.
- Sanz-Pamplona, R., R. Aragues, et al. (2011). "Expression of endoplasmic reticulum stress proteins is a candidate marker of brain metastasis in both ErbB-2+ and ErbB-2- primary breast tumors." Am J Pathol **179**(2): 564-79.
- Sanz-Pamplona, R., J. Garcia-Garcia, et al. (2012). "A taxonomy of organ-specific breast cancer metastases based on a protein-protein interaction network." Molecular bioSystems **8**(8): 2085-2181.
- Sardi, F., L. Fassina, et al. (2011). "Alzheimer's disease, autoimmunity and inflammation. The good, the bad and the ugly." Autoimmun Rev **11**(2): 149-53.
- Sarris, M., R. A. Scolyer, et al. (2004). "Cytoplasmic expression of nm23 predicts the potential for cerebral metastasis in patients with primary cutaneous melanoma." Melanoma Res **14**(1): 23-7.
- Sattler, R. and J. D. Rothstein (2006). "Regulation and dysregulation of glutamate transporters." Handb Exp Pharmacol(175): 277-303.
- Savarin, C., S. Stohlman, et al. (2010). "Monocytes regulate T cell migration through the glia limitans during acute viral encephalitis." Journal of Virology **84**(10): 4878-4966.

- Savarin, C., S. A. Stohlman, et al. (2010). "Monocytes regulate T cell migration through the glia limitans during acute viral encephalitis." J Virol **84**(10): 4878-88.
- Schackert, G. and I. J. Fidler (1988). "Site-specific metastasis of mouse melanomas and a fibrosarcoma in the brain or meninges of syngeneic animals." Cancer Res **48**(12): 3478-84.
- Schackert, G., R. D. Simmons, et al. (1988). "Macrophage infiltration into experimental brain metastases: occurrence through an intact blood-brain barrier." J Natl Cancer Inst **80**(13): 1027-34.
- Schenkel, A. R., Z. Mamdouh, et al. (2004). "Locomotion of monocytes on endothelium is a critical step during extravasation." Nat Immunol **5**(4): 393-400.
- Schmid, B. C., G. A. Reznicek, et al. (2007). "The neuronal guidance cue Slit2 induces targeted migration and may play a role in brain metastasis of breast cancer cells." Breast Cancer Res Treat **106**(3): 333-42.
- Schneider, A., H. G. Kuhn, et al. (2005). "A role for G-CSF (granulocyte-colony stimulating factor) in the central nervous system." Cell Cycle **4**(12): 1753-7.
- Schouten, L. J., J. Rutten, et al. (2002). "Incidence of brain metastases in a cohort of patients with carcinoma of the breast, colon, kidney, and lung and melanoma." Cancer **94**(10): 2698-705.
- Scott, I. A. and D. W. Jeremy (2012). "Identification of a G-CSF-Granulocytic MDSC axis that promotes tumor progression." Onc Immunology **1**(5): 550-551.
- Sedgwick, J., S. Schwender, et al. (1991). "Isolation and direct characterization of resident microglial cells from the normal and inflamed central nervous system." Proceedings of the National Academy of Sciences of the United States of America **88**(16): 7438-7480.
- Segal, A. W. (2005). "How neutrophils kill microbes." Annu Rev Immunol **23**: 197-223.
- Seike, T., K. Fujita, et al. (2011). "Interaction between lung cancer cells and astrocytes via specific inflammatory cytokines in the microenvironment of brain metastasis." Clin Exp Metastasis **28**(1): 13-25.
- Semerad, C., F. Liu, et al. (2002). "G-CSF is an essential regulator of neutrophil trafficking from the bone marrow to the blood." Immunity **17**(4): 413-436.
- Serres, S. b., M. Soto, et al. (2012). "Molecular MRI enables early and sensitive detection of brain metastases." Proceedings of the National Academy of Sciences of the United States of America **109**(17): 6674-6683.
- Sharma, K., Z. Korade, et al. (1995). "Late-migrating neuroepithelial cells from the spinal cord differentiate into sensory ganglion cells and melanocytes." Neuron **14**(1): 143-52.
- Shinonaga, M., C. C. Chang, et al. (1988). "Immunohistological evaluation of macrophage infiltrates in brain tumors. Correlation with peritumoral edema." J Neurosurg **68**(2): 259-65.
- Shintani, Y., S. Higashiyama, et al. (2004). "Overexpression of ADAM9 in non-small cell lung cancer correlates with brain metastasis." Cancer Res **64**(12): 4190-6.
- Shmueli, E., N. Wigler, et al. (2004). "Central nervous system progression among patients with metastatic breast cancer responding to trastuzumab treatment." Eur J Cancer **40**(3): 379-82.

- Shojaei, F., X. Wu, et al. (2009). "G-CSF-initiated myeloid cell mobilization and angiogenesis mediate tumor refractoriness to anti-VEGF therapy in mouse models." Proc Natl Acad Sci U S A **106**(16): 6742-7.
- Shulman, Z., V. Shinder, et al. (2009). "Lymphocyte crawling and transendothelial migration require chemokine triggering of high-affinity LFA-1 integrin." Immunity **30**(3): 384-96.
- Sidani, M., J. Wyckoff, et al. (2006). "Probing the microenvironment of mammary tumors using multiphoton microscopy." J Mammary Gland Biol Neoplasia **11**(2): 151-63.
- Sierra, A., J. E. Price, et al. (1997). "Astrocyte-derived cytokines contribute to the metastatic brain specificity of breast cancer cells." Lab Invest **77**(4): 357-68.
- Simard, A. R., D. Soulet, et al. (2006). "Bone marrow-derived microglia play a critical role in restricting senile plaque formation in Alzheimer's disease." Neuron **49**(4): 489-502.
- Singh, P., P. Hu, et al. (2012). "hematopoietic stem and progenitor cells." Leukemia **26**(11): 2375-83.
- Sivaparvathi, M., R. Sawaya, et al. (1996). "Expression of cathepsin D during the progression of human gliomas." Neurosci Lett **208**(3): 171-4.
- Sivaparvathi, M., M. Yamamoto, et al. (1996). "Expression and immunohistochemical localization of cathepsin L during the progression of human gliomas." Clin Exp Metastasis **14**(1): 27-34.
- Smalley, S. R., E. R. Laws, Jr., et al. (1992). "Resection for solitary brain metastasis. Role of adjuvant radiation and prognostic variables in 229 patients." J Neurosurg **77**(4): 531-40.
- Smith, M. C., K. E. Luker, et al. (2004). "CXCR4 regulates growth of both primary and metastatic breast cancer." Cancer Res **64**(23): 8604-12.
- Sofroniew, M. (2005). "Reactive astrocytes in neural repair and protection." The Neuroscientist : a review journal bringing neurobiology, neurology and psychiatry **11**(5): 400-407.
- Sofroniew, M. and H. Vinters (2010). "Astrocytes: biology and pathology." Acta neuropathologica **119**(1): 7-42.
- Sofroniew, M. V. (2009). "Molecular dissection of reactive astrogliosis and glial scar formation." Trends Neurosci **32**(12): 638-47.
- Spicer, J., B. McDonald, et al. (2012). "Neutrophils promote liver metastasis via Mac-1 mediated interactions with circulating tumor cells." Cancer Research **72**(16): 3919-27.
- Stamenkovic, I. (2000). "Matrix metalloproteinases in tumor invasion and metastasis." Semin Cancer Biol **10**(6): 415-33.
- Stark, A. M., K. Tongers, et al. (2005). "Reduced metastasis-suppressor gene mRNA-expression in breast cancer brain metastases." J Cancer Res Clin Oncol **131**(3): 191-8.
- Steiner, O., C. Coisne, et al. (2010). "Differential roles for endothelial ICAM-1, ICAM-2, and VCAM-1 in shear-resistant T cell arrest, polarization, and directed crawling on blood-brain barrier endothelium." J Immunol **185**(8): 4846-55.

- Stemmler, H. J., S. Kahlert, et al. (2006). "Characteristics of patients with brain metastases receiving trastuzumab for HER2 overexpressing metastatic breast cancer." Breast **15**(2): 219-25.
- Stone, J. P. and D. D. Wagner (1993). "P-selectin mediates adhesion of platelets to neuroblastoma and small cell lung cancer." J Clin Invest **92**(2): 804-13.
- Streit, W., C. Davis, et al. (2005). "Role of fractalkine (CX3CL1) in regulating neuron-microglia interactions: development of viral-based CX3CR1 antagonists." Current Alzheimer research **2**(2): 187-196.
- Sugiura, K. and C. C. Stock (1955). "Studies in a tumor spectrum. III. The effect of phosphoramides on the growth of a variety of mouse and rat tumors." Cancer Res **15**(1): 38-51.
- Sumagin, R., H. Prizant, et al. (2010). "LFA-1 and Mac-1 define characteristically different intraluminal crawling and emigration patterns for monocytes and neutrophils in situ." J Immunol **185**(11): 7057-66.
- Suratt, B. T., J. M. Petty, et al. (2004). "Role of the CXCR4/SDF-1 chemokine axis in circulating neutrophil homeostasis." Blood **104**(2): 565-71.
- Tao, K., M. Fang, et al. (2008). "Imagable 4T1 model for the study of late stage breast cancer." BMC Cancer **8**: 228.
- Tavazoie, S. F., C. Alarcon, et al. (2008). "Endogenous human microRNAs that suppress breast cancer metastasis." Nature **451**(7175): 147-52.
- Teplyuk, N., B. Mollenhauer, et al. (2012). "MicroRNAs in cerebrospinal fluid identify glioblastoma and metastatic brain cancers and reflect disease activity." Neuro-oncology **14**(6): 689-1389.
- Tepper, R. I. (1994). "The eosinophil-mediated antitumor activity of interleukin-4." J Allergy Clin Immunol **94**(6 Pt 2): 1225-31.
- Toft-Hansen, H., R. Buist, et al. (2006). "Metalloproteinases control brain inflammation induced by pertussis toxin in mice overexpressing the chemokine CCL2 in the central nervous system." J Immunol **177**(10): 7242-9.
- Tosoni, A., M. Ermani, et al. (2004). "The pathogenesis and treatment of brain metastases: a comprehensive review." Crit Rev Oncol Hematol **52**(3): 199-215.
- Tran, E. H., K. Hoekstra, et al. (1998). "Immune invasion of the central nervous system parenchyma and experimental allergic encephalomyelitis, but not leukocyte extravasation from blood, are prevented in macrophage-depleted mice." J Immunol **161**(7): 3767-75.
- Tsao, N., H. P. Hsu, et al. (2001). "Tumour necrosis factor-alpha causes an increase in blood-brain barrier permeability during sepsis." J Med Microbiol **50**(9): 812-21.
- Tsuruo, T., H. Kawabata, et al. (1986). "Tumor-induced platelet aggregation and growth promoting factors as determinants for successful tumor metastasis." Clin Exp Metastasis **4**(1): 25-33.
- Ullian, E. M., S. K. Sapperstein, et al. (2001). "Control of synapse number by glia." Science **291**(5504): 657-61.
- Unanue, E. R. (1984). "Antigen-presenting function of the macrophage." Annu Rev Immunol **2**: 395-428.

- Updyke, T. V. and G. L. Nicolson (1986). "Malignant melanoma cell lines selected in vitro for increased homotypic adhesion properties have increased experimental metastatic potential." Clin Exp Metastasis **4**(4): 273-84.
- Urban, C. F., U. Reichard, et al. (2006). "Neutrophil extracellular traps capture and kill *Candida albicans* yeast and hyphal forms." Cell Microbiol **8**(4): 668-76.
- Vajkoczy, P., M. Laschinger, et al. (2001). "Alpha4-integrin-VCAM-1 binding mediates G protein-independent capture of encephalitogenic T cell blasts to CNS white matter microvessels." J Clin Invest **108**(4): 557-65.
- Varin, A. and S. Gordon (2009). "Alternative activation of macrophages: Immune function and cellular biology." Immunobiology **214**(7): 630-41.
- Varon, D. and A. Brill (2001). "Platelets cross-talk with tumor cells." Haemostasis **31** (Suppl 1): 64-6.
- Villringer, A., U. Dirnagl, et al. (1991). "Imaging of leukocytes within the rat brain cortex in vivo." Microvasc Res **42**(3): 305-15.
- Voisin, M.-B. t., A. Woodfin, et al. (2009). "Monocytes and neutrophils exhibit both distinct and common mechanisms in penetrating the vascular basement membrane in vivo." Arteriosclerosis, thrombosis, and vascular biology **29**(8): 1193-1202.
- von Hundelshausen, P. and C. Weber (2007). "Platelets as Immune Cells: Bridging Inflammation and Cardiovascular Disease." Circulation Research(100): 27-40.
- von Zahn, J., T. Moller, et al. (1997). "Microglial phagocytosis is modulated by pro- and anti-inflammatory cytokines." Neuroreport **8**(18): 3851-6.
- Voskuhl, R. R., R. S. Peterson, et al. (2009). "Reactive astrocytes form scar-like perivascular barriers to leukocytes during adaptive immune inflammation of the CNS." J Neurosci **29**(37): 11511-22.
- Wagner, S., M. Tagaya, et al. (1997). "Rapid disruption of an astrocyte interaction with the extracellular matrix mediated by integrin alpha 6 beta 4 during focal cerebral ischemia/reperfusion." Stroke **28**(4): 858-65.
- Waight, J., Q. Hu, et al. (2011). "Tumor-derived G-CSF facilitates neoplastic growth through a granulocytic myeloid-derived suppressor cell-dependent mechanism." PLoS One **6**(11): 27690.
- Wang, J., R. Loberg, et al. (2006). "The pivotal role of CXCL12 (SDF-1)/CXCR4 axis in bone metastasis." Cancer Metastasis Rev **25**(4): 573-87.
- Warnick, R. E., B. J. Darakchiev, et al. (2004). "Stereotactic radiosurgery for patients with solid brain metastases: current status." J Neurooncol **69**(1-3): 125-37.
- Welch, D. and D. Schissel (1989). "Tumor-elicited polymorphonuclear cells, in contrast to" normal" circulating polymorphonuclear cells, stimulate invasive and metastatic potentials of rat mammary adenocarcinoma cells." Proceedings of the National Academy of Sciences **86**(15): 5859-63.
- Wengner, A. M., S. C. Pitchford, et al. (2008). "The coordinated action of G-CSF and ELR + CXC chemokines in neutrophil mobilization during acute inflammation." Blood **111**(1): 42-9.
- Wilson, E., W. Weninger, et al. (2010). "Trafficking of immune cells in the central nervous system." The Journal of clinical investigation **120**(5): 1368-1447.

- Winkler, F., Y. Kienast, et al. (2009). "Imaging glioma cell invasion in vivo reveals mechanisms of dissemination and peritumoral angiogenesis." *Glia* **57**(12): 1306-15.
- Wojtasiak, M., D. Pickett, et al. (2010). "Depletion of Gr-1+, but not Ly6G+, immune cells exacerbates virus replication and disease in an intranasal model of herpes simplex virus type 1 infection." *The Journal of general virology* **91**(Pt 9): 2158-2224.
- Wolburg, H. and A. Lippoldt (2002). "Tight junctions of the blood-brain barrier: development, composition and regulation." *Vascul Pharmacol* **38**(6): 323-37.
- Woodfin, A., M.-B. Voisin, et al. (2011). "The junctional adhesion molecule JAM-C regulates polarized transendothelial migration of neutrophils in vivo." *Nature immunology* **12**(8): 761-770.
- Woodfin, A., M.-B. Voisin, et al. (2009). "Endothelial cell activation leads to neutrophil transmigration as supported by the sequential roles of ICAM-2, JAM-A, and PECAM-1." *Blood* **113**(24): 6246-6303.
- Wosko, T. J., D. T. Ferrara, et al. (1984). "Histological comparison of the B16 melanoma and its F1 variant." *Cancer Lett* **24**(1): 57-63.
- Wu, Q. D., J. H. Wang, et al. (2000). "Neutrophil-induced transmigration of tumour cells treated with tumour-conditioned medium is facilitated by granulocyte-macrophage colony-stimulating factor." *Eur J Surg* **166**(5): 361-6.
- Wu, Q. D., J. H. Wang, et al. (2001). "Human neutrophils facilitate tumor cell transendothelial migration." *Am J Physiol Cell Physiol* **280**(4): C814-22.
- Wu, W., K. Wong, et al. (1999). "Directional guidance of neuronal migration in the olfactory system by the protein Slit." *Nature* **400**(6742): 331-6.
- Wu, Y., L. Muldoon, et al. (2012). "Targeting α (V)-integrins decreased metastasis and increased survival in a nude rat breast cancer brain metastasis model." *Neuro Oncol* **110**(1): 27-36.
- Wyckoff, J. B., Y. Wang, et al. (2007). "Direct visualization of macrophage-assisted tumor cell intravasation in mammary tumors." *Cancer Res* **67**(6): 2649-56.
- Xie, T. X., F. J. Huang, et al. (2006). "Activation of stat3 in human melanoma promotes brain metastasis." *Cancer Res* **66**(6): 3188-96.
- Yan, H. H., M. Pickup, et al. (2010). "Gr-1+CD11b+ myeloid cells tip the balance of immune protection to tumor promotion in the premetastatic lung." *Cancer Res* **70**(15): 6139-49.
- Yang, J., Y. Hao, et al. (2012). "Therapeutic Application of MicroRNAs against Human Cancers." *J Lab Autom Epub ahead of print*.
- Yano, S., H. Shinohara, et al. (2000). "Expression of vascular endothelial growth factor is necessary but not sufficient for production and growth of brain metastasis." *Cancer research* **60**(17): 4959-5026.
- Yoneda, T., P. J. Williams, et al. (2001). "A bone-seeking clone exhibits different biological properties from the MDA-MB-231 parental human breast cancer cells and a brain-seeking clone in vivo and in vitro." *J Bone Miner Res* **16**(8): 1486-95.
- Yong, K., H. Cohen, et al. (1991). "Lack of effect of granulocyte-macrophage and granulocyte colony-stimulating factors on cultured human endothelial cells." *Blood* **77**(8): 1675-80.

- Yoo, J., S.-H. Yang, et al. (2012). "E-cadherin as a predictive marker of brain metastasis in non-small-cell lung cancer, and its regulation by pioglitazone in a preclinical model." Journal of neuro-oncology **109**(2): 219-27.
- Yoshimasu, T., T. Sakurai, et al. (2004). "Increased expression of integrin alpha3beta1 in highly brain metastatic subclone of a human non-small cell lung cancer cell line." Cancer Sci **95**(2): 142-8.
- Youn, J.-I., M. Collazo, et al. (2012). "Characterization of the nature of granulocytic myeloid-derived suppressor cells in tumor-bearing mice." Journal of leukocyte biology **91**(1): 167-248.
- Zaccaria, M. L., F. Di Tommaso, et al. (2001). "Dystroglycan distribution in adult mouse brain: a light and electron microscopy study." Neuroscience **104**(2): 311-24.
- Zhang, C., F. Zhang, et al. (2009). "Transforming growth factor-beta2 is a molecular determinant for site-specific melanoma metastasis in the brain." Cancer Res **69**(3): 828-863.
- Zhang, C., F. Zhang, et al. (2009). "Transforming growth factor-beta2 is a molecular determinant for site-specific melanoma metastasis in the brain." Cancer Res **69**(3): 828-35.
- Zhang, E. T., C. B. Inman, et al. (1990). "Interrelationships of the pia mater and the perivascular (Virchow-Robin) spaces in the human cerebrum." J Anat **170**: 111-23.
- Zhang, L., P. Sullivan, et al. (2011). "MicroRNA-1258 suppresses breast cancer brain metastasis by targeting heparanase." Cancer research **71**(3): 645-699.
- Zhang, M. and Y. Olsson (1995). "Reactions of astrocytes and microglial cells around hematogenous metastases of the human brain. Expression of endothelin-like immunoreactivity in reactive astrocytes and activation of microglial cells." J Neurol Sci **134**(1-2): 26-32.
- Zhang, W., S. Dang, et al. (2012). "A humanized single-chain antibody against beta 3 integrin inhibits pulmonary metastasis by preferentially fragmenting activated platelets in the tumor microenvironment." Blood **120**(14): 2889-98.
- Zhang, Z., T. Hatori, et al. (2008). "An experimental model of brain metastasis of lung carcinoma." Neuropathology **28**(1): 24-8.
- Zhou, J., S. A. Stohlman, et al. (2003). "Neutrophils promote mononuclear cell infiltration during viral-induced encephalitis." J Immunol **170**(6): 3331-6.
- Zhou, S. L., Z. Dai, et al. (2012). "Overexpression of CXCL5 mediates neutrophil infiltration and indicates poor prognosis for hepatocellular carcinoma." Hepatology **56**(6): 2242-54.
- Zlotnik, A. (2004). "Chemokines in neoplastic progression." Semin Cancer Biol **14**(3): 181-5.
- Zujovic, V., J. Benavides, et al. (2000). "Fractalkine modulates TNF-alpha secretion and neurotoxicity induced by microglial activation." Glia **29**(4): 305-15.

APPENDIX

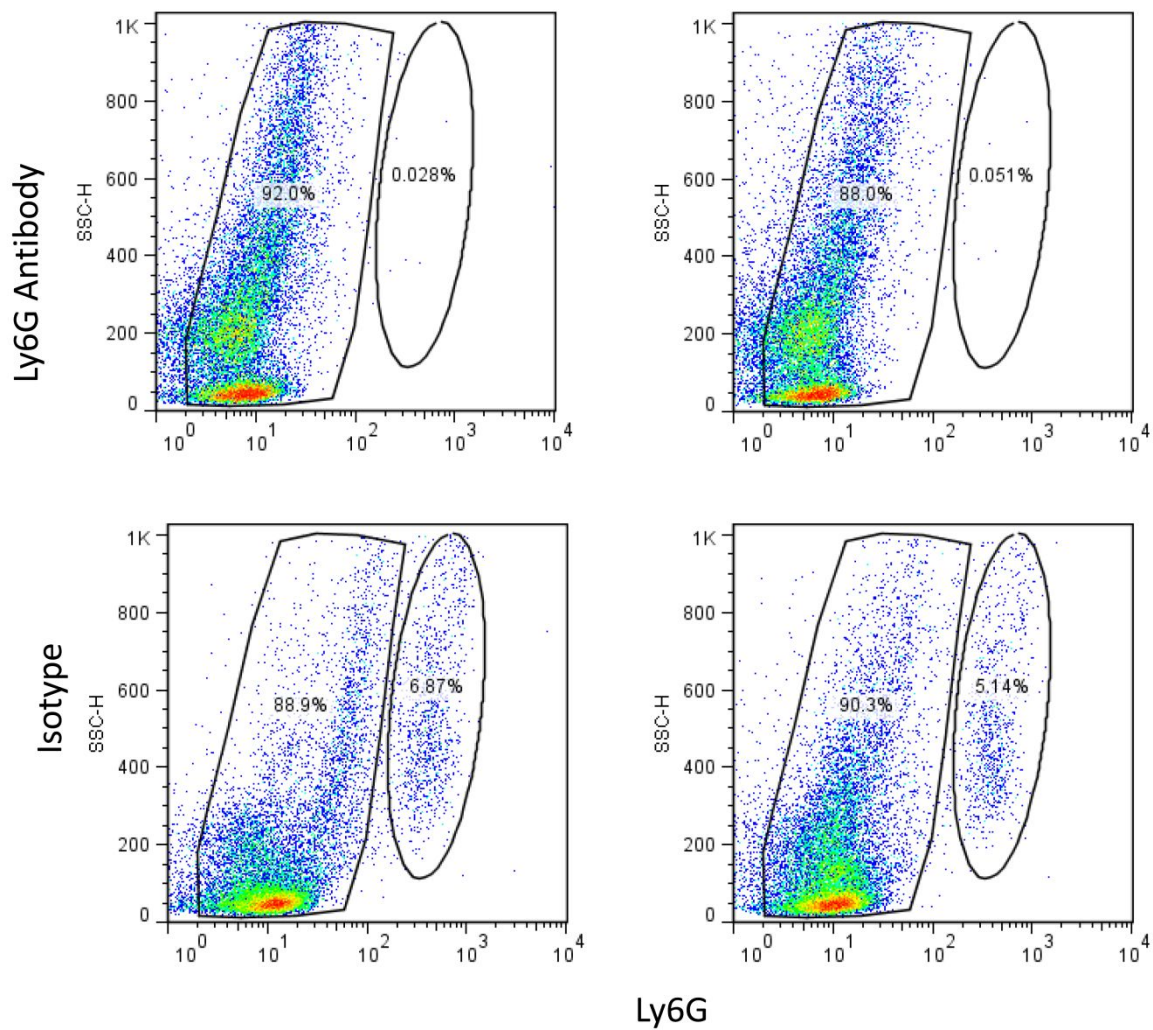
SUPPLEMENTARY TABLE

Supplementary Table 1: In Vivo Adverse Effects

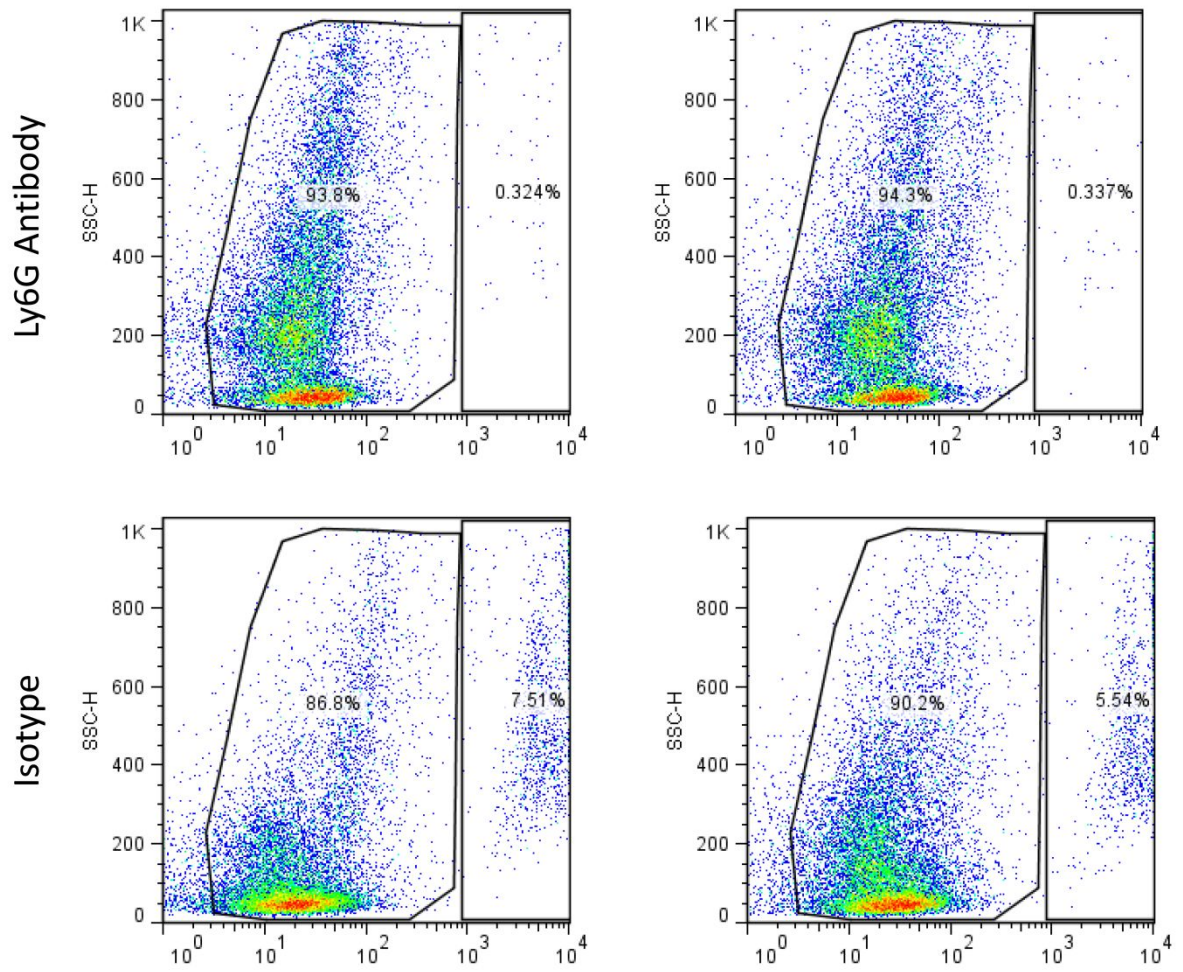
Procedure	Adverse Effects	Expected	Actual
Intracardiac (blind)	Haemorrhage following tumour cell injection	up to 30%	17% (2/12)
Intracardiac (Ultrasound)	Anaesthetic deaths	<5%	0%
	Haemorrhage following tumour cell injection	up to 30%	0%
Intracarotid	Anaesthetic deaths	<5%	0%
	Haemorrhage/ischemia following tumour cell injection	up to 30%	16% (5/31 due to ischemia)
Cranial windows/ <i>in vivo</i> imaging	Anaesthetic deaths	<5%	<1% (1/23 during imaging)
	Haemorrhage following cranial surgery	<5%	0%
	Toxicity of drugs or fluorescent or coloured markers and other adjuvants	<1%	<1% (1/23 after i.v injection of fluorescent beads)
	Neurological sequelae due to cranial window placement and/or laser microlesions	< 5%	0%

SUPPLEMENTARY FIGURES

A

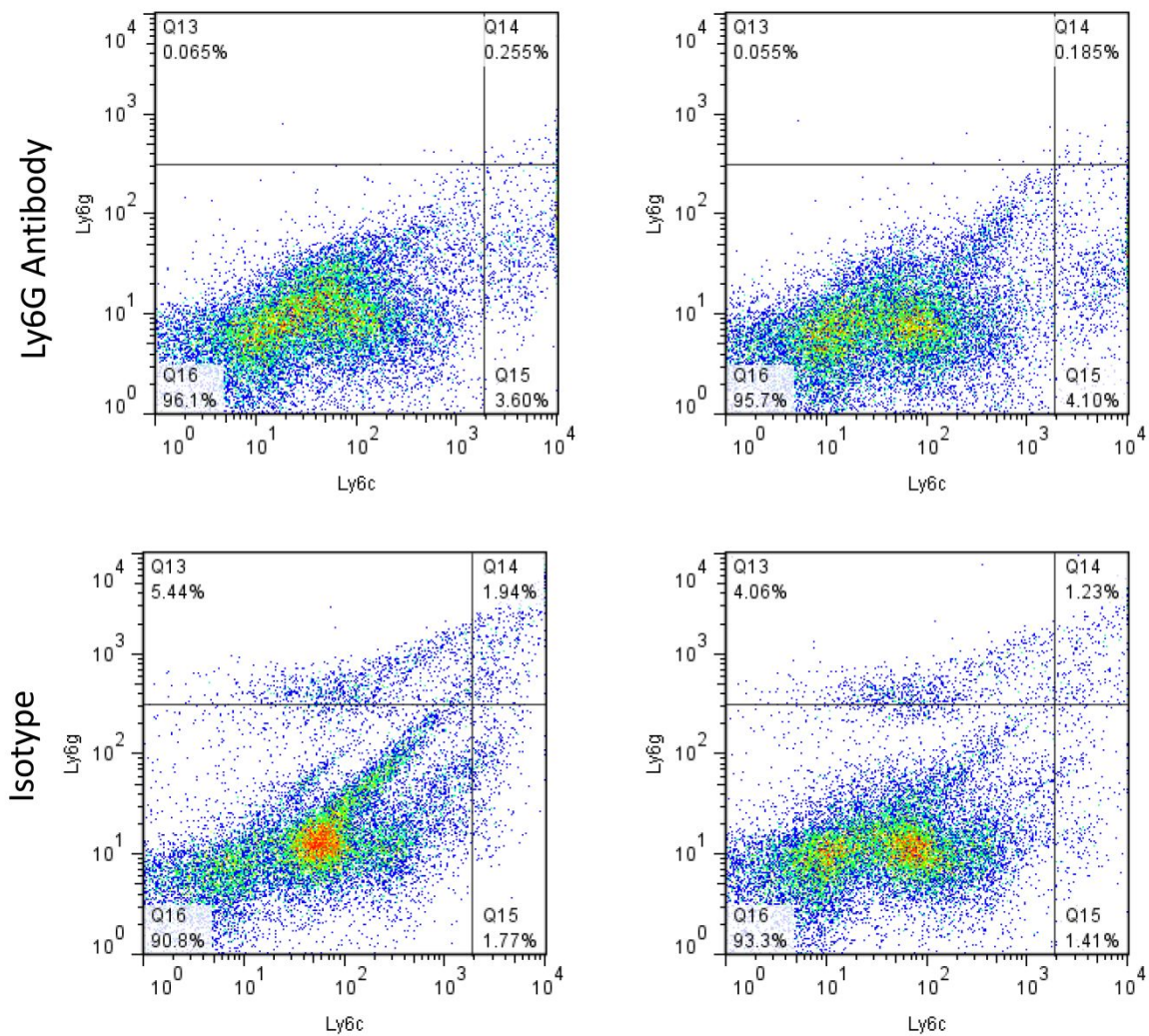


B



Gr-1

C

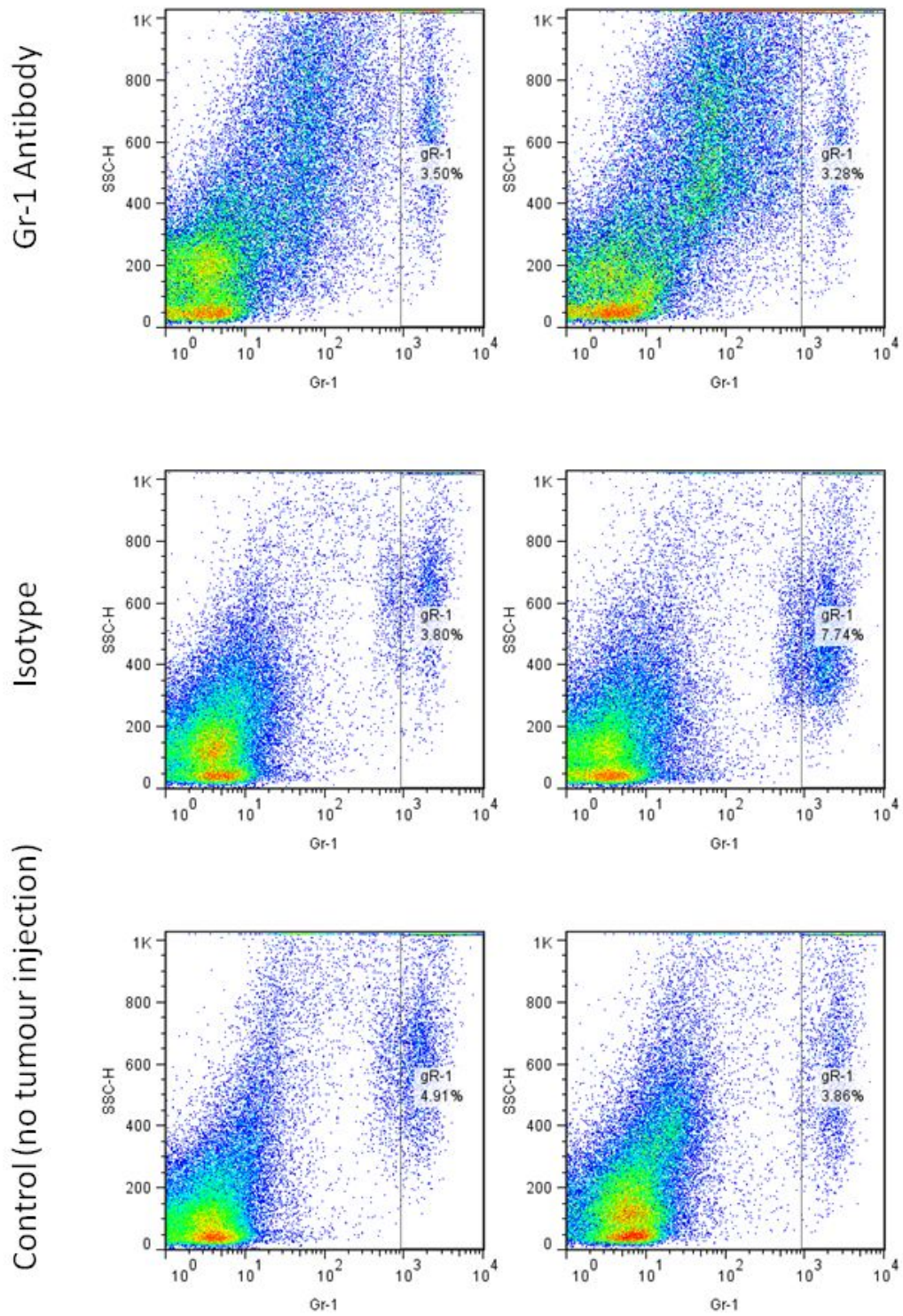


Supplementary Figure 1: Ly6g antibody depletes Ly6G⁺ cells but may mask Gr-1⁺ cells

Balb/c mice were injected daily for 7 days with 12.5 μg of Ly6G antibody or isotype matched control antibody. 24 h after the first dose of antibody, mice were intracardiac injected with 10^5 4T1-GFP tumour cells. Mice were culled on day 8 and blood was collected. Blood was labelled *ex vivo* with fluorescent antibodies against Ly6G, Ly6C and Gr-1 and analysed by FACS. A-B: Both the Ly6G⁺ and Gr-1⁺ population were depleted in Ly6G antibody injected mice. However, in plot B, an increase in the number of Gr-1⁻ cells population in Ly6G antibody depleted mice was found. C: Representative images of FACS plot of blood stained with Ly6G (y-axis) and Ly6C (x-axis). In isotype injected mice there was a population of Ly6G⁺Ly6C⁻ cells (neutrophils) and Ly6G⁺Ly6C⁺ (Gr-1⁺) cells. Both these populations disappeared in Ly6G antibody injected mice. However, the Ly6C⁺ cells are retained in Ly6G antibody depleted mice but shifted down so that they are appeared Ly6G⁻. This shift implies a masking effect of the Ly6G antibody on the Ly6G epitopes of Gr-1⁺ cells.

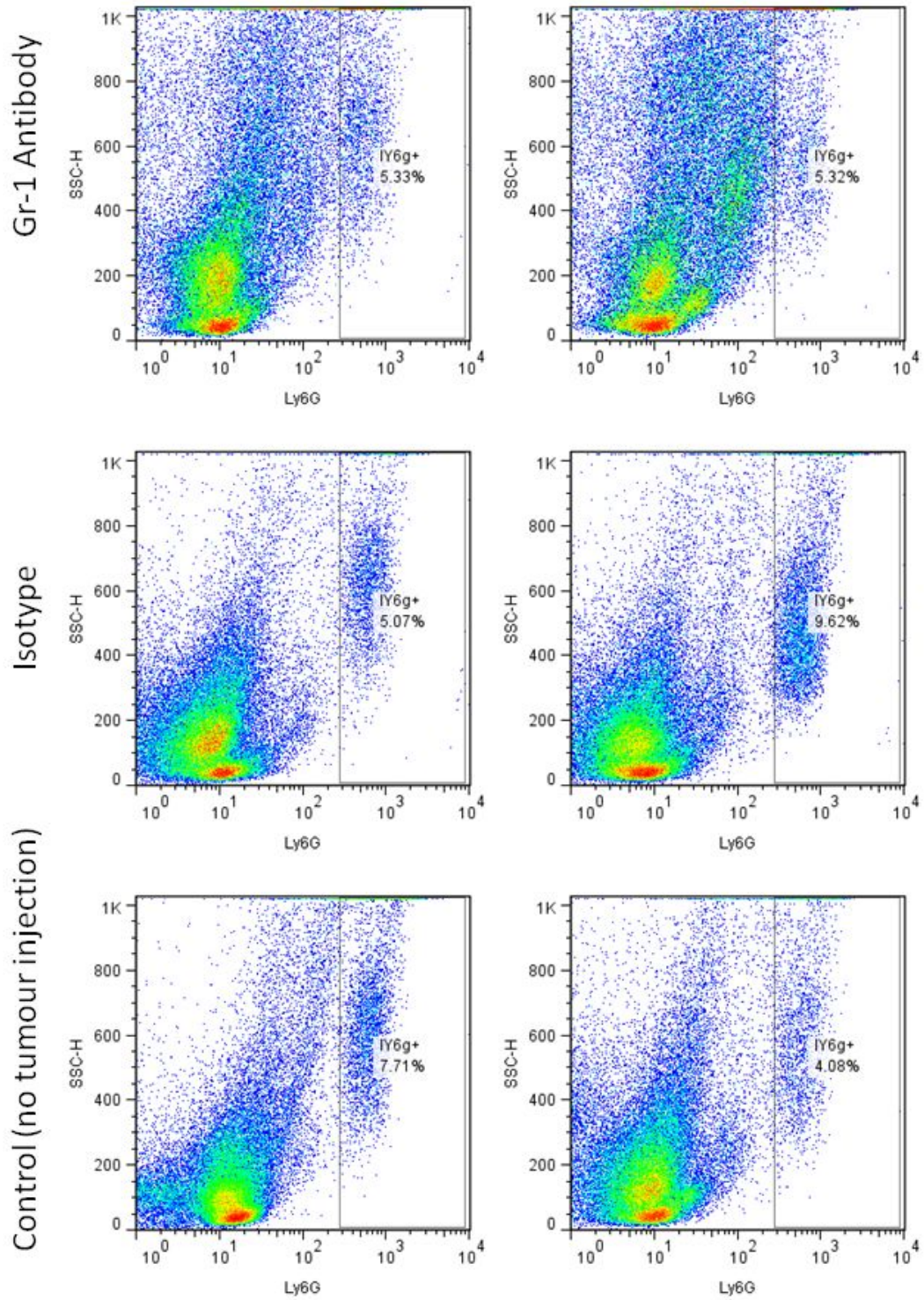
A

SSC vs. Gr-1



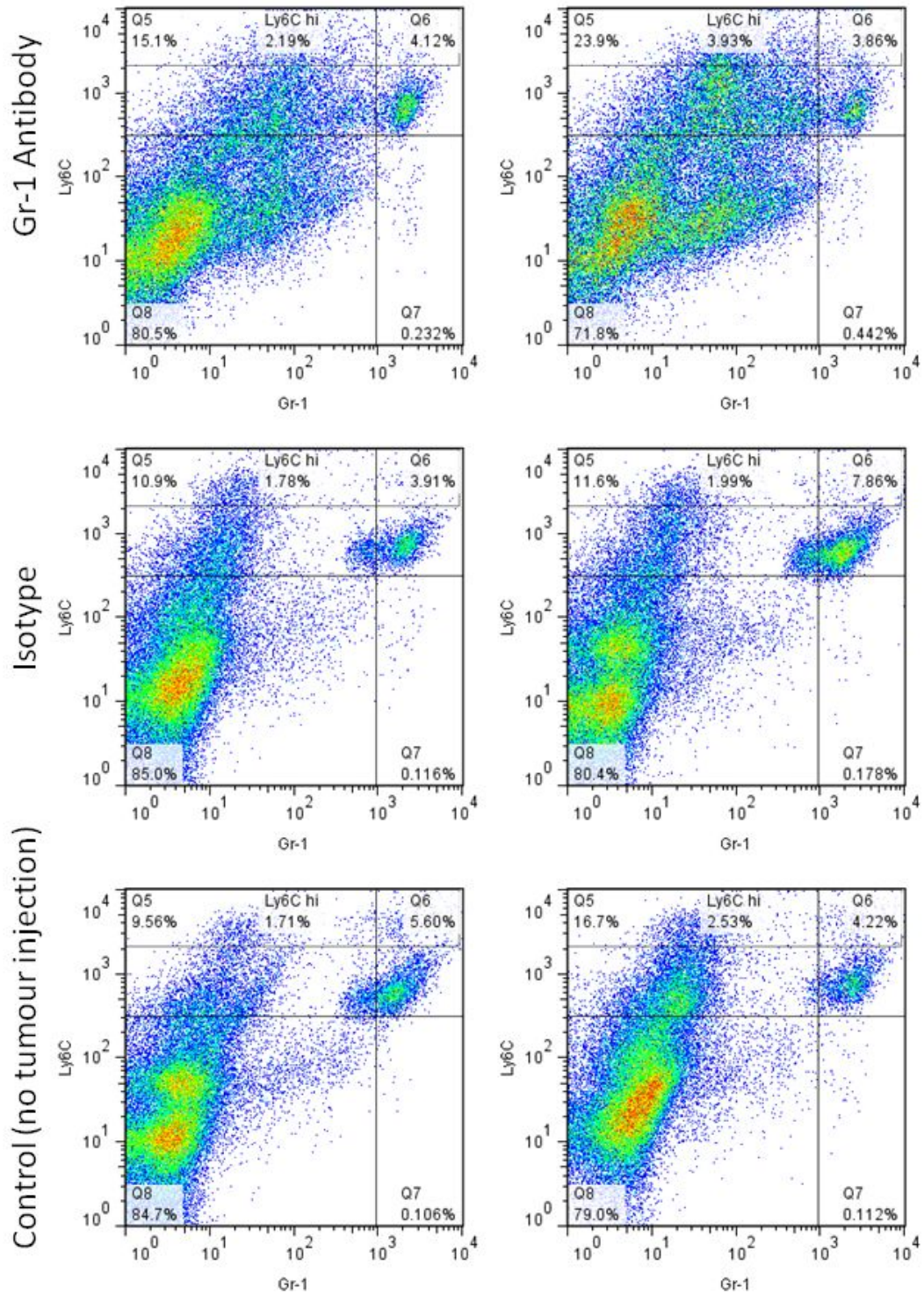
B

SSC vs. Ly6G



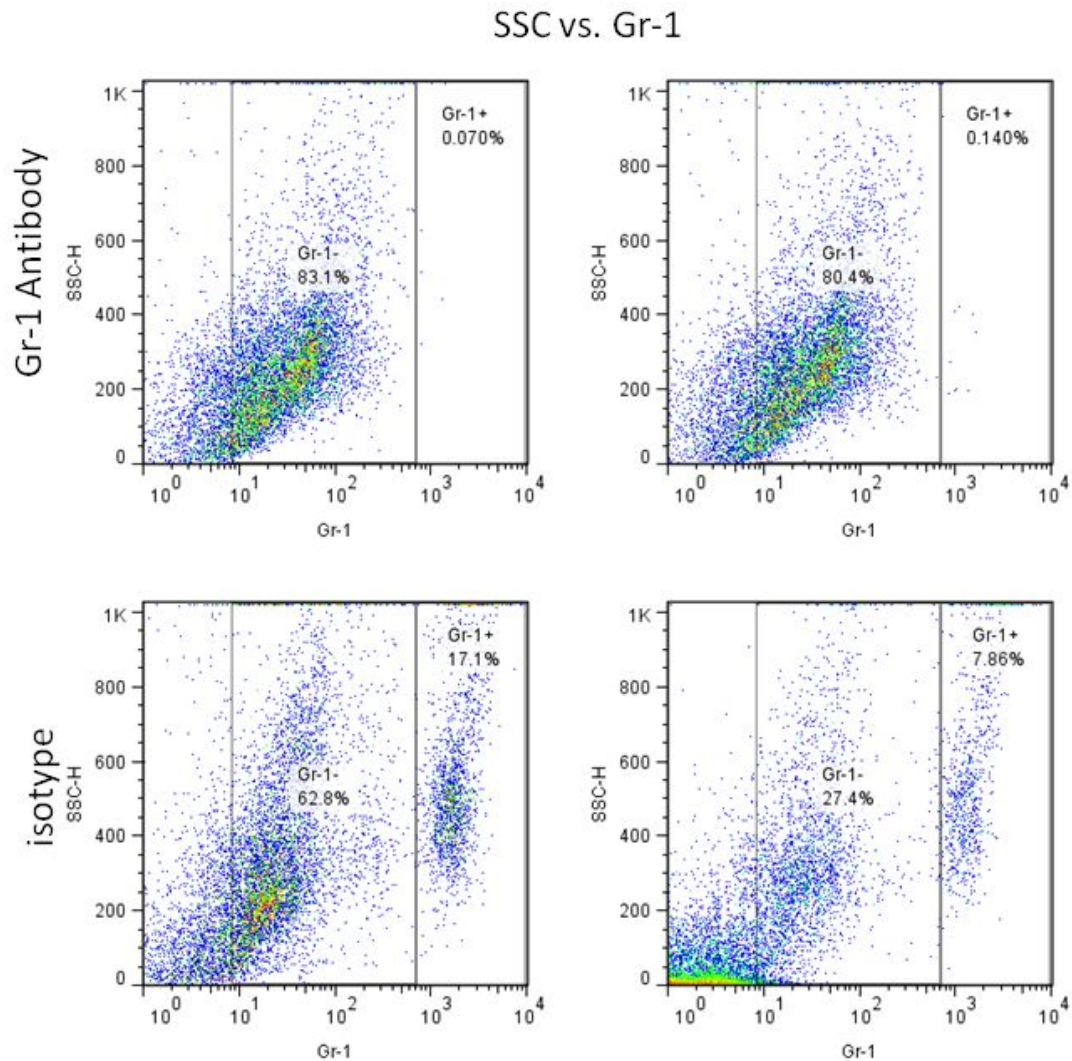
C

Ly6c vs. Gr-1



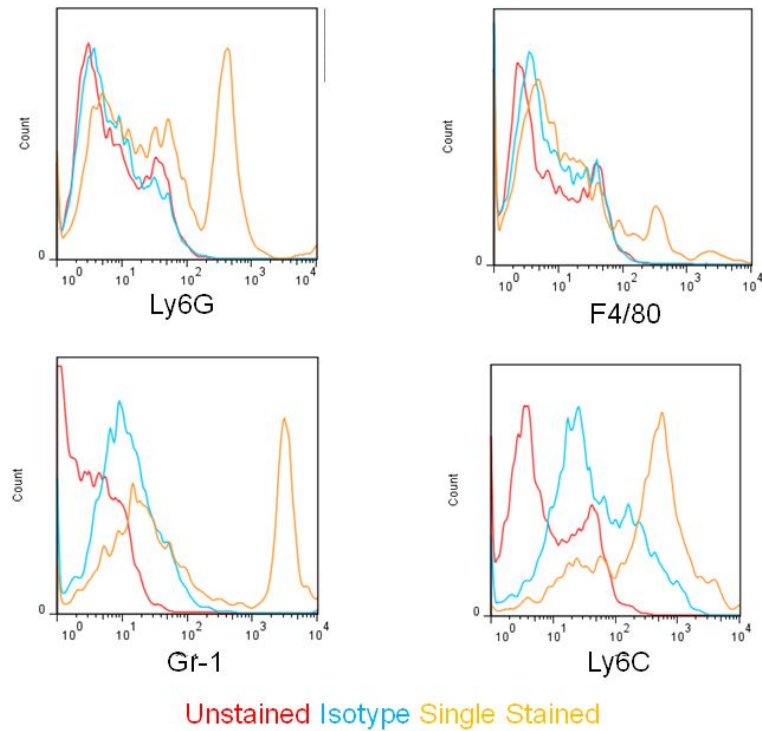
Supplementary Figure 2: Gr-1 antibody does not sustain depletion of Gr-1⁺ cells in 4T1 injected mice

Balb/c mice were injected daily for 7 days with 50 µg of Ly6G antibody or isotype matched control antibody. 24 h the first dose of antibody, mice were intracardiac injected with 10⁵ 4T1-GFP tumour cells. Mice were culled on day 8 and blood was collected. Blood was labelled *ex vivo* with fluorescent antibodies against Ly6G, Ly6C and Gr-1 and analysed by FACS. Blood collected from an age-matched naïve Balb/c mouse was included as control. A-B: Both Gr-1⁺ and Ly6G⁺ cells were found in blood of Gr-1 antibody injected mice. There was also an increase of Gr-1⁻ and Ly6G⁻ cells in Gr-1 antibody injected mice. C: Blood was analysed based on Ly6C and Gr-1 expression. In Gr-1 antibody injected mice there was an increase in Ly6C⁺ and Ly6C^{hi} cell populations implying myelopoiesis due to antibody injection and not due to tumour growth.



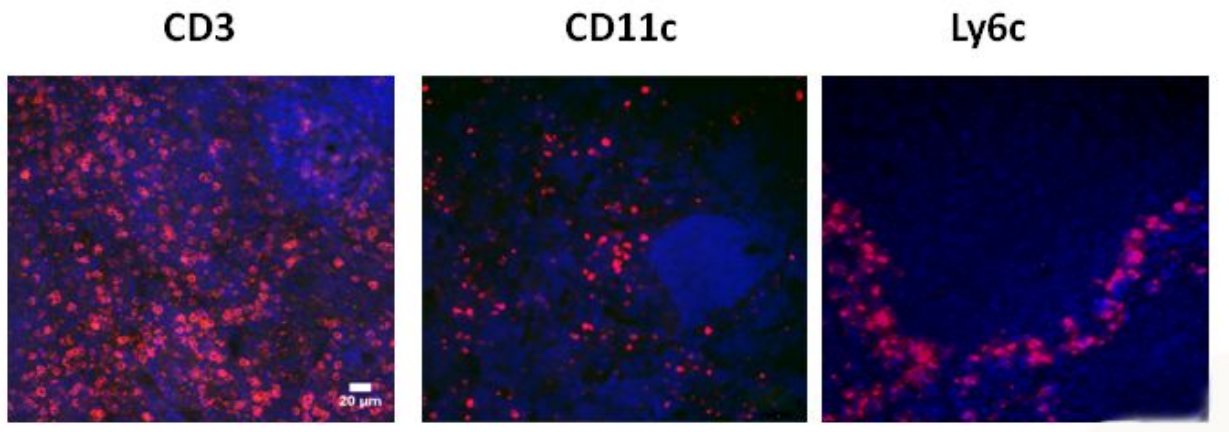
Supplementary Figure 3: Use of Gr-1 antibody to deplete Gr-1⁺ cells in MDA 231 injected SCID mice.

SCID mice were injected daily for 5 days with 50 μ g of Gr-1 antibody or isotype matched control antibody. 24 h the first dose of antibody, mice were intracardiac injected with 10^5 MDA 231-GFP tumour cells. Mice were culled on day 6 and blood was collected and labelled *ex vivo* with fluorescent antibodies against Gr-1 and analysed by FACS. Although it seems like Gr-1⁺ cells were depleted in mice injected with Gr-1 antibody, there seemed to be an increase in the number of cells in the Gr-1⁻ gate in Gr-1 antibody injected mice compared to isotype control. Injected of Gr-1 antibody may deplete some cells but may also mask the Gr-1 epitope in other cell types therefore shifting non-depleted Gr-1⁺ cells into the Gr-1^{low/-} gate.



Supplementary Figure 4: Single staining and isotype control staining of blood cells from MDA 231 injected SCID mice.

Blood from SCID mice intracardiac injected with MDA 231 was analysed by FACS after *ex vivo* staining with Ly6G, F4/80, Gr-1 and Ly6C antibodies and isotype controls. Cells were single stained with each antibody to determine specificity of staining and to use for the gating strategy to analyse cells stained with all 4 antibodies.



Supplementary Figure 5: Antibody labelling of spleen sections as positive controls

CD3, CD11c and Ly6c cells are not normally found in the brain, therefore we stained spleen sections as positive controls. Antibodies against CD3 (T-cells), CD11c (dendritic cells/macrophages), and Ly6C (monocytes, MDSC) labelled immune cells in the spleen. Labelling was not seen when spleen sections were labelled without adding primary antibodies (not shown).

SUPPLEMENTARY VIDEOS

Videos corresponding to legends are found in the accompanying DVD

Supplementary Video 1: Adoptive transfer of Dil labelled immune cells can be visualised through the cranial window

Balb/c mice fitted with a cranial window were intracarotid injected with 2.5×10^5 4T1-GFP cells and 10^6 Dil labelled peripheral blood cells collected from a naïve age-matched Balb/c mouse. Mice were imaged within 30 mins of injection. Mice were injected i.v with 100 μ l of Oregon Green 514 dextran prior to imaging. Very few Dil labelled cells can be seen within the circulation.

Supplementary Video 2: CD45-PE antibodies label circulating immune cells

Balb/c mice fitted with a cranial window were intracarotid injected with 2.5×10^5 4T1-GFP cells and imaged 24 h later. Prior to imaging, mice were injected i.v with 100 μ l of PE labelled anti-CD45 antibody and imaged using confocal microscope. PE labelled cells were recorded using confocal imaging. Free unbound antibody circulating in the blood highlighted blood vessels.

Supplementary Video 3: Injecting mice with 10^6 4T1-GFP tumour cells causes slowing down of circulating immune cells.

Mice were injected into the carotid artery with 1×10^6 4T1-GFP cells and confocal imaging commenced 24 h after tumour injection and repeated every day for 7 days. Prior to each imaging session, mice were injected i.v with 100 μ l of anti-mouse CD45-PE. Video recordings were made over the same areas on days 1, 2 and 3(A) or only day 2 and 3 in another mouse (B). Substantial slowing down of CD45-PE labelled cells was seen 3 days after tumour cell injection.

Supplementary Video 4: Injecting mice with 5.0×10^5 4T1-GFP tumour cells or PBS does not cause slowing down of circulating immune cells.

Mice were injected into the carotid artery with 5.0×10^5 4T1-GFP cells and confocal imaging commenced 24 h after tumour injection and repeated every day for 7 days. Prior to each imaging session, mice were injected i.v with 100 μ l of anti-mouse CD45-PE. A: Video recordings were made over several areas of the brain 3 days after mice were injected with PBS and CD45 bright cells showed similar movements within the circulation 3 days after PBS injections as they did 24 h after PBS injection (not shown). B – Video recordings were made 10 days after mice were injected with 5.0×10^5 4T1-GFP cells and CD45 bright cells were seen moving at the same speed as CD45 bright cells within the vasculature of PBS injected mice.